EPITHERMAL NEUTRON ACTIVATION ANALYSIS FOR BACTERIAL TRANSFORMATIONS OF CHROMIUM

N.Ya. Tsibakhashvili[1,2], L. Mosulishvili[1], E. Kirkesali[1], T. Kalabegishvili[1,2], S. Kerkenjia[2], M.V. Frontasyeva[3], Gh. Duca[4] , I. Zinicovscaia[3,4]

[1]*Andronikashvili Institute of Physics, Tbilisi, Georgia,*
[2]*Chavchavadze State University, Tbilisi, Georgia*
[3]*Frank Laboratory of Neutron Physics, Joint Institute for Nuclear Research,Dubna,Russia*
[4]*University of the Academy of Sciences of Moldova*
E-mail: zing@nf.jinr.ru

Abstract: Most powerful primary analytical technique, neutron activation analysis, was applied to study indigenous bacteria, namely, *Arthrobacter* genera which can be successfully used in detoxification and immobilization of toxic substances. In the present study the effect of Cr(VI) on the elemental content of these bacteria has been examined. The concentrations from 12 to 19 elements such as Na, Al, Cl, K, Fe, Co, Zn, As, Br, Rb, Sr, Sb, Ba, Tb, Th, U were determined in the bacterial cells. The high rate of Cr accumulation in the tested bacterial cells was shown. In bacteria treated with chromate some similarity in the behaviour of the following essential elements − potassium, sodium, chlorine − was observed. Such non-essential elements as Ag, As, Br and U were determined in all bacteria and have to be considered by cells as toxins.

Keywords: neutron activation analysis, electron spin resonance spectrometry, *Arthrobacter*

Introduction

Environmental pollution by chromium is widespread in soils, sediments and groundwater [1]. Being a transition element, it occurs in a number of oxidation states from Cr(II) to Cr(VI). However, only two stable, trivalent and hexavalent, species are significant in environmental systems. Hexavalent chromium compounds are highly soluble and toxic [2]. Epidemiological**,** animal and cellular studies have also established that Cr(VI) compounds are carcinogenic [3]. In contrast to Cr(VI), most Cr(III) compounds are less soluble and less toxic. Moreover, trace amounts of Cr(III) appear to be essential for animal and human glucose and lipid metabolism. The biological effect of Cr(VI) is generally attributed to cellular uptake, because Cr(VI), unlike Cr(III), is easily uptaken by cells via SO_4^{2-} and HPO_4^{2-} channels [4]. The toxicity of Cr(VI) compounds is ascribed to reactive intermediates (such as Cr(V), Cr(IV), radicals) generated during their reduction by living cells. Relatively, long-lived Cr(V) intermediates have been detected in the reduction of Cr(VI) both in vitro and in vivo [4,5]. However, to the best of our knowledge, there have been only a few studies that examined the in vivo formation of Cr(V) (in algae and fangs) [5,6] and none on the dynamic detection of Cr(V) and its effect in bacteria. Toxic chromium compounds can be removed by chemical reduction, which is both difficult and expensive.

Indigenous bacteria can be successfully used to either detoxify or immobilize toxic heavy metals. These bacteria are under continuous investigation, and in-depth molecular understanding has been developed for some of them. However, up to date the dependence between the ability of bacteria to reduce or immobilize metals and their elemental compositions is not clear yet [7, 8].

In the present study the effect of Cr(VI) on the elemental content of these bacteria has been examined. Specifically, we tested three Gram-positive bacterial strains of *Arthrobacter* genera – *A. oxydans* (isolated in the USA from polluted Columbia basalt rocks), *Arthrobacter* sp. (61 B), and *A. globiformis* (151 B) (isolated from the most polluted regions in the Republic of Georgia).

Materials and Methods

Sample cultivation and preparation for analysis

The bacteria were grown aerobically in the following nutrient medium: 10 g of glucose, 10 g of peptone, 1 g of yeast extract, 2 g of caseic acid hydrolysate, 5 g of NaCl, and 1 liter of distilled water. To provide the chromium concentration of 35 and 200 mg/L, Cr(VI) [as K_2CrO_4] was added to the nutrient medium at an early stationary phase of growth.

After being cultivated for 4 days the cells were harvested by centrifugation (10,000 rpm, 15 min, 4 °C), rinsed twice in a 20 mM phosphate buffer and analyzed by NAA method.

To prepare bacterial samples for NAA, wet biomass was placed in an adsorption-condensation lyophilizer, dried, and pelletized to 5 mm pieces (~ 0.5 g) by means of titanium press form.

Instrumental Neutron Activation Analysis (INAA) at the reactor IBR-2

ENAA was conducted at the IBR-2 pulsed fast reactor in FLNP, JINR, Dubna, which is characterized by a very high ratio (~100) of epithermal neutrons to thermal ones. The IBR-2 reactor provides activation with the whole fission spectrum: thermal, epithermal, and fast neutrons. Thermal NAA takes advantage of the high intensity of neutrons available from the thermalization of fission neutrons and the large thermal neutron cross sections for most isotopes.

Epithermal is taken to be neutrons with energies from the Cd "cutoff" of 0.55 eV up to ~1 MeV. ENAA is a useful extension of thermal (conventional) NAA in that it enhances the activation of a number of trace elements relative to the major matrix elements. ENAA is particularly advantageous for radionuclides produced from a stable isotope with a high resonance activation integral relative to its thermal neutron activation cross section. In general, the activation cross sections of the matrix elements of environmental samples are inversely proportional to the neutron energy (1/*v* law). The trace elements also follow this general trend, but many of them have large activation cross sections at specific energies in the epithermal energy region. In our case, the following advantages are evident: (i) improved detection limits for As, Br, Rb, Sr, and Sb; (ii) reduction of high matrix activity, e.g., from ^{28}Al, ^{56}Mn, ^{24}Na, ^{46}Sc, ^{60}Co.

Bacterial samples of about 0.5g were heat–sealed in polyethylene foil bags for short–term irradiation and for long-term irradiation were packed in aluminum cups. To determine the short–lived isotopes Cu, I, Br, Mn, Mg, Na, V, K, Cl and Ca, channel 2(Ch2) was used. Samples were irradiated for 3 minutes and measured twice after 3−5 and 20 minutes, respectively for 5 and 15 minutes. In case of long–lived isotopes of Na, K, Sc, Cr, Fe, Co, Ni, Zn, As, Se, Br, Rb, Sr, Ag, Cd, Sb, Cs, La, Ce, Sm, Tb, Yb, Hf, Au, Th and U, channel 1 (Ch1) was used. Samples were irradiated for five days, re-packed and then measured twice after 4−6 and 20 days, respectively. Measure time varied from 1−3 hours. γ-Ray spectra were measured using a large-volume Ge(Li) detector with a resolution of 1.96 keV at the 1332.4-keV line of ^{60}Co with an efficiency of 30% relative to a 3 in.× 3 in. NaI detector for the same line. The data processing and element concentration determination were performed on the basis of certified reference materials and comparators using software developed in FLNP JINR [9].

Three certified reference materials (CRMs), namely, IAEA Lichen-336, Donnye SL-1and Coal, fly ash SRM-1633b were used for quality assurance purpose.

Electron Spin Resonance Spectrometry

The ESR investigations were carried out on a RE 1306 radiospectrometer with 100 kHz modulation at 9.3 GHz [10]. Detection of Cr(V) was carried out at liquid nitrogen temperature (77 K) to avoid a decrease in sensitivity of the ESR spectrometer caused by the water content in bacterial samples. The detection of the broad line for Cr(III) was complicated at low temperatures due to the presence of oxygen impurity in liquid nitrogen, which shifts the zero line. To avoid this problem, we measured Cr(III) at room temperature after drying the samples at 100 °C. The typical settings for the registration of Cr(V) and Cr(III) are described in detail in [10].

Results and discussions

Metals play an integral role in life processes of microorganisms. In the present work, we focused on the determination of metal contents in bacteria cells. Some metals, such as Co, Cr, Fe, Na, K, and Zn, are required nutrients and are essential. Others have no definite biological function (Ag, Al, Cd) and are non-essential [11].

The concentrations from 12 to 19 elements such as Na, Al, Cl, K, Fe, Co, Zn, As, Br, Rb, Sr, Sb, Ba, Tb, Th, and U were determined in the bacterial cells of 3 strains of *Arthrobacter*.

Data on chromium shows the high rate of Cr accumulation in tested bacterial cells (**Fig.1**). The chromium content in the control cells was less than 10 *μg/g*, while the same values in the treated cells were much higher. For example, in *Arthrobacter* sp. it reached to 3 10^3 *μg/g* after exposure to 35 *mg/L* of Cr(VI) for 4 days. Reduction of Cr(VI) to Cr(III) begins at the surface of bacteria with the formation of Cr(V) complexes **(Fig.2)** and the main part of reduced chromium (Cr(III hydroxide) is tightly bound to bacterial cells. Our current ENAA data provide evidence that one part of chromium penetrates inside cells as well.

Bacteria can use chromium (VI) as terminal electron acceptor during oxidation of organic compounds. The capability of Cr (VI) reduction is not uncommon among Cr(VI)-resistant microorganisms. Investigation of oxidation-reduction potential (ORP) of nutrient medium during microbial chromate reduction has shown that Cr(VI) reduction takes place effectively at ORP level +400 – +200 mV. This is a potential range of aerobic processes. Standard

electrode potential (E_0) of reaction: $Cr_2O_4^{2-} + 8H^+ + 3e = Cr^{3+} + 4H_2O$ is 1477 mV. The potential is higher then potential of oxygen reduction process: $O_2 + 4H^+ + 4e = 2H_2O$ (E_0=1228 mV). The reactions take place in bacterial cells during respiration. Therefore, the presents of oxygen is necessary to supply high OPR level in cultural medium. Thus, the reduction of Cr(VI) to Cr (III) has to take place in aerobic condition [12].

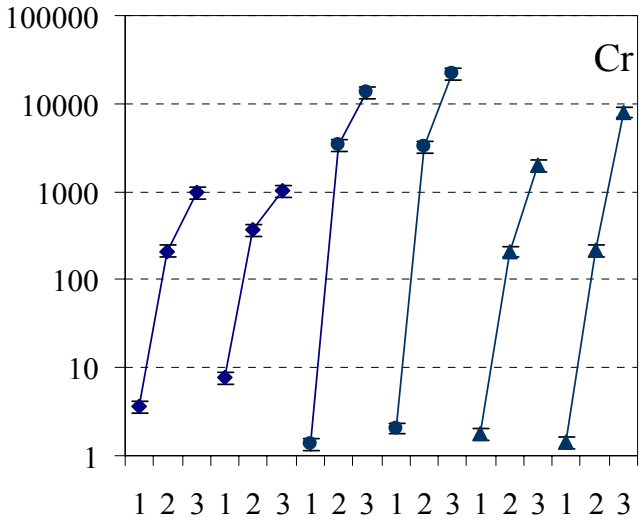

Fig. 1. Concentration of chromium (*μg/g*) in different species of *Arthrobacter*: 1 – control; 2 – 35 *mg/L* Cr(VI); 3 – 200 *mg/L* Cr(VI)

◆ *Arthrobacter oxydans*; ■ *Artrobacter* sp. (61B); ▲ *Arthrobacter globiformis* (151B)

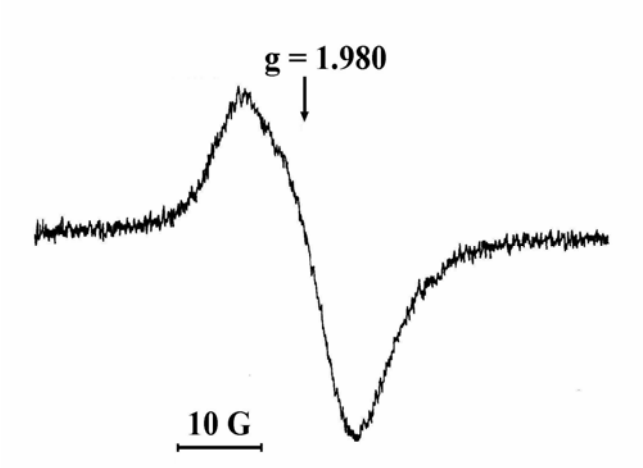

Fig. 2. An ESR spectrum of Cr(V) from tested bacteria after growing in the nutrient medium containing Cr(VI), line width = 12 gauss and g-factor = 1.980

In bacteria treated with chromate some similarity in the behaviour of the following essential elements – potassium, sodium, chlorine – was observed (**Fig. 3)**.

Potassium is known to play an important role in maintaining cellular osmotic pressure; it is involved in non-specific activation of many enzymes, in bacterial energy metabolism (as the coupling ion), and in the regulation of intracellular pH. Potassium is the principal positively charged ion (cation) in the fluid inside of cells, while sodium is the principal cation in the fluid outside of cells. Potassium concentrations are about 30 times higher inside than outside cells, while sodium concentrations are more than ten times lower inside than outside cells.

The concentration differences between potassium and sodium across cell membranes create an electro-chemical gradient known as the membrane potential. A cells membrane potential is maintained by ion pumps in the cell membrane, especially the sodium, potassium−ATPase pumps. These pumps use ATP (energy) to pump sodium out of the cell in exchange for potassium [11].

First, exposure to Cr(VI) caused a lower potassium concentrations in cells and the decrease of K content was almost equal at both low (35 mg/L) and high (200 mg/L) concentrations of Cr(VI). Second, concentrations of sodium and chlorine changed in a parallel way to each other, but in an opposite way to that of potassium. Decrease of K content, in other words extrusion of K from cells to maintain the acidity of their cytosol, concomitant with increase of Na (and correspondingly Cl) content, suggests that, one part of Cr(V)-diols (as well as Cr(VI) ions (via HPO_4^{2-} channels)) were able to penetrate inside bacterial cells.

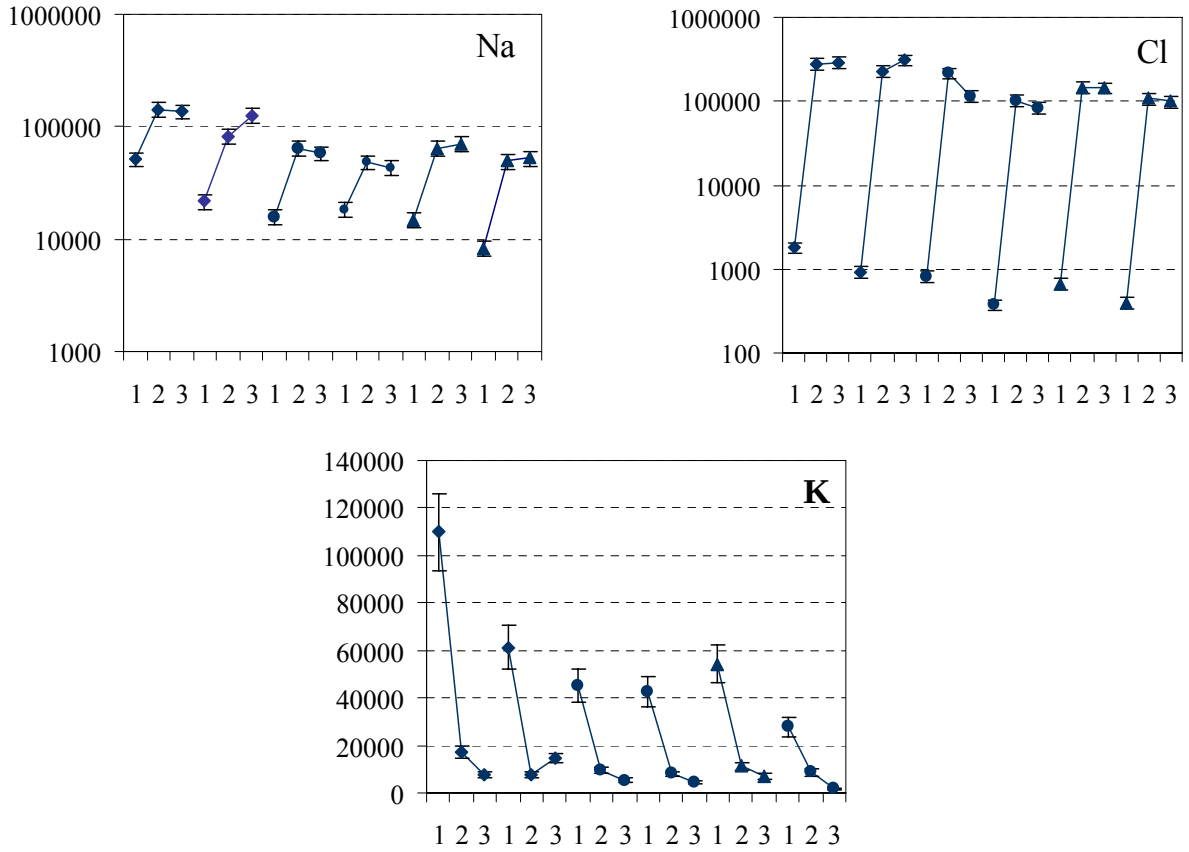

Fig. 3. Concentration of Na, Cl and K (*μg/g*) in different species of *Arthrobacter* under different Cr(VI) loadings

NAA measurement of iron content in bacteria supports this conclusion **(Fig. 4.)**. As is known, iron is the most important metal biologically. It is a many-functional constituent ofcomplex molecules. **Fig. 4** demonstrates that in the tested bacteria the Fe content significantly increased in response to Cr(VI) loading, indicating that the bacterial protective system was activated significantly against chromium toxic impact.

In *A. globiformis*, contrary to *A. oxydans* and *Arthrobacter* sp, the content of iron increased almost linearly with increase of Cr(VI) dose. It seems that Cr(VI) transformation mechanism is rather different in *A. globiformis* than in *Arthrobacter oxydans* and *Arthrobacter* sp.

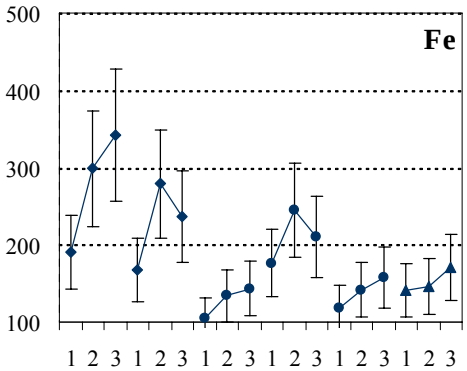

Fig. 4. Concentration of Fe (*μg/g*) in different species of *Arthrobacter* under different Cr(VI) loadings

This result suggests what the chemical composition of basalts influenced the elemental composition of bacteria. Really the Georgian basalt samples from the studied sites are rocks with high content of total iron (Fe_2O_3+FeO), which is due to the abundance of ferromagnesial minerals-pyroxenes [(Ca, Na, Mg, Fe)(Al, Si)O_3], olivine ($Mg_{1.8}Fe_{0.2}SiO_4$), magnetite($Fe^{2+}Fe_2^{3+}O_4$). Ferrous monoxide form is predominant in all samples (FeO = 4.2-8.4%), while ferrous oxide is also present in quantity (Fe_2O_3= 3.0-5.9% of iron) [13].

As, Br, Nd, Rb, Sb, U were also determined in all bacteria (**Fig. 5**). These non-essential elements have no beneficial function and have to be considered by cells as toxins, however their behavior illustrates that the permeability of bacterial cell wall changed after treatment with chromium.

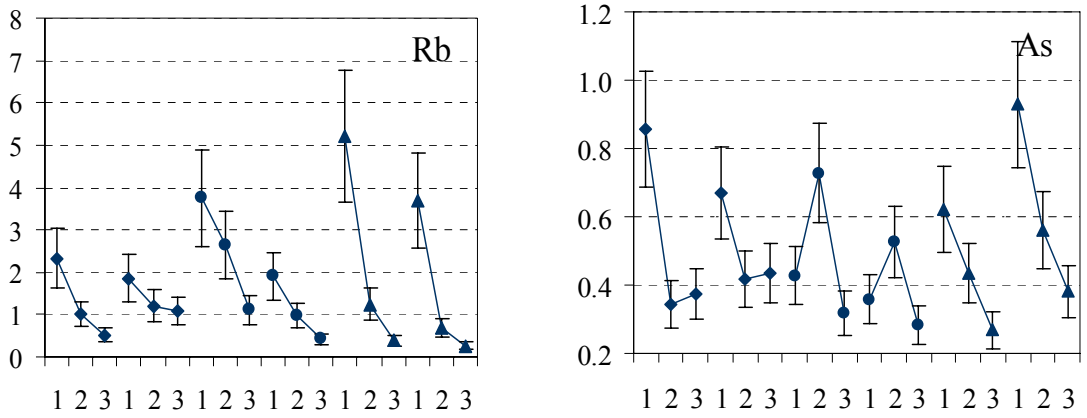

Fig.5. Concentration of As and Rb (*μg/g*) in different species of *Arthrobacter* under different Cr(VI) loadings

Conclusions

- By application of INAA and ESR spectrometry the behavior of chromium in basalt-inhabiting bacteria of *Arthrobacter* genera exposed to high concentrations of Cr(VI) was studied. It was shown that the tested bacteria of *Arthrobacter* genera can efficiently detoxify high concentrations of Cr(VI).
- The concentrations of 12−19 elements were determined in each bacterium simultaneously. The concentration range was over 8 orders of magnitude, from major- to ultra trace elements. Some similarity in the elemental composition of bacteria was observed.
- In all bacteria, potassium and sodium were the dominant elements. The concentrations of both Na and K were in the range of 10^5*μ*g/g. In the tested bacteria the concentrations of the other elements were much less.
- The relatively high contents of Fe detected in bacteria indicate bacterial adaptation to the environmental conditions typical for basalts.
- Elemental analysis of these bacteria also revealed that basalt-inhabiting bacteria are distinguished by relative contents of essential metals such as Na, K, Fe, Zn, Co.

References

[1]. Cary, E. E. Chromium in air, soils and natural waters, in Biological and Environmental Aspects of Chromium, S. LANGARD (Ed.), Elsevier, Amsterdam, the Netherlands, 1989.
[2]. Langard, S. The carcinogenicity of chromium compound in men and animals, in: Chromium Metabolism and Toxicity, S. Borrow (Ed.), CRS Press, 1983.
[3]. Deflora, S.; Wetterhahn, K. E. Life Chem. Rep., 7 (1989) 169.
[4]. Codd, R.; Dillon, C. T.; Levina A.; Lay, P. A. Coord. Chem. Rev., 216.217 (2001) 537.
[5]. Appenroth, K. Y.; Bischoff, M.; Gabrys, H.; Stoeckel, J.; Swartz, H. M.; Walczak, T.; Winnefeld, K. J. Inorg. Biochem., 78 (2000) 235.
[6]. Liu, K. J.; Jiang, J. J.; Shi, X. Biochem. Biophys. Res. Commun., 206 (1995) 829.
[7]. Lloyd, J. R. *Microbiology Today*. 2002, V. 29, p. 67.
[8]. Rudic V.; Dencicov L. Microbiologie genetrală, manulal pentru studenții ciclului universitar, Centrul editorial USM, 2002.
[9]. Ostrovnaya, T. M.; Nefedyeva, L. S.; Nazarov, V. M.; Borzakov, S. B.; Strelkova, L. P. Proceedings, Activation Analysis in Environment Protection, Dubna, 1993; p 319, preprint D-14-93-325

[10]. Kalabegishvili, T.; Tsibakhashvili, N.; Holman, H.-Y. *Environ. Sci. Technol.* 2003, *37*, 4678-4684.
[11]. Hoghes M. N.; Peele R. K. Metals and Microorganisms, Chapman and Hall, 1989.
[12]. Dmytrenko G.M.; Ereshko T.V.; Konovalova V.V. Reduction of Chromium (VI) by bacteria collection strains of different physiological groups, Microbiology, 6 .2007, 125-130
[13]. Tsibakhashvili N.; Frontasyeva M. V.; Kirkesali E.; Aksenova N.; Kalabegishvili L.; Mosulishvili L.; Tsertsvadze T.; Holman H-Y. Epithermal neutron activation analysis of Cr(VI)-reducer basalt-inhibiting bacteri, Jornal of analytical chemistry, 2005, vol.53.

(-)-DRIMENOL – A VALUABLE STARTING COMPOUND FOR THE SYNTHESIS OF DRIMANIC SESQUITERPENOIDS

Aculina Aricu

Institute of Chemistry of the Academy of Sciences of Moldova, Chişinău,
MD-2028, 3 Academiei str., Republic of Moldova
Tel: +7 (373 2) 739963; Fax: +7 (373 2) 739775;. E-mail: aricu_aculina@yahoo.com

Abstract: (-)-Drimenol is a relatively accessible compound, that has been and may be further used as a starting material to prepare sesquiterpenoids. The present review deals with the methods of obtaining of this compound as well as its usage.

Keywords: drimenol**,** albicanol, drimenyl acetate, polygodial, warburganal, synthesis.

1. Introduction

Drimenol (1) is a very important reprezentative of drimanic sesquiterpenoids. This terpenol served as a starting compound in the synthesis of diverse natural drimanes [1-5]. According to [1], drimenol (1) has the plant growth regulatory activity comparable with that of heteroauxin.

Besides the South American tree *Drimys winteri*, drimenol (1) was also found in many other natural sources [1,2]. It has been isolated from some species of the plants of the *Warburgia* [6] and *Porella* [7] families, from *Polygonum hydropiper* [8], *Ferula ceratophylla* [9] and fungi [10].

The importance of drimenol (1) as a starting compound for the synthesis of drimanic compounds, on the one hand, and the fact that its contents in natural sources is relatively low, on the other hand, have stimulated studies of its synthesis.

In this comunication, the methods of drimenol (1) preparation and the syntheses elaborated on its basis are discussed.

2. Synthesis of (-)-drimenol and its acetate

One of the first syntheses of drimenol (1) was accomplished by Wenkert and Strike [11] from dehydroabietic and podocarpic derivatives of type (2) obtained from resin acids. Because of its complexity and a great number of steps (~ 25), it is not of practical importance.

Pelletier et al. [12] carried out the drimenol (1) synthesis from ambreinolide (3) - the product obtained from a series of available labdanoids [13] (Scheme 1). Dehydrogenation of the ambreinolide (3) with 2,3-dichloro-5,6-dicyano-1,4-benzoquinone (DDQ) led to Δ^{12}-dehydroambreinolide (4), whose ozonolysis, followed by reduction of the resulting products with Red-Al, gave (+)-drimane-8α,11-diol (5). Its monoacetate (6) on successive dehydration with $POCl_3$, and saponification gave the mixture of alcohols (1) and (7) separated by column chromatography on silica gel. The total yield of drimenol (1) in this seven-step synthesis was about 13%.

Scheme 1

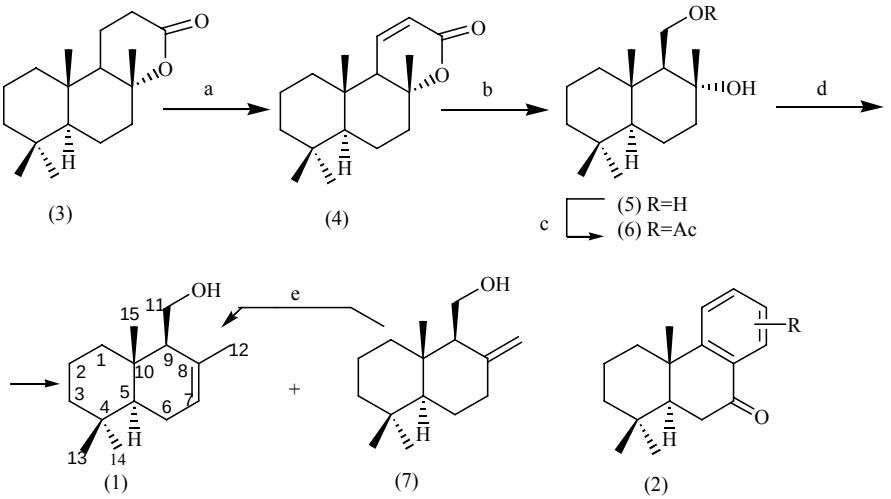

a) DDQ, dioxane, Δ, 40%; b) O_3, CH_2Cl_2, -70°C; Red-Al, C_6H_6, 85%; c) Ac_2O, Py, 92%; d) $POCl_3$, Py; KOH, MeOH, 53%; e) $BF_3 \cdot Et_2O$, CH_2Cl_2, 93%.

It is necessary to mention that authors [14] showed that albicanol (7) isomerizes into drimenol (1) in high yield (93%) on treatment with boron trifluoride etherate.

Scheme 2

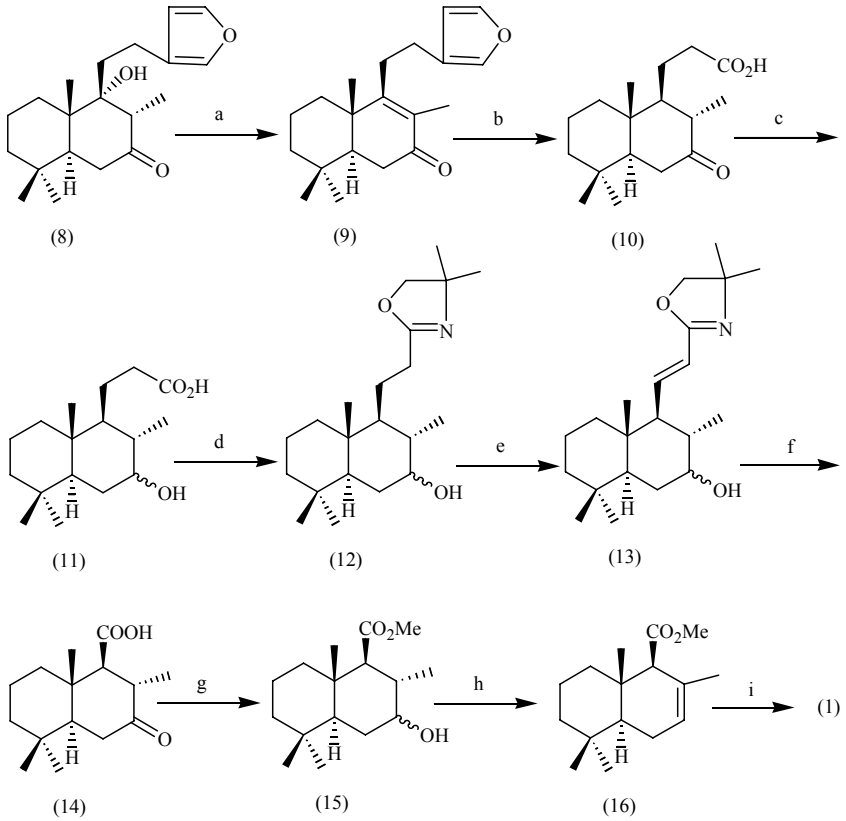

a) $SOCl_2$, Py, 95%; b) $Na_2S_2O_4$, PTC; O_3, CH_2Cl_2, MeOH; H_2O_2, NaOH, 80%; c) $NaBH_4$, MeOH, 95%; d) $(CH_3)_2C(NH_2)CH_2OH$, H_3BO_3, 85%; e) PhSeOH, H_2O_2, 80%; f) O_3, CH_2Cl_2, MeOH; CrO_3, H_2SO_4, 75%; g) $NaBH_4$, MeOH; CH_2N_2; h) HMPA, Δ; i) $LiAlH_4$, THF, 80%.

Drimenol (1) was also synthesized from the available labdanoid gispanolone (8) [15] (Scheme 2). The latter was dehydrated into the unsaturated ketone (9), the conjugated double bond of which was reduced, and the resulting product was ozonolyzed giving the keto acid (10). Its reduction with $NaBH_4$ led to a mixture of epimeric hydroxy acids (11) which on interaction with 2-amino-2-methylpropanol-1 afforded a mixture of 4,5-dihydrooxazols (12). This mixture was dehydrogenated with phenyl seleninic acid into a mixture of compounds (13), converted into the keto acid (14) by ozonization and subsequent oxidation of the ozonolysis product by the Jones reagent. Reduction of this keto acid with $NaBH_4$, followed by methylation with CH_2N_2, afforded the hydroxy ester (15). On its heating with HMPA the drimic acid ester (16) has been obtained. Its reduction with $LiAlH_4$ led to drimenol (1). This synthesis of drimenol (1) includes 11 steps, the overall yield being 8%.

Synthesis of drimenol (1) from larixol (17) has been recently described in [16] (Scheme 3). The exocyclic double bond of larixol has been selectively epoxidized with oxone. The obtained epoxy diol (18) was then reduced into triol (19), whose C-6 hydroxy group was selectively acetylated and the resulting compound was cleaved with OsO_4-$NaIO_4$ into the diacetoxy aldehyde (20). This compound was converted into the mixture of the silyl enol eters (21), ozonolysis of which resulted the diacetoxy aldehyde (22). On subsequent heating, compound (22) eliminated acetic acid affording the diene aldehyde (23). Reduction of (23) with $NaBH_4$ gives drimenol (1) as a result of selective 1,4-addition. The overall yield of this eight-step synthesis made up 32.5%.

A short synthesis of the drimenyl acetate (27) was elaborated by Barrero et al. [17] from the sclareol (24) (Scheme 4). Oxidative cleavage of the sclareol (24) side chain by osmic acid and sodium periodate led to the acetoxy aldehyde (25), whose enol silylation gave a mixture of the acetoxy silyl esters (26). On its ozonolysis, followed by reduction of the ozonolysis products with $NaBH_4$, the 11-monoacetate of drimanediol (6) has been formed. On its interaction with $SnCl_4$ the drimenyl acetate (27) was obtained in low yield. The total yield of the desired product in this four-step synthesis was about 17%.

Scheme 3

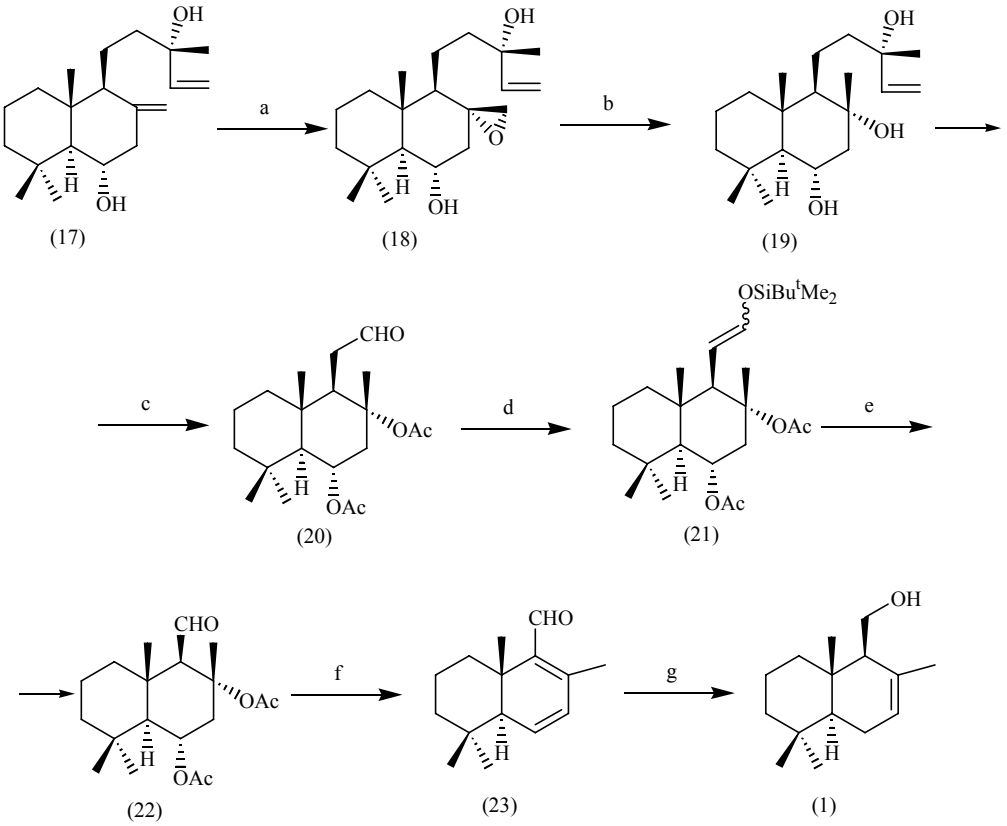

a) oxone, CH_2Cl_2, acetone, H_2O, $NaHCO_3$, 18-crown-6, 81%; b) $LiAlH_4$, THF, 94%;
c) Ac_2O, Py, 99%; OsO_4, $NaIO_4$, THF, H_2O, 84%; d) Bu^tMe_2SiCl, NaH, THF, 96%;
e) O_3, CH_2Cl_2, MeOH, -78^{o}C, Me_2S, 78%; f) collidine, 200^{o}C, 77%; g) $NaBH_4$, EtOH, 0^{o}C, 89%.

Scheme 4

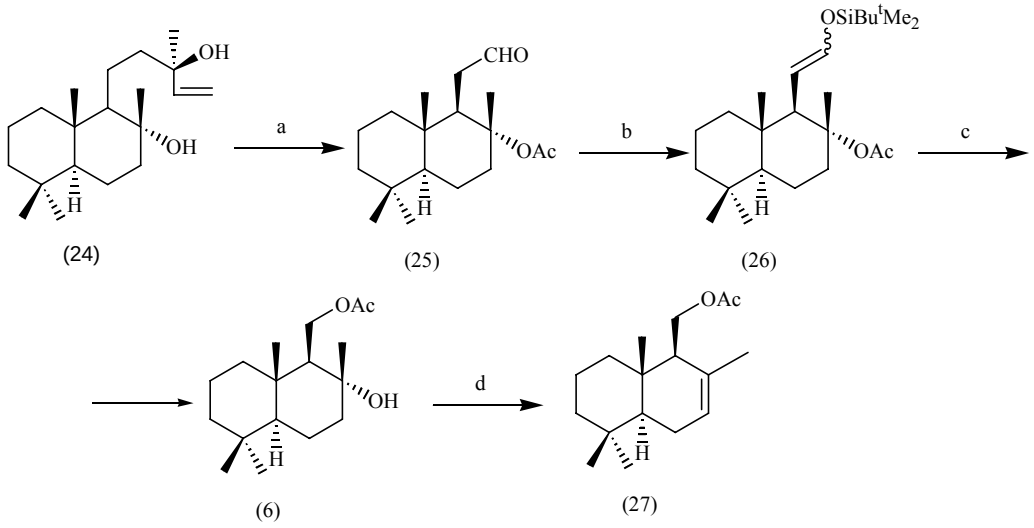

a) OsO_4, $NaIO_4$,, 73%; b) Bu^tMe_2SiCl, NaH, 99%; c) O_3, CH_2Cl_2, MeOH, -78^{o}C; $NaBH_4$, MeOH, 95%;
d) $SnCl_4$, CH_2Cl_2, 25%.

The authors [18] accomplished the drimenol (1) synthesis from sclareol (24) (Scheme 5). This was the first synthesis of a drimanic sesquiterpenoid from a labdanic diterpenoid. This synthesis that correlated these two groups of terpenic compounds firmly confirmed the stereochemistry of drimenol (1).

Scheme 5

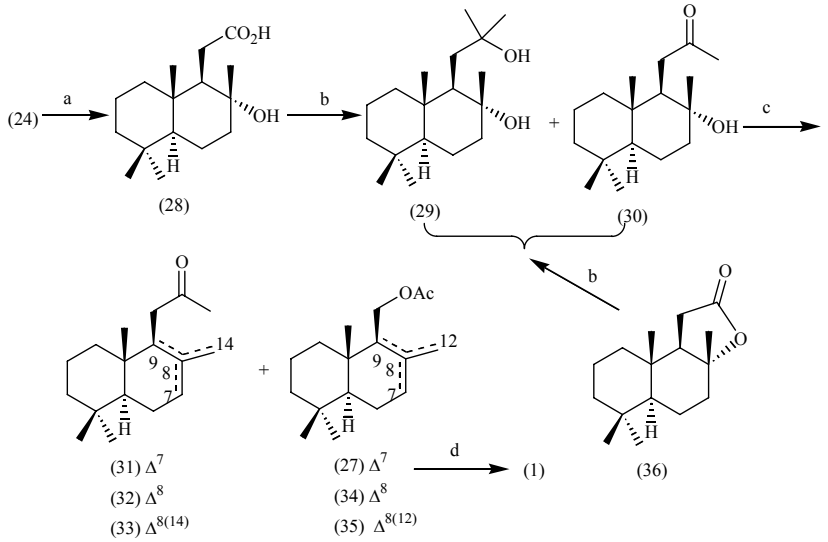

a) $KMnO_4$, AcOH, H_2O; KOH, MEOH, Δ; H_2SO_4, 92%; b) CH_3Li, Et_2O, 80%;
c) H_2O_2, $BF_3 \cdot Et_2O$; d) KOH, EtOH, Δ., 100%.

Sclareol (24) was oxidized according to the method [19] and the obtained hydroxy acid (28) was introduced in the reaction with methyl lithium. The reaction product was a mixture of the ditertial diol (29) (18%) and of the hydroxy ketone (30) (80%). The latter, on interaction with a mixture of concentrated (93.6%) hydrogen peroxide and boron trifluoride etherate, afforded a mixture of the unsaturated ketones (31)-(33) and of the isomeric acetoxy drimenes (27), (34) and (35). All these substances were separated and isolated in individual form by column chromatography on $SiO_2 \cdot AgNO_3$ and characterized. On saponification of acetate (27), drimenol (1) was obtained. Later it was established [20] that in the reaction with methyl lithium it is possible to use the commercially available norambreinolide (36), a common cleavage product of many labdane diterpenoids. In this case the yield of the hydroxy ketone (30) is a little lower (65%), but this reaction is more convenient to carry out. The total yield of drimenol (1) in this synthesis is small (6.5%).

It is necessary to note that later on an alternative, shorter synthesis of the hydroxy keton (30) from sclareol (24) was elaborated [21] (Scheme 6). On the ozonolysis of sclareol (24) and subsequent treatment of the ozonolysis products with ammonium chloride, the dimeric product (37) was formed [22]. Its further ozonolysis gave the β-diketone (38).

Scheme 6

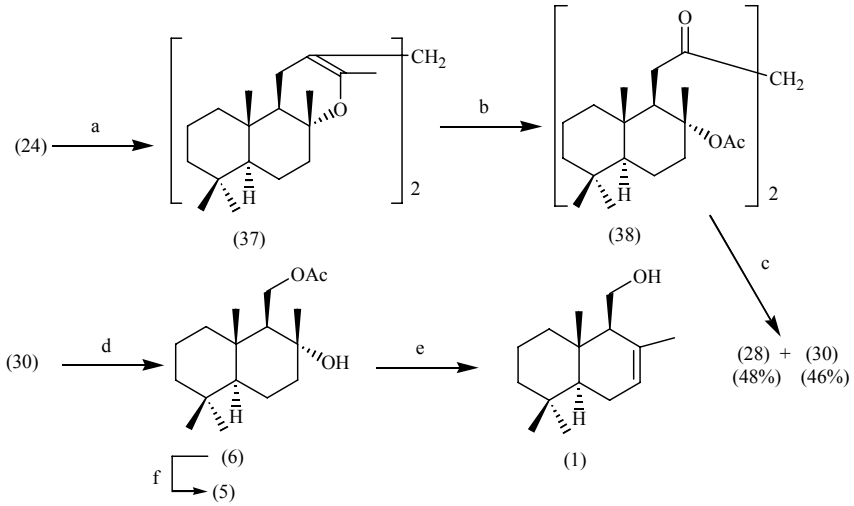

a) O_3, MeOH, 5-10°C; NH_4Cl, 80%; b) O_3, hexane, -65…-70°C; H_2O, Δ , 100%; c) NaOH, EtOH, Δ;
d) H_2O_2, CH_2Cl_2, $(CF_3CO)_2O/NaHCO_3$ (1:1), 100%; e) H_2SO_4, EtOH, r.t., 56%; f) KOH, MeOH, 98%.

On the treatment of β-diketone (38) with an alkaline base, the (1:1) mixture of the hydroxy acid (28) and the hydroxy ketone (30) was formed. As a result, this three-step synthesis led to the hydroxy ketone (30) in 37% overall yield. Furthermore, the hydroxy acid (28) can be converted into (30) as is indicated in scheme 5.

Scheme 7

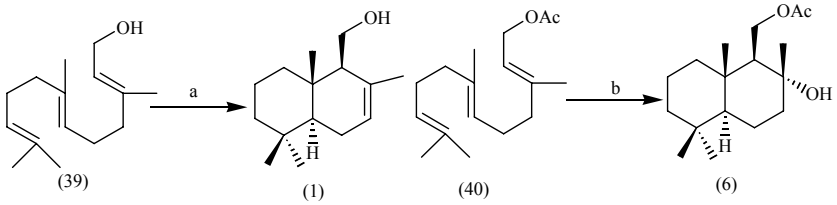

a) 1 mmole FSO_3H, $C_3H_7NO_2$, -80…-85°C, 1 h, 71%; b) 10 mmole FSO_3H, -80…-85°C, 5 min, 77%.

The authors [23] elaborated a highly efficient method for the synthesis of the racemic drimenol (1) and of the hydroxy acetate (6) by the superacidic, low temperature cyclization of *E,E*-farnesol (39) and its acetate (40), respectively (Scheme 7).

We have investigated the dehydration reaction of monoacetate (6) when treated with a series of dehydrating agents: oxalil chloride in DMSO, TsOH, iodine, oxalic acid, $POCl_3$ [24], $Sc(OTf)_3$, $CF_3SO_3SiMe_3$, PCl_5, amberlyst-15, $CH_3SO_3SiMe_3$ [25]. Besides, hydroxy acetate (6) was acetilated in diacetate (41), which was pyrolized on heating in the prezence of SiO_2 in hexane or in DMSO [26]. In all cases, the reaction afforded mixtures of acetates (27), (34), and (35), which could not be separated by chromatography. Besides these acetates, the drim-7,9(11)-diene (42) was formed as a secondary compound in many cases. On the treatment of the monoacetate (6) with $CF_3SO_3SiMe_3$ in CH_3CN or with amberlyst-15 in CH_2Cl_2 [25], the drim-7,9(11)-diene (42) became the only product of this reaction (Scheme 8). The same results were obtained by the authors [24] and [27].

A good selectivity of the dehydration reaction was reached on the interaction of hydroxy acetate (6) with an excess of $CH_3SO_3SiMe_3$ in CH_3CN: the yields of drimenil acetate (27) and of diene (42) were 65 and 14%, respectively [25]. This method for the synthesis of drimenil acetate (27) was patented [26]. In most reactions of the hydroxy acetate (6) dehydration, the drimenol acetate (27) dominates.

Scheme 8

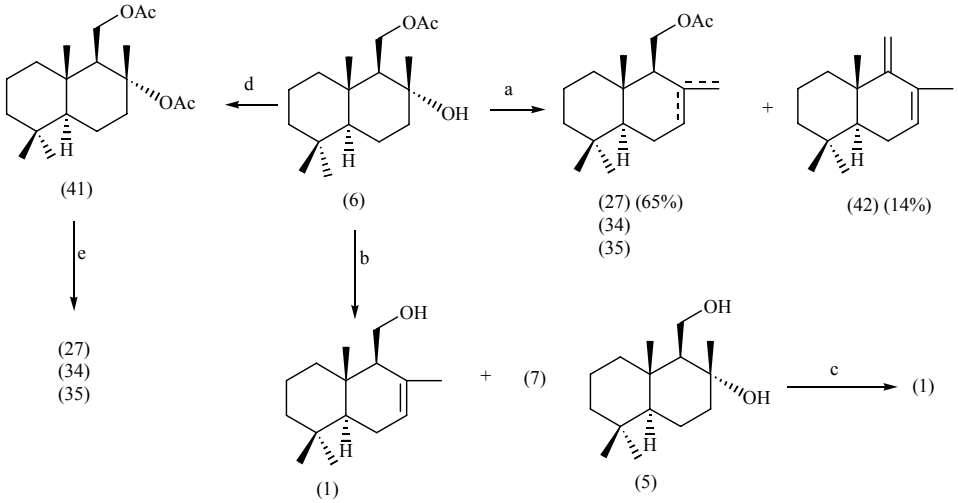

a) $CH_3SO_3SiMe_3$, CH_3CN, 65%; b) H_2SO_4, EtOH, 60%; c) DEAD, PPh_3, 92%; d) AcCl, $C_6H_5NMe_2$; e) DMSO, $NaHCO_3$, Δ, 77%.

We have proposed a simple and efficient method for the transformation of monoacetate (6) into the desired drimenol (1) [25]. It was found that treatment of monoacetate (6) with an ethanolic solution of H_2SO_4 under mild conditions induced the dehydration accompanied by deacetylation to give a crystalline product that was a mixture of drimenol (1) and albicanol (7) at 10 : 1 ratio formed in a (60%) overall yield. Recrystallization of this mixture from hexane gave pure drimenol (1) (56%) [28].

It should be mentioned that recently Spanish chemists [29] have synthesized drimenol (1) in a high yield (92%) on the treatment of driman-8α,11-diol (5) with dietilazadecarboxilat (DEAD) and trifenil phosphine in C_6H_6 (Scheme 8).

3. The synthesis of drimanic sesquiterpenoids on the basis of drimenol (1)

3.1. The synthesis of the drimanic aldehydes

The synthesis of the drimane dialdehyde polygodial (43) was carried out starting with drimenol (1) (Scheme 9). According to [30], drimenol (1) was oxidized into drimenal (44), the aldehyde group of which was protected and compound (45) was oxidized into aldehyde (46) with selenium dioxide. The treatment of aldehyde (46) with p-toluene sulfonic acid gave the target polygodial (43) (30% overall yield), isolated earlier from some plants and marine organisms [1, 2].

According to the synthesis [31], drimenol (1) was acetylated and its acetate (27) was oxidized with selenium dioxide into the hydroxy acetates (47) in a 45% yield. If the oxidation of drimenyl acetate was carried out with a catalytic amount of SeO_2 in the presence of bis(4- metoxifenol) selenoxide as a co-oxidant gives, apart from compound (47) (60%), a small amount of 11-acetoxydrim-7-en-12-ol (48) (30%) .

Saponification of the latter gave diol (49) which was oxidized by the Swern reagent into polygodial (43) in high yield.

The particular interest of researchers in polygodial can be explained by its various biological activities: anti-feedant [32, 33], antibacterial [7, 34], cytotoxic [7, 35], allergenic [7], piscicidal, molluscicidal, anticomplemental, and plant-growth regulatory [1, 2].

Scheme 9

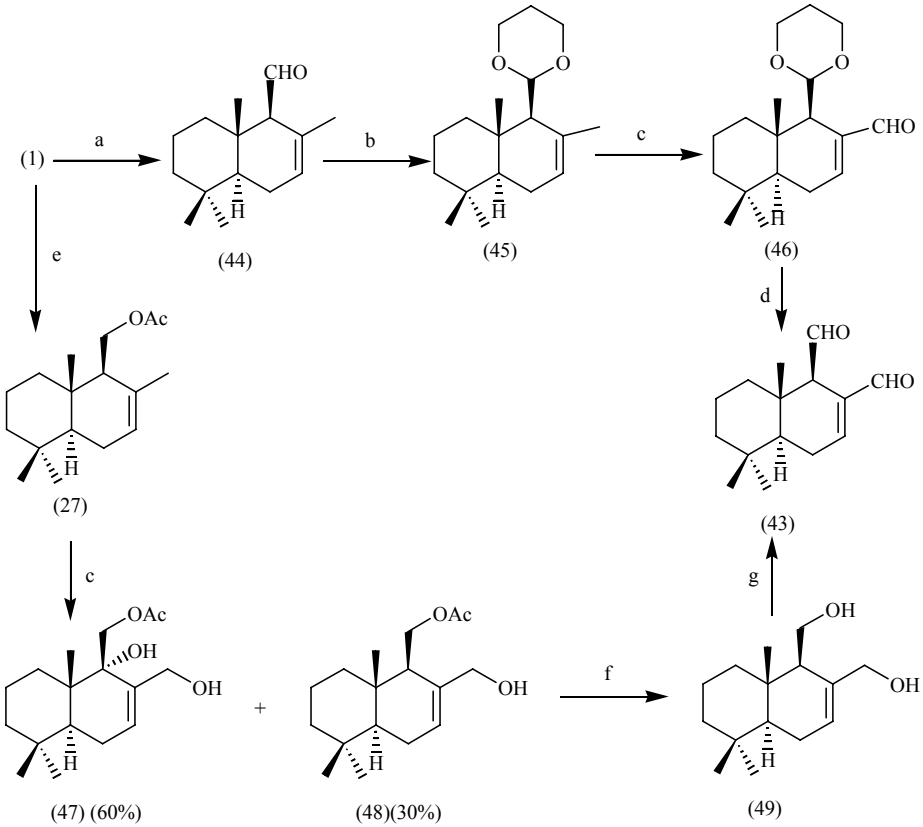

a) PCC, CH_2Cl_2,75%; b) $CH(CH_2OH)_2$, H^+, 88%; c) SeO_2 (cat), $(p\text{-}MeOC_6H_4)_2SeO$, 45%;
d) TsOH, acetone, 100%; e) Ac_2O, Py, 98%; f) K_2CO_3, MeOH, 100%; g) $(COCl)_2$, DMSO, 98%.

The hydroxy acetate (47) has been used as a starting compound for the synthesis of another drimanic dialdehyde, warburganal (50), that is similar to polygodial (43) in the variety and level of biological activities [36] (Scheme 10).

Scheme 10

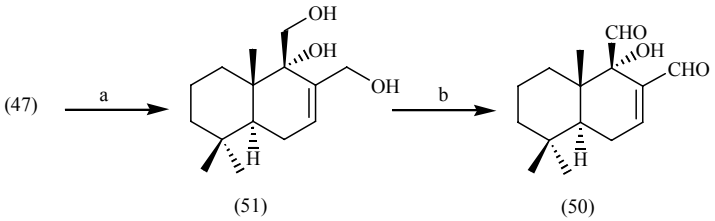

a) KOH, MeOH, 100%; b) DMSO, $(CF_3CO)_2O$, 64%.

Compound (47) was saponified into triol (51) which, on oxidation with DMSO and $(CF_3CO)_2O$, gave the final product (50) in high yield.

Cinnamodial (52) was obtained from drimenol (1) in 13 steps in 10% overall yield. The diol (59) was synthesized from drimenol (1) according to the method [37], and further synthesis was continued as described in [38] (Scheme 11). Its acetate (60) has been successively subjected to oxidation with selenium reagents and to selective saponification giving acetoxy triol (62) that oxidizes with Swern's reagent into cinnamodial (52).

Scheme 11

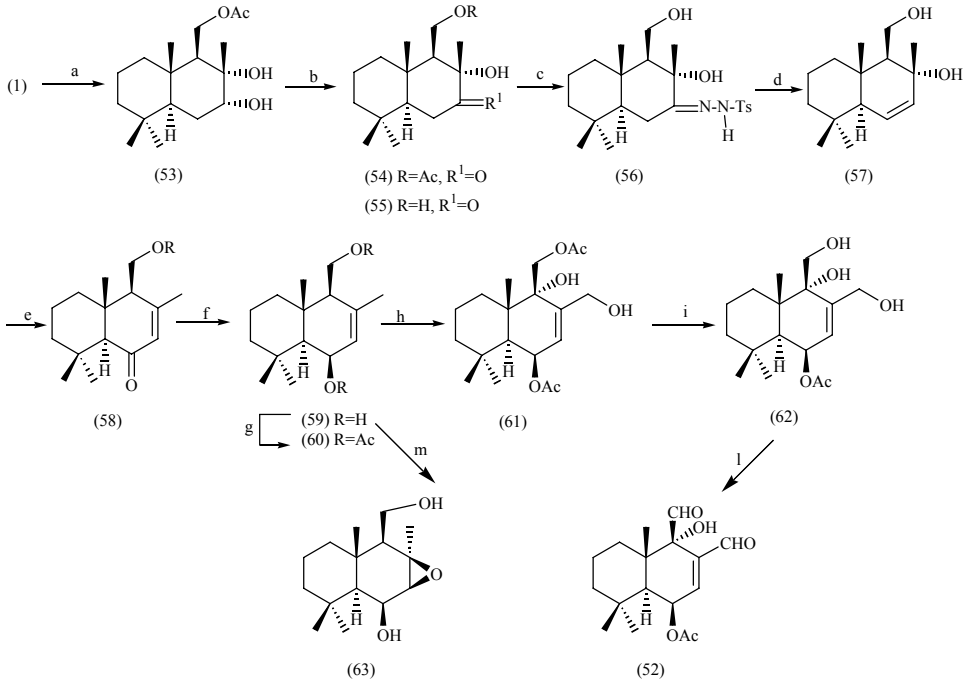

a) Ac_2O/Py; OsO_4, NMO, 56%; b) NBS,CH_2Cl_2; KOH, MeOH, 90%; c) $TsNHNH_2$, $BF_3{\cdot}Et_2O$, C_6H_6;
d) BuLi, THF, 91%; e) Ac_2O, Py; PCC; f) DIBAL, THF;, 100%; g) Ac_2O, Py, DMAP;
h) SeO_2 (cat), $(p\text{-}MeOC_6H_4)_2SeO$, dioxane; i) K_2CO_3, MeOH; l) $(COCl)_2$, DMSO; m) m-CPBA, CH_2Cl_2, 95%.

Drimenol (1) has been also used as a starting material for the preparation of uvidin C (63), metabolite of fungi *Lactarius uvidus Fries* [39]. By acetylation and dihydroxylation of drimenol (1), compound (53) was obtained in an overall yield of 56%. Oxidation of (53) with N-bromosuccinimide afforded ketol (54) in good yield. Saponification of (54) followed by treatment of the resulting diol (55) with tosylhydrazide gave compound (56). Tosyl hydrazone (56) was converted to the allylic alcohol (57) in 91% yield. Acetylation of (57) and subsequent oxidative rearrangement with pyridinium chlorocromate gave enone (58). Reduction of (58) with DIBAL afforded the allylic alcohol (59) in quantitative yield. The treatment of (59) with m-chloroperbenzoic acid afforded uvidin C (63) in 95% yield.

3.2. The synthesis of drimanic ketones

Starting from drimenol (1), Swedish chemists [40] accomplished the synthesis of drim-8-en-7-one (64), thus confirming its structure and stereochemistry (Scheme 12). 7α,8-Epoxidriman-11-ol (65), preparation by epoxidation of drimenyl acetate, was converted in good yield to drim-8-en-7α-11-diol (68) in three steps. These were performed *in situ* and involved oxidation to the epoxyaldehide (66) followed by base-catalyzed isomerization to the conjugated aldehyde (67). Acetylation of the diol (68) at low temperature furnished 11-acetoxydrim-8-en-7α-ol (69) as the major product which on oxidation with the Jones reagent yielded keto ester (70). Hydrogenolysis of the conjugated keto ester (70) applying zinc in acetic acid gave drim-8-en-7-one (64) in excellent yield.

Schema 12

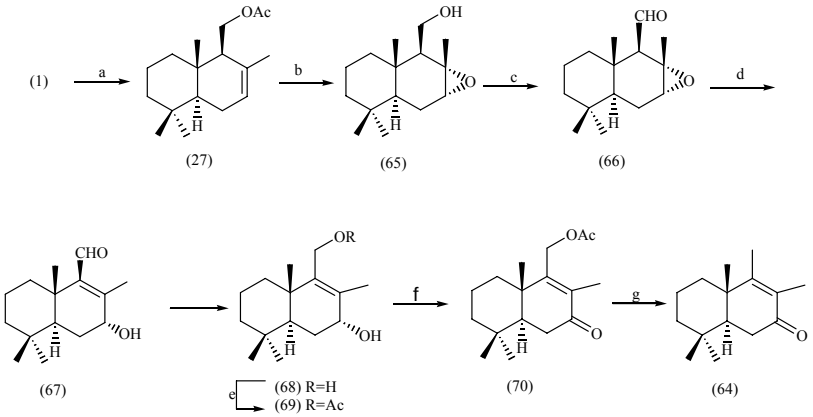

a) Ac_2O, Py, 100% ; b) m-CPBA, CH_2Cl_2; KOH, MeOH, 80%; c) CrO_3, Et_2O, 100%;
d) KOH, MeOH; $NaBH_4$, MeOH, 82%; e) Ac_2O, Py; f) Jones reagent, 78%; g) Zn, AcOH, 100%.

3.3. The synthesis of the drimanic alcohols

We studied the reaction of drimenol (1) with SeO_2 in order to perform further functionalization of compound (1) [24]. Refluxing of alcohol (1) with SeO_2 in ethanol gives known diols (71) and (49) and the new compound (72) (Scheme13), the structure of which was established based on the spectral data. Under the optimal conditions, the yield of the reaction products (71) and (49) was 44 and 8%, respectively. It should be mentioned that diols (71) and (49) are the known precursors of biologically active drimanes, warburganal (50) and poligodial (43) [2, 4, 41, 42, 43] – natural compounds possessing a wide range of biological activities, and of other natural drimanes [44].

Schema 13

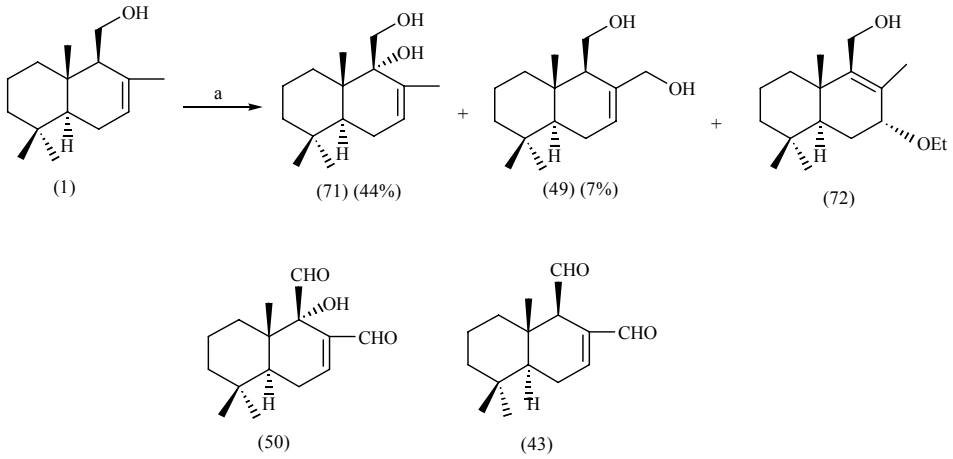

a) SeO_2, EtOH, Δ;

The (-)-ent-drim-9(11)-en 8α-ol (73) and its dextrorotatory C(8)- epimer (74) [45] (Scheme14) were isolated from the culture filtrate of the fungi *Aspergillus oryzae* used in breadmaking and in the production of some beverages in Japan.The structure of these drimanic compounds was confirmed on the basis of the spectral data and synthesis of racemic alcohols. But its stereochemistry remains unknown.

To determine the absolute configuration of compounds (73) and (74), we [46] carried out the stereoselective synthesis of compound (75) from sclareol (24) (Scheme 14). Sclareol (24) was transformed in its diacetate (76). A detailed investigation of its reactions with different oxidants was carried out [46]. However, either the reaction did not occur or the yeld of the expected product (77) was low (25%). A reasonable yield of acetoxy ketone (77) (52%) was obtained on decomposition of the ozonolysis products of sclareol diacetate (76) on heating with $Cu(OAc)_2 \cdot H_2O$ in toluene.

To prepare 8α-acetoxydrim-9(11)-ene (75), acetoxy ketone (77) was subjected to photolytic cleavage according to the Norrish II reaction. The reaction product was saponified giving the dextrorotatory compound (75). This result proves that the natural products (73) and (74) belong to the enantiomeric series (Scheme14). It should be noted that this reaction has also been studied by Spanish chemists [47], and drim-7,9(11)-diene (42) has been isolated as the only reaction product. This result was difficult to explain and we suggested that the primary reaction product, unsaturated acetate (78), decomposes during chromatography on SiO_2.

Schema 14

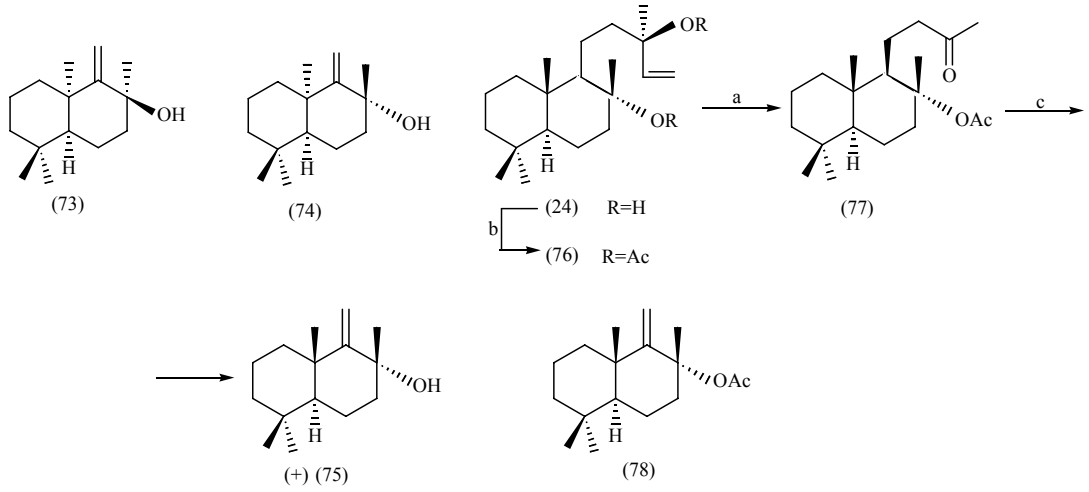

a) 1. O_3, 2. $Cu(OAc)_2 \cdot H_2O$, 52%; b) AcCl, $C_6H_5NMe_2$, 80%; c) 1. hν/hexan, 2. KOH/EtOH, 44%.

Later on, we elaborated an alternative route for preparation of drim-9(11)-en-8α-ol (75) and its epimer (79) starting from drimenol (1) [48].

Oxidation of drimenol (1) by the Swern reagent or DMSO and P_2O_5 produced the known aldehyde drimenal (43) in yields of 94 and 95%, respectively. We note that the method using P_2O_5 is more convenient because the reaction occurs at ambient temperature whereas oxidation by Swern's reagent occurs at -60°C. Previously, drimenal (43) was prepared through oxidation of drimenol (1) by pyridinium chlorochromate (PCC) (75% yield) or CrO_3 in pyridine (30% yield). At the next step, compound (43) was isomerized into the known isodrimenal (80). Isodrimenal was reduced by $NaBH_4$ into isodrimenol (81). Reaction of alcohol (81) with *m*-chloroperbenzoic acid afforded a liquid mixture of the known 8,9α-(82) and 8,9β-(83)-epoxydriman-11-ols at a 3.4:1 ratio. The mixture of compounds (82) and (83) was used without separation in the next step. There reaction with *p*-tosyl chloride in Py gave the mixture of epoxy tosylates (84) and (85) in a good yield. Subsequent reaction of the mixture of (84) and (85), first on heating with KI in an acetone:DMF mixture, and then with Ph_3P, afforded a mixture of drim-9(11)-en-8α-ol (75) and drim-9(11)-en-8β-ol (79) at a 2.5:1 ratio and in 60% overall yield. The mixture was separated by chromatography. Compounds (75) and (79) were identified by comparing their physicochemical and spectral properties with the published data. Thus, drim-9(11)-en-8-ols (75) and (79) were synthesized from drimenol (1) in six steps in ~26% overall yield (Scheme 15).

Scheme 15

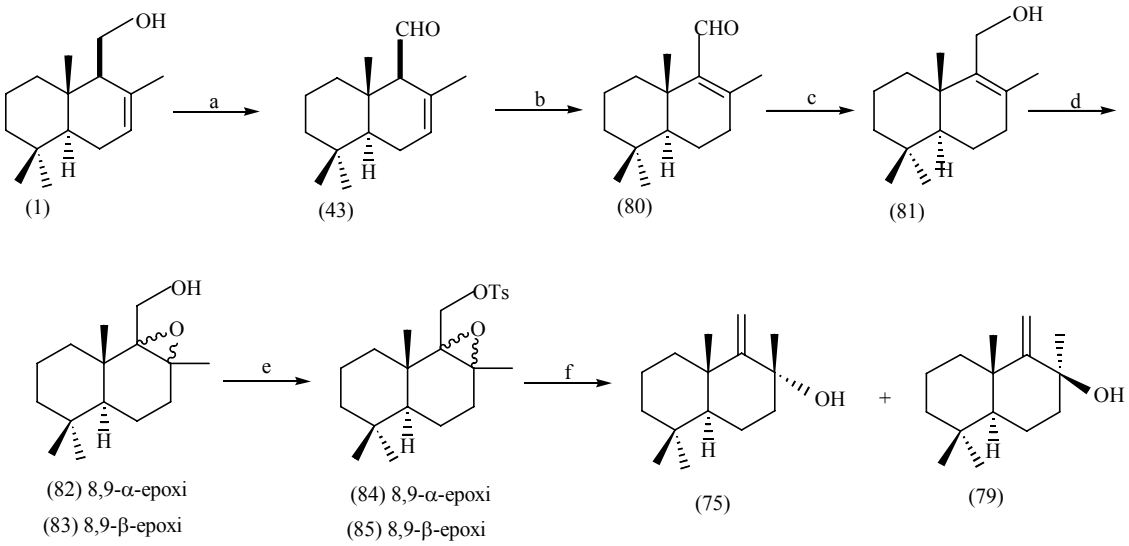

a) P_2O_5, DMSO, 95%; b) TsOH, C_6H_6, Δ, 82%;c) $NaBH_4$, EtOH, 75%; d) mCPBA, CH_2Cl_2, 95%; e) pTsCl, Py, 77%; f) 1.KI, DFA, 2. Ph_3H, 60%.

4. Conclusion

The data mentioned above demonstrated that drimenol (1) proves to be a valuable and convenient compound for the synthesis of various natural drimanes including those with biological activities.

5. References

[1]. Jansen, B. J. M.; de Groot, A. *Nat.Prod. Rep*., 1991, 8, Nr. 3, 309-318.
[2]. Jansen, B. J. M.; De Groot, A. *Nat. Prod. Rep*., 2004, 21, Nr. 4, 449-477.
[3]. Jansen, B. J. M.; de Groot, A. *Nat. Prod. Rep.,* 1991, 8, Nr. 3, 319-337.
[4]. Влад, П. Ф.; Колца, М. Н.; Миронов, Г. Н. *Изв. АН, сер. хим*., 1997, 46, № 5, 896-913.
[5]. Vlad, P.F. *In Studies in Natural Products Chemistry, Bioactive Natural Products* (Part M), Atta-ur Rahman /Editor, Elsevier, Amsterdam, 2006, 33, 393-432.
[6]. Brooks, C .J .W; Draffan, G. H. *Tetrahedron*, 1969, 25, 2865-2885; Kioy, D.; Gray, A. I.; Waterman, P. G. *Phytochemistry,* 1990, 29*,* 3535-3538.
[7]. Asakawa, Y.; Toyota, M; Takemoto, T. *Phytochemistry,* 1978, 17, 457-460.
[8]. Fukuyama, Y.; Sato, T.; Asakawa, Y.; Takemoto, T. *Phytochemistry,* 1982*,* 21, 2895-2898.
[9]. Dembitskii, A. D.; Crotova, G. I.; Zamcova, V. V. *Izv. Acad. Nauk Kaz. SSR,* ser. khim., 1991, *№ 6,* 63-65.; Fraga, B. M. *Natur. Prod. Rep., 1*995, 12, 303-321.
[10]. De Bernardi, M.; Mellerio, G.; Vidari, G.; Vita-Finzi, P. *J. Chem. Soc., Perkin Trans. 1,* 1980, 221-226.

[11]. Wenkert, E.; Strike, D. P. *J.Am. Chem. Soc.,* 1964, 86, 2044-2050.
[12]. Pelletier, S.W.; Lajsic, S.; Ohtsuka, Y.; Djarmati, Z. *J. Org. Chem.,* 1975, 40, 1607-1609.
[13]. Vlad, P. F.; Koltsa, M. N. *Synthesis and Application of Odorous Compounds from Labdane Diterpenoids,* Kishinev, Shtiintsa, 1988 (in Russian).
[14]. Akita, H.; Nozawa, M.; Mitsuda, A.; Ohsawa, H. *Tetrahedron Asymmetry,* 2000, 11, 1375-1388.
[15]. Hueso-Rodriguez, J. A.; Dominguez, G.; Rodriguez, B. *An. Quim., ser C,* 1988, 84, 215-218.
[16]. Lagnel, B. M. F.; Morin, C.; De Groot, A. *Synthesis,* 2000, 1907-1916.
[17]. Barrero, A. F.; Manzaneda, E. A.; Altarejos, J.; Salido, S; Ramos, J. M. *Tetrahedron Lett.,* 1994, 35, 2945-2948.
[18]. Vlad, P. F.; Kryshtal, G. V.; Lazurievskii, G. V. *Zh. Obshch. Khim*., 1967, 37, 2187-2190.
[19]. Schumacher, J. N. ; Henley, W. M.; Teague, C. E. *US Patent* 3050532.
[20]. Kuchkova, K. I.; Chumakov, Y. M.; Simonov, Y. A.; Bocelli, G.; Panasenco, A. A.; Vlad, P. F. *Synthesis,* 1997, 1045-1048.
[21]. Aricu, A. N.; Koltsa, M.N.; Vlad, P. F.; Kukovinets, O. S.; Odinokov, V. N.; Tolstikov, G. A. *Khim. Prirod. Soedin, (Chem. Nat. Comp.)*, 1991, 343-349.
[22]. Odinokov, V. N.; Vlad, P. F.; Kukovinets, O. S.; Isakova, L. A.; Lindeman, S. V.; Struchkov, Yu. T.; Tolstikov, G. A. *Dokl. Akad. Nauk SSSR,* 1983, 269*,* 853-855.
[23]. Vlad, P.F.; Ungur, N. D.; Perutsky, V. B. *Khim. Prirod. Soedin, (Chem. Nat. Comp.)*, 1986, 793; Vlad, P. F. *Pure Appl. Chem*., 1993, 65*,*1329-1336; Polovinca, M. P.; Korchagina, D.V.; Gatilov, Y. G.; Bagrianskaya, I. Y.; Barkhash, V. A.; Shcherbukhin, V. V.; Zefirov, N. S.; Perutskii, V. B.; Ungur, N. D.; Vlad, P. F. *J. Org. Chem.,* 1994, 59*,* 1509-1517; Vlad, P. F.; Ungur, N. D.; Hung, N. V.; Perutsky, V.B. *Russ. Chem. Bull. (Engl. Transl.),* 1995, 44, 2390-2403.
[24]. Кучкова, К. И.; Арыку, А. Н.; Драгалин, И. П.; Влад, П. Ф. *Изв. АН, сер. хим.,* 2004, № 12, 2745-2748.
[25]. Кучкова, К. И.; Арыку, А. Н.; Барба, А. Н.; Влад, П.Ф. *Химия природ. соедин*., 2007, №4, с. 340-343.
[26]. Vlad, P; Cucicova, C.; Arîcu, A.; Barba, A. *Brevet de invenţie a Republicii Moldova* Nr. 3273. Data publicării hotărârii de acordare a brevetului 31.03.2007, BOPI, 2007, Nr. 3.
[27]. Poigny, S.; Huor, T.; Guyot, M.; Samadi, M. *J. Org. Chem,* 1999, 64, 9318-9320.
[28]. Vlad, P.; Cucicova, C.; Arîcu, A. *Brevet de invenţie a Republicii Moldova* Nr. 2018. Data publicării hotărârii de acordare a brevetului 31.10.2002, BOPI, 2002, Nr. 10.
[29]. Alvarez-Manzaneda, E.J.; Chahboun, R.; Barranco Perez, I.; Cabrera, E.; Alvarez, E.; Alvarez-Manzaneda, R. *Organic Lett*., 2005, 7, Nr.8, 1477-1480.
[30]. Cortes, M.J.; Razmilic, I.; Sierra, J.R.; Lopez, J.; *Chem.Ind.,* 1985, 735.
[31]. Razmilic, J.; Lopez, J.; Sierra, J.; Cortes, M. *Synth. Commun.,* 1987, 17*,* 95-103.
[32]. Kubo, I.; Lee, Y. W.; Pettei, M.; Pilkiewicz, F.; Nakanishi, K. *J. Chem. Soc., Chem. Commun,* 1976, 1013-1014.
[33]. Caproli, V.; Cimino, G.; Colla, R.; Gavagnin, M.; Sodano, G.; Spinella, A. *J. Nat. Prod.,* 1987, 50, 146-151.
[34]. Paul, V. J.; Seo, Y.; Cho, K. W.; Rho, J. R.; Shin, J.; Bergguist, P. R. *J. Nat. Prod.,* 1997, 60, 1116-1120.
[35]. Banthorpe, D. V.; Brooks, C. J. W.; Brown, J. T.; Leppin, G. J.; Morris, G. S. *Phytochemistry,* 1989, 28, 1631-1633.
[36]. Oyarzum, M. L.; Cortes, M.; Sierra, J. *Synth. Commun.,* 1982, 12, 951-958.
[37]. Lopez, J.; Sierra, J.; Cortes, M. C*hem. Lett.,* 1986, 2073-2074.
[38]. Cortes, M.; Razmilic, I.; Lopez, J. *J. Nat. Prod*., 1990, 53, 1369-1371.
[39]. De Bernardi, M.; Mellerio, G.; Vidari, G.; Vita-Finzi, P. *J. Chem. Soc., Perkin Trans. 1*, 1983, 2739-2743.
[40]. Aasen, A. J.; Vogt, C. H. G.; Enzell, C. R. *Acta Chem. Scand.,* 1975*,* B29*,* 51-55.
[41]. Barrero, A. F.; Cortes, M.; Marzaneda, E. A.; Cabrera, E.; Chahboun, R.; Lara, M.; Rivas, A. R. *J. Nat. Prod*., 1999, 62, Nr.11, 1488-1491.
[42]. Urones, J. G.; Marcos, J. S.; Perez, B. G.; Diez, D.; Lithgow, A. M.; Gomes, P. M.; Basabe, P.; Garrido, N.M. *Tetrahedron*, 1994, 50, Nr. 37, 10995 – 11012.
[43]. Razmilic, I.; Lopez, J.; Sierra, J.; Cortés, M. *Synth. Commun*, 1987, 17, 95-103.
[44]. Hollinshead, D.M.; Howell, S.C.; Ley, S.V.; Mahon, M.; Ratcligffe, N.M.; Worthington, P.A. *J. Chem. Soc., Perkin. Trans. I,* 1983, 1579 – 1589.
[45]. Wada, K.; Tanaka, S.; Marubo, S. *Agric. Biol. Chem.,* 1983, 47, 1075 – 1078.
[46]. Влад, П. Ф.; Арыку, А. Н.; Чокырлан, А. Г. *Изв. АН, сер. хим*. 2003, № 2, 423-426.
[47]. Lithgow, A.M.; Marcos, J.S.; Basabe, P.; Sexmero, J.; Diez, D.; Gomez, A.; Estrella, A.; Urones, J. G. *Natur. Prod. Lett.,* 1995, 6, Nr.4, 291-294.
[48]. Кучкова, К.И.; Арыку, А.Н.; Драгалин, И.П.; Влад, П.Ф. *Химия природ. соед*., 2005, № 2, 152-155.

ADSORPTION WAVE OF VANADIUM COMPLEX WITH 2,3–DIHYDROXYBENZALDEHYDE

Ludmila Kiriyak[a], Natalia Cecoi[a], Tatiana Cazac[a]*, Mihail Revenco[b]*

[a] *Institute of Chemistry, Academy of Sciences of Moldova, MD-2028 Chisinau, 3 Academiei str., Republic of Moldova.*
[b] *State University of Moldova, MD-2009 Chisinau, A. Mateevici str., 60, Republic of Moldova.*
**E-mail: revenco@usm.md; phone 373-22-57-74-04*
cazac_t@yahoo.com;phone 373-22-73-97-81

Abstract: The polarographic behavior of the complex formed by V(V) and 2,3–dihydroxybenzaldehyde (2,3–DHBA) in the solution containing acetate buffer (pH 5,2) has been investigated. By means of a.c. polarography, chronovoltammetry and other techniques, it has been shown that the electrode process is complicated by the adsorption of 2,3-DHBA and its vanadium complex. The kinetic and adsorption parameters of the electrode process have been determined: adsorption equilibrium constant B= $1{,}32\cdot10^{5}$ $mol^{-1}\cdot dm^{3}$, the attraction constant $\gamma = 1{,}2$, the maximum surface concentration $\Gamma_{max} = 9{,}10\cdot10^{-11}$ $mol\cdot cm^{-2}$; the share of the electrode surface occupied by one particle of the adsorbed complex S = 1,81 nm^2 and the free adsorption energy ΔG = - 39,1 $kJ\cdot mol^{-1}$.

Keywords: Voltammetry, 2,3–dihydroxybenzaldehyde, vanadium.

Introduction

Numerous investigations have shown [1,2] that V(V) interacts easily with substances containing oxygen atoms as donors. The formation of the complexes with hydroxyl-containing ligands is especially characteristic for V(V). When trihydroxyglutaric acid [3], catechol [4,5], pyragallol [6], catechol violet [7], 2,5-dichloro-3,6-dihydroxy-1,4-benzoquinone [8,9], dihydroxynaphthaline [10] and other hydroxyl-containing aromatic compounds [11-14] are added to solution containing V(V), the formation of the stable complexes has been observed . These species can be adsorbed on the surface of the mercury electrode and reduced considerably easier than V(V). This behavior made possible to use them in the adsorptive stripping voltammetry with a significant increase of the sensitivity of vanadium determination. The main shortcoming of these methods, as mentioned in [10], is the reagents instability and the overlapping of V(V) waves as well as the interferences of some metals ions which can be reduced at potentials close to the reduction potential of V(V). Thus, the solutions of catechol and pyrogallol [4-6] had to be prepared daily due to their quick oxidation by air oxygen. That is why it is often necessary to look for new and more stable ligands able to be used for determination of vanadium.

The purpose of this work is to investigate the electrochemical behavior of V(V) in the presence of 2,3-dihidroxybenzaldehyde (2,3-DHBA), as well as the peculiarities of the adsorption of the produced complex on the mercury electrode.

Experimental

Apparatus

Voltammetric measurements were carried out on a PU-1 polarograph (Russia) in a thermostated (25±0,1)^{o}C three–electrode cell. A three-electrode system consisting of a mercury drop electrode (MDE, 2,45 $mg^{2/3}s^{-1/2}$) as the working electrode, a saturated calomel reference electrode (SCE) and a platinum wire as a auxiliary electrode.

The potential scan rate, *v*, was 2 mV/s, the amplitude of alternating voltage, ΔE, was 15 mV. The drop-time curves were obtained by measuring drop-time in tree-electrode cell with a slowly dropping capillary (12 s).

The voltammetric adsorptive complex waves of V(V) with 2,3-DHBA were recorded with Model 03 Oscillopolarograph PO-5122 (Russia) with linear-sweep potential: the scan rate - 1,0 V/s; the starting potential – 0,35 V; the delay after the breaking away of the drop - 10 s.

The solution acidity was measured by a universal pH-meter of OP-204/1 type (Hungary). The analyzed solutions were deaerated by electrolytic hydrogen.

Reagents

Analytical reagent grade chemicals and twice distilled water were used for preparation of the solutions. Stock solution of V(V) ($1\cdot10^{-2}$ $mol\cdot dm^{-3}$) was prepared by dissolving the appropriate amount of the sodium metavanadat in a 100 cm^3 volumetric flask. The working standard solutions were prepared daily by diluting the stock solution. The $1\cdot10^{-3}$ $mol\cdot dm^{-3}$ 2,3-DHBA solution was prepared by dissolving the weighted sample in 1,0-1,5 ml of ethanol in a 100 cm^3 volumetric flask followed by addition of the water up to mark. All solutions were prepared in an acetate buffer (0,4 M CH_3COONa+ 0,1 M CH_3COOH, pH 5,2).

Procedure

In all cases, the investigated solutions were prepared as follows: an appropriate volume of 2,3-DHBA solution was added to the sodium metavanadat solution in the volumetric flask followed by adding 2.5 cm^3 the buffer solution (pH 5.2) and diluting with water up to mark.

The solution was transferred into the polarographic cell, deaerated with electrochemically generated hydrogen and an a. c. polarogram was recorded under the following condition: starting potential E_s = - 0,35 V (SCE), ΔE = 15 mV, ν=2 mV / s.

Results and discussion

The polarographic behavior of vanadium (V) species is strictly depending on the pH-value of the solutions. In [10] it is shown the presence of diverse vanadium containing forms in solutions with concentrations of V(V) < 1· 10^{-5} mol·dm^{-3} . For the pH < 3,5 the dominating particles are VO_2^+. In the range of pH 3,5 – 7,8 the formation of the form $VO_2(OH)_2^-$ is favored. For pH > 8 the main form present in solution is HVO_4^{-2}. The electroreduction of the vanadium containing solutions at pH 3,5 – 7,8, two waves can be recorded. The first wave characterizes the reduction $VO_2(OH)_2^- + 2H^+ + e \rightarrow VO(OH)_2 + H_2O$, and the second one - the further reduction of V(IV) [1 – 3]. The both waves appear at a potential more negative that -1.0 V (SCE).

The supporting electrolyte formed by acetate buffer solution, and ensuring the pH 5,2 is inactive up to E = -1.0 V. Adding V(V) and 2,3-DHBA, a new well expressed peak can be recorded at the potential -0.590 V. (Fig.1) The height of the peak (Ip) and its potential (E) for a constant concentration of vanadium and 2,3-DHBA are depending on the pH value of solution.

When pH is increased, the height of the peak increases and reaches its maximum value in the pH range of 4,7 – 5,3. With the increase of pH, the peak's potential shifts to the more negative values. This is an indicative of hydrogen ions participation in the electrode process.

The increase of the 2,3-DHBA concentration gives rise to the augmentation of the height peak. When the concentration surpasses 1·10^{-4} mol·dm^{-3} the height remains constant. For a content of vanadium 2·10^{-7} mol·dm^{-3} the optimal concentration of the organic reagent is 1·10^{-4} mol·dm^{-3} for a pH 5,2. Under these conditions the signal can be recorded as well expressed peak on the a.c. polarogram.

The height of this peak increases with the increase of V(V) concentration (Fig. 2, curve 2). The linear dependence of I_p with V(V) content was observed in the concentration range 2·10^{-7} – 5 ·10^{-6} mol/dm^3.

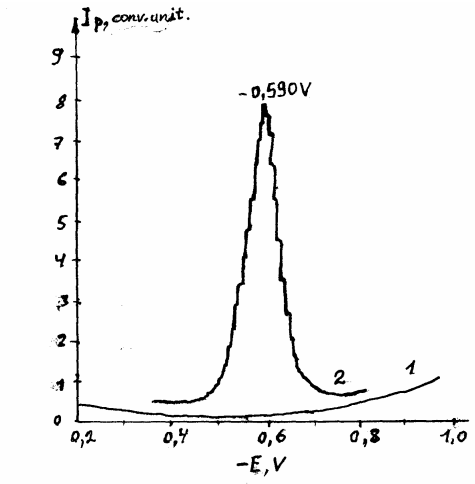

Fig. 1. A. c. Voltammogram of V(V): ***1. 0,4M CH_3COONa, 0,15M CH_3COOH, pH 5,15; 2. 1 + 2 ·10^{-6}M V(V) + 1 ·10^{-4} M 2,3-DHBA ν= 2mV/s, amplitude 15mV, r.c. 0,25 x 100, τ = 2,1 s, E_s = - 0,35V·***

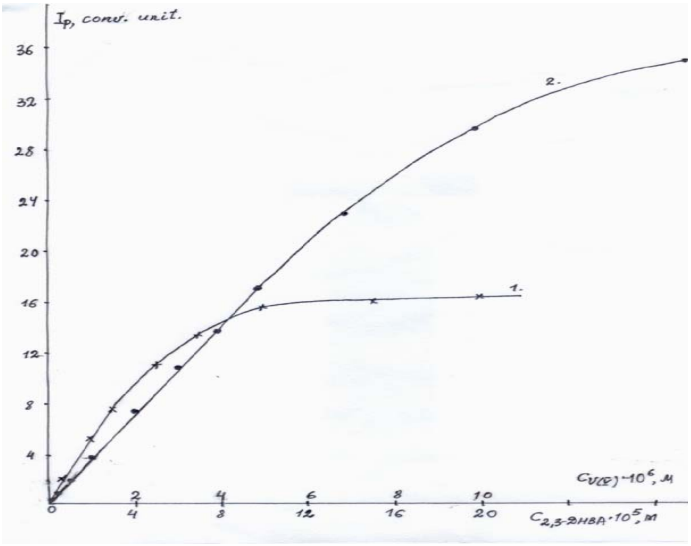

Fig. 2. Dependence of I_p on concentration of 2,3-DHBA (curve 1) and V(V) (curve 2) in solution. Conditions as in Fig. 1.

Using the amperometric titration composition of the formed complexes has been established. As it is seen from Fig. 3, the amperometric curve reflects the following processes occurring in the solution. Up to ratio V(V) : 2,3-DHBA = 1 : 1, vanadium (V) species oxidizes 2,3- DHBA and reaches the oxidation state V(IV). The second section reflects the formation of V(IV) complex with 2,3-DHBA which finishes at the ratio V(IV) : 2,3-DHBA = 1:3. In [5] a detailed discussion of the question concerning the formation of the tris-chelate

complex V(IV) with catechol can be found. Besides that, in the same paper it is emphasized that the tendency of forming tris-chelate complexes is common for ortho-diphenol compounds.

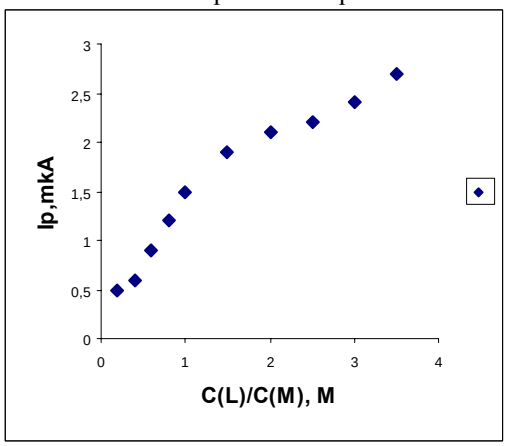

Fig. 3. Amperometric titration curve of vanadium (V) – 2,3-DHBA

In acid aqueous solutions [2], only the following ion pairs : VO^{3+} - VO^{2+}; VO^{2+} - V^{3+}; V^{3+} - V^{2+} can exist simultaneously. All other ions combinations of vanadium are impossible due to immediate redox reactions leading to the formation of the above mentioned redox pairs. That is why, in acid solutions it is possible to carry out the process of electrolytic reduction of vanadat- ions according to the scheme:

$$\mathbf{V(V)} \xrightarrow{e} \mathbf{V(IV)} \xrightarrow{e} \mathbf{V(III)} \xrightarrow{e} \mathbf{V(II)}$$

It should be noted that unless all V(V) is reduced in V(IV) it is impossible to observe the next step (reduction of V(IV)) a. s. o. In our case V(V) is reduced to V(IV) by the ligand, while complex V(IV) with 2,3-DHBA is reduced electrochemically on the electrode giving a well expressed peak on the a. c. polarogram in the presence of the acetate buffer (pH 5,2) as supporting electrolyte.

For establishing the composition of the complex which is adsorbed on the surface of the mercury electrode, we have used the following equation [11] : $1/I_p = 1/I_{p,max} + 1/(\beta I_{p,max} \cdot C_L^m)$, where I_p is the peak's current at a certain concentration of the ligand, $I_{p,max}$ is peak's current when all metal ions are bound in a complex, C_L is the concentration of the ligand. The dependence $1/I_p$ on $1/C_L^m$ is linear only for the case when m = 3. This result confirms that the electroactive complex on the surface of the electrode is of the same composition as in the solution, i. e. 1:3.

To establish the nature of the current an oscillopolarografic investigation has been undertaken. The height of the peak, recorded in the same condition as was indicated for a.c. polarography, increases simultaneous with the increase of the scan rate. The value of "X" (the slope of dependence lg 1_p – lg v) was found to be 0,92. Such a value of "X", as well as the shape of the oscillopolarogram, reminding of an isosceles triangle, is characteristic for electrode processes controlled by adsorption of the complex on the electrode. The value of the current depends on the initial potential and reaches its maximum value at E_s = (-0,35 – 0,45) V. The peak's height decreases with the temperature increase. The temperature coefficient is – 2,1% per degree. All these dependences and the negative value of the temperature coefficient are characteristic for electrode processes complicated by adsorption.

The dependence of drop-time curves on the electrode's potential is shown in Fig. 4.

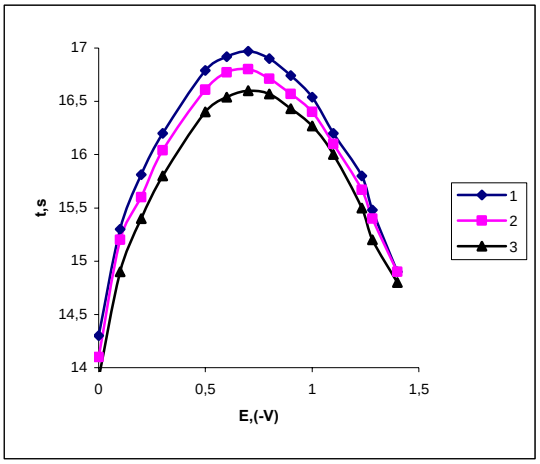

Fig. 4. Drop-time curve: *1. 0,4M CH_3COONa – 0,15M CH_3COOH, pH 5.20; 2. 1 + 1·10^{-4}M 2,3-DHBA; 3. 2 + 2 · 10^{-6} M V(V).* Conditions as in Fig. 3.

The introduction of vanadium(V) into the solution containing 2,3-DHBA decreases the drop-time curves (Fig. 5, curve 3), which is indicative of the fact that adsorption of complexes V(V) with 2,3-DHBA is more significant than the adsorption of the free ligand (Fig. 5, curve 2). The parameters, characterizing the adsorption of V(V) complexes with 2,3-DHBA on the dropping mercury electrode, has been determined. The maximum surface concentration $\Gamma_{max} = 0{,}91 \cdot 10^{-6}$ mol · cm^2 was calculated from the dependence of the discharge current on the complexes concentration. The surface of the electrode per one particle of the adsorbed complex S = 1,81nm^2 was calculated.

Proceeding from the areas of complexes discharge peaks, the quantity of electricity (Q) was calculated for various concentrations of complexes in the solution [16]. The filling degree (θ) was determined from relationship Q/Q_{max}. The attraction constant γ = 1,82, whose positive value points to the mutual attraction of particles on the electrode's surface, was found from the slope of the straight line in lgθ/(1-θ)·C - θ coordinates (Fig. 5). The adsorption equilibrium constant $B = 1{,}32 \cdot 10^5 \cdot$ mol^{-1}·dm^3 was determined from the same dependence. Using the value of the equilibrium constant, the free adsorption energy ΔG = -39,1 l· kJ·mol^{-1} was calculated.

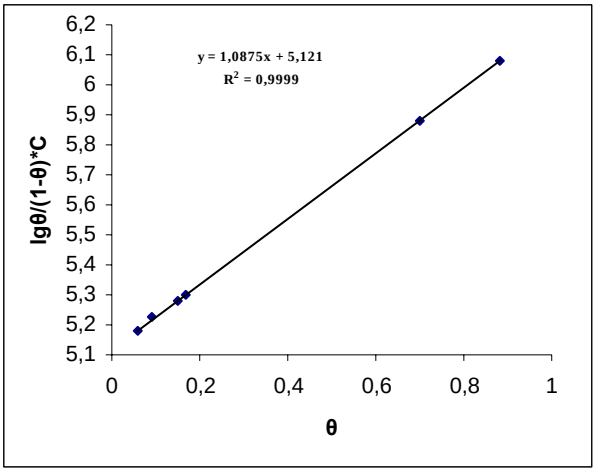

Fig. 5. Isotherm of V(V) - 2,3-DHBA complexes adsorption on the mercury electrode surface. Conditions as in Fig. 3.

Conclusion

The electrochemical behavior of the vanadium (V) complex of with 2,3-DHBA is controlled by the adsorption of the product on the surface of the mercury electrode. The effect of experimental conditions on the peak of adsorbed species has been studied. The adsorption parameters were determined.

References

[1]. Музгин, В.Н.; Хамзина, Л.Б.; Золотавин, В.Л.; Безруков, И.Я. Аналитическая химия элементов. Ванадий; М.: Наука, 1981, pp 25-27.
[2]. Гончаренко, А.С. Электрохимия ванадия и его соединений; М.: Металлургия, 1969, pp 49-51.
[3]. Chikryzova, E.G.; Kiriyak, L.G.; Meryan, V.T. Zh. Anal. Khim. 1971, 26, 33-37.
[4]. Van den Berg, C.M.G. ; Huang, Z. A. Anal. Chem.1984, 56, 2383-2386.
[5]. Ivanov, V.D.; Kaplun, M.M. Zh. Anal. Khim. 1997, 52, 362-368.
[6]. Adeloju, S. B. O.; Pablo, F. Anal. Chim. Acta. 1994, 288, 157-222.
[7]. Vucomanovic, D.V.; Van Loon G.W. Talanta, 41, 387-391.
[8]. Sander, S. Anal. Chim. Acta. 1999, 394, 81-89.
[9]. Novotny, L.; Navratil, T.; Sander, S. Electroanalysis 2002, 14, 1105-1109.
[10]. Li, H.; Smart, R.B. Anal. Chim. Acta. 1996, 333, 131-138.
[11]. Lu, J., Jin, W; Wang, S. Anal. Chim. Acta. 1990, 238, 375-381.
[12]. Meryan V. T., Latichewski, I.; Taragan, N.; Zayat, G. Bull. ASM. Ser. Boil. Chem. 1994, N 5, 33-37.
[13]. Pelzer, J.; Scholtz, F., Henrion, G.; Heininger, P. Frezenius Z. Anal. Chem. 1989, 334, 331-336.
[14]. Hsein, A. – K., Ong, T. –H. Mikrochim. Acta. 1991, 3, 117-123.
[15]. Meryan, V. T., Vataman I.I. Zh. Anal. Khim. 1990, 45, 222-232.

REACTIVE EXTRACTION OF TARTARIC ACID

Natalia Marchitan

Department of Industrial and Ecological Chemistry, Faculty of Chemistry and Chemical Technology,
Moldova State University, 60 A. Mateevici str., MD 2009, Chisinau, Republic of Moldova
E-mail: n_marchitan@yahoo.com, (+373 22) 57 77 96

Abstract. The present paper describes the results of reactive extraction of tartaric acid in model systems, which can be used for its separation from secondary wine products. As extractant have been used a normal/isododecyl mixed secondary amine Amberlite LA-2. The following parameters of the separation process have been varied: nature of diluent and modifier; modifier concentration; concentration, temperature and pH of the tartaric acid solution and the stirring time, and the work intervals have been established. It was concluded that in determinated conditions the extent of tartaric acid extraction attains value 85-95%.

Keywords: reactive extraction, tartaric acid, Amberlite LA-2.

Introduction

Liquid extraction has been used already for a very long time for separation of metals from production or waste water streams [1-4]. It is an efficient, economical, and environmentally friend method for the recovering of different compounds from waste water, for separation of some biologically active products from fermentation liquids, for extraction of some carboxylic acids [5-14] etc.

Extraction with conventional solvents such as alcohols and ketones are not efficient when applied to dilute carboxylic acid solutions because of the low aqueous activity of carboxylic acids resulting in low distribution coefficients. The strong amine interaction with the acid allows for formation of acid-amine complexes and thus provides for high distribution coefficients. When using amine extragents, a proton transfer occurs during the extraction and the acid prevails in the organic phase as an amine-acid ion pair complex [12].

The difference between the two extraction techniques is due to the appearance of a hydrophobic complex, which is the product of the interfacial chemical reaction between solute and extractant [10].

Primary and secondary amines are stronger bases than tertiary amines and in many cases are also stronger than the anion of the extracted carboxylic acid. These strong bases protonate, therefore, even in equilibrium with solutions, the pH of which is too high to allow considerable amounts of undissociated carboxylic acids. In that sense carboxylic acid extraction by amine more basic than the anion of the extracted acid (at $pH<pK_a$), nearly complete protonation takes place to reach stoichiometric extraction through ion-pair formation with dissociated acid molecules. In equilibrium with aqueous phases of high pH ($pH>pK_a$) ion-pair formation is the dominating mechanism [15].

In this paper the reactive extraction of tartaric acid from aqueous solution with Amberlite LA-2 was examineted. The separation efficiency depends on solute physical and chemical characteristics (hydrophobicity, acidity), extractant proprieties (reactivity, the ability to form hydrophobic compounds with the solute) and process conditions (pH-values, concentration of solute, mixing time, temperature of aqueous solution). Thus, the mentioned factors constitute the subject of this study.

Experimental Section

Materials. The aqueous phase was prepared by dissolving tartaric acid (*Reahim*, *Russia*) in distilled water. The initial concentration of tartaric acid solution was 1,56 g/dm^3. Several solvents were used as inert diluents for organic phase - benzene, chloroform, carbon tetrachloride, kerosene, butyl acetate, heptane, methyl isobutyl ketone (MIBK), n-dodecane, 1-butanol, 1-octanol, 1-decanol (all from *Sigma-Aldrich, Germany*). The last two alcohols also were used as modifiers. The organic phase was prepared by dissolving Amberlite LA-2 (*Sigma-Aldrich, Germany*) in diluent and adding modifier. The concentration of Amberlite LA-2 in organic phase was 16,62 g/dm^3. Glacial acetic acid (*Reactivul, Romania*) and sodium metavadanate (*Reahim, Russia*) were used for determination of tartaric acid concentration, hydrochloric acid (*HaricovPromHim, Ukraine*) and sodium hydroxide (*Chimicomplex, Romania*) for pH value adjustment.

Procedure. The experiments were carried out in 200 cm^3 glass flasks. Equal volumes of aqueous phase and organic phase (50 cm^3 of each) were mixed by universal stirrer type WU-4 (*Premed, Poland*) for 15 min at room temperature, time sufficient to attain equilibrium. The obtained mixtures were let for phase separation for 15-30 min, in same cases it was used centrifugal separator. The process development has been followed by determination the solute concentration in the initial and in the final solution. For the calculation of the solute concentration in the solvent phase mass transfer balance was used.

Methods. Concentration determination of tartaric acid was realized by photocolorimetric method on colorimeter (*Zomz, Russia*). For measurements 5 cm^3 of analyzed solution were passed into 50 cm^3 flask, 4 cm^3 of sodium metavanadat solution (5 %) and 1 cm^3 of glacial acetic acid were added, then flask was fitted with distilled water. Obtained solution is left for 15-20 min at dark for the formation of the stable colour in 24 h. Measurements were done at 525 nm wave length (green filter) in cells with 20 mm working side length, against a blank similarly prepared without tested solution [16].

Definition of Characteristic Parameters. The extraction is represented by the extent of extraction η (%) and the distribution coefficient D:

$$\eta = \frac{V_{in}C_{in} - V_{eq}C_{eq}}{V_{in}C_{in}} \cdot 100 \quad (1)$$

$$D = \frac{C_{eq(o)}}{C_{eq(aq)}} \quad (2)$$

where V – volume of the phase, cm^3; C – concentration of tartaric acid (of undissociated molecules and of tartaric anions) g/dm^3, index *in* – initial solution, index *eq* – solution after reaching equilibrium, index *o* – organic phase, and index *aq* – aqueous phase.

Theory

The general interfacial equilibrium that is established in the reaction between organic oxyacids and Amberlite LA-2 is following:

$$mR(COOH)_{n(aq)} + pQ_{(o)} \rightleftharpoons [R(COOH)_n]_m \cdot Q_{p(o)} \quad (3)$$

where $R(COOH)_n$ represent the oxyacid (n=2 for tartaric acid), and Q – Amberlite LA-2.

Depending on molar ratio between the components, tartaric acid and extraction agent, three types of chemical inter-phase reactions used for reactive extraction may be distinguished:

1) in the case of m:p proportion close to 1, the tartaric acid and extraction agent form the hydrophobic complex in a equimolar proportion (formation of an ion-pair):

$$R(COOH)_{n(aq)} + Q_{(o)} \rightleftharpoons R(COOH)_n \cdot Q_{(o)} \quad (4)$$

2) in the case of molar proportion between the carboxylic acid and the extraction agent much lower than 1 (m:p <<1), reactive extraction results in the formation of particular complexes $R(COOH)_n \cdot Q_n$ in the organic phase:

$$R(COOH)_{n(aq)} + nQ_{(o)} \rightleftharpoons R(COOH)_n \cdot Q_{n(o)} \quad (5)$$

3) in the case of reactive extraction in nonpolar solvents (e.g. butyl acetate) of existent high initial concentrations of oxyacids in aqueous solutions, a third phase is possible to appear, representing a stable emulsion, with a high content of acid complexes, insoluble in aqueous phase as well as in the organic one:

$$mR(COOH)_{n(aq)} + Q_{(o)} \rightleftharpoons [R(COOH)_n]_m \cdot Q_{(o)} \quad (6)$$

Analysis of the individual mechanism of tartaric acid reactive extraction shows that at concentrations lower than 7,6 g/dm^3 the reactive extraction takes place according to mechanism (2) - $R(COOH)_2 \cdot Q_2$. At the rise of tartaric acid concentration there establishes an intermediate mechanism between theoretic mechanisms (1) and (2). This phenomenon may be explained by formation of tartaric acid specific dimmers. Accordingly, one molecules of Amberlite LA-2 extracts more than one molecule of tartaric acid [6-9, 11].

Moreover, in low concentration domain, for a molar ratio between solute and extractant below 1, the separation occurs mainly by reactive extraction. Contrarily, at molar ratio higher than 1, the contribution of the physical extraction becomes considerable [10].

Results and Discussion

Generally, the distribution coefficients of carboxylic acids between aqueous and organic phases, in absence of the extractants, are very low, being higher in polar solvents. This phenomenon is the result of acid dissociation in aqueous solutions because the formed ionic species having a low solubility especially in non-polar solvents [10].

The type of diluent and its concentration in the mixture extractant-diluent have an important effect on the distribution coefficients because the diluent affects basicity of the amine and the stability of the ion-pair complex formed and consequently its extracting power [12].

In this study were used next nonpolar diluents: kerosene, carbon tetrachloride, benzene, dodecane, and heptane; and polar diluents: chloroform, 1-butanol, methyl isobutyl ketone (MIBK) and butyl acetate. The organic

solution of amine in 1-octanol and 1-decanol were used for separation of tartaric acid. All tests were done using Amberlite LA-2 as extracting reagent.

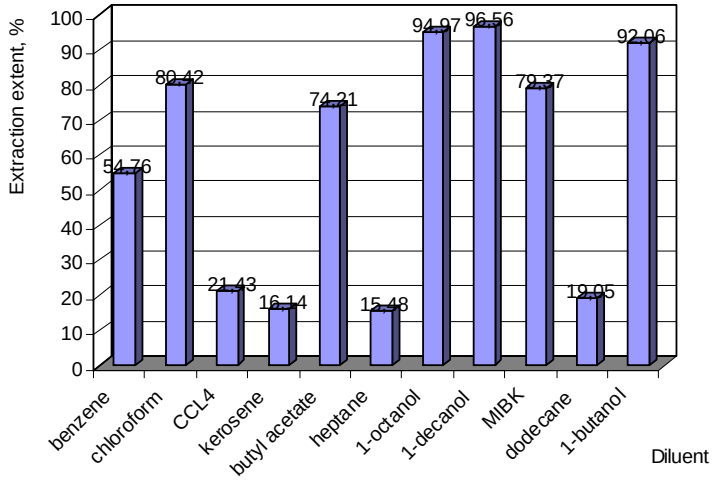

Fig. 1. The influence of diluents on efficiency of the tartaric acid extraction from aqueous phase

The best extraction efficiency was gained for 1-octanol, 1-decanol, and 1-butanol, but using of these solvent caused stable emulsions formation. The same effect was observed in case of dodecane. Thus, were selected benzene, chloroform, butyl acetate and MIBK.

The role of diluent is not only to improve the physical properties of the extraction system, but also removes the interaction product. In the presence of modifier, the inert diluent may enhance its extraction ability as a solvent. Addition of a modifier, such as a high molecular weight alcohol, to overcome third phase and emulsion formation in the system was necessary in case of resulting high concentration of the acid-amine complex in the organic phase [1, 13].

1-octanol and 1-decanol were tested as modifier by their separate addition of (10 cm^3, 20 % v/v) in organic phase.

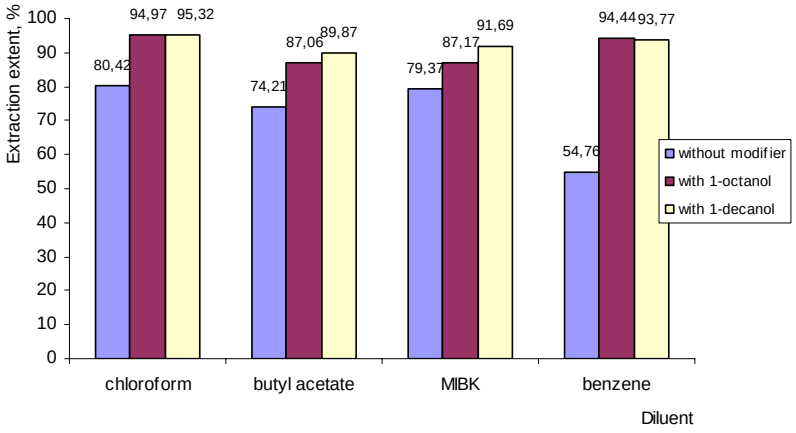

Fig. 2. The influence of the modifiers (10 %) on efficiency of the tartaric acid extraction from aqueous phase

Fig. 2 shows that 1-octanol and 1-decanolul increased the tartaric acid removal efficiency of organic solution. The results are very similar, thus both modifiers can be used for practical application.

In next studies MIBK wasn't used as solvent because of stability of its formed emulsion (separation time of the phases minimum 90 min), and benzene because of its toxicity. The chloroform and butyl acetate were selected as diluents for preparing the amine solution.

It was studied the dependence between the efficiency of tartaric acid extraction and the modifier's concentration in organic solution, which was varied from 2 % (v/v) to 50 % (v/v).

In figure 3 can be seen that for a good extraction of tartaric acid the concentration of 1-octanol as modifier should be 10 % in chloroform solution, and 20 % in butyl acetate solution. The 1-octanol concentration higher that 30 % increased tartaric acid extraction just with 2-3 %, but made phase separation time after stirring much longer.

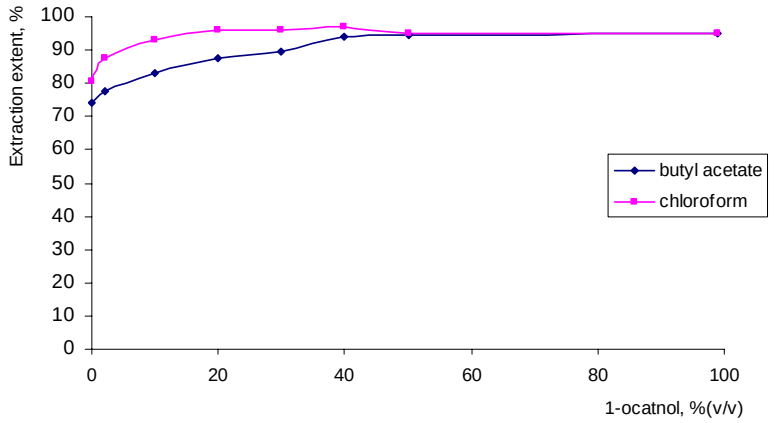

Fig. 3. The effect of 1-octanol concentration on the extraction extent of tartaric acid from aqueous phase

Figure 4 reflects the increase in the extraction extent at the same time with the concentration of tartaric acid in the initial solution, which is due to the lowering of the pH of the aqueous solution upon elevation of the concentration of tartaric acid. The concentration of tartaric acid was varied from 0,5 g/dm^3 to 10 g/dm^3. In this way, the highest efficiency of separation process was observed for organic solutions of amine in butyl acetate at tartaric acid concentration of 2-3 g/dm^3, and 0,5-2 g/dm^3 for solutions of amine in chloroform.

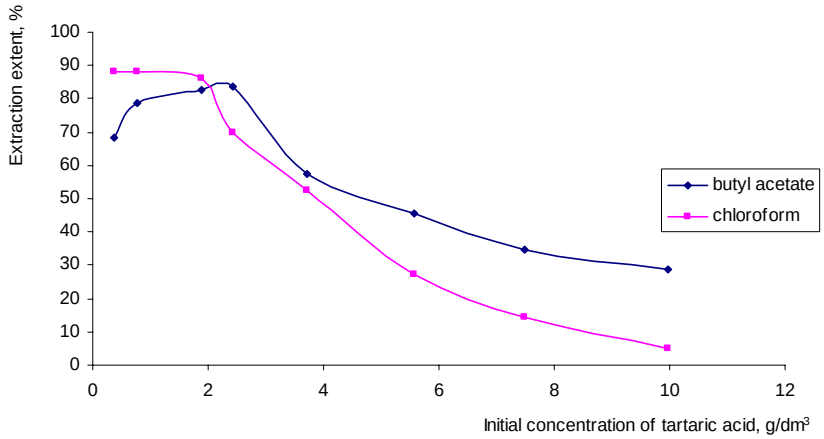

Fig. 4. The effect of the tartaric acid concentration in aqueous solution on its using 1-octanol (10 %) as modifier

The complexation reactions in the organic phase involve proton transfer or hydrogen-bond formation and are thus expected to be exothermic. Moreover, formation of a complex makes the system more ordered and, therefore decreases the entropy. Thus, as the temperature is increased, the amount of tartaric acid extracted decreases [11, 17].

To find the optimal extraction temperature value the determinations were made in interval from 25 ^{0}C to 75 ^{0}C, the last one is the temperature of obtained vinasses after wine or grape must distillation, the other secondary wine produces obtained at lower temperatures. It must be mentioned that for the system which contents chloroform as solvent the higher temperature was 50 ^{0}C (boiling point of chloroform 61 ^{0}C). It was shown that the efficiency of the tartaric acid separation process from model solution is constant until 35 ^{0}C, and after that decreases.

The physical extraction is controlled by the system components diffusion only. For the reactive extraction, a new resistance appears, namely the resistance induced by the interfacial chemical reaction between solute and extractant (the extraction degree increases).

The relative participation of physical extraction increases with rotation speed. In the same time, the evolution of the mass flows with rotation speed for reactive extraction indicated two variation regions corresponding to the diffusional (the increase of the mass flow with rotation speed) and kinetic region (the constant level of mass flows beside the rotation speed increase), respectively [10].

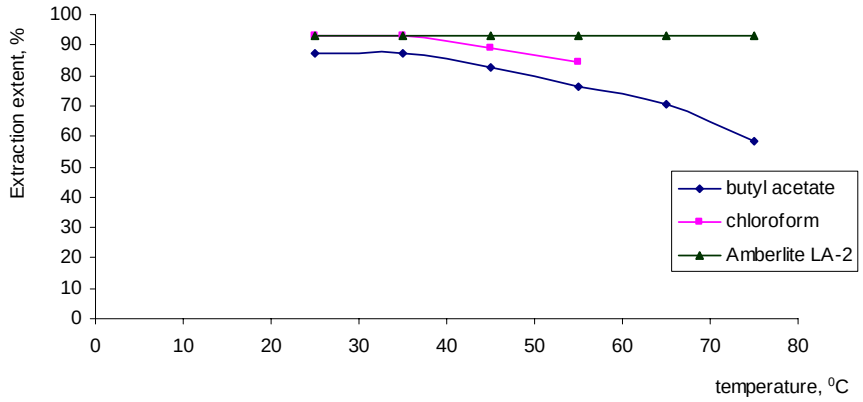

Fig. 5. The influence of temperature on the extraction extent of tartaric acid from aqueous phase

For the stabilization of the equilibrium between tartaric acid content in aqueous solution and in organic solution it was necessary 1 min of stirring (fig.6).

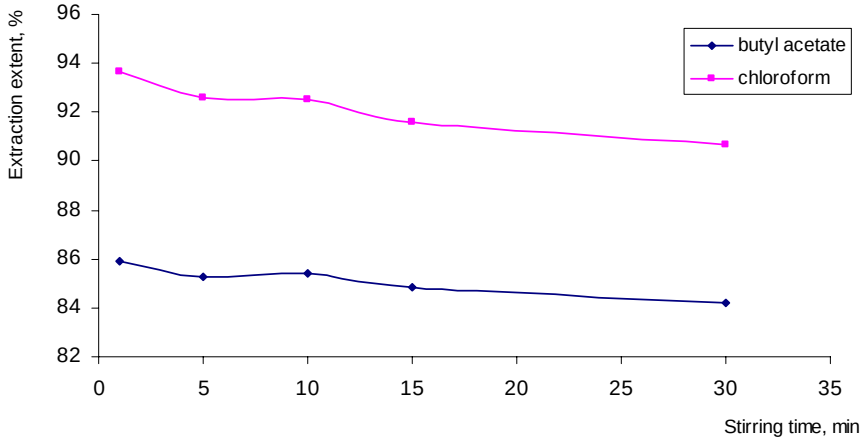

Fig. 6. The effect of the stirring time on the extraction extent of tartaric acid from aqueous solution

To identify the dependency of the reactive extraction process to the model solution pH values, initially was prepared a solution of tartaric acid with concentration of about 1,56 g/dm^3 with pH of 2,5. The pH value of every 50 cm^3 of initial solution was adjusted with concentrated solutions of HCl and NaOH.

As it was shown, the efficiency of reactive extraction process decreases brusque at insignificant modifications of pH of the tartaric acid solution through acid values, because tartaric acid is a weak acid and does not dissociate at low values of pH. In can be concluded that adjusting low values of pH by adding of hydrochloric acid to the solution of tartaric acid should lead to simultaneous separation of both acids, moreover, that HCl would be extracted preferentially. At intermediate values of pH protonation of amine is reduced and an increasing amount of undissociated tartaric acid may be separated, both through the ion-pair and H-bonding mechanisms. Experimental results from the runs in which pH has been adjusted with aqueous solution of NaOH showed that the amount of acid equimolar to the added base may be regarded as bound in form of acid sodium tartrate and, therefore, inseparable. Thus only the remaining free acid takes part in ion-exchange equilibrium. Simultaneously, the sodium hydrogen tartrate present affects the ionic strength of the solution and thus the activity of free acid [14].

Conclusions

The secondary amine Amberlite LA-2 was found to be efficient in the extraction of tartaric acid. The best physico-chemical conditions of the process have been determinated. Butyl acetate and chloroform were selected as diluents. 1-octanol was selected as modifier and its concentration in chloroform solution is 10 %, and in butyl acetate solution 20 %. The stabilized parameters of aqueous solution were: concentration of tartaric acid - 2-3 g/dm^3 in case of organic solutions of amine in butyl acetate, and 0,5-2 g/dm^3 for solutions of amine in chloroform; temperature – 20-35 ^{0}C; stirring time - 1 min; pH value – initial (pH=2,5 for concentration of tartaric acid in solution 1,56 g/dm^3).

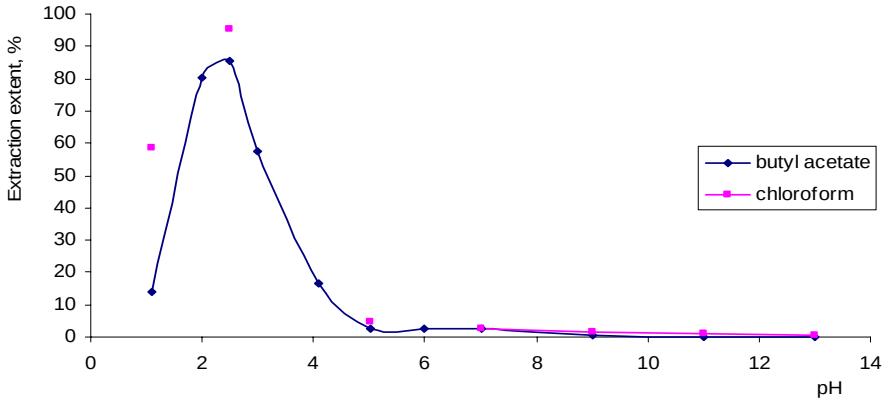

Fig. 7. The effect of initial pH of aqueous solution on extraction extent of tartaric acid

With a view to the practical application of the system the optimization of the reactive extraction and studies on solution of secondary wine products should be performed.

References

[1]. San Martin, M.; Bart, H. J. Recovery of Zinc from Pickling Baths with Amberlite LA-2. Influence of Modifier on the Extraction Equilibrium. Chem. Eng. Tech. 1994, 17, pp. 397-400.
[2]. Zaboska, W.; Leszko, M.; Krzymowska-Hachuka, A. Extraction of Cu(II) from Hydrochloric Acid Media by Amberlite LA-1 Hydrochloride Dissolved in 1,2-dichloroethane.Talabta, 1989, vol. 36, № 12, pp. 1295-1299.
[3]. Alguacil, F.J.; Alonso, M. Liquid-liquid Extraction of Au(I) by Amberlite LA-2 and its Application to a Polymer-Immobilized Liquid Membrane System. Gold Bulletin, 2005, 38/2, pp. 68-72.
[4]. Chatterjee, A.; Basu, S. Solvent Extraction of Silver(I) with Amberlite LA-2 Using ^{110m}Ag as Trager. J. Radioanal. Nuclear Chem., Articles, 1992, vol. 162, № 2, pp. 259-265.
[5]. Hauer, E.; Marr, R. Liquid Extraction Processes in Biotechnology. Chem. Ing. Tech. 1991, vol. 63, № 8, pp. 809-816.
[6]. Oniscu, C.; Mereuța, A.; Caşcaval, D.; Duca, Gh. Selective Separation of Organic Oxyacids from Aqueous Phase by Reactive Extraction. Roum. Biotechnol. Lett. 2002, vol. 7, № 5, pp. 933-940.
[7]. Caşcaval, D.; Oniscu, C.; Dumitraşcu, A.; Chichirău, Al.; Toma, L. Extracția selectivă a acizilor carboxilici din lichidul rezultat de la fermentația citrică. Revista de chimie. 1998, 49, № 1.
[8]. Oniscu, C.; Caşcaval, D. Studies on Separations of Biosynthesis Products by Reactive Extraction. Roum. Biotechnol. Lett. 1996, vol. 1, № 1, pp. 23-33.
[9]. Caşcaval, D.; Tudose, R.; Oniscu, C. Reactive Extraction of Dicarboxylic Acids Selective Extraction. Hung. J. Ind. Chem. Veszprém. 1997, vol. 25, pp. 245-248.
[10]. Caşcaval, D.; Oniscu, C. Comparative Study of Some Monocarboxylic Acids I. Correlations for mass flow. Hung. J. Ind. Chem. Veszprém. 2000, vol. 28, pp. 99-103.
[11]. Juang, R. S.; Huang, W. T. Equilibrium Studies on the Extraction of Citric Acid from Aqueous Solutions with Tri-n-octylamine. J. Chem. Eng. Japan. 1994, vol. 27, № 4, pp. 498-504.
[12]. Malmary, G. H.; Mourgues, J. F.; Bakti, J.; Conte, T. S.; Achour, D.; Smagghe, F. J.; Molinier, J. R. Partition Coefficients of Tartaric and Malic Acids between Dilute Aqueous Solution and Amine Extractants Dissolved in Various Diluents. J. Chem. Eng. 1993, 38, pp. 537-539.
[13]. Kyuchoukov, G.; Labbaci, Ab.; Albet, J.; Molinier, J. Simultaneous Influence of Active and "Inert" Diluents on Extraction of Lactic Acid by Means of Tri-n-octylamine (TOA) and Tri-iso-octylamine (TIOA). Ind. Eng. Chem. Res. 2005, page est. 7,9.
[14]. Tomovska, R.; Poposka, F.; Heyberger Al.; Prochazka, J. pH-Dependence of Tartaric Acid Extraction. Chem. Biochem. Eng. Q. 1999, vol. 13, № 4, pp. 185-190.
[15]. Eyal, A. M.; Canari R. pH Dependence of Carboxylic and Mineral Acid Extraction by Amine-Based Extractants: Effects of pK_a, Amine Basicity, and Diluent Properties. Ind. Eng. Chem. Res. 1995, vol. 34, № 5, pp. 1789-1798.
[16]. Razuvaev, N.I. Complexnaya pererabotka vtoricnih productov vinodelia. 1975, Moscova.
[17]. Juang, R. S.; Huang, R. H. Comparison of Extraction Equilibria of Succinic and Tartaric Acids from Aqueous Solutions with Tri-n-octylamine. Ind. Eng. Chem. Res. 1996, vol. 35, № 6, 1944-1950.

EFFECT OF COMPLEX FORMATION ON ELECTROCHEMICAL BEHAVIOUR OF METAL-CONTAINING WASTE WATERS

Olga Covaliova

Research Centre of Applied and Ecological Chemistry of the State University of Moldova
60, Mateevici Street, MD 2009, Chisinau, Moldova
Email: olga196cov@yahoo.com, phone: (373 22) 577707

Abstract. The problem of preventing the heavy metals and other toxic substances release in environment due to the discharges of untreated plating and rinsing solutions is actual from both ecologic and economic point of view. It is crucial to prevent the environmental pollution and uncontrolled losses of resources (metals and other substances). The treatment technologies used today are not always efficient and cost saving and in some cases they may even provoke the secondary pollution of environment. Electrochemical treatment of industrial waste waters is one of the most promising technologies as it implies the same principles as the main technological processes and does not require introducing of chemicals into the treated solution. However, until now this method was given insufficient attention, although there are certain publications in this field [1].

The electrochemical behaviour of some *d*-metal complexes was studied and discussed from the viewpoint of water treatment requirements. The studies performed in the model plating solutions of Zn, Ni, Cu ammonia and pyrophosphate complexes, polynuclear Cr complexes have shown that the application of conventional reagent waste water treatment methods for such solutions would be inefficient. Examination of potentio-dynamic polarization curves registered in studied solutions have shown, that due to the formation of series of Zn ammonia complexes, alkaline treatment will not ensure Zn removal from such solutions, and application of electrocoagulation treatment method will not be efficient enough. It was also found that in case of Ni-, Cr-containing solutions electrochemical treatment can be used for Cu removal, whereas for the effective Cr(VI) removal the electrocoagulation would be required, which entails the redox processes resulted in the formation of hydroxides. The research has shown that the approach on the heavy metal removal from the used plating solutions may be different depending on the plating bath composition.

Keywords: electrochemical processes, model plating solutions, ligands, complex salts, polarization curves.

1. Introduction

The presence of metal complex salts, specifically of Zn(II), Cr(III) and Cr(VI), Ni(II), Cu(II), etc. in the plating solutions play an important role in electrochemical processes of heavy metal removal from them. There are numerous works in the field of plating processes, in which the influence of complex salts on the cathode processes is studied only from the point of view of the quality of cathode coatings formed [2-6]. However, cathode processes in the low-concentrated model waste water solutions were practically paid no attention. Therefore, the special research in this field was undertaken by us. Taking into account that the most broadly distributed ligands in plating industry are ammonia salts, pyrophosphate-, citrate-, tartrate-ions, organic amines and others, which are coordination-active with regard to the metal ions, this research was focused on the study of the specifics of cathode processes in the presence of some of the mentioned ligands.

The above listed metals possess amphoteric properties, and in alkaline solutions they can form hydroxide complexes of $[Me(OH)_n]^{(z-n)}$ type. So, the chemical (alkaline) treatment of waste waters containing these metals will be inefficient. In the presence of ligands, metal hydroxides participate in complex formation reactions, which can be schematically presented as follows:

$$\begin{aligned}
&Me(OH)_{z\downarrow} + nNH_3 \rightarrow [Me(NH_3)_n]^{z+} + z\ OH^- \\
&Me(OH)_{z\downarrow} + nP_2O_7^{4-} \rightarrow [Me(P_2O_7)_n]^{z-4n} + z\ OH^- \\
&Me(OH)_{z\downarrow} + nCit^{3-} \rightarrow [Me(Cit)_n]^{z-3n} + z\ OH^- \\
&Me(OH)_{z\downarrow} + nTart^{2-} \rightarrow [Me(Tart)_n]^{z-2n} + z\ OH^- \\
&Me(OH)_{z\downarrow} + nOx^{2-} \rightarrow [Me(Ox)_n]^{z-2n} + z\ OH^- \\
&Me(OH)_{z\downarrow} + nH_2NR \rightarrow [Me(H_2NR)_n]^{z+} + z\ OH^-
\end{aligned} \qquad (1)$$

As the function of water pH, the number of coordinated ligands (*n*) can be widely varied, and this brings out certain difficulties in the data interpretation for electrolytic processes. The various standpoints were expressed with regard to the mechanisms of such processes. Thus, in [7] it is supposed that, in spite of the exclusively low concentration of free metal ions in ligand-containing solutions, the discharge of simple cations occurs on cathode. In favour of such mechanism, the authors suggest that the accelerated dissociation of complex ions proceeds within the double electric layer. However, this concept has not been experimentally proved so far. The other assumption is related to the direct discharge of complex

ions on cathode. As far back as in the mid 50-ies of XXth century, A.N. Frumkin with team [8], based on the theory of delayed discharge, have explained this by the effect of repulsing action of negative charge, due to the anions deforming in double electric field and their dipole orientation. According to the third point of view, metal is deposited on cathode as a result of the secondary process.

With the scope to improve the existing methods of electrochemical treatment of low-concentrated waste waters and make them more efficient, we studied the behaviour of ammonia and pyrophosphate complexes in diluted model plating solutions.

2. Materials and Methods

The effect of complex forming substances (ligands) concentration on complex composition and distribution was studied in solutions where the ratio metal ions : ligands concentrations was varied from 1:1 to 1:10. Standard behaviour of ligands during the complex formation was taken into account. Thus, ammonium salts in solutions with the pH increase to the alkaline area can produce ammonia, following the well-known scheme:

$$NH_4^+ + OH^- \rightleftharpoons NH_3 + H_2O \quad (2)$$

Ammonia molecules thus formed can participate in complex formation with heavy metal ions which make part of metal aquacomplexes in water solutions, substituting a number of coordinated water molecules, following the scheme:

$$[Me(H_2O)_n]^{z+} \cdot mNH_3 \rightleftharpoons [Me(NH_3)_m(H_2O)_{n-m}]^{z+} + mH_2O \quad (3).$$

It is known that the coordination-active properties of ammonia are in many ways similar to those of the organic amines. This makes it possible to consider ammonia as a model ligand, which electrochemical behaviour can be extended to the entire family of other complex-forming agents.

A typical representative of the anion-type ligand is pyrophosphate-ion ($P_2O_7^{4-}$). Like ammonia ligands, they are often used in industrial plating processes, therefore it was also chosen for our research.

Table 1

Composition of waste water model solutions studied

Waste waters model solutions	*Components*	*Concentrations, g/l*			
		1	*2*	*3*	*4*
Zn- containing	$ZnSO_4$	0,01	0,01	0,01	0,1
	NH_4Cl	-	0,01	0,1	0,024
Ni- containing	$NiSO_4$	0,01	0,01	0,01	0,01
	NH_4Cl	-	0,004	0,01	0,1
Cu-containing	$CuSO_4$	0,01	0,01	0,01	0,01
	$Na_4P_2O_7$	-	0,01	0,1	0,156
Cr- containing	CrO_3	0,01	-	-	-
	$CrCl_3$	-	0,01	-	-

Electrochemical behaviour of heavy metal containing model waste water solutions was studied on the base of potentiodynamic polarization curves – PDPC. The curves were registered using the P-5827 potentiostate and the PDPI-002 potentiometer in the commercial glass electrolytic cell, in which the anodic and cathodic compartments were separated with the porous glass partition. The potential elevation rate (2 and 10 mV/s) was selected in such a way that the first regime made it possible to register PDPC in the regime close to the stationary electrolysis, while the second one – made it possible to estimate the influence of concentration limitations on the electrode process. The electrode potentials were measured with regards to the saturated chlorine-silver electrode.

The cathodic PDPC were registered on iron (Armko-Fe), copper and nickel electrodes, the anodic ones – on iron and aluminium, in order to receive the results under the conditions close to the electrocoagulation treatment of waste waters.

The PDPCs were registered with the strictly fixed position of the Luggin-Gaber capillary to exclude the resistance of the solution layer between the electrode surface and capillary.

3. Results and discussion

Some data related to the Zn behaviour in acid ammonium chloride solutions are given in the work [9]. According to our results **(**Fig.1), all the potentio-dynamic polarization curves (PDPC) registered on iron electrode in the simulated zinc-containing ammonium-free galvanic waste waters, are characterized by the presence of two portions:

1) Initial portion with low values of electrode potential, with low slope with regard to the potentials' axis, and
2) A sharper portion, ascending and laying within the more negative potentials area.

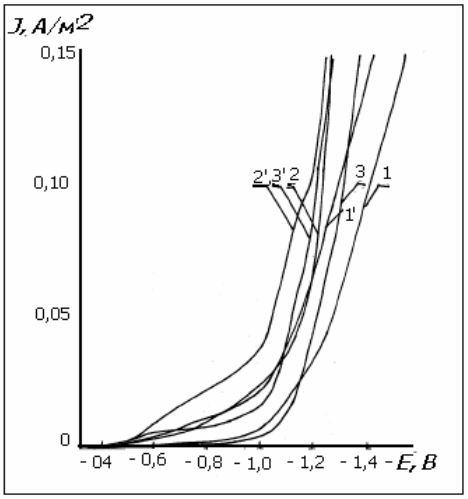

Fig. 1. Cathode PDPC of Fe-electrode in the solution of Zn(II) ions – 0,01 g/l at pH: 1, 1' – 6,1; 2, 2' – 8,1; 3, 3' – 10. Potential sweep speed, mV/s: 1,2,3, - 2; 1', 2', 3' – 10.

The initial portion of cathode PDPC is corresponding to the predominant evolving of hydrogen and gradual covering of iron electrode surface with zinc, which can result in the growth of hydrogen evolving overpotential, compared to the iron cathode, not covered with zinc.

On the ascending portion of PDPC the hydrogen evolving is mainly proceeding, causing the alkalization of by-electrode layer up to pH 9-10 and higher. In our experiments, the cathodic compartment was separated from the anodic one with the porous glass partition.

At the same time, with faster potential reaming (10 mV/s), PDPC are shifted to more positive potential area.

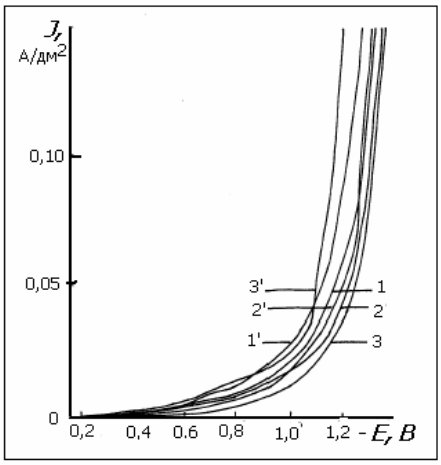

Fig. 2. Cathode potentiodynamic polarization curves of Ni –electrode in the solution (g/l) of Zn(II) – 0,01 and NH_4Cl – 0,024 under pH: 1, 1' – 6,5; 2, 2' – 8,0; 3, 3' – 10. Potentials sweep speed, mV/s: 1,2,3, - 2; 1', 2', 3' – 10.

Such result may be explained by two reasons: 1) acceleration of protons donor reducing on cathode in comparison with the zinc (II) complexes reducing, and 2) lower size of zinc-coated cathode surface and easing of hydrogen evolving on the zinc-free surface of iron electrode, as the hydrogen evolving overpotential on this metal is lower than on zinc surface.

According to the PDPC's obtained, the influence of model solution's pH seems to be more complicated. With the pH growth, no shifting of curves was observed towards any potential area, as soon as the curves 2 and 2' are not placed between the appropriate curves 1,3 and 1'3'. Apparently, this is connected with the change in chemical composition of both zinc donors and hydrogen donors during their reduction on the cathode. It is to be noted that there are two limited currents plateaus PDPC (curve 2'). At the same time, the shift of this curve, and also of curve 2 is observed, towards the more positive potentials area, more than the shift of all the other PDPC. Perhaps, such a result is associated with the low concentration of electrochemically active Zn(II) compounds under pH 8,1 in the model solution (presence of limiting current portions on PDPC 2'), which causes higher iron electrode surface uncovered with zinc, hydrogen evolving and significant alkalization of by-cathode layer. The latter fact should provoke the change in the nature of proton donor in the cathode reaction: water molecules instead of hydroxonium ions.

The research of electrochemical behavior of zinc-containing model solutions with the contents in ammonium chloride (Fig.2), carried out on Ni electrode under various pH with various potentials sweep speed, has shown that the polarization curves are placed within the same potentials area as those obtained in the model solution with no ammonium ions. However, the potential of electrode to which no voltage is applied, in the ammonium-free solution is shifted to more positive area (by about 1 mV). By their form, these cathode PDPC are distinguished with that the initial portions of curves for different pH values are grouped in a more compact way. The lower dispersion is observed for the ascending PDPC branches. These insignificant differences can be attributed to the effect of electrode material (Ni) and the involvement of ammonium ions, equally with zinc complexes and proton donors, in the formation of double electric layer.

Therefore, formation of zinc (II) complexes with ammonia in water solutions starts under the lower pH values (5,0), than the formation of its hydroxides (pH 9,7). In dependence on Zn^{2+} ions and ammonia concentrations ratio under the various pH, the following zinc ammonia complexes may be present in waste waters, with the appropriate instability constants: $[Zn(NH_3)]^{2+}$ ($4{,}26.10^{-3}$); $[Zn(NH_3)_2]^{2+}$ ($1{,}54.10^{-5}$); $[Zn(NH_3)_3]^{2+}$ ($4{,}87.10^{-8}$); $[Zn(NH_3)_4]^{2+}$ ($3{,}46.10^{-10}$); $[Zn(NH_3)_5]^{2+}$ (in very low concentration) and $[Zn(NH_3)_6]^{2+}$, existing within very broad pH area (from 8 up to 13 and higher).

Ammonia complexes with higher coordination number, exist outside the limits of zinc hydroxides formation pH (pH=12). All of them are water soluble and will remain in solution after the alkaline treatment of zinc-containing waste waters, and also after the electrocoagulation treatment of such waters. So, the alkaline treatment of such type of waste waters in view to remove heavy metal would be inefficient, as during this treatment, equally with zinc (II) ammonia complexes, the anion-type hydroxide complexes $Zn(OH)_3^-$ and $Zn(OH)_4^{2-}$ will be present in water solution, due to the amphoteric character of zinc hydroxide. This testifies that with using the above-mentioned treatment methods, the satisfactory removal of zinc from Zn-containing waste waters cannot be reached.

Fig. 3A shows the cathode PDPC obtained in the ammonia-free model solutions. The curves, as in the case of zinc-containing solutions, have initial and ascending branches. The initial branch is thus characterized by the presence of limiting current, which can be attributed to the cathodic process of nickel aqua-complexes reducing, masked by the reduction of protons donors. This conclusion is based on the low value of hydrogen overvoltage on iron surface. With the pH increase, polarization curves are shifted to more negative potentials, due to the involvement in electrode reaction of the available and newly forming nickel (II) hydroxocomplexes, under the higher pH in the by-electrode layer.

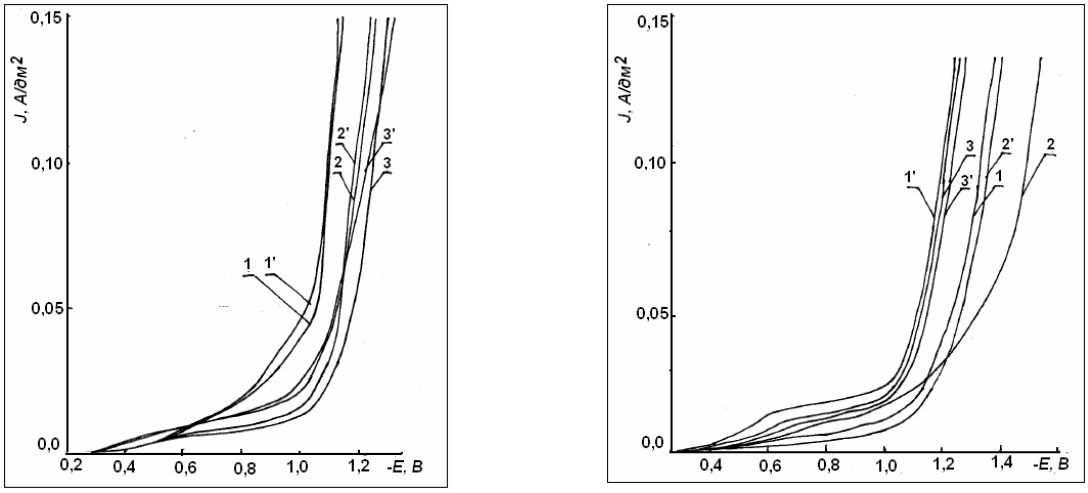

A **B**

Fig. 3. Cathode potentiodynamic polarization curves of Fe-electrode in the solutions, containing (g/l): Ni(II) – 0,01 (A); Ni(II) – 0,01 and NH_4Cl – 0,0037 (B) under pH: 1, 1' – 6,15; 2, 2' – 8,1; 3, 3' – 9,95. Potentials sweep speed, mV/s: 1,2,3, - 2; 1', 2', 3' – 10.

Presence of ammonia ions in model solutions and their effect on the cathode process, in the case of iron electrode, is illustrated by Fig.3B. The higher value of limiting current for the initial PDPC portions is explained by two factors: 1) catalytic effect of labile protons donors, adsorbed on the negatively charged surface of iron electrode and 2) proton-donor and buffer effect of ammonium ions, which to some degree prevent alkalinization of by-cathode layer. We should note that the effect of ammonium ions is most clearly shown on the initial PDPC portions and in the model solutions with lower pH values (6,5), where their buffering role is most clearly pronounced.

As follows from Fig.4, the portions of limited diffusion current with respect to copper ions are clearly shown on PDPC obtained in copper sulphate solution. As could be expected, with the increase of potentials sweep speed, PDPC are slightly shifted to more positive area. The data presented demonstrate that the electrochemical method can be successfully applied for the pre-treatment of the galvanic copper-containing waste waters for the elimination of copper ions.

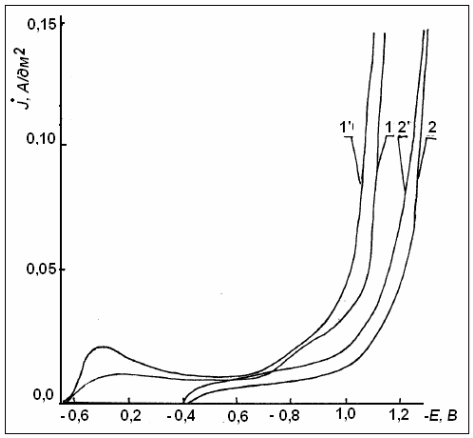

Fig. 4. Cathodic PDPC of Ni-electrode (1, 1') and Fe -electrode (2, 2') in 0,01 g/l Cu(II) solution under pH = 5,3 and potentials sweep speed, mV/s: 1,2 - 2; 1', 2' – 10.

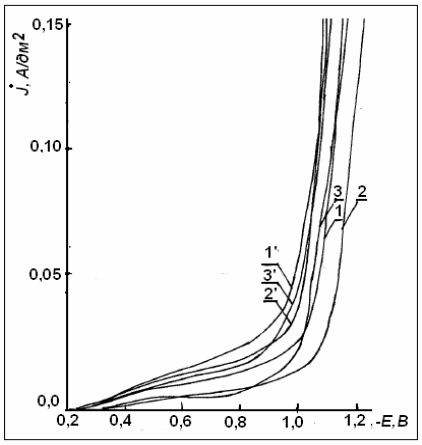

Fig. 5. Cathodic PDPC of Fe – electrode in the solution of ions (g/l): Cu(II) – 0,01 and $Na_4P_2O_7$ – 0,1566 under pH: 1, 1' – 5,8; 2, 2' – 8,2; 3, 3' – 10. Potentials sweep speed, mV/s: 1,2,3, - 2; 1', 2', 3' – 10.

With the decrease in copper ions concentration in by-electrode layer, an increase in current density is observed as a result of the beginning of another cathodic reaction – electrochemical reducing of proton donors with hydrogen evolving on electrode [10]. The overvoltage growth is thus connected with copper, which covers the surface of nickel and iron electrode.

Electrochemical behaviour of copper in pyrophosphate-containing solutions was studied on iron electrode (Fig. 5). Polarization curves, like in previous cases, are characterized with the initial and ascending portions, although they are shifted to about 200 mV in the negative potentials area, compared to the PDPC obtained in the model solutions of acid copper electrolytes. The limiting current is not fixed here in most cases, whereas the smooth ascending of PDPC initial branch is specific.

Thus, at less negative potentials, copper (II) complexes with pyrophosphate-ions having less negative charge, should participate in the cathode reaction. With the by-electrode layer depletion as regards to copper complexes $[Cu(P_2O_7)^{2-}]$, electrode potential and its surface charge becomes more negative. Under these conditions, the cations of alkali elements or hydroxonium ions are mainly adsorbed on the cathode surface. They play the role of cation bridges, which ease the formation of transition state (surface complex) on copper-covered iron electrode surface with participation of both above-mentioned complexes and $Cu(P_2O_7)_2]^{6-}$. The cathodic reaction potential will be thus shifted to the more negative values, and PDPC elevation becomes sharper.

At the ascending PDPC branch both the reactions of electrochemical reduction of copper pyrophosphate complexes occur, along with the process of proton donors reduction. The effect of the potentials elevation rate is similar to the previous case (Fig. 4).

Special attention should be paid to the effect of pH of pyrophosphate-containing model solution on its electrochemical behaviour.

Fig. 5, at first glance, gives no possibility to discern the strict regularities in pH effect on the cathodic process: PDPC are intersecting with each other many times. The curves obtained in more alkaline solutions (pH=8,2), are sometimes in more positive potentials area. It should be considered however, that the conditions of cathodic reactions are determined not only and not so much by pH in the bulk of solution, but sooner the pH value in the by-electrode zone. It could be concluded that it is factor that determines the electrochemical behaviour of pyrophosphate-containing model solutions of plating waste waters (used copper electrolytes). The change in the ration of copper (II) complexes cathodic reduction rates and proton donors reduction (H_3O^+, H_2O, $H_4P_2O_7$, $H_3P_2O_7$, $H_2P_2O_7^{2-}$, $HP_2O_7^{3-}$) will, accordingly, modify the pH of by-cathode layer.

PDPC registered in model solutions of Cr (VI)-containing industrial waste waters on different electrodes (Fig.6) show the step-by-step electrochemical reduction of chromium compounds. There are four portions and two clearly expressed limiting currents on these curves.

The initial portion with low inclination angle is related to the reduction of chromate-ions up to the nearest intermediate oxidation degree of Cr with the involvement of labile protons, playing the role of electron bridges. Starting from -0,8B, the most probably, proceeds the formation and reduction of Cr (III) to Cr (II). The ascending PDPC branch in the area of -1,2 V can be attributed to the joint reduction of proton donors and cationic forms of Cr(III) aquacomplexes and Cr (II) to Cr^0. The similar course is specific for PDPC of chromate-ions reduction on cathode from model solution on Ni-electrode (Fig. 6B).

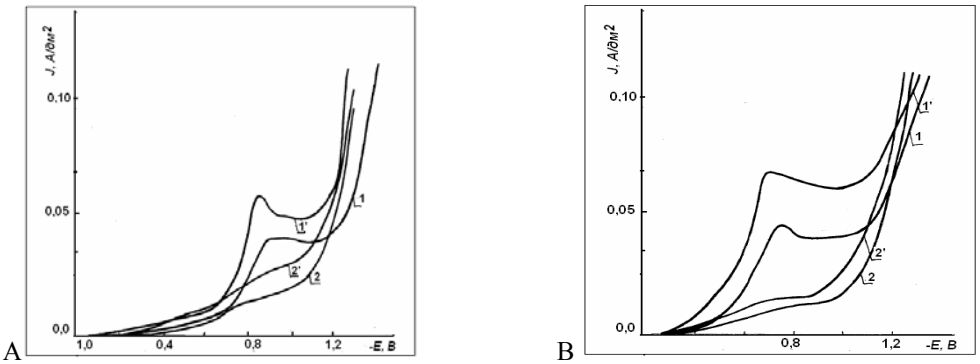

Fig. 6. Cathodic PDPC Cu – electrode (A) and Ni-electrode (B) in the solution of Cr(VI) – 0,01 g/l under pH: 1, 1' – 2,8; 2, 2' – 4,8. Potentials sweep speed, mV/s: 1,2 - 2; 1', 2' – 10.

The following conclusions can be made on the basis of data obtained. Chromium compounds in soluble state can exist equally in acid and neutral and alkaline solutions. The oxidation degree of chromium during the electrochemical treatment can be varied from Cr(VI) to Cr^0.

The specifics of chromium complexes behaviour in acid solutions is interesting from the viewpoint of Cr(III) ions removal from them. Thus, when the alkaline-chemical treatment is applied to obtain $Cr(OH)_3$ hydroxide, it should be taken into account that hydrato-formation reaction proceeds with time. Cr(III) polynuclear aquahydroxocomplexes can be destroyed with difficulty. Besides, chromium hydroxides formed with time are becoming less and less easily dissolvable, due to the transformation to polynuclear forms. "Ageing" of heavy metal hydroxides with time is known for a long time [11].

The amphoteric character of Cr(III) hydroxide and its transformation in soluble anionic hydroxycomplexes should be considered, as well. Such transformation of polymerized ("inveterate") hydroxides also proceeds with time.

Therefore, the alkaline treatment of Cr(III)- and Cr(VI)-containing galvanical waste waters treatment is rather problematic and cannot be recommended for practical uses. Removal of Cr from used solutions requires the application of oxidation-reduction methods combined with the pre-treatment, or using of the appropriate selective sorption methods, or other modern treatment methods, among them electrocoagulation with soluble Fe-electrodes.

Conclusion

Based on the study of electrochemical behaviour of some *d*-metal with amphoteric properties (Zn^{2+}, Ni^{2+}, Cu^{2+}, Cr(VI) and Cr^{3+}) complexes with ammonia and pyrophosphate ligands under the low concentrations in water solutions within the broad pH range, it was shown a complex approach is required to provide the efficient metal removal from such waste waters. As the chemical alkaline treatment for such low-concentrated solutions with the scope to obtain insoluble products which can be separated, would be unacceptable, the electrochemical approach was proposed for the removal of metal ions.

Therefore, it may be recommended to apply the electrochemical method of metal deposition on flow-through carbon fibre cathode. Such electrodes possess high specific surface, which makes it possible to provide the selective deposition of metals under the energy-saving conditions, due to the low specific current densities applied, corresponding to the potential of metal deposition [12].

References

[1]. Juttner, K., Galla, U., Schmieder, H. Electrochemical approaches to environmental problems in the process industry. Electrochimica Acta, Vol.45, Is.15-16 May 2000; pp. 2575-2594.
[2]. Vinogradov S.S. Ecologically safe plating industry/ Ed. V.N. Kudeavtsev. Moscow: Globus, 2002; 352 p.
[3]. Vysomirskis, R.M. Kinetics of Metal Plating from Complex Electrolytes. Moscow: Nauka, 1969; 244 p.
[4]. European Committee for Surface Treatment. "Surface Treatment of metals and plastic materials using electrolytic or chemical process". Reference Document on best available techniques for Integrated Pollution Prevention Control (IPPC). June, 2001, 69p.
[5]. Kozin, L.F. Electrodeposition and Dissolving of Polyvalent Metals. Kiev: Naukova Dumka, 1989; 464 p.
[6]. Popov, K.I., Djokic, S., Grgur, B. Fundamental Aspects of Electrometallurgy. Springer US, 2002; pp. 191-196.
[7]. Antropov, L.I. Theoretical Electrochemistry. Moscow: Vysshaia Shkola, 1984; 520 p.
[8]. Frumkin, A.M., Bagotzky, V.S., Iofa, Z.A., and Kabanov, B.N. Kinetics of Electrode Processes. Moscow: Izd.Mosk.Univ., 1952; 336 p.
[9]. Shishkina S.V., Maslenikova I Yu. Electrodialysis of Solutions Simulating Water in Rinsing Tanks after Zinc Plating from Weak-Acid Ammonium Chloride Baths / Electroplating & Surface Treatment, VI., nr.3, 1998, pp. 41-46.
[10]. Khobotova, E.B., Zaretchenski, V.M. Regeneration of Rinse Water Containing Copper and Ammonia. Electroplating & Surface Treatment, V.3, 1997; pp 43-49.
[11]. Yakovlev, S.V., Volkov, L.S., Voronov, Yu.V., Volkov, V.L. Treatment and utilization of solid wastes from the industrial waste waters. Moscow: Khimia, 1999; 448 p.
[12]. Maslyi, A.I., Medvedev, A.J., Poddubnyi, N.P. Dynamics of copper electro-deposition on the flow-through porous electrode. Electrochemistry, Vol.41, Nr.11, 2005; pp.1335-1339.

PREPARATION OF MICROBIOLOGICAL AGENTS FOR ORGANIC POLLUTANTS REMOVAL IN WASTEWATER

Angela Cincilei*[1], Svetlana Tolocichina[1], Inna Rastimesina[1], Ion Dragalin[2], Veronica Dumbraveanu[2], Nina Streapan[1], Vera Mamaliga[1]

[1]*Institute of Microbiology and Biotechnology, Academy of Sciences of Moldova, MD-2028 Chisinau, R.Moldova*
[2]*Institute of Chemistry, Academy of Sciences of Moldova, MD-2028 Chisinau, R.Moldova*
E-mail: angela_cincilei@yahoo.fr

Abstract: The present article is dedicated to biochemical aspects of degradation processes of persistent organic pollutant benzothiazole by immobilized *Rhodococcus rhodochrous* cells, such as entrapped in Ca-alginate beads, as being immobilized on some solid carries. The mineralization of toxicant was complete and biodestructive capacity of entrapped in alginate rhodococci increased with each new experimental cycle.

Keywords: Benzothiazoles, biodegradation, immobilized cells, *Rhodococcus* sp.

Introduction

Biotechnological processes based on immobilized viable cells have developed rapidly over the last 30 years. The use of immobilized microbial cells (IC) to carry out biotransformation or biosynthesis, and to improve fermentation processes, has been one of the most interesting techniques and has been extensively investigated [1,2]. A large part of published data on IC systems concerns their operation in bioreactors where they perform biosyntheses or bioconversions leading to a variety of compounds. IC cultures have also been widely applied to the treatment of domestic or industrial wastewaters containing different types of pollutants such as nitrate/nitrite ions, heavy metals or organic compounds recalcitrant to biodegradation due high resistance of IC to environmental stresses, in particular, the exposure to toxic compounds.

As physiological point of view, IC systems can be separated into wholly artificial and naturally occurring ones. In the first category, microbial cells are artificially entrapped in or attached to various matrices/supports where they keep or not a viable state, depending on the degree of harmfulness of the immobilization procedure. Polysaccharide gel matrices, more particularly Ca-alginate hydrogels, are by far the most frequently used materials for harmless cell entrapment [3].

In comparison with free suspended cells, immobilized cells exhibit tolerance to toxic substances [4], enhance fermentation productivity [5], can adapt to a wide range of pH environments [6] and high process temperature [7,8] and are re-usable [9,10] (Tab.1). Published results show contradictory effects of immobilization on growth rate, i.e. decreased, unchanged or enhanced growth rates of IC compared to free cultures [11-13]. Mass transfer limitation in IC systems gives the most evident explanation to reduced IC growth rate. On the other hand, the growth-promoting action of immobilization has been attributed to protective effects of the support, e.g. against high-shear environment [14] or acidification [6,15].

Table 1

Potential advantages of viable IC systems over conventional fermentations (adapted by Junter a.Jouenne, 2004 from Mattiasson, 1983)

(a)	**Higher reaction rates due to increased cell densities**
(b)	Possibilities for regenerating the biocatalytic activity of IC structures
(c)	Ability to conduct continuous operations at high dilution rate without washout
(d)	Easier control of the fermentation process
(e)	Long-term stabilization of cell activity
(f)	Reusability of the biocatalyst
(g)	Higher specific product yields

The biodegradation of toxic compounds also represents a preferential application field of IC systems. The high biodegradation efficiency and operational stability of IC cultures, highlighted for instance, during continuous biodegradation assays of phenol and phenolic derivatives, is typically ascribed to some protecting effect of the immobilization support [16], rather than to enhanced specific degradation capacity that might involve physiological modification in IC. IC is also characterized by a high resistance to antimicrobial agents such as biocides and antibiotics. This resistance has been observed for artificially immobilized microbial cultures, e.g. alginate entrapped bacteria exposed to sanitizers [17] or antibiotics [18], but more frequently for natural IC systems, namely biofilms, which are implied in a variety of industrial, environmental and medical situations.

Benzothiazole (BT) and its derivatives (BTs) belong to an extensive family of synthetic compounds. BTs are used in various fields e.g. in the tire industry as catalysts in vulcanization processes, as medicines, as pesticides/ biocides and in the manufacture of azo-dyes [19]. As a consequence of their large range of applications, these compounds are often found in the aquatic environment [20]. Some of these compounds are attributed to persistent organic compounds with carcinogenic properties [21]. Therefore, it is important to investigate the processes of pollutant detoxication with the help of active micro organisms capable of bringing about a complete degradation of the target compound.

Results and Discusion

***Cells immobilization on alginate*:** Generally, the biodegradation of benzothiazole by active cells of bacteria *R.rhodochrous* OBT 18 in suspension is complete in the first 3 hours from the start of the experiment. The process is accompanied by the appearance of two metabolites - 2-hydroxybenzothiazole (OBT), and dihydroxybenzothiazole (diOBT), which transformations to the complete disappearance occur quickly. Thus, the complete mineralization of BT (including metabolites) lasts 10 hours [22].

We know about successful examples of degradation of organic pollutants with the active bacteria, immobilized in alginate of 2.0% [23], 2.5% [24], 2.6% [25], 2.7% [26]. Therefore, we tried to find the minimal useful concentration of alginate career in order to avoid the mass transfer limitation in IC system. For this purpose, the repeated (3 cycles) degradation of BT by rhodococci immobilized in five different concentrations of alginate (1.5 …. 3.5% w/v) was compared. The beads forms, shapes, their stability were analyzed visually for 3 cycles 24 hours each and more (till 7 days of incubation). Neither changing of the beads shape, no opalescence of BT solution was noted for variants 2.0-3.5% alginate. For the next experiments the optimal concentration of alginate – 2.0% has been chosen, to assure a good diffusion of xenobiotic, metabolites, and oxygen in alginate / water system.

BT, with a concentration from 300 mg L^{-1}, or 2.2 mMol, is toxic for *R.rhodochrous* bacteria. Or, one of recognized advantages of immobilization of active microorganisms on solid supports is the protection of microbial cells against the toxic action of organic compounds and its metabolites subdued to the transformation. In the variant of BT 1.0 mMol degradation, the experimental analyze of data obtained by the HPLC method showed the high destructive efficiency of the alginate immobilized bacteria during the 3 consecutive cycles. More than that, the destructive capacity of immobilized bacteria increases by every cycle (Tab.2).

Table 2

Degradation of 1.0 mMol BT by immobilized in Ca-alginate 2% rhodococci, the 3 cycles of degradation

Incubation, hours	BT 1.0 mMol + 2% (alginate with cells)				BT 1.0 mMol + free cells			
	BT, mMol	OBT, mMol	diOBT, area	% degr.	BT, mMol	OBT, mMol	diOBT, area	% degr.
Ist cycle of degradation								
0	0,94	-	-	6,0	0,99	0,008	-	1,0
3	0,48	0,17	2,6	52,0	0,26	0,37	3,8	74,0
5	0,22	0,28	4,4	78,0	0,03	0,41	8,5	97,0
24	-	0,01	-	100,0	-	-	-	100,0
2nd cycle of degradation								
5	-	0,19	5,5	100,0				
24	-	0,01	-	100,0				
3rd cycle of degradation								
5	-	0,11	5,8	100,0				
24	-	0,01	-	100,0				

Thus, after 5 hours of the 1st cycle in the water were found 22% of residual BT that was missing in the 2nd and 3rd cycles, after 5 hours. This phenomena shows the good estate of immobilized in alginate bacteria. The chosen organic support allowed the multiplication, inside of it, of the active bacteria, so that the rate of biodestruction increases with each new cycle of treatment.

The decrease of destructive capacity of immobilized in alginate bacteria when high concentrations of BT can be attributed to the decreasing of the number of bacteria cells inside of the alginate through the duration of a degradation cycle. For verifying this hypothesis, there was measured the number of viable cells (colony-forming units, CFU) inside the alginate beads before and after first cycle of degradation, in two extreme concentration of BT – 1.0 and 5.0 mMol. The obtained data showed the strong reduction of the number of bacteria in the alginate - to 0,64 x 10^7 CFU per alginate bead – in the variant 5.0 mMol BT after 24h of the first cycle of degradation. In opposition to this, as it was confirmed by the HPLC analyzes, the alginate assured the good state and the destructive efficiency of *R.rhodochrous* bacteria, for the concentration of BT 1 mMol: the number of rhodocci increased with approx.206%

(or by 3.1 times) and was 3,3 x 10^7 CFU per bead (after 24h of the Ist cycle of degradation) compared to 1,08 x 10^7 CFU per initial bead.

Thus, the chromatographic researches of biodestructive efficiency of alginate immobilized active microorganisms were completed and confirmed by microbiological complementary studies of the interested bacteria.

Mainly, by applying two essentially different methods, we showed the preservation of good physiological state of the cells, immobilized in 2% alginate. In case of concentration of approx 135 mg/L BT (1 mMol), the chosen organic support respects the natural metabolic activity and the multiplication of bacteria, so that the rate of biodestruction of toxicants and the number of rhodococci increase with each new cycle of biotransformation. This phenomena comes to confirm the special capacities of calcium alginate hidrogels, that are frequently used as support for a light, tolerant, non-agressive immobilization („harmless cell entrapment") of the living cells, in our case - of the microorganisms, and that respect the natural phisiological state of the immobilized cells [27].

***Cells adsorption on solid support*:** One of the major objectives of our researches was to provide a simple, low-cost and efficient carrier and to find immobilization techniques for preparing immobilized microbial cells with the goal of application in waste water treatment. Readily available, low-cost carrier, namely sawdust, alluvial quartz sand, activated carbon (from walnut shell, and from grapes seeds), and diatomite-containing material were tested as supports for adsorptive immobilization of *R.rhodochrous* cells. Physico-chemical modification (hydrophobization) of sawdust was performed, in order to increase the adhesion of bacteria. Results of laboratory trials showed that solid supports (sand, diatomite, and activated carbon) demonstrated significant level (11,2-7,0 mg dry cells g^{-1}) of bacterial immobilization. However, even with the saturation before experiment, the carbon support produces a strong absorbtion of toxicant and doesn't permit to observe the real BT biodegradation process.

In the case of immobilized in the tested solid support bacteria, unlike those immobilized in alginate, complete biodestruction of the toxicant didn't occured. Nevertheless, the results show the superiority of diatomite-immbolized bacteria, that assures 53,2% (I cycle) and 35,5% (II cycle) of BT degradation after 24h of incubation. Also we noticed a clear apparition of OBT in a incubation medium during two cycles.

Although the sand assures a good immobilization of 52,8% from initial quantity of bacteria, the efficiency of BT biodestruction with immobilized in sand rhodococci is low – 19.3%, from which 4.7% can be atributed to abiotic phenomena.

Our experiments of cells entrapment and adhesion on the support materials were confirmed by scanning electron microscopy investigations (Fig.).

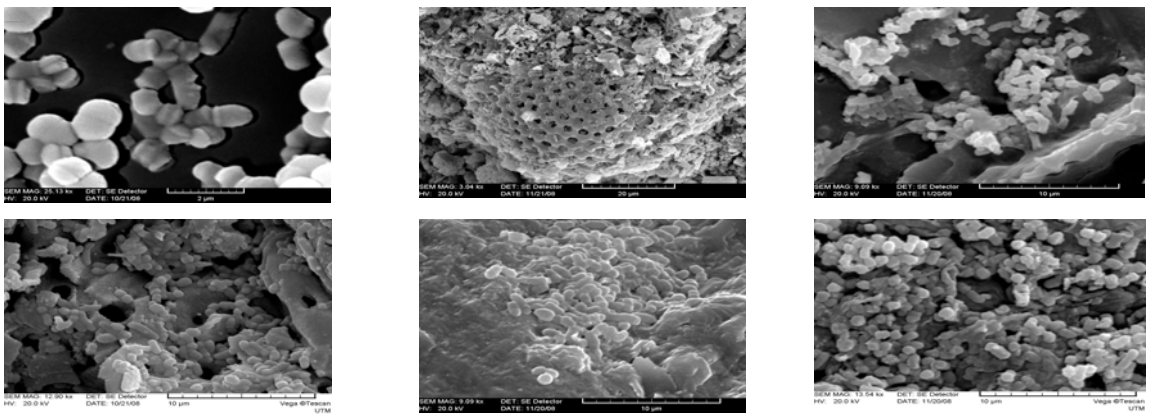

Fig.: (left to right): free and immobilized bacterial cell of *R.rhodochrous* on the support materials: diatomite-containing material, activated carbon from walnut shell, sawdust, quartz sand, and within alginate beads.

The sand, diatomite-containing material and activated carbon as support materials have been shown to assure a good absorbance of bacteria (52.8, 38.7, and 32.8%, respectively), and were selected as carriers in the new combined photo-catalytical bio-reactor [28].

Conclusions

In conclusion, immobilized in alginate active *R.rhodochrous* OBT 18 bacteria assures the complete mineralisation of pollutant in pure water in the first 5h of experiment, and these biodestructive capacity increases with each new cycle. More than that, the alginate support offers the necesary conditions for the natural metabolic activity and multiplication of active bacteria within it. The optimal conditions, that assures the complete elimination of BT by the strain *R.rhodochrous* OBT18 through several repeated cycles are: concentration of bacteria in alginate – 2.5%, of alginate – 2.0%, of BT – up to 135 mg/L.

The prezented researches contributed to the elaboration of the efficient microbiological method of distruction of organic compounds, using the microorganisms immobilized on solid support, and will be implemented in modern regional biotechnologies of environmental decontamination. The diatomite and alginate were recommended as carriers in the new hybrid solid support of immobilizing.

Experimental

The object of study was water solution of benzothiazole, purchased from Aldrich Ltd (Gillingham, Kent, UK).

BT transformations by rhodococci were studied in "resting cells" experiments with free and immobilized cells by HPLC method. Bacterial strain *R.rhodochrous* OBT18 from LSEESIB (Blaise Pascal University, France) were used. Cell immobilization was performed by entrapping in calcium alginate matrices (2.0% w/v) [27], or by absorption in solid supports (2,1% w/w) [29]. The percentage of immobilized biomass was estimated by two different methods: 1) indirectly through turbidity measurement as absorbance at 540 nm before and after immobilization procedure, 2) directly, by counting the CFU in serially diluting samples of aliquots planted onto nutrient agar. The resting or immobilized cells were incubated with 1.0 mMol BT in 300-mL Erlenmeyer flaks at 28°C under agitation (200 rpm) [22]. The negative controls lacking BT, supports or cells were incubated under the same conditions.

HPLC analyses were performed in isocratic conditions using an Agilent 1200 chromatograph fitted with a pre-column and reversed-phase column Zorbax Eclipse XDB 5 µm (C_8 150 x 4.6 mm) at room temperature. The mobile phase was acetonitrile-water (25/75, v/v), with a flow rate of 1 mL/min, vol.inj. – 5 mcL; λ=265 nm.

Scanning electron microscopy investigations were performed by VEGA TS-5130 microscop.

Acknowledgements

This cycle of researches was supported by Institutional project 06.411.016 A, and INTAS Ref.Nr.05-104-7596.

References

[1]. Wijffels, R.H., Ed. Immobilized cells. Springer Verlag: Heidelberg, 2001.
[2]. Junter, G.A.; Jouenne, T. Biotechnol.Advances. 2004, 22, 633-658.
[3]. Gerbsch, N.; Buchholz, R. FEMS Microbiol Rev. 1995, 16, 259-269.
[4]. Lee, S.L.; Cheng, H.Y.; Chen, W.C.; Chou, C.C. Process Biochem. 1998, 33, 453-459.
[5]. Kim, D.J.; Chang, H.N. Biotechnol.Bioeng. 1990, 36, 460-466.
[6]. Buzas, Z.S.; Dallmann, K.; Szajani, B. Biotechnol.Bioeng. 1998, 34, 882-884.
[7]. Bajpai, P.; Margaritis, A. Biotechnol.Bioeng. 1987, 30, 306-313.
[8]. Tan, Q.; Day, D.F. Appl.Microbiol.Biotechnol. 1998, 42, 22-27.
[9]. Paik, H.D.; Glatz, B.A. Appl.Microbiol.Biotechnol. 1994, 42, 22-28.
[10]. Lee, S.L.; Cheng, H.Y.; Chen, W.C.; Chou, C.C. Process Biochem. 1999, 34, 845-850.
[11]. Galazzo, J.L.; Bailey, J.E. Biotechnol.Bioeng. 1990, 36, 417-426.
[12]. Muyima, N.O; Cloete, T.E. Water Res. 1995, 29, 2461-2466.
[13]. Pashova, S.; Slokoska, L.; Sheremetska, P.; Krumova, E. et al. Proc.Biochem. 1999, 35, 15-19.
[14]. Chun, G.-T.; Agathos, S.N. Biotechnol.Bioeng. 1991, 37, 256-265.
[15]. Taipa, M.A.; Cabral, J.M.; Santos, H. Biotechnol.Bioeng. 1993, 41, 647-653.
[16]. Dervakos, G.A.; Webb, C. Biotech.Adv. 1991, 9, 559-612.
[17]. Trauth, E.; Lemaitre, J.-P. Rojas, C.; Divies, C.; Cachon R. Lebensm-Wiss Technol. 2001, 34, 239-243.
[18]. Coquet, L.; Junter, G.-A. ; Jouenne, T. J.Antimicrob.Chemother. 1998, 42, 755-760.
[19]. Bunescu, A.; Besse-Hoggan, P; Sancelme, M.; Cincilei, A. et al. In: Wang B., Ed. Environmental Biodegradation Research Focus. Nova Publishers: New York, 2008; 159-187.
[20]. De Wever, H.; Weiss, S.; Reemtsma, T.; Vereecken, J. et al. Wat. Res. 2007, 41, 935-945.
[21]. Gaja, M.A.; Knapp, J.S. J.of Appl.Microbiol., 1997, 83, 327-334.
[22]. Besse, P.; Combourieu, B.; Boyse, G.; Sancelme, M.; De Wever, H.; Delort, A.M. Appl. Environ. Microbiol. 2001, 67, 1412-1417.
[23]. Paje, M.L.; Marks, P.; Couperwhite, I. World J. of Microbiol. and Biotechnol. 1998, 14, 675-680.
[24]. Velankar, H.R.; Heble, M.R. Electronic J.of Biotechnol. 2003, 6 (2), 90-103.
[25]. Chang, Y.; Chou, C. Biotechnol.Appl.Biochem. 2002, 35, 69-74.
[26]. Mordocco, A.; Kuek, C.; Jenkins, R. Enzyme Microb. Technol. 1999, 25, 530-536.
[27]. Chorao, C.; Charmantray, F; Besse-Hoggan, P.; Sancelme, M.; Cincilei, A. et al. Chemosphere. 2009, 75, 121-128.
[28]. Covaliova, O.; Covaliov, V.; Delort, A.-M.; Mailhot, G.; Cincilei, A. Patent MD 3911 F1 2009.
[29]. Kitova, A.E.; Kuvichkina, T.N.; Ilyasov, P.V. et al. Appl.Biochem and Microbiology (Russian), 2002, 38, 585-590.

THE CONTENT OF OCHRATOXIN A IN MOLDAVIAN WINE PRODUCTS

Boris Găină[1], Rodica Sturza[2], Violeta Bejan[2], Constantin Bodean[1]

Moldavian Academy of Science[1], Technical University of Moldova[2]
E-mail: sturzar@yahoo.com

Abstract: The basic objective of this work is studying the content of ochratoxin A (OTA) in grapes, grape juice, and wine. This is an analysis of their origin, the conditions of contamination and ways decontamination, toxiconogenes mushrooms, toxicity, world and European regulations. It was estimated the methods of detection of mycotoxins in wine products. It has examined the contents of OTA in the moldavian juice/wine from different varietals at different stages of winemaking and obtained by different proceeds winemaking.

Keywords*:* mycotoxin, OTA, wine, grape juice.

Introduction

The United Nations Food and Agriculture Organization (FAO) estimates that about 25% of world production of food is contaminated by mycotoxins and the burden of mycotoxins causes the loss of nearly 1000 million tons of food each year. Mycotoxins may be listed without our knowledge in our everyday dishes [1].

On completion of toxicological tests, the OTA has been shown nephropathy, carcinogenic, teratogenic and immunosuppressive and was listed in the list of dangerous molecules [14]. Several human diseases attributed to this mycotoxin, such as kidney disease endemic countries in the Balkans and tumors of the urinary tract and kidney observed in Tunisia and Egypt and the detection of this molecule in the blood of healthy individuals or not around the world have shown great danger and the large exposure of humans to this mycotoxin. If the air and building materials are recognized as agents of exposure to this molecule food remains the main vector of contamination.

Whether in the animal or plant products, different levels have been detected. The products from the cereal sector are the most contaminated and participate for 50 to 80% by ingestion of OTA by men. The contamination by OTA products in the pipeline grape has been detected in 1996. This path is then ranked 2nd after the cereal sector for its contribution to the ingestion of human OTA estimated at 15% [14,15]. The factors influencing OTA production are:

- OTA formation in grapes is mainly due to berry contamination by certain mould species, belonging essentially to the black *Aspergillus* species (in particular *Aspergillus carbonarius* species and to a lesser extent *Aspergillus niger*), but also to *Penicillium* species in cool temperatures regions;
- The growth of these molds occurs at air humidity levels of 72% to 90% and temperatures of 12°C to 39°C (optimum 28°C);
- The presence and spread of such fungus in vineyards are influenced by:
  - environmental and climatic factors (high humidity, hot and dry environments)
  - nocturnal dampening condition of grapes
  - grape bunch shape
  - aeration level of grape bunch
  - susceptibility of vine varieties
  - health status of grapes and berry injuries which are the main entry points for ochratoxinogenic fungus
  - skin thickness
  - use of fungicides
  - winemaking procedures
  - Damaged berries by Lobesia Botrana (worm grape).

Some importing countries have introduced restrictions on the content of mycotoxins and particularly of OTA in wines [5,15]. It is known that the European Union (EU) has already set a maximum limit of 2 μg/l of OTA in wine (red, white and rose) and other beverages based on mash of wine and / or grape. This limit applies to products from the 2005 harvest. Other countries, like Canada refuses imports of wine with more than 1 μg/l of ochratoxin A.

Requests for the harmless of wine products are becoming more stringent, limits or permissible concentrations of different toxins increasingly reduced, which requires that the source of an outbreak are considered multilaterally and complexity. That is why it is necessary to know this toxin (structure, properties, and regulatory acts) to study the sources of mycotics pollution, molds that attack vines producing OTA and for the development of processed effective prevention of the occurrence of toxins, complete decontamination or decrease the concentration under the permissible limits of international mash of wine and wine. In a context of increased competition, consideration of this very important issue by all wine is a priority.

In this context the study of mycotoxins in wine is very current and important, particularly by the fact that their toxicity has been demonstrated and we must know our wines to be exported.

Two vilifications technology were studied to monitor the OTA throughout the winemaking: the white wine and red. The purpose of the study was to determine the concentration of OTA in wine products at different stages of winemaking. It focused on the analysis of samples of reds: Cabernet Sauvignon, Merlot, Pinot noir, Lidia, Bastard and those white Feteasca, Muscat, Saperavi.

Materials and Methods

The analytical methods for OTA determination in foodstuffs are [9,13]:

- AOAC–2001.01IAC-HPLC with fluorescence detection
- CEN – EN 14133:2003
- MA-F-AS315-10-OCHRAT
- ELISA quantitative method
- Screening method (strip, yes/no response).

Moldovan wines in the detection of OTA done in the laboratory of the National Center for Quality of Wines by the enzymatic method with quantitative spectrophotometrical (650 nm) detection (ELISA quantitative method) [3,4]. It applies to the reds, whites, roses and the special wines and beer in the concentration limit of 0,2 - 25 μg/l (ppb). In the situation of higher concentrations are diluted samples in accordance with the instruction. The detection limit is 0,1 μg/l, the limit of quantification of 0,2 μg/l. This method can be applied to the determination of OTA in sparkling wines and sparkling after a PMD.

The principle of this method is a test immunosorbent directly connected with enzymes (CD-ELISA), which allows to obtain accurate concentrations in parts per billion (ppb). Ochratoxin samples and control substances involved together with other enzymes for places Liaison antibodies. After washing, adding the substrate, this reacts with the substance combined process accompanied by the appearance of the color blue. The intensity of color is inversely correlated with the content of the OTA in the sample. The results of this test are discussed in a micro alveolus for checking optical densities. The optical densities of control samples are the standard curve, to calculate the exact concentrations of OTA for tests.

This procedure is automated; the calculation is done directly by the Neogene-VERATOX device that presents information in the form of an analyst with the Packing of the curve indicating the contents of the OTA and fidelity of this test. For red wine is made sedimentation tannins with a special set Veratox.

For this study 22 samples of juice, mash of wine, and wine were analyzed. It was selected wines of our republic in dependence of the following criteria:

- by color
- depending on the contents of residual sugar
- Manufacturing Technology

Depending on the color used on a juice/must/white wine and red, while the manufacturing technology of sparkling wine and alcoholic dessert. Regarding the content of residual sugar and wine taste dry and semisweet were analyzed.

The absolute difference of two results of independent analysis conducted on identical material, using the same equipment in a short period of time not exceeding the limit r repetition more than 5% of all cases.

Results and Discussions

In the world we know more than 1000 species of fungi that grow on different parts of the vine. With us this number is reduced is less is more than 400 species. The microflora exchange dependence on environmental conditions, climacteric, the system of protection against disease and insects, agricultural technology used [2]. Macroclimate thus has a significant impact on the burden and fungal contamination OTA grapes.

In addition to the factors temperature, humidity and rainfall, the composition of sugar and acidity of the grapes direct substrate are critical factors in the mycotoxinogenesis.

Moldova has a temperate continental climate with a slight influence sea view near the Black Sea. The winters are cold, relatively mild in the south, with average temperatures ranging between - 3 - 5 degrees C in January. Summers are hot and sunny: the average temperature exceeds 20 ° C in July to about 40 ° C. The summer heat is tempered by a strong breeze blowing an almost permanent south-east. So the temperature is optimal for the development of fungi. *Aspergillus ochraceus* is developing moderate temperatures ranging between 8 and 37 ° C with an optimum between 24 and 37 ° C [6].

Another factor favoring the development and growth of mold is moisture. In our rainfall is low and irregular. The average rainfall per year is 450 mm in the south, 560 mm in the center and 680 mm in the north. The availability of water combined with other favorable factors is sufficient to result in the emergence and development of fungi producing OTA.

There are generally two types of risk: the risk biological and chemical hazards. Biological hazards are due to uncontrolled development of living organisms. The prevention of risks of contamination by microorganisms is an important issue for all players in the wine industry. The case of OTA is an example.

In the literature review conducted earlier, it was a synthesis of multiple factors that influence the content of OTA in wine products [6,7,11]. Some of them are interested for us that are why the part of this test was examined. It was interesting to know the content of the toxin for different types of wine at different stages of winemaking, the role of certain technological processes as well as the health cluster, sort of harvest, developments during the OTA the conservation of bottled wines.

Table 1

The comparative content of OTA in certain wine products*

Nr	Witness	OTA content in µg/l (ppb)
1	white grape juice	0.1
2	red grape juice	2.6
3	Muscat mash of wine	0.5
4	Cabernet mash of wine	3.0
5	Merlot row material	0.5
6	Muscat	0.3
7	Muscat Blanc	0.1
8	Feteasca	0.1
9	Saperavi	> 2
10	Sangria	0.12
11	Merlot	< 0.1
12	Cabernet-Sauvignon	0.9
13	Bastard	> 2
14	Lidia	0.4
15	Zemfira	0.2
16	Rosu de Etulia	< 0.1
17	Chardonnay dry wine	< 0.1
18	Pinot dry wine	0.5
19	Semisweet wine Chardonnay	< 0.1
20	Kahor	0.6
21	Sparkling Wine	0.1

** r = 0,982*

Our study was proposed to determine the degree of contamination by OTA Moldovan wines. Following this analysis has been obtained very important and surprising. The data obtained are presented in the table 1. The maximum of OTA content (3 µg/l) was detected in the must from the red grape Cabernet Sauvignon. In the majority of witnesses studied the minimum level of the toxin did not exceed 0,1 µg/l. We can conclude that our wines are not beyond the maximum permissible ochratoxin A in all types of wine, but also drinks made from wine or grape, grape juice and ingredients based juice grapes, 2 µg/l, set by the Regulation of the European Commission in 2005. This fact once again demonstrates that the Moldovan wines are harmless. So we can conclude that the wines of our Republic can compete with New World wines (Chile, Argentina, New Zealand, Australia, etc.) regarding this health problem [9-11].

One of our goals was to establish the content of the mycotoxin at different stages of winemaking evolution of OTA during the red wine which is presented below (Figure 1).

The evolution of OTA during the red winemaking includes five steps:

1: from veraison to mature;
2: after a few days of maceration;
3: at the end of fermentation;
4: at bottling (3 months after completion ALF and collage FML + + filtration);
5: stage after bottling.

The concentration of the mycotoxin has been studied in grapes and wine and its evolution from veraison until bottling.

The first step includes the ripening period until maturation. The OTA may appear very early on grape (30 days before harvest). During this period there was a reduced level of OTA. The fungus is installed on grape berries

damaged, develops preferentially at the heart of clusters, and it continues to harvest. 15 days before harvesting the concentration of the toxin begins to increase the award of costs of the must.

The second period is that of obtaining the must charge until maceration for 15 days. It is observed that the wine fermentation reached a level close to the maximum OTA because of existing factors that promote its extraction.

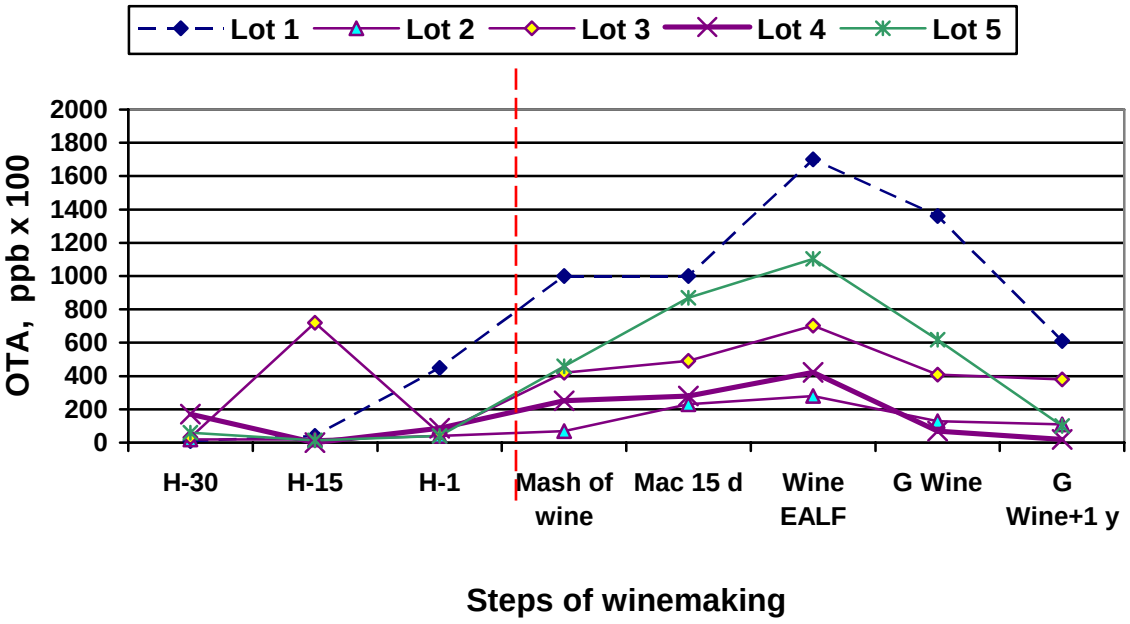

Figure 1. **OTA content evolution during the winemaking of red wine**

The third stage is the end of the fermentation (ALF) when OTA reached a maximum. The fourth step is bottling (3 months after completion ALF and collage FML+filtration), OTA has decreased by 39% on average. We can conclude that the collages are made effective in lowering the content of the mycotoxin.

The last step is after bottling and storage for a year. OTA content seems to diminish after bottling what makes us think that during the breeding OTA migrates in the filing.

Thanks to research that has been able to make the comparison between the content of the OTA in various alcoholic beverages and raw materials necessary for obtaining beverage was analyzed. In the first study it was determined the OTA in white grape juice and red in the must obtained from a white and red grape and wine in a white and red. The varieties were studied Muscat, Merlot and Cabernet Sauvignon. It was observed that the content of OTA is highest in juice, must and red wine, the maximum being prepared for the must Cabernet (3µg /l), so the reds are more susceptible to contamination.

In this study we have concluded that red wine is more contaminated by the toxin than white what has demonstrated the truthfulness of theoretical data available so far on this subject. The red wine requires a skin maceration that occurs before and during fermentation. The white wine this process completely excludes. This study confirms the work [11], that the OTA on this film, is found more easily in winemaking where maceration are important. The maceration process is a physical rather than chemical based on the extraction, distribution and adsorption which consists of maintenance of solids and liquids in contact for some time in certain conditions. It is likely that toxins on the solid berries are extracted in the juice along with the color, tannins and aromas. That is why OTA quantities are larger in red wine than in white or rose wines. The high contamination red mash of wine is also explained by the presence of conditions favorable for the development of mushroom toxin. The temperature and humidity play a role on growth, development and physiology of mushrooms. *Aspergillus ochraceus* indeed develops at moderate temperatures ranging between 8 and 37 °C with an optimum between 24 and 37 ° C, temperatures existing during the process of maceration.

To make a more complex analysis of wine we used as samples of grapes from different species of wine from various groups: Eurasian Group (Vitis vinifera) and group of North America (Vitis labrusca). Vitis vinifera is represented by Muscat Blanc, Merlot, Cabernet-Sauvignon. The varieties of Vitis labrusca group studied are: Lidia, Zemfira. The result turns to the wines made from Vitis labrusca have a higher content OTA from 2 µg/l than Vitis vinifera (Table 1).

The conservation of bottled wines is reflected by a decline in toxin by processes known and poorly studied. Several samples were used; the conclusion is that the content in bottled OTA decreased each wine (red or white wine). The average decrease is higher than 40%.

The results suggest that there is a continuous decline of the toxin from up to the end of vinification. The OTA who "disappeared" on the wine bottle is found mostly in the filing it is probably precipitated or adsorbed by the compounds that make up the deposit. The failure to find any deposit in the OTA initially present in the wine comes, probably, the difficulty of the determination of mycotoxin in the filing. While the bulk of the decline in the OTA on wines is reflected in the deposit, the runway part of its metabolism is not excluded.

The red grape juice shows that the content is higher - 2,6 ppb, but it is less compared to the mash of wine. Among the factors favoring the production of the toxin is the states of maturity at which the grapes were crushed, his health status, sort of harvest (Figure 2). In this context, we can mention that the sorting of the grapes is a process not commonly practiced in enterprises with Moldovan wine.

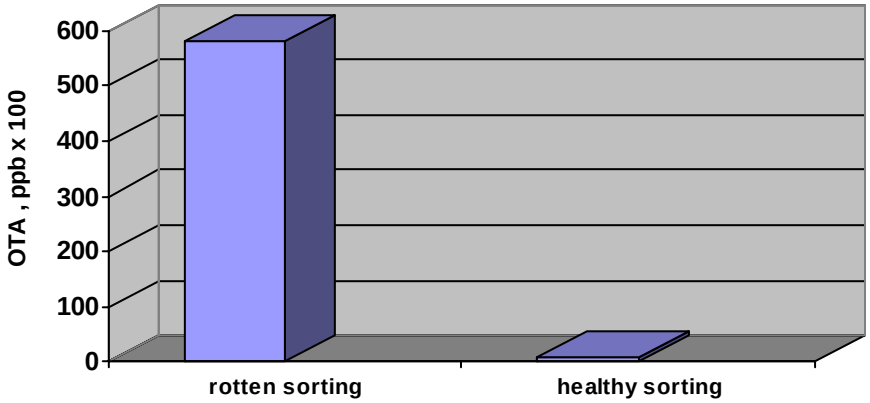

Figure 2. **Content of the OTA in wines from the rotten sorting and healthy sorting**

The ill health of the grapes is considered the main factor for the development of OTA in wine. A rotten harvest does not provide optimal security products. There is evidence that a high contamination of grapes by OTA involves a heavy contamination of wines produced. The master plant becomes a priority for the development of healthy wine with levels limits OTA. With the increasing maturity of grapes increases the risk of contamination with OTA and if the grapes are in a bad health risk becomes higher (Figure 3).

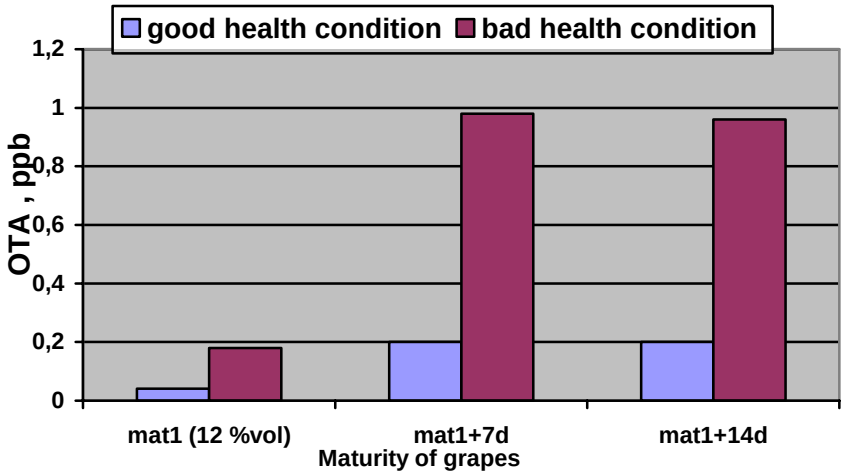

Figure 3. **Impact of health status and level of maturity of grapes on the contamination of wines in OTA (ICV data on 84 wines)**

This work took aim studying the content of OTA in different types of wines. The dry wine and white grape semisweet of Chardonnay and Pinot noir red were also discussed the purpose of determining the dependency of the presence/absence of residual sugar and the concentration of toxin. From table 1, we find that the content is 0,1 μg/l corresponding to the regulation, both for red wines than for whites. This allows us to say that the residual sugar is not a factor influencing the emergence and development of fungi producing toxins. The dry wine Pinot noir is the most contaminated (0,5 μg/l) but yet its content does not exceed the permissible level of OTA. The content of the OTA in wine is generally lower than in must by the fact that the content in the bottle decreases.

According to literature reviews found that among the factors influencing the presence of the toxin: temperature, humidity, type of substrate, and is the gaseous composition. Technology sparkling wines requires the formation of CO_2 content is very low, we can assume that this is probably the pressure and the presence of CO_2 gas that affects the content of the OTA. It is already known that the formation of this toxin is inhibited to 30 % CO_2.

Regarding the presence of alcohol, conducted according to a convex model, there is a significant inhibition of growth from a concentration of 2% ethanol. From 1 until 3% of ethanol production is stimulated and OTA has achieved the most important values to the concentration of 2% or an increase of 6 times for *Aspergilius carbonarius* Mu243 and 13 times for *Aspergilius niger* G731. Beyond 3% inhibition of total production of OTA was observed. The fermentation, implemented in the manufacture of wine, is deteriorating largely OTA present in grape juice or cereals used. OTA content decreases by 35% on average during the fermentation.

The yeast fermentation ensuring adsorption capacity of OTA more or less important depending strains. Tests in 2004 showed that the adsorption was higher in musts contaminated red white. The 2005 results confirm that over a yeast adsorb the color of it adsorb OTA. A choice in the strain of yeast is possible. These differences between yeast are significant red wine; one possible explanation is that the polyphenols may interact with these phenomena adsorption. Different groups of yeast have been identified, some of whom may trap 30% of OTA, further to 57%.

However, it is unclear today what the metabolites from this are and what stages of fermentation process occurs degradation. Such knowledge is essential to determine the dangers associated with the presence of the OTA in musts: they are not necessarily restricted to OTA remaining in the wine, but may also include those related to metabolites of degradation.

Regarding the malolactic fermentation research is needed because we do not know until now its influence on the evolution of the content of the toxin.

References

[1] Pfohl-Leszkowicz. Les mycotoxines dans l'alimentation. Evaluation et gestion du risque. Conseil supérieur d'hygiène publique de France, coord. Paris: 1999, pp. 3-14, 17-30, 141-169, 409-427.
[2] Gaina, B. Biotehnologii ecologice viti-vinicole, Chisinau, 2007, pp. 34-37.
[3] Gaina, B.; Sturza, R.; Bejan, V. Ochratoxina A- una dintre toxinele din vinuri, Viticultura si vinificatia in Moldova, 2007, 5(11), pp. 19-20.
[4] Cutzach-Billard. Etude comparative d'une methode semi-quantitative pour la détection de l'Ochratoxine A, Revue des œnologues, 2006, 121, pp. 43-45.
[5] Dumoulin, M., Riboulet, J. M. Réflexions sur la présence d'ochratoxine A dans les vins et les jus de raisin. Revue Française d'œnologie, 2002, 104, pp. 11-13.
[6] Esteben, A., Abarca, M. L., Bragulat, M. R. Cabanes, F. J. Effects of temperature and incubation time on production of ochratoxin A by black aspergilli. Research in Microbiology, 2004, 155, pp. 861-866.
[7] Fleet, G. H. Yeast interactions and wine flavour. International Journal of Food Microbiology, 2003, 86, pp. 11-22.
[8] Höhler, D. Ochratoxin A in food and feed: occurrence, legislation and mode of action. Z Ernahrungswiss, 1998, 37, pp. 2-12.
[9] Merkaki, P., Delpont-Binet, C., Grosso, F., Dragacci, S. Determination of ochratoxin A in red wine and vinegar by immunoaffinity high-pressure liquid chromatography. Journal of Food Protection, 2001, 64, 533-537.
[10] Pretet –Lataste, J-L Berger, B. Molot. Analyse du risque dans les vins: l'exemple de l'Ochratoxine A, Revue des œnologues, 2006, 119, pp. 43-45.
[11] Ramos, A. J., Sanchis, V., Marin, S. Incubation time and water activity effects on ochratoxin A production by Aspergillus section Nigri strains isolated from grapes. Letters in Applied Microbiology, 2004, 38, pp. 72-77.
[12] Rouseau, J., Blateyron, L. Ochratoxine A dans les vins: pas de solution curative dans les vins, priorite a la maitrise sanitaire au vignoble. Revue des Œnologues, 2002, 104, pp. 14-16.
[13] Visconti, A., Pascale, M., Centonze, G. Determination of ochratoxin A in wine by means of immunoaffinity column clean-up and high performance liquid chromatography. Journal of Chromatography A, 1999, 864, pp. 89-101.
[14] WHO. Evaluation of certain mycotoxins in food. Fifty-sixth report of the joint FAO/WHO expert committee on food additives. WHO technical report series, Geneva, 2002, 906, pp. 27-28.
[15] Varga, J., Kevei, E., Rimyu, E., Teren, J. & Kazakiewicz, Z. Ochratoxin production by Aspergillus species. Appl. Environ. Microbiol., 1996, 62, pp. 4461-4464.

COMPARISON OF SENSITIVITY OF ANALYTICAL METHODS FOR SAMPLES INJECTION IN THE DETECTION OF COMPOUNDS WITH FLAVOURING POTENTIAL OF WINES

Rodica Sturza[1], Constantin Sîrghi[1], Mariana Vrîncean[1], Susanne Böhme[2]

Technical University of Moldova[1], Shimadzu Europa GmbH[2]
E-mail:utm.marianav@gmail.com

Abstract: The study has been focused on the comparative analysis of various analytical techniques for the injection of samples applied to detect the additives with flavouring potential that are used to obtain illicitly the "Muscat" and "Isabela" wines, by implementing the GC/MS method with injection of liquid samples directly into the capillary column, using the "Head-space" method and the solid phase microextraction (SPME).

Keywords: GC/MS, Head-space, SPME, Wine and Flavours

Introduction

The wine aroma is a basic element of the quality of wine obtained from grapes. Aroma compounds are most closely associated with the volatile fraction of food [1].

The study of the volatile fraction in enological products has become necessary and is more than sufficiently justified, considering these compounds make a major contribution to the consumer's overall perception of the quality of particular food and drink products. In fact, these complex volatile compounds largely determine the acceptance or rejection of many products by the consumer. In addition, product characteristics known as "off-flavours", caused by the presence of volatiles that give rise to disagreeable odour and flavours, often imply microbial contamination; therefore the study of volatiles becomes part of the larger subject of food safety [2].

In other words, the wine flavour results from a harmonious compound of several chemicals having different origin and structure. The main focus is on the terpenoids substances that are capable to release smelling volatile substances (terpenes) through hydrolysis. The methoxypyrazines, some compounds with thiol functions, phenolic acids also belong to this category. Through decarboxylation they form the aldehydes, alcohols, and later esters, which can have the flavour of flowers or fruits [3].

The determination of the volatile fraction is normally performed by gas chromatography (GC), a technique which in recent years has made great advances.

Given that SPME is very appropriate for application in the field of volatile compounds, this technique is being widely used for the characterization of wines [4]. Bonino and others [5] utilized HS-SPME for the extraction of aroma compounds characterizing a Piedmont wine (Ruché) derived from a non-aromatic wine. The most aromatic monoterpenes, are in the form of monoterpenic alcohols, namely linalool, α-terpineol, nerol, geraniol, citronellol, hotrienol (HO-trienol, (5E)-3,5-dimethylocta-1,5,7-trien-3-ol), which express the rose flavour [6], [7]. The citronellol and linalool are the most aromatic, playing an important role in the formation of Muscat varieties flavour, where their concentration is higher the perception threshold [8].

In order to improve the gustatory and olfactory properties of grape wines or in order to give them certain characteristics, the wine aromatisation often is carried out illegally by adding different flavoured substances both of plant and synthetic origin. The usage of any type of flavoured elements, of synthetic origin included, for the natural wine production is prohibited by the EU and RM legislation [9].

The information concerning the toxic action of ethanol in combination with synthetic aromatizing compounds often does not have a relevant character. While carrying out the research in the field of alcohol products toxicology and detection of compounds which are harmful or potentially dangerous for the human body, the role of the control over such unauthorized applications of additives in the process of wine making increases.

The objective of this research was to compare the efficiency of various analytical techniques for the injection of samples used to detect the additives with flavouring potential that are utilised for the illicit obtaining of "Muscat" and "Isabel" wines on the basis of raw material wine with neutral aromatic potential.

Materials and Methods

For the analysis, the raw material wine of „Mixture of European white varieties" and „Mixture of European red varieties" type were used, to which have been added naturally identical aromatizers of "Muscat" (white wine) and "Isabel" (red wine) type from commerce, in the recommended amount (1:10000). Subsequently, the comparative analysis of the composition of raw material wine and of the "variety" wine has been carried out using the GC/MS method by injecting liquid samples directly into the capillary column, the „*head-space*" (HS) method and the solid phase microextraction (SPME).

Experimental conditions:

All tests have been carried out using the Shimadzu GC system coupled with a single quadrupole mass-spectrometer GCMS-QP2010 Plus equipped with the three-dimensional automated system for the injection of samples AOC-5000 (GCMS-QP2010 PlusxAOC-5000) (figure 1a).

The experimental conditions for the analysis of the injection of liquid samples directly into the capillary column are presented in figure 1b; of the injection of samples using the HS method - in figure 1c; of the injection of samples using the SPME method - in figure 1d.

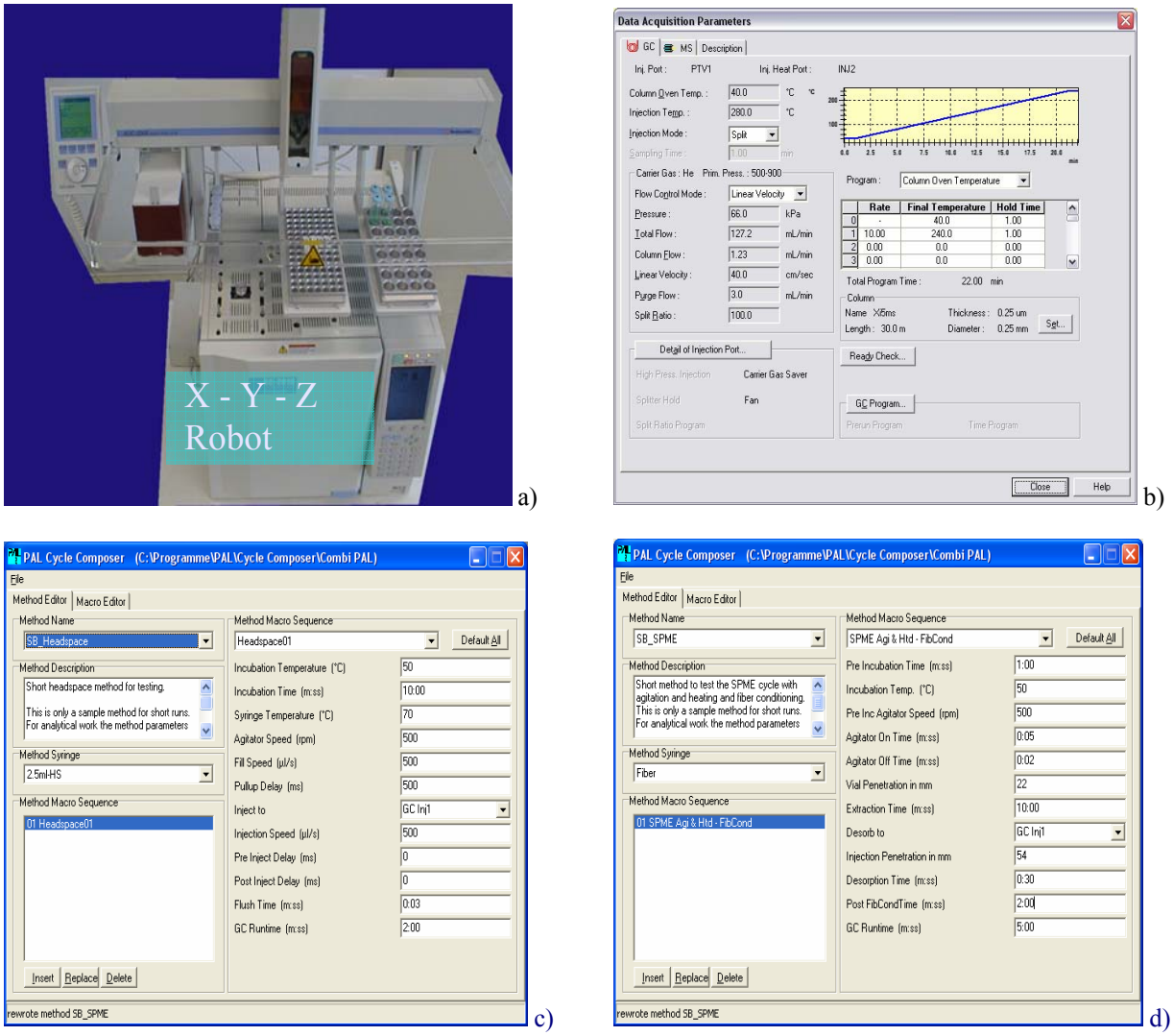

Figure 1. Three-dimensional automated system for the injection of samples AOC-5000 (GCMS-QP2010xAOC-5000) (a) and the experimental conditions for the analysis of the injection of liquid samples directly into the capillary column (b); using the „head-space" method (c) and using the solid phase microextraction (SPME) (d)

In the case of injection of samples by the HS and SPME methods, the 20 ml vials have been used, in which 10 ml of sample and 4 g of NaCl were administered. For the solid phase microextraction (SPME), the 100µm Carboxen-PDMS fibre was used, which provides the extraction of volatile and semi-volatile compounds on a concentration range from tenths of ppb up to tens of ppm [10].

For the identification, the general library of NIST-5 mass spectra and the FFNSC 1.3, a library which was specially developed for flavours and fragrances (available from Shimadzu Europa GmbH) were used. The accuracy of displacement has been verified according to the library of Covatz retention indices (MLRI). The analysis of the experimental data was carried out with the GC/MS Solution software (Shimadzu), which contains the SCAN/SIM options (Fast Automated Scan/SIM Type (FASST); creation of automatic SIM (Scan/SIM) table (COAST).

Results and Discussions

The comparative analysis of the composition of raw material wine of "Mixture of white European varieties" and "variety" types, by adding naturally identical aromatizers of "Muscat" type, carried out using the GC/MS method with the injection of liquid samples directly into the capillary column, indicates the presence of unessential differences (*figure 2*).

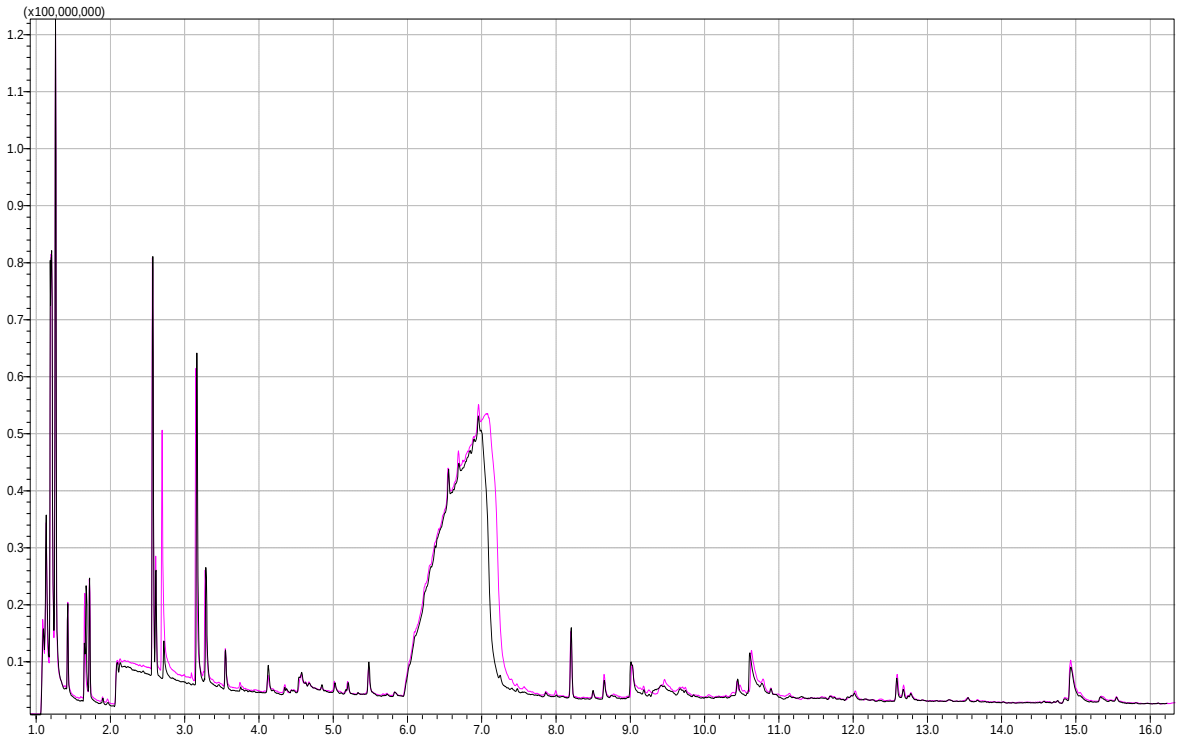

Figure 2. The comparative analysis of the composition of raw material wine (white) and "Muscat" wine using the GC/MS method with the injection of liquid samples directly into the capillary column

The reason of this phenomenon consists in the matrix effect of the majority components of wine - ethanol, organic acids, esters, and, in particular, glycerine, which has an extremely large trace. This fact demonstrates the minor sensibility of the GC/MS method with the injection of liquid samples directly into the capillary column for the analysis of wine components with flavouring potential [11].

The "*headspace*" method refers to the determination of volatile organic substances in the gaseous phase, which are in equilibrium with those from liquid or solid phase [12]. The sample is thermostated until the establishment of balance of the components which are in gaseous, and respectively liquid or solid phases. The HS mode advantages are:

- The position in agitator allows overlapping analysis of precursor sample and incubation of following samples, respectively
- Sample will be gained only when GC is in ready state
- After injection heated syringe is automatically cleaned by purge gas
- Flexible definition of method parameters

The initial concentration of a component from sample in the field of Henry's law validity is given by equation (1):

$$C_{OL} = \frac{C_G(K_{VL} + V_G)}{V_L} \quad (1)$$

where: C_{OL} – is the initial concentration of component in the liquid phase;
C_G – component concentration in the gaseous phase;
K – coefficient of gas - liquid reference for a certain component at the analysis temperature;
V_G – volume of the gaseous phase;
V_L – volume of the liquid phase.

This technique of introducing the sample is used when the interest components are situated in non-volatile and dirty matrices or that contain large amounts of water.

The matrix effects can be reduced by saturation of aqueous samples with salt in order to obtain the "salting out" effect, or by saturation of an organic sample with water. The temperature control and reproducibility are essential for obtaining the reproducible results. In case of quantitative determination, the method requires a prior calibration, because the distribution coefficient K of the equation is not known (1). The method is recommended, especially, for the analysis of volatile pollutants, of the components with flavouring potential from food, beverages and pharmaceutical products.

The differential analysis of the composition of raw material wine and of "variety" wine, made by the administration of "Muscat" naturally identical aromatizer using the GC/MS method with the injection of samples by HS method, demonstrates the presence of some significant differences (*figure 3*).

In the "Muscat" wine, the presence of a range of monoterpenes ($C_{10}H_{16}$) is identified: *beta*-myrcen (2,6,7-octatriene), *p*-cymen, D-limonen, *beta* (Z, E)-ocimene and terpineol. All these monoterpenes were identified in grapes of flavoured varieties [13], although these are formed in insignificant amounts and are not of interest in the olfactory field. At the same time, they are part of the composition of essential oils extracted from exotic and flavoured plants: limonen - from lemons and oranges, terpinol - from coriander, myrcenelum - from Myrcia acris plant, ocimenum – from basil leaves, p-cymen - from camphor tree wood. The presence of an insignificant trace, from the point of view of intensity, but identified with certainty (camphor) demonstrates once again that the concerned monoterpenes were not formed in grapes, but come from essential oils extracted from plants (but in any case are not of synthetic origin).

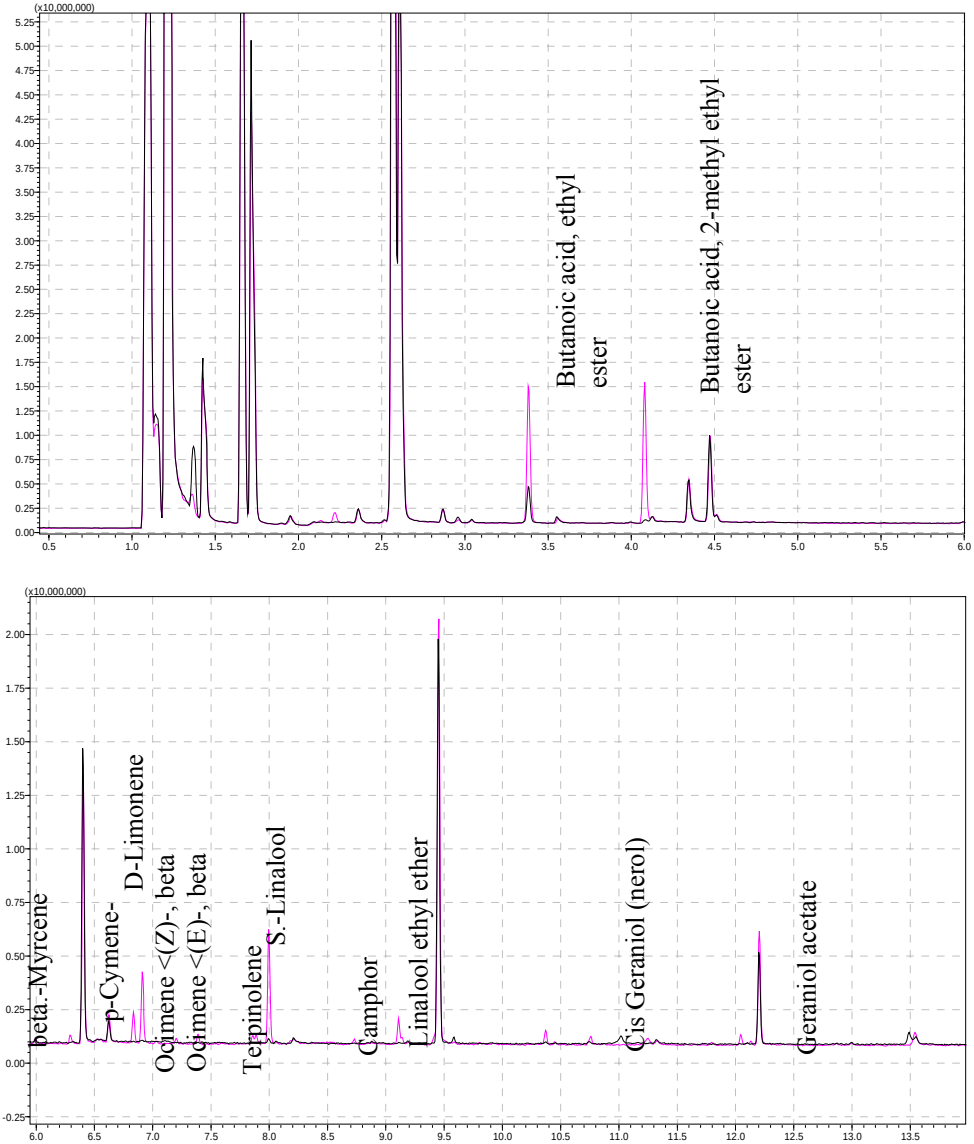

Figure 3. The identification of differences between the composition of raw material wine (white) and "Muscat" wine using the GC/MS method with sample injection by HS method (the identified substances are lacking in the row materials wine

The terpene monohidroxilic alcohols (terpenols) are the most important compounds with flavouring potential, because these represent volatile free flavours from aromatic grapes. From the quantitative point of view, they represent about 40-50% of dosed volatile aromatic substances, having a very low threshold of volatile perception, of 0,1-0,5 mg/L of wine [14]. The main terpenols are linalool, geraniol, nerol, citronelol, hotrienol (HO-trienol, (5E)-3,5-dimethylocta-1,5,7-trien-3-ol) and α -terpineol.

In the case of "Muscat" wine, obtained by using the naturally identical aromatizer, the presence of *S*-linalool and of ethyl ester of linalool was identified. The *S*-linalool trace abundance is maximum compared to other compounds with flavouring potential. It is known that namely this tertiary acyclic terpenic alcohol possesses muscatel flavour.

The linalool presence has been identified in the essential oils of many plants (linaloil - a tree in Central America, orange, bergamot, rose, etc.). In the grapes of "Muscat" varieties, the linalool represents 53.4% of the total of terpenic alcohols, nerol and geraniol, that always accompany the linalool, represent only 17,6-31,8% [15]. In the examined case, the presence of nerol and geraniol acetate were detected, the abundance of traces being insignificant. This acyclic terpenic alcohol is present in essential oils of rose, lavender, citronel. By oxidation this is converted into aldehyde (geranial), with an odorous impact much weaker than geraniol.

The fatty acids and their volatile esters represent real indicators of the fermentation aroma, which prints the "vinous" character through odorous nuances of fruits. In the raw material wine, an important number of volatile esters of inferior fatty acids with short and medium chain have been found (Table 1).

Table 1

The chemical composition of volatile fraction of raw material wine "Mixture of white European varieties"

Peak Report TIC

Peak#	R.Time	Area	Area%	Height	Height%	A/H	Name
1	1.369	15220650	2.37	7931129	1.98	1.92	1-Buten-3-yne, 1-chloro-, (Z)-
2	1.425	29537686	4.59	16918729	4.22	1.75	Propane, 1,2-dimethoxy-
3	1.662	118982681	18.50	64613207	16.11	1.84	1,3-Dioxolane, 2-methyl-
4	1.716	75116469	11.68	49678347	12.38	1.51	o-Allylhydroxylamine
5	1.950	1510728	0.23	891844	0.22	1.69	Cyclopentane, methyl-
6	2.359	2321591	0.36	1428268	0.36	1.63	Propanoic acid, ethyl ester
7	2.567	220919591	34.35	133093986	33.18	1.66	1-Butanol, 3-methyl-
8	2.608	89391431	13.90	64739321	16.14	1.38	1-Butanol, 2-methyl-
9	2.868	1992157	0.31	1359676	0.34	1.47	Propanoic acid, 2-methyl-, ethyl ester
10	2.958	841221	0.13	562401	0.14	1.50	Spiro[2.4]hepta-4,6-diene
11	3.041	457562	0.07	333759	0.08	1.37	Propanoic acid, 2-oxo-, methyl ester
12	3.382	5310773	0.83	3724880	0.93	1.43	Isobutyrate <ethyl->
13	3.552	957883	0.15	611089	0.15	1.57	Acetic acid, methoxy-, ethyl ester
14	4.085	563240	0.09	305472	0.08	1.84	Butanoic acid, 2-methyl-
15	4.126	842501	0.13	570415	0.14	1.48	Butanoic acid, 3-methyl-, ethyl ester
16	4.343	6598608	1.03	4322961	1.08	1.53	1-Heptene, 2,6-dimethyl-
17	4.471	12567387	1.95	8895998	2.22	1.41	2,3-Pentanedione, 4-methyl-
18	6.401	18814779	2.93	13688347	3.41	1.37	Hexanoic acid, ethyl ester
19	6.623	1351913	0.21	929153	0.23	1.45	Acetic acid, hexyl ester
20	7.994	259434	0.04	201309	0.05	1.29	1,6-Octadien-3-ol, 3,7-dimethyl-
21	8.050	156101	0.02	79323	0.02	1.97	Nonanal
22	8.207	344769	0.05	215963	0.05	1.60	Phenethyl alcohol
23	9.450	27217854	4.23	18851410	4.70	1.44	Octanoate <ethyl->
24	9.584	515303	0.08	286335	0.07	1.80	Decanal
25	12.202	6484313	1.01	4266728	1.06	1.52	Decanoate <ethyl->
26	14.655	186027	0.03	111184	0.03	1.67	Phthalate <diethyl->
27	14.708	274765	0.04	206338	0.05	1.33	Pentanoic acid, 2,2,4-trimethyl-3-carboxyi
28	15.543	1805999	0.28	867404	0.22	2.08	3,5-Diisopropoxy-1,1,1,7,7,7-hexamethyl-
29	17.278	1503831	0.23	803174	0.20	1.87	3-Butoxy-1,1,1,7,7,7-hexamethyl-3,5,5-tri
30	17.926	1111936	0.17	669875	0.17	1.66	Benzamide, N-[2-(1,1,2,3,3,3-hexafluorop
		643159183	100.00	401158025	100.00		

The differential scanning of the chromatograms of raw material wine and "variety" wine allowed to detect an essential increase of the content of an ester with fruit aromatic notes: ethyl butanoate (pineapple). As well, the presence of 2-ethyl methylbutanoate with apple aromatic nuance was detected (figure 3). These two aromatic compounds, which characterize the wines of "Muscat" type, have an extremely low olfactory perception threshold: 0, 02 mg/L for the ethyl butanoate and 1μg/L for ethyl methylbutyrate. In the raw material wine, the 3-ethyl methylbutanoate is present, but the abundance of this trace is much lower than of its isomers found in wine with "variety" flavour. It is obvious that the presence of these two abundant traces in wine with "variety" flavour cannot

be attributed to the accumulation of these compounds in grapes, a fact also confirmed by the difference between the two isomers.

The carried out research shows with certainty that the GC/MS technique with sample injection by the "Headspace" method, allows the assessment of qualitative and semi-quantitative composition of the substances with wine flavouring potential even in the absence of respective standards. Meanwhile, the method also allows the detection of residues of contaminants or pollutants - for example, in the raw material wine, the signs of diethylftalat have been found (table 1).

As the purpose of this research was to compare the sensibility of the analytical methods for samples injection in detecting the compounds with wine flavouring potential, the analysis of raw material wine and of "variety" wine with samples injection by the solid phase microextraction (SPME) was carried out. The differential scanning of chromatographic traces for the basic wine and for the "variety" flavoured wine demonstrated the presence of the following compounds (figure 4).

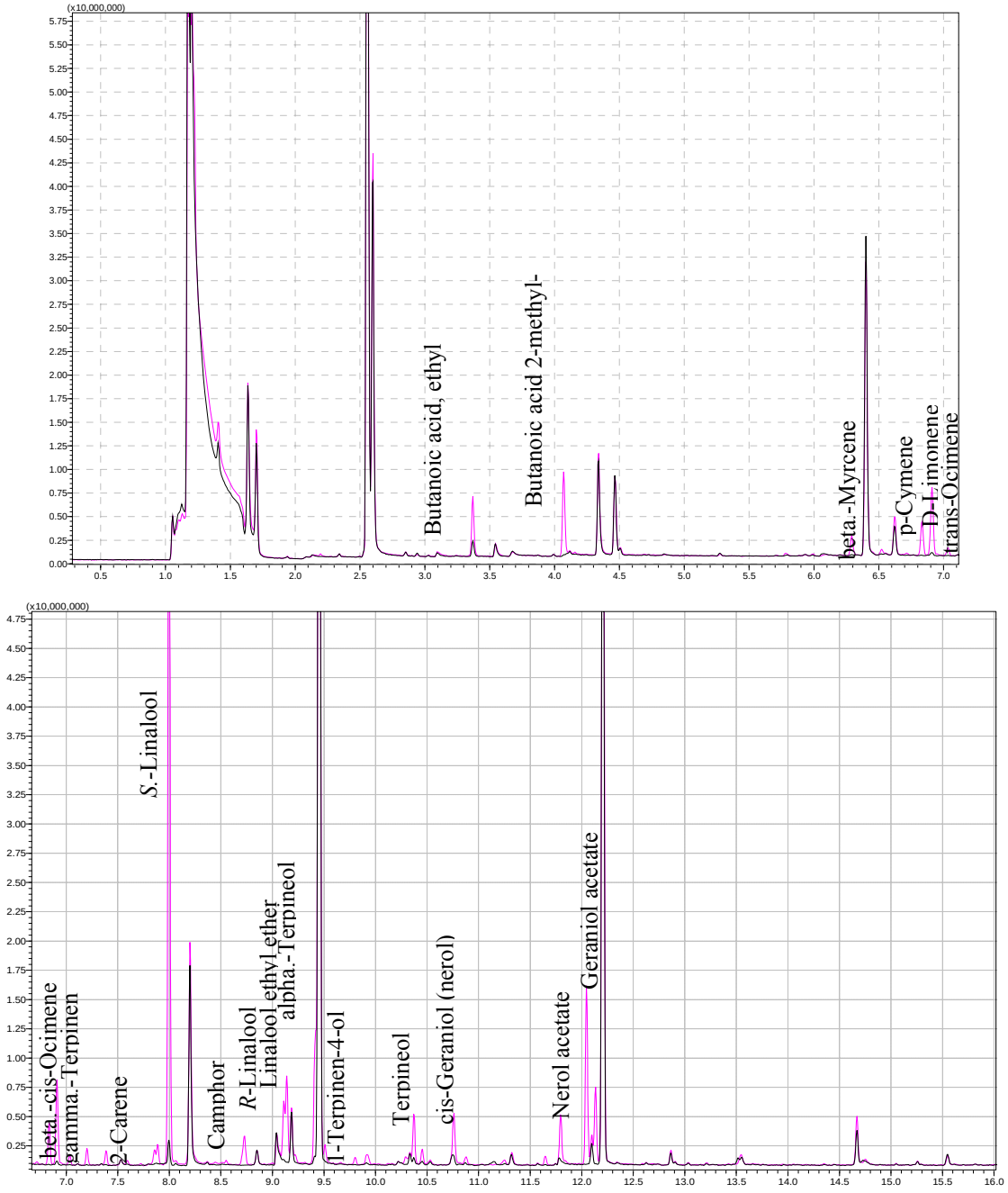

Figure 4. The identification of differences between the composition of raw material wine (white) and "Muscat" wine using the GC/MS method with samples injection by the solid phase microextraction (SPME)

SPME is a solvent less extraction technique that can be used to extract analytes from both liquid and solid matrices. The quantitative use of this technique has been proven with the automatic robot. The use of SPME for the analysis of flavours and off-flavours in food and beverages is an important preparation tool.

In addition to the compounds detected by the "Headspace" sample injection method, the presence of following monohidroxylic terpenic alcohols was reported: terpineol, alpha-terpineol and 1-terpinen-4-ol. The presence of nerol acetate was also additionally detected. The presence of these compounds with flavouring potential, although in insignificant quantities, demonstrates the natural origin of the used aromatizer (essential oils).

The intensity of chromatographic traces in the case of SPME method is considerably higher (figure 5). Thus, the beta-linalool trace in the case of SPME is saturated. The alpha-terpineol trace, masked in the case of *"Headspace"* method by the ethyl decanoat trace, a less volatile ester, but present in significant quantities in the raw material wine, is detected in the case of samples injection using the SPME method. The chromatograms comparison for the "variety" wine obtained by these two methods of samples injection indicates that the *"Headspace"* method, although it can be applied successfully to the analysis of compounds with wine flavouring potential, has certain drawbacks – the vapour phase composition varies essentially from the liquid phase composition. The volatility of components has a predominant role in this case.

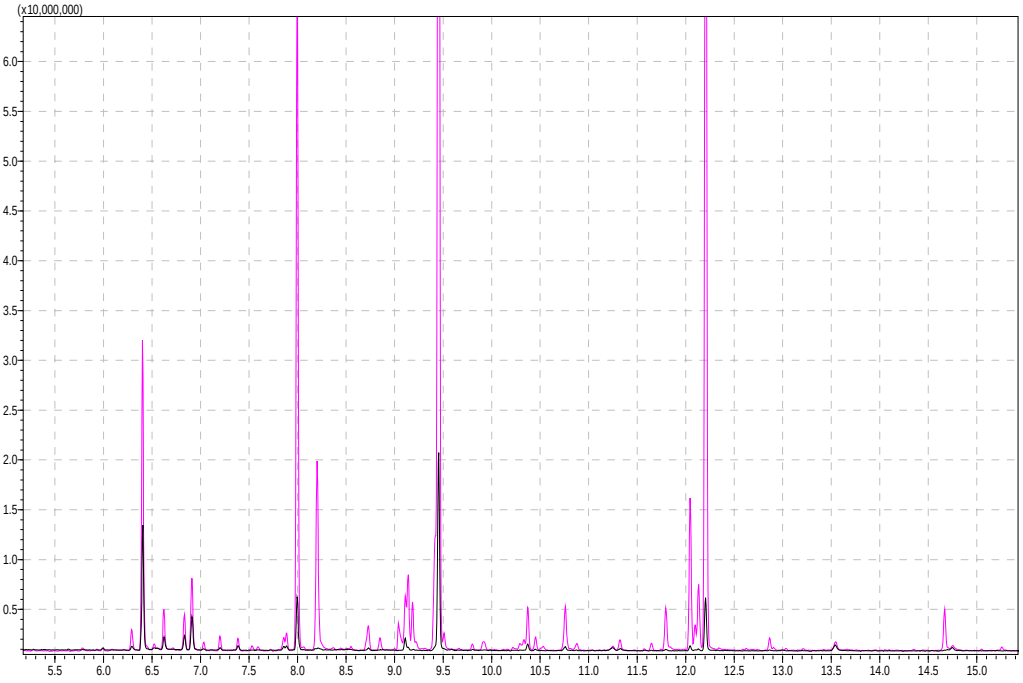

Figure 5. The comparison of the sensibility of the GC/MS method with samples injection by the solid phase microextraction (SPME) (red) and "Headspace" (black)

The sensibility and the resolution of chromatographic separation are considerably higher when the SPME method is applied. The quantity of sample extracted from the solution can be determined by the relationship:

$$m = \frac{K_{f/s}.V_f.C_o.V_{sol}}{K_{f/s}.V_f + V_{sol}}, \quad (2)$$

where: V_f and V_s are the stationary phase volume and the solution volume;
$K_{f/s}$ - coefficient of distribution of the component at the interface of stationary phase / solution phase;
C_0 – initial concentration of component in solution.

The relationship (2) demonstrates the linearity between the component mass absorbed by the organic fibre and its concentration in the solution. Because the organic substances being in the aqueous solution have a higher net affinity towards the organic fibre (in the examined case - carboxen), which has a much less polar character than the aqueous phase, these will be distributed essentially in the organic phase, that is $V_{sol} >> K_{f/s}$, and the equation (2) becomes:

$$m = K_{f/s}.V_f.C_o \quad (3)$$

Thus, the quantity of sample extracted from the solution to be analyzed is independent of the sample volume, which is an extremely important fact that assures the repeatability and reproducibility of the analysis results.

The testing of raw material wine "Mixture of European red varieties" using the GC/MS method with samples injection through the solid phase microextraction (SPME) has allowed the identification of 60 compounds, these belonging to different classes of substances (table 2).

Table 2

The chemical composition of raw material wine "Mixture of European red varieties"

Peak Report TIC

Peak#	R.Time	Area	Area%	Height	Height%	A/H	Name
1	1.639	44866981	6.00	30945919	6.32	1.45	Acetic acid, 1-methylethyl ester
2	1.704	29377050	3.93	21375333	4.37	1.37	Propane, 2-nitro-
3	1.940	1015107	0.14	730563	0.15	1.39	1-Butanol
4	2.341	960214	0.13	564456	0.12	1.70	Propanoic acid, ethyl ester
5	2.500	1895982	0.25	1681600	0.34	1.13	Acetylpropionyl
6	2.558	168166787	22.49	113834147	23.25	1.48	1-Butanol, 3-methyl-
7	2.599	103284327	13.81	66062336	13.50	1.56	Propanoic acid, 2,2-dimethyl-, methyl este
8	2.854	2646200	0.35	1177555	0.24	2.25	Propanoic acid, 2-methyl-, ethyl ester
9	2.905	262675	0.04	201661	0.04	1.30	Butane, 1-(ethenyloxy)-3-methyl-
10	2.944	1449636	0.19	1067057	0.22	1.36	Spiro[2.4]hepta-4,6-diene
11	3.028	323650	0.04	245888	0.05	1.32	Acetic acid, 2-methylpropyl ester
12	3.085	9380493	1.25	3417608	0.70	2.74	2,3-Butanediol, [R-(R*,R*)]-
13	3.227	2304773	0.31	600036	0.12	3.84	2,3-Butanediol
14	3.373	1867274	0.25	1307942	0.27	1.43	Isobutyrate <ethyl->
15	3.545	6657408	0.89	3799158	0.78	1.75	Acetic acid, methoxy-, ethyl ester
16	3.705	413943	0.06	314100	0.06	1.32	1,3-Butadiene, 1,4-dimethoxy-, (Z,Z)-
17	3.874	306601	0.04	218463	0.04	1.40	1-Pentanol, 4-methyl-
18	3.995	668372	0.09	454231	0.09	1.47	1-Pentanol, 3-methyl-
19	4.075	524624	0.07	384810	0.08	1.36	Butanoic acid, 2-methyl-
20	4.120	1182375	0.16	777910	0.16	1.52	Butanoic acid, 3-methyl-, ethyl ester
21	4.342	12479103	1.67	7605333	1.55	1.64	1-Heptene, 2,6-dimethyl-
22	4.468	13566349	1.81	9941119	2.03	1.36	2,3-Pentanedione, 4-methyl-
23	4.727	226118	0.03	154789	0.03	1.46	Benzene <ethyl->
24	5.936	703016	0.09	430731	0.09	1.63	2-Octene, 3,7-dimethyl-, (Z)-
25	5.998	561120	0.08	287825	0.06	1.95	N-Acetylisoxazolidine
26	6.062	1576702	0.21	552331	0.11	2.85	Ethanol, 2,2-diethoxy-
27	6.207	686573	0.09	199286	0.04	3.45	Ethane, 1,1,1-triethoxy-
28	6.403	33096736	4.43	22726267	4.64	1.46	Hexanoic acid, ethyl ester
29	6.627	333807	0.04	250597	0.05	1.33	Acetic acid, hexyl ester
30	7.534	1043067	0.14	560141	0.11	1.86	1-Octanol
31	7.961	522462	0.07	368118	0.08	1.42	Heptanoic acid, ethyl ester
32	8.000	439696	0.06	346271	0.07	1.27	1,6-Octadien-3-ol, 3,7-dimethyl-
33	8.202	67685812	9.05	39032807	7.97	1.73	Phenethyl alcohol
34	8.370	589534	0.08	320902	0.07	1.84	Octanoate <methyl->
35	8.851	1935948	0.26	1128687	0.23	1.72	Heptanal <cyclic-, ethylene-> acetal
36	9.072	1786362	0.24	873580	0.18	2.04	1-Nonanol
37	9.186	8422817	1.13	5628783	1.15	1.50	Succinate <diethyl->
38	9.455	145228511	19.42	99505411	20.33	1.46	Octanoate <ethyl->
39	10.223	729368	0.10	267367	0.05	2.73	Hexanoate <isopentyl->
40	10.336	937456	0.13	532431	0.11	1.76	Phenethyl acetate <2->
41	10.531	606487	0.08	301959	0.06	2.01	Decyl alcohol
42	10.742	2875592	0.38	1728550	0.35	1.66	Isoaromadendrene epoxide
43	10.869	896156	0.12	684897	0.14	1.31	Nonanoate <ethyl->
44	11.248	674000	0.09	321817	0.07	2.09	1,3-Dioxolane, 2-(5-bromopentyl)-
45	11.319	1522606	0.20	776612	0.16	1.96	Hexasiloxane, 1,1,3,3,5,5,7,7,9,9,11,11-do
46	12.099	1044406	0.14	644610	0.13	1.62	4-Decenoic acid, ethyl ester, (Z)-
47	12.206	52638024	7.04	35256483	7.20	1.49	Decanoate <ethyl->
48	12.628	192135	0.03	171167	0.03	1.12	Hexanedioic acid, bis(1-methylethyl) ester
49	12.866	738451	0.10	459589	0.09	1.61	Octanoate <isopentyl->
50	13.211	377891	0.05	239501	0.05	1.58	Pentafluoropropionic acid, tridecyl ester
51	13.546	1923562	0.26	771944	0.16	2.49	2-Propenoic acid, 2,3,3-tris[(trimethylsilyl)
52	14.670	6239169	0.83	3865254	0.79	1.61	Dodecanoate <ethyl->
53	14.756	2044330	0.27	975819	0.20	2.09	Propanoic acid, 2-methyl-, 1-(1,1-dimethyl
54	15.261	280038	0.04	227353	0.05	1.23	Sulfurous acid, dipentyl ester
55	15.550	1421638	0.19	792088	0.16	1.79	D-Arabinonic acid, 2,3,5-tris-O-(trimethyls
56	16.895	545695	0.07	320225	0.07	1.70	Tetradecanoic acid, ethyl ester
57	17.282	1221285	0.16	666669	0.14	1.83	3-Butoxy-1,1,1,7,7,7-hexamethyl-3,5,5-tris
58	17.699	521151	0.07	315682	0.06	1.65	1,2-Benzenedicarboxylic acid, dipropyl est
59	18.641	530401	0.07	333600	0.07	1.59	1,2-Benzenedicarboxylic acid, bis(2-methy
60	18.912	1326010	0.18	789269	0.16	1.68	Ethyl hydrogen dodecanedioate
		747724056	100.00	489516637	100.00		

The differential scanning of chromatograms of the raw material wine and of the Izabela ”variety” wine, obtained by the administration of "naturally identical" aromatizer (according to commercial features) demonstrated the presence of the following traces (*figure 6*). The presence of methylanthranilat is attested - a component of the primary flavours of American hybrid grapes. The abundance of this trace is prevalent among the registered flavouring components.

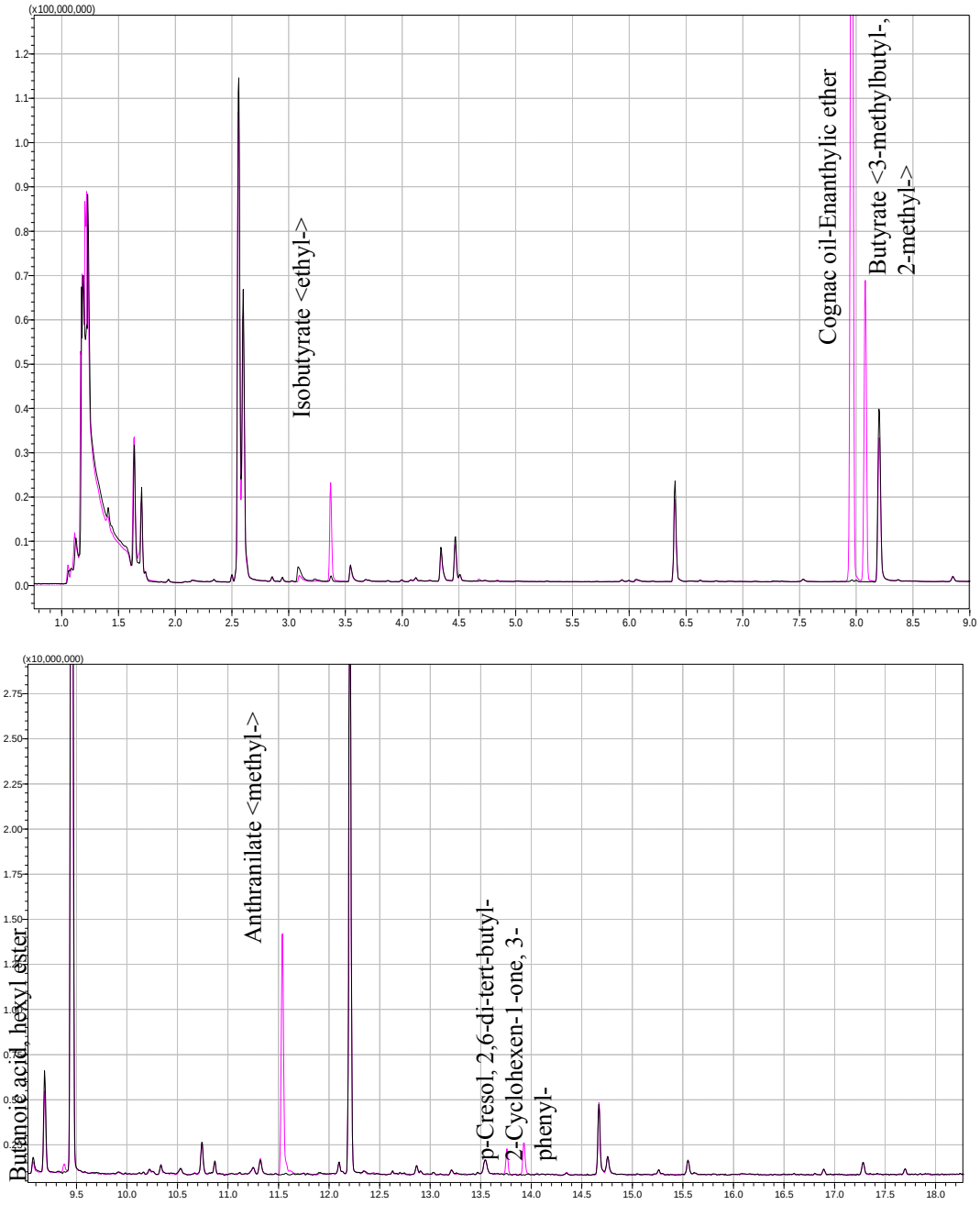

Figure 6. The identification of the differences between the composition of raw material wine (red) and "Izabela" wine using GC/MS method with samples injection by the solid phase microextraction (SPME)

The ethyl izobutirat was found, an ester with a nuance of fruit and fusel flavour, which is characteristic for the wines of Muscatel type, with a very low threshold of olfactory perception - 0.02 mg/L. Its presence in the composition of flavouring substances is not characteristic for the wines of *Vitis Labrusca* varieties. As well, two significant traces of enantilic and butyrate ether <3-methylbutil, 2-methyl-> were recorded - two chemicals of synthetic origin with pineapple flavour (enantilic ether) and fruit caramel (butyrate < 3-metilbutil-, 2-methyl->). The hexilic ester of the butanoic acid, present in extremely low quantity (pineapple flavour) can be of synthetic origin, but is also detected in the composition of natural wines [16].

The presence of the *p-Cresol, 2,6-di-tert-butyl-* compound, an antioxidant agent of synthetic origin, restricted to food products, demonstrates eloquently the synthetic origin of the concerned aromatizer. This compound, which manifests allergic effect and is suspected to be carcinogenic, is not part of the flavouring compounds, but is included in the composition of the synthetic aromatizer for its antioxidant effect.

3 - phenyl-2-cyclohexene-1-ona also represents a synthetic compound that could be used as a solvent for *p-Cresol, 2,6-di-tert-butyl*.

The carried out research demonstrated that the usage of the GC/MS method with sample injection by "Headspace" method and with the solid phase microextraction (SPME) can be successfully applied to identify the aromatic profile of wines, to detect the wine counterfeiting (by using naturally identical and synthetic aromatizers). It is also relatively easy to detect the origin of the aromatizer. In the case of the naturally identical, the presence of a greater number of traces, characteristic for substances with flavouring potential, is detected. For the synthetic aromatizers, the number of components with flavouring potential is lower (for the "Izabela" aromatizer, only 5 compounds with flavouring potential have been found), but there were recorded two chemicals which have nothing in common with the flavouring substances, but fulfil various functions.

The sensitivity of the method decreases in the order to use the following analytical techniques for samples injection:

SPME> „Headspace" >> injection of liquid samples directly into the capillary column

The GC/MS method with the injection of liquid samples directly into the capillary column can not be applied to identify the aromatic profile of wines, as in this case the effect of the matrix leads to the decrease of sensibility in the detection of substances that are present in very small quantities. The GC/MS method with the samples injection by the solid phase microextraction provides a higher sensibility than the method of samples injection by application of the "*Headspace*" technique.

References

[1]. Natera R, Castro R, Morena MVG, Hernandez MJ, Barroso CG (2003) Agric Food Chem 51: 3345-3351.

[2]. Morales ML, Gonzales GA, Casas JA, Troncoso AM (2001) Eur Food ResTechnol 212 : 676-682

[3]. Flanzy C., Œnologie, fondements scientifiques et technologiques", Londre, Paris, New York, Technique & Documentation, 1998.

[4]. Favretto D, Grandis G, Allegri G, Traldi P (1998) Rapid Commun Mass Spectrom 12 :1595-1600.

[5]. Bonino M, Schellino R, Rizzi C, Aigotti R, Delfini C, Baiocchi C (2003) Food Chem 80 : 125-133.

[6]. Riberau-Gayon P., „Les composées phénoliques des végétaux", Dunod, Paris, 1998, pp.410.

[7]. Sirghi.C, Zironi R., „Aspecte inovative ale enologiei moderne", Editura ''Sigma'', Chişinău, 1994.

[8]. Gholami M., Hayasaka Y., Coombe B.G., Jackson J.F., Robinson S.P., Williams P.J. *Biosynthesis of flavour compounds in Muscat Gordo Blanco grape berries.* Australian Journal of Grape and Wine Research. Volume 1 Issue 1, pp. 19 – 24. Published Online: 12 Mar 2008

[9]. Institutul Național pentru Viticultură și Vinificație din Republica Moldova *„Realizări inovative în domeniul Viti-vinicol"*, Ediție specială a Conferinței Internaționale consacrate comemorării mc. AŞM Petru Ungureanu, 18-19 septembrie, 2008, Chişinău.

[10]. Mohamed A., Menno B., Hans-Ulrich B., Rene J.J. Vreuls, Brinckman Udo A.TH., Comprehensive Two-Dimensional Gas Chromatography coupled to rapid-scanning Quadrupole Mass Spectrometer (GC×GC–qMS): *Principles and Applications.* Journal of Chromatography A, Volume 1067, Issues 1-2, 4 March 2005, pp. 245-254.

[11]. Van Wyk C. J., Dinsmoor W., Kepner R. E., Some *Volatile Components of Vitis Vinifera Variety White Riesling 1, Grape Juice*. Journal of Food Science, Volume 32 Issue 6, 2006, pp. 660 – 664.

[12]. Gocan S., " *Cromatografia de înaltă performanță*" Partea 1., Cromatografia de gaze. Ed. Dacia, Cluj-Napoca, 1998.

[13]. Sanchez-Palomo E., Diaz-Maroto C., "*Rapid determination of volatile compounds in grapes by HS-SPME coupled with GC–MS*", Talanta, Volume 66, Issue 5, 15 June 2005, pp. 1152-1157.

[14]. Rosillo L., Salinas M.R., Garijo J., Alonso G.L., "*Study of volatiles in grapes by dynamic headspace analysis - Application to the differentiation of some Vitis vinifera varieties"*. Journal of Chromatography A, Volume 847, Number 1, 25 June 1999 , pp. 155-159(5).

[15]. Țirdea C., " Chimia și analiza vinului", Editura „*Ion Ionescu de la Brad*", Iaşi, 2007.

[16]. *Analysis of Grape Volatiles by Solid Phase Microextraction and Comprehensive Two-Dimensional Gas Chromatography with Time-of-Flight Mass Spectrometry (GCxGC-TOFMS)*. Form No. 203-821-270 3/08-REV ©2008 LECO Corporation MI 49085].

SYNTHESIS, CRYSTAL STRUCTURE AND MAGNETIC BEHAVIOUR OF NOVEL 4*f*-2*s* HETEROMETALIC ONE-DIMENSIONAL COORDINATION POLYMERS ON THE BASE OF 2-FURAN-CARBOXYLIC ACID

Silvia Melnic[a], Denis Prodius[a,*], Sergiu Shova[b], Helen Stoeckli-Evans[c], Yurii Simonov[b], Alexander Feher[d], Maria Gdaniec[e], Constantin Turta[a]

[a]*Institute of Chemistry of the ASM, Chisinau, Moldova*
[b]*Institute of Applied Physics of the ASM, Chisinau, Moldova*
[c]*Institut de Microtechnique, Neuchâtel, Switzerland*
[d]*Institute of Inorganic Chemistry, Bratislava, Slovakia*
[e]*Faculty of Chemistry, A. Mickiewicz University, Poznan, Poland*
[*]*denis_prodius@yahoo.com, phone: +373 22 739722; fax: +373 22 739954*

Abstract: Nine new complexes with the general formula $\{[Ln_2Ba(\alpha\text{-}Fur)_8(H_2O)_4]\}_n$, where Ln = Nd^{3+}, Sm^{3+}, Eu^{3+}, Pr^{3+}, Gd^{3+}, Tb^{3+}, Ho^{3+}, Er^{3+} and La^{3+}; α-Fur ≡ C_4H_3OCOO, were synthesized and characterized by IR spectra, magnetism, X-ray single crystal and powder diffractions. The X-ray diffraction analysis reveals that all titled compounds are isostructural and possess 1D architecture with Ln ion in an eight-coordination geometry formed by six oxygen atoms from furoate and two oxygen atoms from water molecules. The magnetic behaviour of several synthesised complexes as well as $\{[Gd_2Sr(\alpha\text{-}Fur)_8(H_2O)_4]\}_n$ was investigated in the temperature range of 1.8-300 K. The magnetic data were interpreted in the HDVV approximation with the exchange coupling constant J = - 0.014 cm^{-1} that indicates antiferromagnetic interaction in $\{Gd_2Sr\}$, whereas a ferromagnetic one J = + 0.007 cm^{-1} for $\{Gd_2Ba\}$.

Keywords: heteronuclear lanthanide (III) complexes, furancarboxylates ligand, crystal structure, magnetic properties.

Introduction

The syntheses and magnetic properties of rare metal complexes remain an active field of research in recent years, not only for the relevant theoretical interest to investigate the spin-exchange mechanism on the involvement of the *f* orbital in magnetic interactions, but also for understanding chemical properties, and application of rare earth metal for the synthesis of novel molecular magnets [1-3]. However, the research on molecular materials with lanthanides up to now was mostly focused on the interaction of transition metal with lanthanide ions [4-7], but only few heterometallic complexes with *s* metal are structurally known and not all of them were magnetically investigated [8].

The search through the Cambridge Crystallographic Data Center (CCDC) [9] reveals that the data on the metal complexes with a 2-furan-carboxylic acid is limited to 37 hits. In the most cases, coordination compounds of transition and other metals are formed owing to the diversity of coordination modes for carboxyl group of the ligand. The exceptions are homo- and heterometalic complexes of *s* and *s-f* elements. In the complexes of general formula $[M(\alpha\text{-fur})_2]$, where M = Sr^{2+}, Ca^{2+}, the coordination sphere of metal ions is formed by both tipes of oxigen atoms: carboxilic and from furan ring [10]. The same case was found in [8], where, oxygen atoms of furan rings are involved in coordination of *s*- element. The topology of the 2-furan-carboxylic acid donor groups is similar to 2-pyrydincarboxylic acid, which serves as polidentat ligand, forming a polymer structure with one or more coordination centers [11]. It can be expected the same set of coordination modes for 2-furan-carboxilic acid, despite the fact that 2-pyrydincarboxylic acid is composed of donor nitrogen atom, whose affinity for the 3d metals is very high, that determines the mode of coordination.

It was demonstrated [9-14] that the magnetic coupling between Gd(III) ions in Gd(III) dimmers is antiferromagnetic, but recent reports have found ferromagnetic [15-21] interactions. However, the numbers of polynuclear gadolinium compounds for which structural and magnetic data available are quite low and the factors, which govern the nature of Gd^{3+}-Gd^{3+} interaction, have not been clarified. In order to fill this lack of knowledge and to understand the specific features of this kind of heteronuclear lanthanide (III) complexes we synthesized and studied (by IR, magnetism, X-ray single crystal and powder diffraction) nine new compounds. The magnetic properties of gadolinium complex have been studied in detail.

Results and discussion

The X-ray powder diffraction patterns of titled $\{[Ln_2Ba(\alpha\text{-}Fur)_8(H_2O)_4]\}_n$ complexes (Ln = Nd^{3+} (**1**), Sm^{3+} (**2**), Eu^{3+} (**3**), Pr^{3+} (**4**), Gd^{3+} (**5**), Tb^{3+} (**6**), Ho^{3+} (**7**), Er^{3+} (**8**) and La^{3+} (**9**)) shows that they belong to the group of isostructural compounds. It was independently confirmed by the study of single crystal structures of **1** and **4**. Since the complexes are isostructural the characteristic features of the structure is discussed on the base of the compound **1** (Fig.1). All complexes are related to one-dimensional (1D) coordination polymers (Fig.2). In the crystal with space group P-1

the neodymium atom occupies a general position, while Ba atoms reside on the special position - center of inversion. Such an arrangement ensures the formation of the following metal chain along *b* direction in the crystal ···Ln···Ln···Ba···Ln···Ln···, with the distance of Ln-Ln 4.532(1)Å for **1** and 4.523(1)Å for **4**, Ln-Ba 4.161(1)Å and 4.151(1)Å, respectively.

The polymer structure is formed owning to the bridge coordination mode of 2-furan-carboxylic acid moieties. Earlier we have noted that the coordination behavior of the furoic acid can be considered as analogue of 2-pyridine-carboxylic acid. So, it can be expected the same set of coordination modes for 2-furan-carboxilic acid, that was discussed in [11]. There are four moieties of 2-furan-carboxylic acid with deprotonated carboxylic groups in the independent unit cell; however their structural role in the crystal is significantly different. One group forms a *sin-sin* carboxyl bridge and coordinates two lanthanide atoms through oxygen atoms O1 and O2 (Fig.1). The bond distances of Ln-O are shown in Table 1. The second 2-furan-carboxylic moiety, marked by oxygen atoms O10 and O11, also bridges two Ln-cations via *sin-sin* type (Tab.1), but its structural features are more sophisticated. It is a cyclic tetradenthate bridge ligand that forms a single atom (O10) bridge between Ln and Ba cations and coordinates to Ba through oxygen atom (O12) of a furan ring. Two other 2-furan-carboxylic moieties (O4-O6 and O7-O9) have the same chelating coordination mode and bridges Ba atom by means of one oxygen atom from furan fragment and one atom from carboxyl group. Simultaneously, they form a monoatomic bridge Ba-O-Ln with distances of Ba-O 2.901(2) Å, 2.873(2) Å (**1**) and 2.885(3) Å, 2.862(3) Å (**4**) and Ln-O 2.568(2) Å, 2.544(2) Å (**1**) and 2.570(3) Å, 2.553(3) Å (**4**). The real coordination modes of 2-furan-carboxylic acid moieties were analyzed in [8]. In the present structure there are three coordination modes – bidentate bridging, through carboxyl groups of the ligand, tridentate chelating-bridging, with the formation of a monoatomic carboxyl bridge M-O-M and tetradentate, which is a superposition of the two previous ones. It have been found that there are no complexes, where-the oxygen atom of furan ring coordinates to *d* or *f* - metals.

The Scheme 1 [8] shows that the first and second coordination modes match to 1a and 1b type, and the third to 1c. The lanthanide coordination polyhedron (Fig.2, Tab.1) can be interpreted as Thompson cube with the coordination number of metal equal to 8. The polyhedron is asymmetrical and built by six oxygen atoms from carboxyl groups of acid moieties and two water molecules. The distances of Ln-O for Nd are within the 2.366-2.568Å and for Pr – 2.367-2.570Å (Tab.1). The water molecules are associated with the distances from 2.457 to 2.506Å. The comparison of the lanthanide polyhedrons **1** and **4** with that found in [8] for Er shows that they are close except that the contraction of Er-O distance leads to distortions in the polyhedron. The Ba coordination polyhedron is composed by twelve oxygen atoms from acid moieties. The distances are given in Tab.1. By means of hydrogen bonds the polymer chains form a three-dimensional frame in the crystal (Fig.3). There are two water molecules in the independent unite cell. All protons are involved in hydrogen bonds (Tab.2), with one water molecule forms a link inside the polymer chain, whereas the second one between the chains.

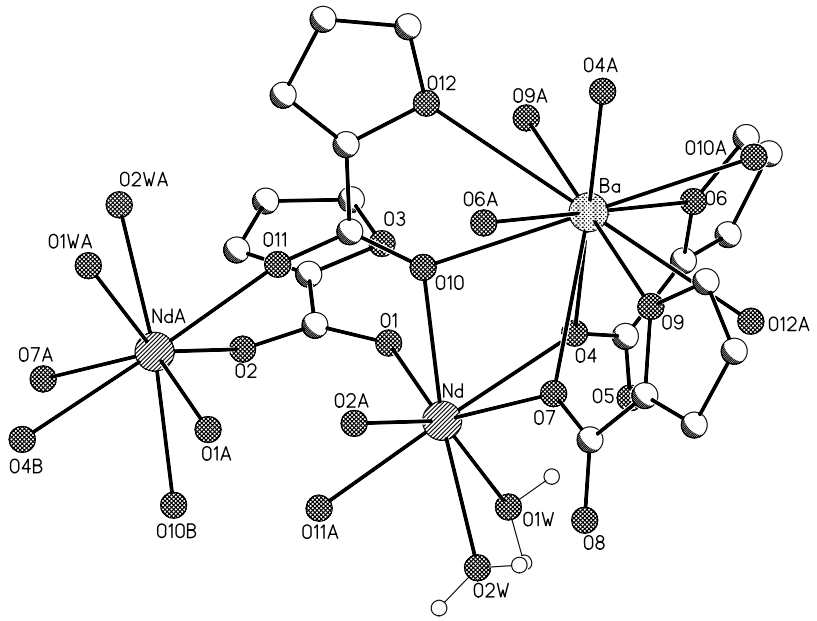

Fig . 1. Structure of the unsymmetrical fragment of the coordination polymer in 1.

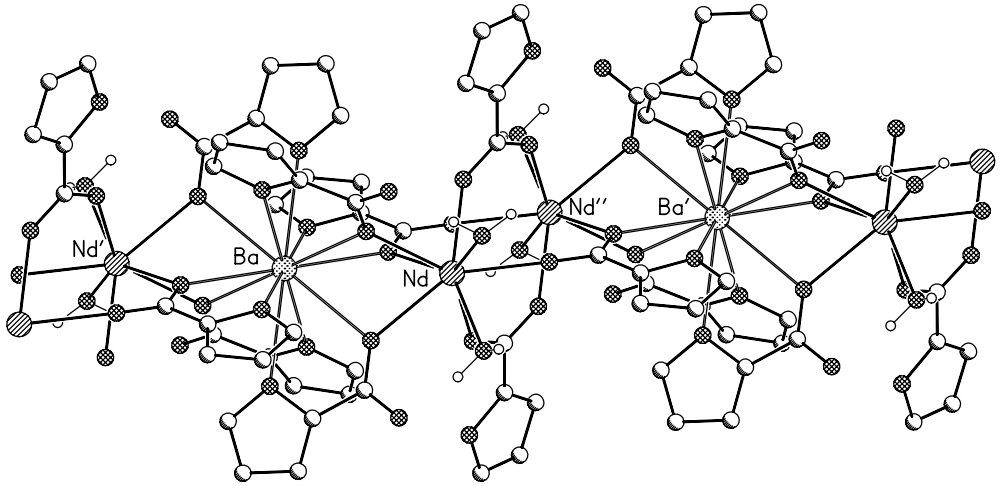

Fig. 2. The fragment of coordination polymer in $\{[Nd_2Ba(\alpha\text{-}Fur)_8(H_2O)_4]\}_n$.

Table 1

Bond lengths and bond angles for compounds 1 and 2

Bond	*d*, Å	
	1 (M = Nd)	**4** (M = Pr)
M-O2	2.366(2)	2.367(3)
M-O11	2.395(2)	2.397(4)
M-O1	2.443(2)	2.444(4)
M-O1*w*	2.464(2)	2.457(4)
M-O10	2.489(2)	2.487(3)
M-O2*w*	2.506(2)	2.503(3)
M-O7	2.544(2)	2.553(3)
M-O4	2.568(2)	2.570(3)
Ba-O10	2.757(2)	2.738(3)
Ba-O9	2.865(2)	2.848(4)
Ba-O7	2.873()	2.862(3)
Ba-O4	2.901(2)	2.885(3)
Ba-O6	2.943(2)	2.924(3)
Ba-O12	3.015(2)	2.996(4)
Angle	ω, deg	
	1 (M = Nd)	**4** (M = Pr)
M-O4-Ba	98.91(6)	98.9(1)
M-O7-Ba	100.19(6)	100.0(1)
M-O10-Ba	104.86(6)	105.1(1)

Table 2

Geometric parameters of hydrogen bonds in the structure 1

Donor (D)	Acceptor (A)	Symmetry codes	R (D···A)	H···A	DHA angle, deg
O1w	05	-x 1-y -z	2,875(5)	2,07	149
O1w	05	x y z	2,640(7)	1,77	167
O2w	08	-x 1-y 1-z	2,927(6)	2,29	128
O2w	08	x y z	2,621(7)	1,77	158

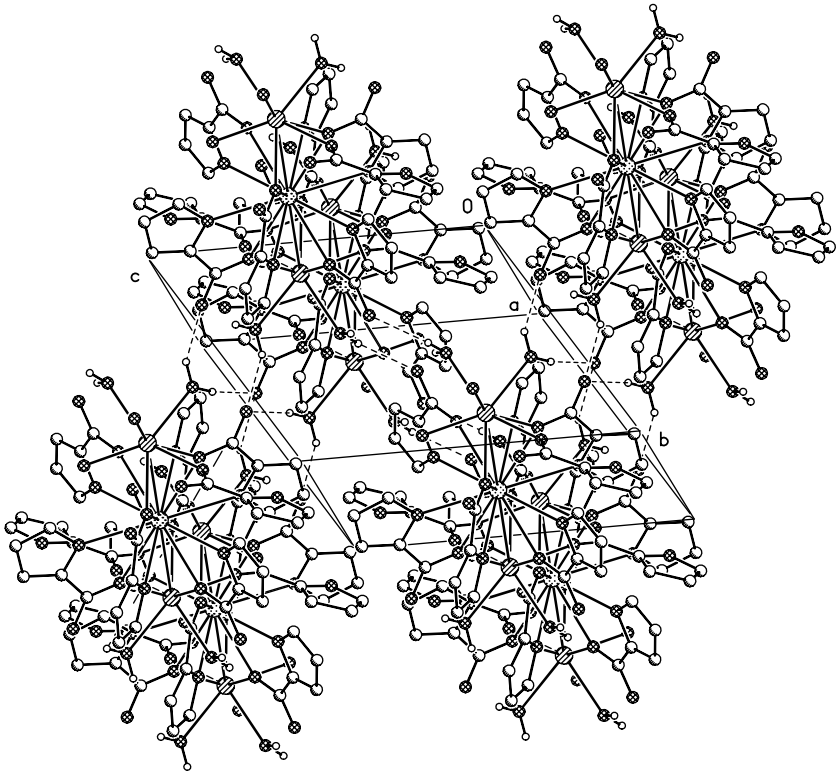

Fig. 3. Projectional view of cell along b axis for 1.

Being interested in the magnetic behaviour of the complexes, variable-temperature (1.8-300K) magnetic susceptibility data were collected for $\{[Nd_2Ba(\alpha\text{-}Fur)_8(H_2O)_4]\}_n$ (1), $\{[Pr_2Ba(\alpha\text{-}Fur)_8(H_2O)_4]\}_n$ (4), $\{[Gd_2Ba(\alpha\text{-}Fur)_8(H_2O)_4]\}_n$ (5) and $\{[Gd_2Sr(\alpha\text{-}Fur)_8(H_2O)_4]\}_n$ (10). complexes, and the results are shown in the form of plots of χ_M *vs.* T and denote magnetic susceptibility per molecule (Fig. 4**,** for **1** and **4**).

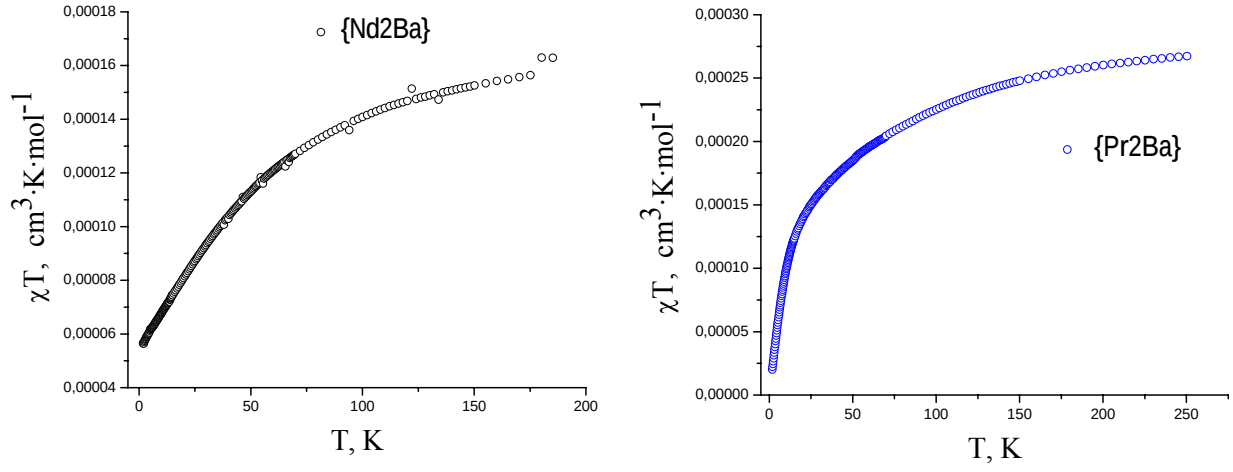

a) **b)**

Fig.4. χT versus T plot for complexes:
$\{[Nd_2Ba(\alpha\text{-}Fur)_8(H_2O)_4]\}_n$ (1) (a) and $\{[Pr_2Ba(\alpha\text{-}Fur)_8(H_2O)_4]\}_n$ (4) (b).

When the rare earth ions different from Gd^{3+} are characterized by orbitally degenerate ground state, the analysis of their magnetic behavior is not straightforward. The best fit of the experimental and theoretical data can be obtained at framework of a classical Crystal Field approach for Pr^{3+}, Nd^{3+} derivatives assuming a pseudo D_4 symmetry with the aim to reduce the number of parameters [8]. In this paper we were interested in magnetic data analysis only of gadolinium containing complexes. The reason for the choice of gadolinium is because Gd(III) ion and its complex are quite simple for a magnetic study. The Gd^{3+} ion has an $^8S_{7/2}$ ground state, which is located at some $3x10^4$ cm^{-1} below the first excited state and is not perturbed by crystal field effects, and has no orbital angular momentum and the anisotropic effect [25]. Based on the inherent nature of Gd(III), the complex $\{[Gd_2Ba(\alpha\text{-}Fur)_8(H_2O)_4]\}_n$ and $\{[Gd_2Sr(\alpha\text{-}Fur)_8(H_2O)_4]\}_n$ are ideal models for studying the magnetic interaction between Ln(III) ions among all title complexes.

The analysis of the measured effective Bohr magneton number (μ_{eff}) for **5** in the temperature range between 1.8 and 300 K shows that with the decrease of the temperature, μ_{eff} increases slowly reaching a maximum value of 11.0 at 3 K, which is slightly less than the spin-only value, 11.23 B.M., calculated from the equation $\mu_{eff} = (\mu^2_{Gd(III)} + \mu^2_{Gd(III)})^{1/2}$, in the absence of exchange interaction for a binuclear Gd(III) ($S_1 = S_2 = 7/2$) system. This behaviour is characteristic for weak intramolecular ferromagnetic spin-exchange interaction between the paramagnetic ions in the complex. But the analysis of magneton number for **10** indicates antiferromagnetic interaction.

In order to further assess the strength of this magnetic interaction quantitatively, a magnetic analysis was performed with the susceptibility equation based on the Heisenberg spin-exchange operator:

$$\hat{H} = -2J\hat{S}_1 \cdot \hat{S}_2 \quad (1),$$

where the exchange parameter J is negative for an antiferromagnetic and positive for a ferromagnetic interaction. For the Gd(III) - Gd(III) ($S_1 = S_2 = 7/2$) system, the theoretical expression of magnetic susceptibility is easily derived from (1):

$$\chi_M = \frac{N\beta^2 g^2}{3kT}\left[\frac{A}{B}\right] \quad (2),$$

where A = 840exp(56x) + 546exp(42x) + 330exp(30x) + 180exp(20x) + 84exp(12x) + 30exp(6x) + 6exp(2x); B = 15exp(56x) + 13exp(42x) + 11exp(30x) + 9exp(20x) +7exp(12x) + 5exp(6x) + 3exp(2x) + 1; x = -J/kT, and χ_M is the molecular susceptibility per complex and the remaining symbols have their usual meaning.

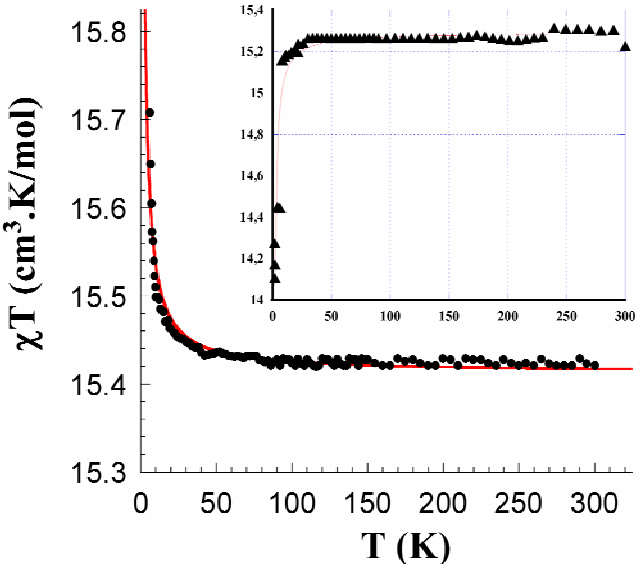

Fig. 5. χT versus T plot for complexes: $\{[Gd_2Ba(\alpha\text{-Fur})_8(H_2O)_4]\}_n$ (5) and $\{[Gd_2Sr(\alpha\text{-Fur})_8(H_2O)_4]\}_n$ (10) (insert).

As shown in Fig. 5, good least-square fits to the experimental data were obtained for J = + 0,007 cm^{-1} and g = 1.98. This results indicate that the complex undergoes a weak ferromagnetic super exchange interaction between Gd(III) - Gd(III) ions.

The analysis of literature [13-17] shows that the different kind of interaction in Gd complexes might be due to the type of the bridging in Gd^{3+}-Gd^{3+} dimmers. Four different homodinuclear units (Fig.6) in Gd^{3+} carboxylates are known. In these units the Gd^{3+} ions are bridged to dimmers by carboxylate groups in a bidentate or tridentate fashion. Beside the pure bridging motifs **a** and **b**, where only bidentate or tridentate modes are involved; there are two other in which both modes are involved (motifs **c** and **d**). As was reported, antiferromagnetic interactions are found for motifs **a** and **c**, and a ferromagnetic one for motifs **b** and **d** [17].

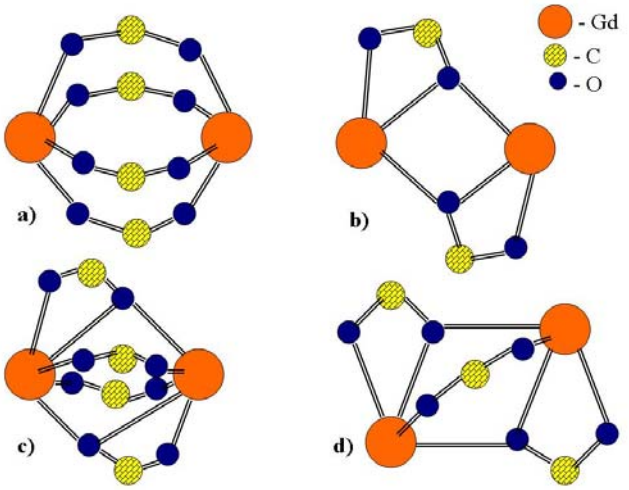

Fig. 6. Bridging motifs in homodinuclear Gd^{3+} carboxylates; (a) for carboxylate groups bridged in a bidentate fashion, (b) two groups bridged in a tridentate fashion, (c) two carboxylate groups bridged in a bidentate, two in a tridentate mode, (d) two carboxylate groups bridged in a tridentate, one in a bidentate fashion.

The values of J and Gd^{3+}-Gd^{3+} distances in the compound **10** are comparable with the ones for other carboxylates contain Gd. The analysis of this complex shows that it is in a good concordance with data given in literature [23-24]. In the compound **10** carboxylate groups bridge the Gd^{3+} ions in a bidentate bridging mode (**a**), that leads to a negative exchange parameter J = -0,014 cm^{-1} and indicates a antiferromagnetic interaction. But in the case of **5**, in spite of bridging of Gd^{3+} ions in a (**a**) fashion, a ferromagnetic interaction was observed. The detailed comparable analysis of **5** and **10** shown that $\{Gd_2Sr\}$ has a rather symmetrical environment, but angles of $\{Gd_2Ba\}$ are quite differ (Table 3).

Table 3

Bond angles

Angles	ω, deg $\{Ln_2Ba\}$	Angles	ω, deg $\{Ln_2Sr\}$ [8]	
O32Nd5O35 O31Nd1O26A	121.50 120.51	O12Er'1O11 O11Er1O12	121.30	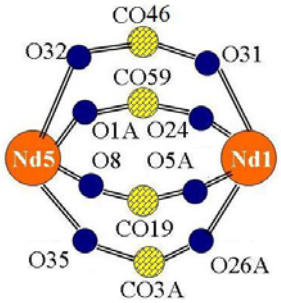
OA1Nd5O8 O24Nd1O5A	118.71 118.52	O6Er'1O5 O5Er1O6	120.66	
O32Nd5O8 O24Nd1O26A	80.15 77.59	O6Er'1O11 O11Er1O6	74.49	
O1ANd5O35 O31Nd1O5A	73.31 72.48	O12Er'1O5 O5Er1O12	73.82	
O32Nd5O1A O26ANd1O5A	75.40 75.65	O5Er'1O11 O11Er1O5	75.63	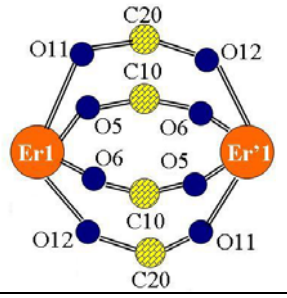
O8Nd5O35 O31Nd1O24	73.67 75.64	O12Er'1O6 O6Er1O12	79.95	
Nd5CO59Nd1 Nd5CO19Nd1	82.17 80.97	Er1C'20Er'1 Er1C20Er'1	81.77	
Nd5CO46Nd1 Nd5CO3ANd1	81.34 79.98	Er1C'10Er'1 Er1C10Er'1	81.63	

Conclusions

Nine new complexes with the general formula $\{[Ln_2Ba(\alpha\text{-}Fur)_8(H_2O)_4]\}_n$, where Ln = Nd^{3+} (**1**), Sm^{3+} (**2**), Eu^{3+} (**3**), Pr^{3+} (**4**), Gd^{3+} (**5**), Tb^{3+} (**6**), Ho^{3+} (**7**), Er^{3+} (**8**) and La^{3+} (**9**); α-Fur ≡ C_4H_3OCOO, were synthesized and characterized by IR spectra, magnetism, X-ray single crystal and powder diffractions. The complexes possess a 1D architecture with Ln ion in a eight-coordination geometry formed by six oxygen atoms from furoate and two oxygen atoms from aqua ligands. The oxygen atom of furan ring coordinates to *s* – metals only. The magnetic data were interpreted in the HDVV approximation with the exchange coupling constant J = - 0.014 cm^{-1} that indicates antiferromagnetic interaction in **10**, whereas a ferromagnetic one J = + 0.007 cm^{-1} for **5**. We suppose that not only the bridging modes of the carboxylate groups influence on the occurrence of ferro-, and antiferromagnetic interaction, but also the distortion among bridging motifs should be taken in consideration.

Experimental

Material. **2-Furoic acid (Aldrich, >98%) was purified by re-crystallization from water/methanol [26]. The starting materials were $Ba(C_4H_3OCOO)_2{\cdot}4H_2O$ and $Ln(ClO_4)_3{\cdot}6H_2O$** (Ln = Nd^{3+}, Sm^{3+}, Eu^{3+}, Pr^{3+}, Gd^{3+}, Tb^{3+}, Ho^{3+}, Er^{3+}, La^{3+})**. $Ba(C_4H_3OCOO)_2{\cdot}4H_2O$ was synthesized by reaction between $BaCO_3$ and 2-furoic acid. $Ln(ClO_4)_3{\cdot}6H_2O$ was prepared by dissolving the respective lanthanide oxides (99.9% pure) in ca. 50% $HClO_4$ and then recrystallizing the resulting salt by evaporating the aqueous solution on a water bath.**

CAUTION: perchlorate salts are potentially explosive and were handled with great care.

Synthesis of $\{[Ln_2Ba(\alpha\text{-}Fur)_8(H_2O)_4]\}_n$, (where Ln = Nd^{3+} (1), Sm^{3+} (2), Eu^{3+} (3), Pr^{3+} (4), Gd^{3+} (5), Tb^{3+} (6), Ho^{3+} (7), Er^{3+} (8) and La^{3+} (9); α-Fur ≡ C_4H_3OCOO). All the nine heterometalic complexes were prepared in a similar fashion and the preparation of $\{[Nd_2Ba(\alpha\text{-}Fur)_8(H_2O)_4]\}_n$ is presented here as an example. Solutions of $Ba(C_4H_3OCOO)_2{\cdot}4H_2O$ (0.30 g, 0.70 mmol) in 10 mL of water and $Nd(ClO_4)_3{\cdot}6H_2O$ (0.40 g, 0.70 mmol) in 15 mL of ethanol were stirred until formation of lilac gel-mass. After 10 days a violet microcrystalline product was filtered off, quickly washed with water and air-dried. Yield: 60 % (on Nd basis). (1) Calc. for $C_{40}H_{32}O_{28}Nd_2Ba$: C, 34.65; H, 2.33; Ba, 9.90%. Found: C, 34.57; H, 2.36; Ba, 10.1%. IR (KBr): ν/cm^{-1}: 3500b, 1627m, 1586vs, 1221m, 1202s, 1136w, 1072s, 1007s, 933m, 883m, 761s, 753w, 611w, 598m, 460s. The IR spectra of other complexes have the same characteristic bands. (**2**) Calc. for $C_{40}H_{32}O_{28}Sm_2Ba$: C, 34.35; H, 2.31; Ba, 9.82%. Found: C, 34.18; H, 2.35;

Ba, 9.78%.(**3**) Calc. for $C_{40}H_{32}O_{28}Eu_2Ba$: C, 34.26; H, 2.30; Ba, 9.79%. Found: C, 33.93; H, 2.36; Ba, 9.80%. (**4**) Calc. for $C_{40}H_{32}O_{28}Pr_2Ba$: C, 34.82; H, 2.34; Ba, 9.95%. Found: C, 34.70; H, 2.36; Ba, 9.93%.(**5**) Calc. for $C_{40}H_{32}O_{28}Gd_2Ba$: C, 34.01; H, 2.28; Ba, 9.72%. Found: C, 33.93; H, 2.35; Ba, 9.71%.(**6**) Calc. for $C_{40}H_{32}O_{28}Tb_2Ba$: C, 33.93; H, 2.27; Ba, 9.69%. Found: C, 33.37; H, 2.33; Ba, 9.55%.(**7**) Calc. for $C_{40}H_{32}O_{28}Ho_2Ba$: C, 33.65; H, 2.26; Ba, 9.63%. Found: C, 33.32; H, 2.29; Ba, 9.53%.(**8**) Calc. for $C_{40}H_{32}O_{28}Er_2Ba$: C, 33.54; H, 2.25; Ba, 9.59%. Found: C, 32.91; H, 2.34; Ba, 9.42%.(**9**) Calc. for $C_{40}H_{32}O_{28}Ln_2Ba$: C, 34.92; H, 2.34; Ba, 9.98%. Found: C, 34.25; H, 2.42; Ba, 9.80%.

Synthesis of {[$Gd_2Sr(\alpha$-Fur)$_8(H_2O)_4$]}$_n$ (10) was performed conform the procedure described in [8]. Yield: 61 % (on Gd basis). Calc. for $C_{40}H_{35}O_{29.5}Gd_2Sr$: C, 34.59; H, 2.54; Sr, 6.30%. Found: C, 34.67; H, 2.51; Sr, 6.10%. IR (cm^{-1}): ν/cm^{-1}: 3500b, 1625m, 1580vs, 1230m, 1200s, 1140w, 1070s, 1010s, 940m, 880m, 820w, 765s, 720w, 615w, 595m, 470s.

Physical measurements. The carbon and hydrogen content of complex was determined by standard micro-methods in the group of microanalysis of the Institute of Chemistry on Vario-EL-III-CHNOS Elemental Analyzer and barium determination was carry out using the Atomic Absorption Spectroscopy (Spectrophotometer AAS-3N Karl Zeiss Jena® DDR) in the Metrology and Analytical Methods of Research Centre of the Academy of Sciences of Moldova.

IR spectrum of each polycrystalline sample was recorded on a Perkin Elmer Spectrum 100 FT-IR Spectrometer.

The magnetic measurements were carried out using a Quantum Design SQUID magnetometer MPMS-XL between 1.8 and 300 K on polycrystalline samples (UT, Karlsruhe). The magnetic data were corrected for the sample holder and the diamagnetic contribution estimated from Pascal constants.

Crystallographic measurements for **1** were carried out at 130 K on KUMA-4CCD diffractometer (Mo-Kα radiation) from a shapeless block of single crystal with the linear dimensions 0.3×0.4×0.2 mm. The crystal was placed 60 mm from the CCD detector chamber. More than hemisphere of reciprocal space was covered by combination of three sets of exposures; each set had a different φ-angle (0, 90, 270) and each exposure of 30 s covered 0.75° in ω. The unit cell determination and data integration were carried out using the CrysAlis package of Oxford Diffraction [27]. Intensity data were corrected for the Lorentz and polarization effects.

The X-ray data for **4** were collected on a STOE Imaging Plate Diffractometer System (IPDS) equipped with an Oxford Cryosystems cooler device using a graphite monochromator (λ = 0.71073 Å). Data were collected [28] using φ rotation movement with the crystal-to-detector distance equal to 70 mm (φ = 0.0–200_, Δφ = 1.0°. All the structure was solved by direct methods [29] and refined by full-matrix least-squares on F^2 with anisotropic displacement parameters for non-H atoms [30]. The hydrogen atoms attached to carbon were included in idealized position in a riding model with isotropic temperature factor fixed at 1.2 × U_{eq} of the relevant carbon atom. Positional parameters of H-atoms of the water molecules were verified by the geometric parameters of the corresponding hydrogen bonds.

The absorption correction was introduced by a semi-empirical method from symmetry equivalent reflections [31]. Scattering factors were taken from the standard compilation [32]. The molecular plots were obtained by using the ZORTEP program [33]. The crystal data and details of the refinement of **1** and **4** are summarized in Table 4, while selected bond lengths and angles – in Table 1.

Table 4
Crystallographic characteristics of the *{[$Nd_2Ba(\alpha$-Fur)$_8(H_2O)_4$]}$_n$ (1) and {[$Pr_2Ba(\alpha$-Fur)$_8(H_2O)_4$]}$_n$ (4)* complexes

Characteristic	1	4
Empirical formula	$C_{40}H_{32}O_{28}Nd_2Ba$	$C_{40}H_{32}O_{28}Pr_2Ba$
FW	1386.48	1379.82
Wavelength, Å	0.71073	0.71073
T, K	293	293
Space group	$P\bar{1}$	$P\bar{1}$
a, Å	10.7619	10.7322
b, Å	11.232	11.1618
c, Å	11.6542	11.5103
α, deg	117.851	117.751
β, deg	93.654	93.603
γ, deg	108.966	108.948
V, $Å^3$	1138.12	1115.74

Z, $\rho_{(calcd.)}$, g/cm^3	1, 2.023	1, 2.054
μ_{Mo}, mm^{-1}	3.202	3.123
Crystal size, mm	0.6×0.15×0.05	0.5×0.25×0.20
θ range, deg	2.69 to 29.76	2.08 to 25.96
Number of reflections: measured/unique	12003/5480 (*R*(int)=0.0185)	8668/4053 (R(int)=0.0942)
Number of refined parameters	317	322
GOOF	1.008	1.011
R (I>2σ(I))	0.0247	0.0488
R (all data)	0.0358	0.0513
$\Delta\rho_{max}$ and $\Delta\rho_{min}$, eÅ^3	2.505 and -0.941	1.926 and -1.582

Acknowledgements

The research described in this publication was made possible in part by CSSDT (#08.819.05.01F) and SNF (SCOPES IB#7320-110823) grants. S.Melnic is grateful to the World Science Foundation. Authors are grateful for providing of magnetic data (**5**, **10**) to the group of Prof. A. K. Powell (University of Karlsruhe, Germany).

References

[1]. Caneschi, A.; Dei, A.; Gatteschi, D.; Poussereau, S.; Sorace, L. Dalton Trans. 2004, 1048-1055.
[2]. Li, X.; Zhang, Z.-Y.; Zou, Y.-Q. Eur. J. Inorg. Chem. 2005, 2909-2918.
[3]. Rohde, A.; Urland, W. Inorg. Chim. Acta. 2006, 359, 2448-2454.
[4]. Kido, T.; Ikuta, Y.; Sunatsuki, Y.; Ogawa, Y.; Matsumoto, N. Inorg. Chem. 2003, 42, 398-408.
[5]. Benelli, C.; Gatteschi, D. Chem. Rev. 2002, 102, 2369-2388.
[6]. Figuerola, A.; Diaz, C.; Ribas, J.; Tangoulis, V.; Granell, J.; Lloret, F.; Mahia, J.; Maestro, M. Inorg. Chem. 2003, 42, 641-649.
[7]. Yin, M.; Lei, X.; Li, M.; Yuan, L.; Sun, J. J. Phys. Chem. Solids. 2006, 67, 1372-1378.
[8]. Turta, C.; Melnic, S.; Bettinelli, M.; Shova, S.; Benelli, C.; Speghini, A.; Caneschi, A.; Gdaniec, M.; Simonov, Y.; Prodius, D.; Mereacre, V. Inorg. Chim. Acta. 2007, 9, 3047-3054.
[9]. Allen, F.N. Acta Crystallogr., Sect.B: Struct.Sci. 2002, 58(2), 380-388.
[10]. Paluchowska, B.; Maurin, J. K.; Leciejewicz, J. Acta Cryst. 1997, C53, 287-289.
[11]. Novitski, G.; Borta, A.; Shova, S.; Kazeva, O.N.; Gdaniec, M.; Simonov, Yu. A. Russ. J. Inorg. Chem. 2008, 53, 202-208.
[12]. Lam, A. W.-H.; Wong, W.-T.; Gao, S.; Wen, G.; Zhang, X.-X. Eur. J. Inorg. Chem. 2003, 149-163.
[13]. Rohde, A.; Hatscher, S.T.; Urland, W. J. Alloys Compd. 2004, 374, 137-141.
[14]. Rohde, A.; Urland, W. Z. Anorg. Allg.Chem. 2004, 630, 2434-2437.
[15]. John, D.; Urland, W. Eur. J. Inorg. Chem. 2005, 4486-4489.
[16]. John, D.; Urland, W. Z. Anorg. Allg.Chem. 2005, 631, 2635-2637.
[17]. Rohde, A.; Urland, W. Dalton Trans. 2006, 2974-2978.
[18]. Costes, J.-P.; Clemente-Juan, J.-M.; Dahan, F.; Necodeme, F.; Verelst, M. Angew. Chem., Int. Ed. 2002, 41, 323-325.
[19]. Hou, H.; Li, G.; Li, L.; Zhu, Y.; Meng X.; Fan, Y. Inorg. Chem. 2003, 42, 428-435.
[20]. Hatscher, S.T.; Urland, W. Angew. Chem., Int. Ed. 2003, 42, 2862-2864.
[21]. (a) Costes, J.-P.; Clemente-Juan, J.-M.; Dahan, F.; Necodeme, F. Dalton Trans. 2003, 1272-1275; (b) Xu, N.; Shi, W.; Liao, D.-Z.; Yan, S.-P.; Cheng, P. Inorg. Chem. 2008, 47, 8748-8756.
[22]. Hernandez-Molina, M.; Ruiz-Perez, C.; Lopez, T.; Lloret F.; Julve, M. Inorg. Chem. 2003, 42, 5456-5458.
[23]. Rohde, A.; Urland, W. Z. Anorg. Allg.Chem. 2005, 631, 417-420.
[24]. Rohde, A.; Urland, W. J. Alloys Compd. 2006, 408-412, 618-621.
[25]. Kahn, O. Molecular Magnetism; VCH Publishers. New York, Weinheim, Cambridge, 1993, p.380.
[26]. Armarego, L. F.; Perrin, D. D. Purification of Laboratory Chemicals, Butterworth-Heinemann, Oxford, 4th ed., 1996, p.529.
[27]. CrysAlis CCD and CrysAlis RED ver. 168, KUMA Diffraction Instruments GmbH, 2001.
[28]. STOE, IPDS Manual. Version 2.93. Stoe & Cie, Darmstadt,Germany, 1997.
[29]. Sheldrick, G. M. SHELX86, Acta Crystallogr. 46A, 1990, 467.
[30]. Sheldrick, G. M. SHELXL-97, University of Göttingen: Göttingen, 1997.
[31]. XEMP ver. 4.2. Siemens Analytical X-ray Inst. Inc. 1990.
[32]. International Tables for Crystallography, vol. C, Kluwer Academic Publishers, Dordrecht, Netherlands, 1992, p.622.
[33]. Zsolnai, L.; Pritzkow, H.; Huttner, G. ZORTEP. Ortep for PC, Program for Molecular Graphics, University of Heidelberg, Heidelberg, Germany, 1996.

SYNTHESIS AND STUDY OF COMPLEXES OF COPPER(II), ZINC, COBALT(II) AND NICKEL(II) WITH NITROFLUORENYLIDENE-9-AMINO(IMINO) DERIVATIVES

S.B. Strashnova*, M.N. Zhuk, O.V.Kovalchukova,
P.V. Strashnov, B.E. Zaitsev

Peoples' Friendship University of Russia, Mikluho-Maklaya str. 5, 117198, Moscow, Russia
** sstrashnova@mail.ru, Phone:+7(495)9550884, Fax:+7(495)9522164*

Abstract: The complexes of general formula $MCl_2 \cdot L^{1-4} \cdot nH_2O$ (where L^1 - *N*-(2,4,7-trinitrofluorenilidene-9)-*p*-dimethyl-aminoanilin, L^2 - *N*-(2,4,5,7-tetranitrofluorenilidene-9)-*p*-dimethylaminoaniline, L^3 - *N*-(2,4,7-trinitrofluorenilidene)-N-(*p*-dimethylaminophenyl)hydroxylamine, L^4 - *N*-(2,4,5,7-tetranitrofluorenilidene-9)-*N*-(*p*-dimethylaminophenyl)-hydroxylamine; M=Cu, Co, Ni, Zn; *n*= 1-3 have been synthesized and investigated by different methods. Spectral criteria of co-ordination of the molecules L^1 – L^4 in electronic absorption spectra were detected. In experimental spectra, the high-frequency band disappears, so the co-ordination occurs through a lone electron pair of a *N*-atom of the amino-group, and the ligand exists in a molecular form. A constant of acidic dissociation of L^3 is determined spectrophotometrically: pKa = 2,07. Geometric optimization of L^1 – L^4 was performed, and the effect of mono-protonation on the electron density was assessed quantum chemically. It was shown that the strongest change of the electron density while protonation occurs at the tertiary amine nitrogen.

Keywords: *3d* metals; complexes; nitrofluoreniliden-9-anilin; amino-group.

Introduction

Among derivatives of polynitrofluorenes, particularly 9-amino-derivatives and 9-hydrazine-derivatives, there are substances which possess anti-tumor activity [1]; or can be used as sensitizers in electrophotography or other fields of technique. Metallocomplexes of nitrofluorenilidene-9-hydroxylamino(imino) derivatives are not studied. Nitrofluorenilidene-9-hydroxylamino(imino)derivatives L^{1-4}, were synthesized by condensation of tris- and tetra-nitrofluorenes with p-nitrozodimethylaniline in solutions of DMF [2]. Two products in approximately equal molar ratio are obtained: N-(nitrofluorenilidene-9-)-*p*-dimethylaminoaniline and N-(nitrofluorenilidene-9-)-N-(*p*-dimethyl-aminophenyl) hydroxylamine. The mixture of the products was separated with the use of chromatography. Mostly possible, L^3 and L^4 are intermediate products of condensation. The structures of L^{1-4} were proved *via* mass spectroscopy and ^{1}H NMR spectroscopy.

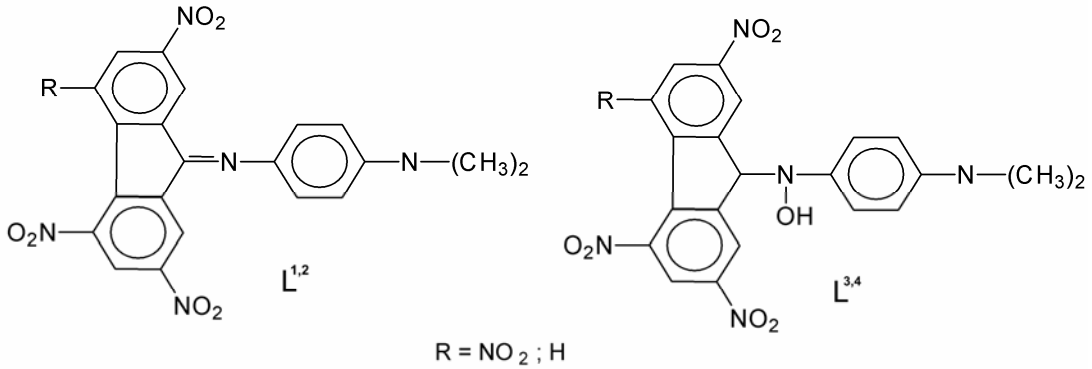

Following on from our earlier work in the field of coordination compounds of nitrofluorene derivatives [3-5] in this paper we discuss our results of the study of new metallocomplexes with L^1-L^4, as far as investigation of their structures and physico-chemical properties.

Results and discussion

The investigated amino(imino)derivatives of polynitrofluorene have several potential centers of co-ordination. They may co-ordinate in molecular as well as in ionic forms through nitro- or imino- (or oximate) groups, the presented organic molecules contain a tertiary amino-group which potentially makes the choice of a center of co-ordination more difficult. In order to determine the most probable way of co-ordination of L^1 – L^4, their geometrical optimization was performed (fig.1), the changes of electron density at mono-protonation were valued. According to

calculations of the models, the strongest change of the electron density while protonation occurs at the tertiary amine nitrogens. Considering protonation as a kind of an analogue of co-ordination, one can propose the N-atom of a diethylamino-group to be the most active co-ordination center of $L^1 - L^4$.

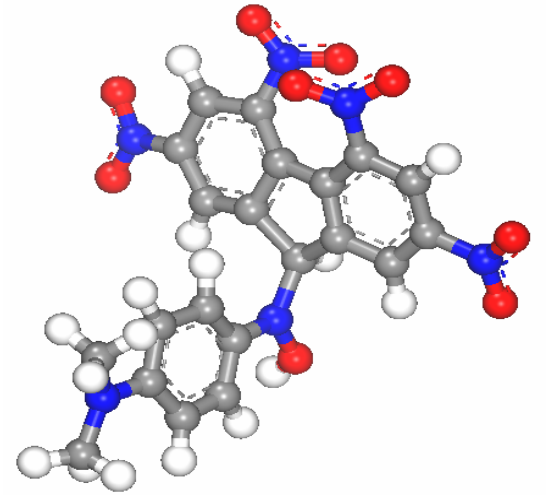

Fig.1. Spatial structure of *N*-(2,4,5,7-tetranitrofluorenilidene-9)-*N*-(*p*-dimethylaminophenyl)-hydroxylamine (L^4)

Spectral investigations of non coordinated ligands and their complexes were performed. IR spectra of $L^1 - L^4$ have characteristic bands in the range of stretching modes of nitro-groups: ν^{as} (NO_2) = 1535-1542 cm^{-1} and ν^{s}(NO_2) = 1349-1355 cm^{-1}[6]. The absorption bands practically do not change while co-ordination. IR spectra of L^1 and L^2 are characterized by intensive absorption band at 1127-1138 cm^{-1}, which is related to stretching modes of C-N bonds of aromatic amines, as far as at 1614-1616 cm^{-1} which can be related to C=C and C=N stretches. In the spectra of complexes (I-IV) these bands shift to 1738 cm^{-1} and sharp bands appear in the area 3445, 3344 and 3090 cm^{-1}. L^3 and L^4 are phenylhydroxylamines. Their IR spectra are characterized by wide bands of ν(OH) = 3420 - 3460 cm^{-1}. Strong widening of the band can be explained by strong inter-molecular hydrogen bonds.

In electronic absorption spectra of non-coordinated ligands were registered bands at 27933cm^{-1} and 14493 cm^{-1} for L^1 as well as at 27778 cm^{-1} and 14578 cm^{-1} for L^2. While deprotonation a series of isobestic points at 38537 cm^{-1}, 36585 cm^{-1}, 33333 cm^{-1} and 29675 cm^{-1} appear. This indicates the equilibrium of neutral and cationic forms of ligands in solution. As it was shown already in [7], in case of co-ordination through an N-atom of an amino-group, a high-frequency band of πl-π* transition with ν_{max}=15122 $см^{-1}$ should disappear as well as in case of co-ordination through a lone electron pair of an imino-group, the maximum of this band should undergo a batochrome shift. Spectrophotometrical titration of solutions of ligands L^1-L^2 with salts of d-metals leads to disappearance of the high-frequency band (fig. 2). It indicates that the co-ordination occurs through a lone electron pair of a N-atom of the amino-group, and the ligand exists in a molecular form. A constant of acidic dissociation of L^1 is determined spectrophotometrically: pKa = 2,07.

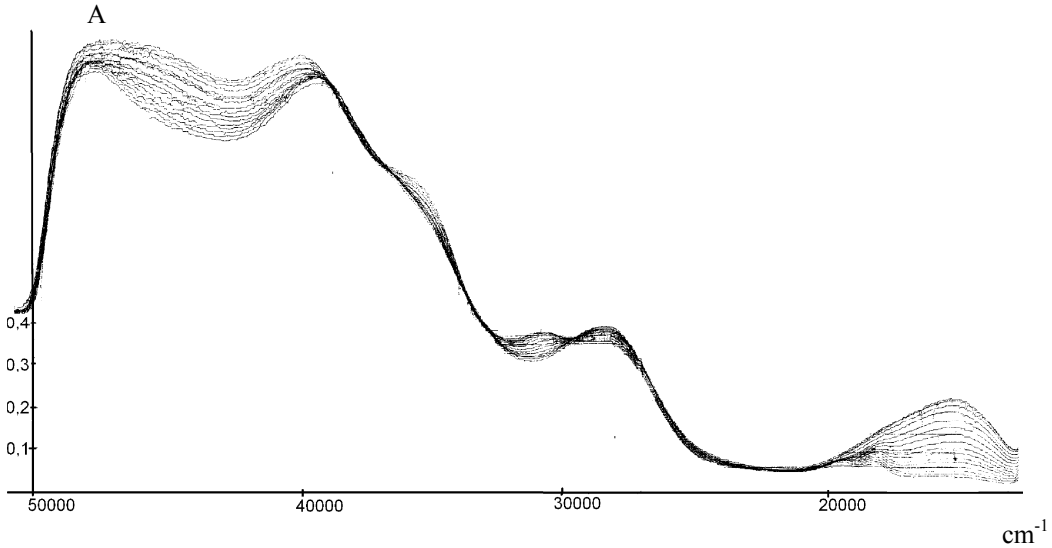

Fig. 2. Spectrophotometrical titration of solution of ligand L^1 with $CuCl_2$ solution.

Electronic absorption spectra of non co-ordinated L^3 and L^4 are characterized by a short-frequency band with a maximum at 27930 cm^{-1} and a band at 14490 cm^{-1} which points the input of the electronic density of amine nitrogen.

Both protonation and complex formation lead to disappearance of absorption at 14490 cm^{-1}. This proves the coordination of ligands through the amine nitrogen. The character of changes of electronic spectra of L^3 and L^4 in ethanol and CCl_4 solution with the rise of pH indicates the process of their alkaline dehydration as the spectra become identical to those of L^1 and L^2. While complexing in neutral and slightly acidic media, the coordination of L^3 and L^4, as far as of L^1 and L^2 takes place through an N-atom of an amino-group.

According to the elemental analysis results metal cation – ligand ratio is 1:1. The presence of two chlorine atoms in complexes (I-VII) proves the neutral form of L^1 – L^4 in complexes. There are up to three water molecules per complex. In order to determine if the character of water molecules binding is complex or cristallizational, thermostability of the complexes was assessed thermogravimetrically in the range of temperatures from 20 to 800 ^oC degrees. It is shown that mass starts to decrease at 120-150 ^oC. The magnitude of this decrease corresponds to the separation of one or two water molecules. So, all of the complexes have one or two water molecules of cristallizational nature whereas complex (III) probably contains one molecule of coordinated water (Table 1)

Experimental

General. The carbon and hydrogen content was determined by standard micro-methods in the microanalytical group. The metals(II) was determined by trilonometric method using the murexid as indicator [8].

IR spectra of non coordinated ligands and synthesized complexes of polycrystalline samples were recorded using Specord 75-IR in frequency range 4000-400 cm^{-1}. UV-visible spectra at different pH values of the ligands and their coordinate compounds were registered on a spectrophotometer Specord UV-VIS in the interval 50000-15000 cm^{-1}.

Geometric optimization of the molecules was performed using the FireFly/PC GAMESS program at the DFT-B3LYP level [9].

Synthesis. 10^{-3} moles of L^3 - L^6 were dissolved in 25 ml of hot DMF (60-65^oC), and a hot ethanol solution of a corresponding metal salt was added dropwise while intensive stirring. After all the ligand underwent the reaction (chromatographic control) the reaction mixture was immediately cooled and left until the crystallization of complexes started. The obtained compounds were filtrated, washed with ethanol and dried in dessicator over P_2O_5 up to a constant mass.

$CuCl_2 \cdot L^1 \cdot 2H_2O$ ***(I)*** Found, % C, 41.12; H, 3.18; N, 11.84; Cl, 11.50; Cu, 10.81. Calc. for $C_{21}H_{19}N_6O_7Cl_2Cu$, M= 603.5 g $mole^{-1}$ %: C, 41.76; H, 3.15; N, 11.60; Cl, 11.76; Cu, 10.52. The yield was 61%. IR spectrum (nujol oil, cm^{-1}): 1138s, 1355s, 1538s, 1616m, 2908m,

$NiCl_2 \cdot L^1 \cdot H_2O$ ***(II)*** Found, % C, 43.08; H, 3.02; N, 12.36; Cl, 12.08; Ni, 10.31. Calc. for $C_{21}H_{17}N_6O_6Cl_2Cu$, M= 581 g $mole^{-1}$ %: C, 43.37; H, 2.93; N, 12.05; Cl, 12.22; Ni, 10.10. The yield was 56%. IR spectrum (nujol oil, cm^{-1}): 1134s, 1351s, 1535s, 1614m, 2912m,

$CuCl_2 \cdot L^2 \cdot 3H_2O$ ***(III)*** Found, % C, 37.12; H, 2.89; N, 14.68; Cl, 10.40; Cu, 9.46. Calc. for $C_{21}H_{20}N_7O_{11}Cl_2Cu$, M= 680.5 g $mole^{-1}$ %: C, 37.03; H, 2.94; N, 14.40; Cl, 10.43; Cu, 9.33. The yield was 65%. IR spectrum (nujol oil, cm^{-1}): 1130s, 1348s, 1538s, 1618m, 2916m,

$CoCl_2 \cdot L^2 \cdot 2H_2O$ (***IV)*** Found, % C, 38.90; H, 2.81; N, 13.16; Cl, 11.11; Co, 8.98. Calc. for $C_{21}H_{18}N_7O_{10}Cl_2Co$, M= 644 g $mole^{-1}$ %: C, 39.13; H, 2.79; N, 13.04; Cl, 11.02; Co, 9.16. The yield was 48%. IR spectrum (nujol oil, cm^{-1}): 1128s, 1355s, 1535s, 1618m, 2908m,

$CuCl_2 \cdot L^3 \cdot 2H_2O$ ***(V)*** Found, % C, 40.02; H, 3.22; N, 13.40; Cl, 11.20; Cu, 10.20. Calc. for $C_{21}H_{20}N_6O_9Cl_2Cu$, M= 634.5 g $mole^{-1}$ %: C, 39.75; H, 3.15; N, 13.25; Cl, 11.20; Cu, 10.02. The yield was 61%. IR spectrum (nujol oil, cm^{-1}): 950s, 1127m, 1340s, 1538s, 2898m, 3426m,

$CuCl_2 \cdot L^4 \cdot 2H_2O$ ***(VI)*** Found, % C, 37.42; H, 3.08; N, 14.40; Cl, 10.40; Cu, 9.20. Calc. for $C_{21}H_{19}N_7O_{11}Cl_2Cu$, M= 679.5 g $mole^{-1}$ %: C, 37.22; H, 3.15; N, 14.41; Cl, 10.44; Cu, 9.34. The yield was 50%. IR spectrum (nujol oil, cm^{-1}): 950s, 1126m, 1344s, 1542s, 2910m, 3432m,

$ZnCl_2 \cdot L^4 \cdot H_2O$ ***(VII)*** Found, % C, 38.12; H, 2.60; N, 14.80; Cl, 11.95; Zn, 9.98. Calc. for $C_{21}H_{17}N_7O_{10}Cl_2Zn$, M= 663 g $mole^{-1}$ %: C, 38.00; H, 2.56; N, 14.78; Cl, 11.71; Zn, 9.80. The yield was 43%. IR spectrum (nujol oil, cm^{-1}): 958s, 1128m, 1354s, 1542s, 2902m, 3460m.

Table 1. Results of the thermogravimetric analysis

compound	m (of weighed part), mg	-Δm(150°), mg	H_2O cryst., %	-Δm (800°) mg	m (rest) (M_xO_y), mg
I	127.2	7.43	5.84	102.97	16.80
II	170.0	5.27	3.00	137.43	27.30
III	132.2	7.00	5.30	105.6	19.60
IV	144.8	8.10	5.50	115.5	21.20
V	178.5	10.14	5.68	145.86	22.50
VI	164.0	8.60	5.24	136.4	19.00
VII	148.0	3.73	2.52	126.47	17.80

Conclusions

The interaction of new ligands *N*-(nitrofluorenilidene-9)-*p*-dimethylaminoanilines (L^1, L^2), and *N*-(nitro-fluorenilidene-9)-*N*-(*p*-dimethyl-aminophenyl)hydroxylamine (L^3, L^4) with the metal salts ($CuCl_2$, $ZnCl_2$, $CoCl_2$ and $NiCl_2$ results the compound of general formula $MCl_2 \cdot L^{1-4} \cdot nH_2O$. The co-ordination of ligands occurs through a lone electron pair of a N-atom of the amino-group in the 1 to 1 mole ratio 1:1, and the ligand exists in a molecular neutral form. A constant of acidic dissociation of L^3 is determined spectrophotometrically: pKa = 2,07.

Acknowledgments

The research described in this publication was made possible in part by the financial support of the RFBR project n° 07-03-00020-a.

References

[1] Degutis J.A., Kurtinaitis J.I. Chemical therahy of tumor. Moskva: 1982, **36**, 240p. (rus).
[2] Organicum (trans. Potapov V.M. Moskva: Mir. –1979, V.2, 434p. (rus).
[3] Zaitsev B.E., Strashnova S. B., Riabov M.A., J. Inorg Chem. 1996, **41**, 1142-1145 (rus).
[4] Minacheva L. Kh., Sergienko V. S., Strashnova S. B. et all, Kristallografiya. 2005, **50**, 79-83 (rus).
[5] Strashnova S. B., Avramenko O.V., Sergienko V. S. et all, J. inorg chem. 2008, **53**, 1697-1702 (rus).
[6] Nakamoto K. Infrakrasnye spectry I spectry KR neorganiceskih I organiceskih soedinenii. Moskva: Mir. 1991, 540p. (rus).
[7] Zaytsev B.E. Spectral coordination chemistry. Moskva: Rudn.-1991, 272p. (rus).
[8] Schwarzenbach G., Flaschka H. Kompleksonometriceskoe titrovanie. Publ. ″Himia″, Moskva, 1970, 359p. (rus.)
[9] Alex A. Granovsky, PC GAMESS/Firefly version 7.1.F,

NEW EFFECTIVE SYNTHESIS OF THE CHINCHONINIC ACIDS FROM (-)-α-PINENE

Oleg Radul, Alexandru Gudima, Fliur Macaev*

Institute of Chemistry of the Academy of Sciences of the Republic of Moldova,
Academy str. 3, MD-2028, Chisinau, Moldova
Tel: +373-22-739-754, fax +373-22-739-954
E-mail: flmacaev@cc.acad.md

Abstract. New effective synthesis of the chiral chinchoninic acids form (-)-α-pinene has been elaborated. It has been shown that, the considerable increase of the yield and purity of chiral acids is achieved applying the method of under phase transfer catalysis.

Keywords: chinchoninic acids, quinoline, pinonic acid, α-pinene.

Introduction

The development of pharmacological agents capable to counteract the mechanisms of drug resistance in malaria therapy has remained a major goal for the past hundred of years. When the mechanisms of multidrug resistance is identified, the hope of identifying molecules capable to simultaneously reverse the resistance to a number of unrelated drugs has to stimulate research in this field.

Early chinchoninic acids have been the main medicine for malaria treatment [1]. Nowadays a great number of analogues of this substance are known, their efficacy being three times greater than that of quinine. Recently, a novel class of optically active chiral oxindoles as specific anti HIV-1 agents from α-pinene **1** has been reported [2,3]. Therefore, these analogues are considered as promising agents for the treatment of other diseases.

This paper describes the resolution of various conditions on obtaining chiral chinchoninic acids form α-pinene **1** via pinonic acid **2**.

Results and Discussion

The target optically active chinchoninic acids **4-7** with the substituents at C2 quinoline moiety were prepared from the keto acid **2a** and isatine **3** as outlined in Scheme 1.

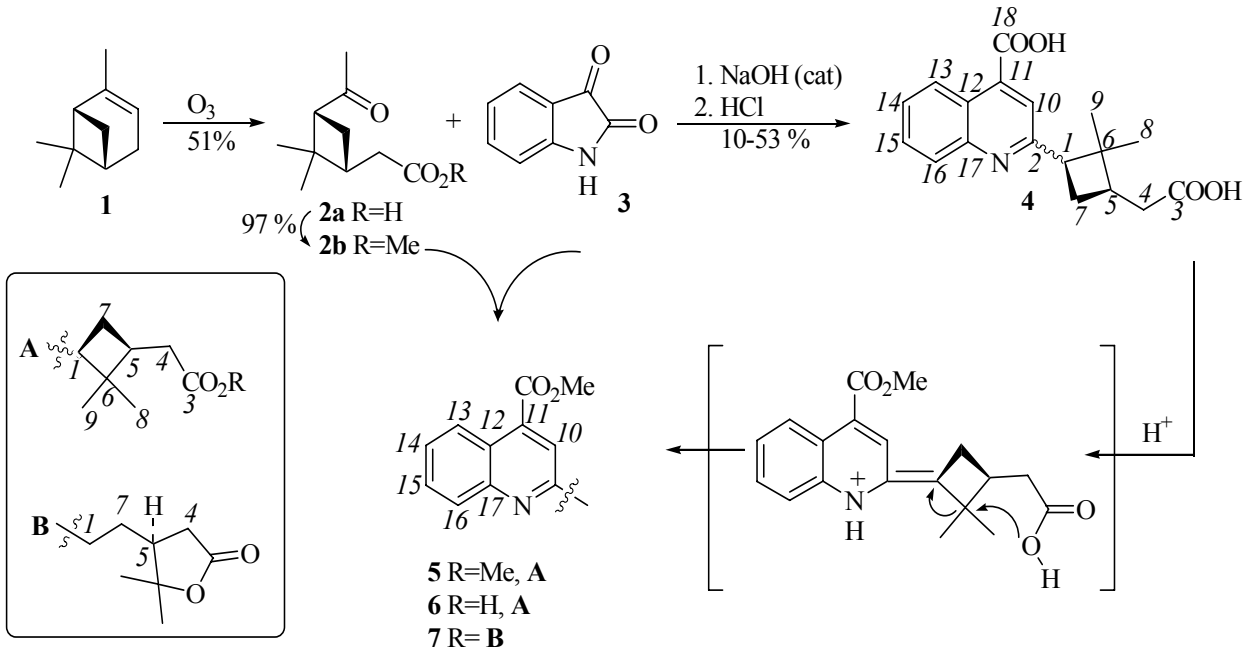

Mixture **2a** and **3** after refluxing (6 hours) in EtOH solution NaOH lead the chinchoninic acids with 10% yield, that is in agreement with data [4] where the authors have attempted to elaborate a technological method for preparation of **4**. The yield of the target acids reaches 50-53% when the time of reaction is increased to 48-50 hours. In ^{1}H NMR spectra of quinolines **4** all peaks are twinned which indicates that the reaction product is a mixture of two epimeric compounds (3:2). In spectra of the major isomer there are signals of the heminal methyl groups at 0.54 and 1.31 ppm, triplet of ^{1}CH group at 3.0 ppm, duplet-duplet signal of the ^{4}CH$_2$ group at 2.423 and 2.434 ppm,

multiplets of the three-protons signals of $^{7}CH_2$ and ^{5}CH groups at 2.19-2.34 ppm, two duplet signals of ^{10}CH, ^{16}CH at 8.0 and 8.62 ppm, multiplet signals of ^{14}CH, ^{15}CH at 7.61-7.79 ppm and carboxylic groups protons at 11-14 ppm. That the reaction product is a mixture of two substances also follows from the data of ^{13}C NMR spectrum there are doubled signals of carbons of both carboxylic groups ^{18}C and ^{3}C at 173.86, 178.05 and 167.65, 167.68 ppm, and carbon ^{2}C at 160.43 and 161.61 ppm. The difference in the values of the position of heminal group signals in *cis*-isomer compared with similar ones of *trans*-isomer in ^{13}C NMR spectra is due to the fact that the first one experience two screening effects of steric character from *cis*-located substitutors of the four-member ring, while in the *trans*-isomer it is less expressed. These data are in agreement with data for similarly constructed derivatives of 2,2-dimethylcyclobutane [5].

Table 1

NMR Spectroscopic Data of Compounds 4

№	Groups	Method	The chemical shifts ($CDCl_3$, δ, ppm, *J*/Hz)	
			Major izomer	Minor izomer
1	CH	^{1}H	3.50, [c]t, $J = 10$	3.58, t, 1H, $J = 7.6$
		^{13}C	48.92	48.22
2	C	^{1}H	-	-
		^{13}C	160.30	161.49
3	CO_2H	^{1}H	10.0	10.0
		^{13}C	172.87	172.67
4	CH_2	^{1}H	2.29, 2.26, [b]d d, $J_{5,4\alpha} = 6.4$, $J_{5,4\beta} = 6.8$	2.30, 2.28, d d, $J_{5,4\alpha} = 6.4$, $J_{5,4\beta} = 6.8$
		^{13}C	29.92	29.92
5	CH	^{1}H	2.42-2.45, [d]m	2.42-2.45, m
		^{13}C	37.91	37.57
6	C	^{1}H	-	-
		^{13}C	43.49	41.60
7	CH_2	^{1}H	2.53-2.64, m	2.53-2.64, m
		^{13}C	24.90	24.34
8	CH_3	^{1}H	0.56, [a]s	0.64, s
		^{13}C	17.52	17.52
9	CH_3	^{1}H	1.33, s	1.23, s
		^{13}C	30.01	30.01
10	CH	^{1}H	7.63, d, $J = 8.0$	7.67, d, $J = 8.4$
		^{13}C	123.00	122.96
11	C	^{1}H	-	-
		^{13}C	135.77	135.85
12	C	^{1}H	-	-
		^{13}C	121.55	122.20
13	CH	^{1}H	8.07, d , $J = 8.0$	8.09, d, $J = 8.0$
		^{13}C	125.32	125.32
14	CH	^{1}H	7.77, 7.79, d d, $J_{13,14} = 8.0$, $J_{14,15} = 8.4$	7.77, 7.79, d d, $J_{13,14} = 8.0$, $J_{14,15} = 8.4$
		^{13}C	129.60	129.23
15	CH	^{1}H	7.64, 7.68, d d, $J_{14,15} = 6.0$, $J_{15,16} = 4.8$	7.64, 7.68, d d, $J_{14,15} = 6.0$, $J_{15,16} = 4.8$
		^{13}C	126.97	126.97
16	CH	^{1}H	8.63, d, $J = 8.8$	8.63, d, $J = 8.8$
		^{13}C	129.33	129.56
17	C	^{1}H	-	-
		^{13}C	148.07	147.96
18	CO_2H	^{1}H	10.0	10.0
		^{13}C	167.65	167.68

[a]s-singlet, [b]d-doublet, [c]t-triplet, [d]m-multiplet

We have shown that the considerable increase of the yield and purity of chiral acids is achieved applying the method of under phase transfer catalysis. In this method, a catalyst is used to carry the nucleophile from the aqueous into the organic phase. As an example, 18-crown-6·CN is added and the product **4** is formed with 81% yield. It is worth noting that not all catalysts, as well as ketones **2a,b,** work equally well in our situations. Experimentation is

required to find benzyltriethylammonium chloride as optimum catalyst under condensation of ester **2b** with **3**. In last case the product **4** has been obtained with yield up to 95%.

Esterification of acids **4** has been investigated, also. There are many ways of performing this reaction. It has been established that treatment of **4** with MeOH in the presence of catalytic amounts of H_3PO_4, $HClO_4$ or H_2SO_4 at room temperature results in the formation of esters **5**, while at high temperature (reflux), the lactone **7** has been isolated.

It's ^{1}H NMR-spectrum is characterized by the presence of the singlet six-proton signal of the hem-dimethyl group at 1.35 ppm, the three-proton signal of the ester group at 3.60 ppm, the multiplet four-proton signals of $^1CH_2$, $^7CH_2$ at 0.59-1.43, 3.38-4.15 ppm, the multiplet three-proton signals of two groups: $^4CH_2$ and ^5CH at 1.05-2.58 ppm and of multiplet signals of quinoline fragment's protons at 7.54-8.74 ppm. Elemental analysis data in combination with characteristic bands of ester, lactone and quinoline groups in the IR-spectrum supplement the spectral characteristics of substance **7.** It should be mentioned that the transformation of the pinonic acid **2** into such types of lactones has been described earlier [5], while the registered signals of the dimethyl-tetrahydrofuran fragment are in good agreement with data for 3-(3'-oxobutyl)-4,4-dimethylbutyrolactone [6].

By action of solution CH_2N_2 in 1.4-dioxane upon **2a,** diesters **5** have been obtained (50% yield). In the ^{1}H NMR spectrum of **5**, all peaks are doubled and one of the products in the mixture predominates. Present in its NMR-spectrum are the characteristic singlet signals of the hem-dimethyl group at 0.52 ppm, 1.28 ppm and esters ones at 3.38 ppm and 3.97 ppm. That the reaction product is a mixture of two substances also results from data of ^{13}C NMR spectrum. In the area of the weak field there are doubled signals of carboxy groups' carbons at 172.60 ppm and 172.58 ppm, as well as the appearance, at 51.06 ppm and 52.66 ppm, of the methyl ester's carbon signal in comparison with the spectrum of the initial **4.**

Conclusions

This report describes new effective synthesis of the chiral chinchoninic acids form (-)-α-pinene. Because of the reactive pinonic acid is a reactive chemical undergoing many reactions of a methyl ketone, carboxyl groups as well as cyclobutane ring. Moreover, in those instances where rupture of the cyclobutane ring has been shown as well as a new methods for liquid/solid phase transfer/catalyst conditions proposed.

Experimental

All the used solvents were of reagent quality, and all commercial reagents have been used without additional purification. Removal of all solvents has been carried out under reduced pressure. Analytical TLC plates were Silufol® UV-254 (Silpearl on aluminium foil, Czecho-Slovakia). Melting points has been determined on the heating table "Boetius" and not corrected. IR spectra have been recorded on a Specord 75 IR instrument. ^{1}H and ^{13}C NMR spectra have been recorded for $CDCl_3$ 2-3% solution on a Bruker AC-80 (80 and 20 MHz) and "Bruker AC-E400" (200.13 and 50.32 MHz). The specific rotation has been recorded on "Jasco-P-2000".

(-)-α-Pinene 1– reagent from Fluka Chemical Company. n_D^{20} 1.466, $[\alpha]_D^{20}$-58.48° (c 0.046, $CHCl_3$).

Acid 2a and **ester 2b** have been prepared according to previously published method [2].

Preparation of (+)-2-[(1*S*)-3(4-carboxy-2-quinoline)-2.2-dimethylclobutyl] acetic acid 4 has been obtained by three methods.

Method a) Solution of 6.72g (120 mmol) KOH in 5 ml of water was added to the solution of 2.4g (16.6mmol) of isatine **3** in 25 ml of EtOH. The mixture was boiled during 5 minutes and then cooled. The obtained solution was supplemented (drop-by-drop) with the solution of 3g (16 mmol) of pinonic acid **2a** in 25ml of EtOH and boiled for 48 hours. The solvent was distilled; water (25ml) was added with following acidification to pH 1 by HCl conc. The solid was filtered out, washed with water, EtOH and dried. 2.13g (53%) of creamy-colored crystals were obtained. M.p. 248-250° (EtOH). $[\alpha]_D^{20}$+6.33° (c 0.016, MeOH). IR-spectrum (ν/cm^{-1}): 1380, 1385 (CMe_2), 1720-1760, 2560-3000 (COOH). It was found %: C 69.03, H 6.09, N 4.44. $C_{18}H_{19}NO_4$. It was calculated, %: C 68.99, H 6.11, N 4.47. The major isomer was isolated for analytical purposes. M.p. 253-254° (EtOH). $[\alpha]_D^{20}$+19.55° (c 0.005, MeOH). IR-spectrum (ν/см$^{-1}$): 1373, 1388 ($C(CH_3)_2$), 1716, 2600-3000 (COOH), 3432 (C=N).

Method b) The solution of 0.8g (0.02 mol) NaOH in 5ml of EtOH has been added to the suspension of 1.47g (0.01 mol) **3** in 30 ml of dry benzene. After 2 hours of stirring the solution of 1.84g (0.01 mol) **2a** in 20 ml of benzene has been added followed by 0.4g (0.01 mol) of NaOH and 0.15g (0.0005 mol) of 18-crown-6·CH_3CN catalyst. The reaction mixture was boiled for 7 hours. The organic phase was separated. The residue was dissolved in 20ml of water and acidified up to pH 2 by conc. HCl. The solid was filtered, washed with water, dried in open air then over NaOH. In result, we have obtained 2.54g (81%) of mixture of isomers similar to those described in point a).

Method c) 20 ml of diethyl ether followed by 1.47g (0.01 mol) **3** were added to the solution of 0.8g (0.02 mol) of NaOH in 6 ml of EtOH. The formed violet suspension was mixed during 1.5 hours and then boiled during 3 hours. At room temperature and while mixing, the solution of 1.98g (0.01 mol) of ester **2b** in 20 ml of ether, 0.4g(0.01 mol) of NaOH and 0.114g (0.005 mol) of benzyltriethylammonium chloride was gradually added to the reaction mixture.

The suspension was boiled during 6 hours under mixing, the ester was distilled, and the residue was dissolved in a minimum quantity of water, acidified to pH2 by conc. HCl. The solid was filtered, washed with water, dried in open air then over NaOH. We obtained 2.98g (95%) of substance **4** in the form of isomers mixture.

Preparation of methyl 2-[2,2-dimethyl-3-(methyl 2-quinoline-4-carboxylate)cyclobutyl] acetate 5.

The solution of diazomethane, obtained from 0.08g (7.8 mmol) of NMU and 2g (36 mmol) of KOH in 15 ml of diethyl ether, was added to the solution of 0.94g (3mmol) of acid **2a** in 10 ml of 1,4-dioxane drop by drop during 30 minutes under mixing. After that, the mixture was stirred for another half an hour, washed by saturated solution of $NaHCO_3$ (3 X 10 ml) and with water (10 ml), dried over Na_2SO_4, steamed in vacuum, and the obtained oily residue (1g) was chromatographed on the column (silica gel 100/400, petroleum ester/ethyl-acetate 2:1). We obtained 0.51g of oily light-yellow product **5**. The yield was 50%. IR-spectrum (ν/cm^{-1}): 1370, 1383 ($C(CH_3)_2$), 1733 ($COOCH_3$), 3444 (C=N). Spectrum NMR ^{1}H of major isomer ($CDCl_3$, δ, ppm, *J*/Hz): 0.52, 1.28 s, s (6H, CMe_2), 2.2-2.52 m (5H, $^4CH_2$, ^5CH,$^7CH_2$), 3.40 t (1H, ^1CH, *J*=7.94), 3.58, 3.97 s, s (6H, $2CO_2Me$), 7.62-8.12 m (3H, ^{13}CH, ^{14}CH, ^{15}CH), 8.47-8.59 m (2H, ^{10}CH, ^{16}CH). Spectrum NMR ^{13}C of the prevailing isomer ($CDCl_3$, δ, ppm): 172.58 (^3C), 166.26 (^{18}C), 160.18 (^2C), 148.06 (^{17}C), 134.45 (^{11}C), 129.62 (^{14}C), 129.39 (^{16}C), 127.11 (^{15}C), 124.71 (^{13}C), 122.25 (^{10}C), 121.58 (^{12}C), 52.66, 51.06 2(CO_2Me), 48.97 (^1C), 43.46 (^6C), 37.51 (^5C), 35.15 (^9C), 29.84 (^4C), 24.89 (^7C), 17.41 (^8C). It was found,%: C 70.52, H 7.67, N 3.88. $C_{21}H_{27}NO_4$. It was calculated, % C 70.56, H 7.61, N 3.92.

Preparation of 2-[-2,2-Dimethyl-3-(methyl 2-quinoline-4-carboxylate)cyclobutyl] acetic acid 6.

Method a). The solution of 0.63g (0.002 mol) of acid **IV** and 0.1 ml of conc. H_2SO_4 in 30 ml of MeOH was stirred at room temperature during 3 days. Then the MeOH was removed and the residue was dissolved in water. The mixture was neutralized by NaOH solution up to pH 6. The white solid was filtered, washed with water, dried and in result has been obtained 0.58g (88%) of product **6**. M.p. 98-99°. The spectrum ^{1}H NMR of the major isomer ($CDCl_3$, δ, ppm, *J*/Hz): 0.72, 1.46 s, s (6H, CMe_2), 2.3-2.60 m (5H, $^4CH_2$, ^5CH,$^7CH_2$), 3.41 m (1H, ^1CH), 3.70 s (3H, CO_2Me), 7.49-8.18 m (3H, ^{13}CH, ^{14}CH, ^{15}CH), 8.83-8.96 m (2H, ^{10}CH, ^{16}CH), 10.0 s (1H, CO_2H). The spectrum ^{13}C NMR of the major isomer ($CDCl_3$, δ, ppm): 171.95 (^3C), 167.65 (^{18}C), 160.95 (^2C), 148.63 (^{17}C), 135.25 (^{11}C), 129.54 (^{14}C), 128.65 (^{16}C), 126.28 (^{15}C), 125.83(^{13}C), 122.54 (^{10}C), 122.07 (^{12}C), 50.77 (CO_2Me), 49.61 (^1C), 38.22 (^6C), 34.71 (^5C), 30.31 (^9C), 29.42 (^4C), 25.18 (^7C), 17.66 (^8C).

Method b).Out of 0.63g (0.002 mol) of acid **2a** and 0.22ml of $HClO_4$ (60%), similar to method a), we obtained 0.28g (43%) of product **6**.

Preparation of methyl 2-{2-[(3S)-2.2-dimethyl-5-oxotetra-hydro-3-furanile] ethyl} 2-quinoline-4-carboxylate 7.

One drop of H_2SO_4 (98% concentration) was added to the solution of 0.47g (1.5 mmol) of acid **2a** in 5ml of MeOH and was refluxed during 12 hours. After that the methanol was distilled and the residue was recrystallized from water. We obtained 0.42g (86%) of crystalline cream-colored product with 205-208°C m.p. IR-spectrum (ν/см$^{-1}$): 1375, 1380 ($C(CH_3)_2$), 1735 ($COOCH_3$), 1760 (COOH), 3400 (C=N). ^{1}H NMR spectrum ($CDCl_3$, δ, ppm, *J*/Hz): 0.75 d (1H, ^5CH, *J*=7.79), 0.94 d (1H, $^4CH_\beta$, *J*=7.79), 1.32, 1.43 s, s (6H, CMe_2), 2.25-3.58 m (5H, $^4CH_\alpha$, $^6CH_2$, $^7CH_2$), 3.68 s (3H, CO_2Me), 7.54-7.72 m (3H, ^{13}CH, ^{14}CH, ^{15}CH), 8.04-8.94 m (2H, ^{10}CH, ^{16}CH). It was found, %: C 69.79, H 6.55, N 4.37. $C_{19}H_{21}NO_4$. It was calculated, %: C 69.71, H 6.47, N 4.28.

References

[1]. Heterocyclic Compounds, V. IV. Foreign Literature Publishers, M. 1955, pp. 232-239.
[2]. Macaev, F.Z.; Radul, O.M.; Gudima, A. Russ.Chem.Bl. 2008**,** 7, 380-383.
[3]. Macaev, F.Z.; Geronikaki, A.; Radul, O.M.; Gudima, A.P. New chiral oxindoles as potential anti HIV-1 agents. The EAMHC- 4th Eurasian Meeting on Heterocyclic Chemistry. Abstracts of communications. Thessaloniki, Greece, 2006, p.175.
[4]. Hendrick, G.W.; Lawrence, R.V. Pinonic acid. Industrial & Engineering Chem. 1960, 52, 853-856.
[5]. Arcus, C.L.; Bennett, G.J. J.Chem.Soc. 1958, 123, 284-289.
[6]. Poulter C.D., King Chi-Hsin R. J.Am.Chem.Soc. 1982, 104, 1420-1422.

FLUORESCENT N-HETEROCYCLES VIA ONE-POT TANDEM REACTIONS

Rodica Dinica*[1], Bianca Furdui[1], Geta Cârâc[1] and Constantin Stanciu[1]

[1] *"Dunarea de Jos" University, Galati, Chemistry Department, Domneasca street, 47, Romania, E-mail: rodinica@ugal.ro*

Abstract. Synthetic indolizines have attracted special attention in the past years mainly due to their manifold practical utilities. An improved preparation of bis-indolizines using microwave-assisted synthesis is described. The microwave-mediated three component reaction of acyl bromide, bipyridine and dipolarophyl is catalyzed by basic alumina to give corresponding bis-indolizines in excellent yields in a one –pot reaction. This strategy would provide access to fast synthesis of bis-indolizines which otherwise are accessible only through multistep synthesis.

Keywords: microwave, "one-pot" reaction, indolizine

Introduction

The conception of molecules with biologic properties is very interesting and opens a field of research important for molecular biology and pharmacology. Microwave irradiation is known to accelerate organic reactions and is a powerful tool in organic synthesis and in biocatalysis. The microwave-promoted solid phase heterogenous reaction is well-known as an environmentally benign reaction methodology that usually provides improved selectivity, enhanced reaction rates, cleaner products and manipulative simplicity [1-10]. The objective of the present study was to establish the viability of a three-component reaction (3-CR) involving a 1,3-dipolar cycloaddition reaction between an *in situ* generated dipole (from ω-bromacetophenones and 4,4'-bipyridine) and ethyl propiolate, using a fast and facile reaction strategies that involve microwave energy as unconventional energy source. This strategy would provide access to fast one-pot synthesis of bis-indolizines which otherwise are accessible only through multistep synthesis [14-16]. 1,3-Dipolar cycloaddition has been widely used for the synthesis of heterocyclic compounds because of its utility for creating two sets of bonds in a single operation and because stereoselectivity and regioselectivity are easily predictable [11]. Among a number of 1,3-dipoles, azomethine ylides are useful intermediates for the synthesis of various five-membered nitrogen-containing heterocycles. They belong to the class of 1,3-dipoles of the allyl type with a cationic nitrogen atom and react with several dipolarophiles to give pyrrolidine derivatives, respectively [12-13].

Results and discussion

We report here the synthesis of novel nitrogen heterocycles, with fluorescent properties. These compounds are easy prepared using microwave-assisted synthesis. The microwave-mediated three component reaction of phenacyl bromide, bipyridine and dipolarophyl is catalyzed by basic alumina to give corresponding bis-indolizines in excellent yields in a one–pot reaction.

Previously, we have studied the synthesis of this type of compounds using multistep reactions. Substituted indolizines are very attractive heterocyclic units, as a number of representatives of this class and, especially their partially or completely reduced analogues, indolizidine alkaloids and related natural compounds which exhibit important biological properties. As a part of our program on developing efficient methods for differently substituted indolizines, we were particularly interested in elaborating efficient approaches toward three-component reaction of these compounds which are very interested from the point of view fluorescent properties, certain of them being useful for securely marking articles, such as documents and security paper.

If successful, such a strategy would provide access to fast one-pot synthesis of cycloadducts which otherwise are accessible only through multistep synthesis. The first successful examples of the application of this approach are described here in (Scheme 1).

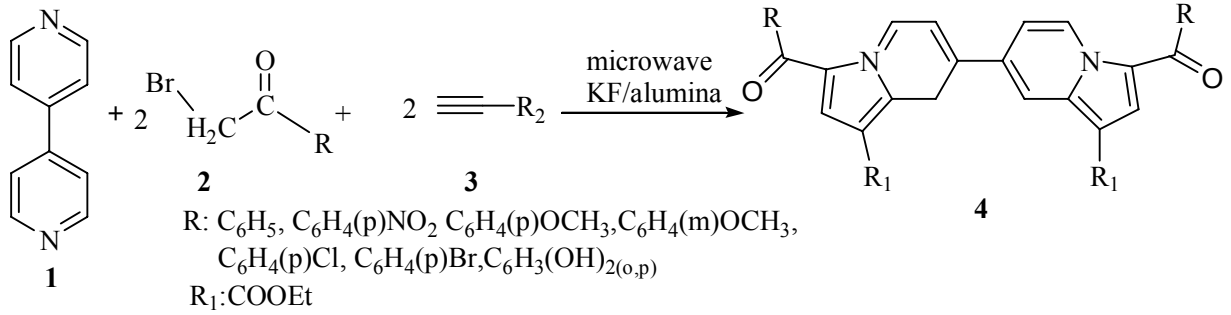

Scheme 1. One-pot synthesis of bis-indolizines

The design of multicomponent reactions (MCR) is an important field of research from the point of view of combinatorial chemistry. Being a one-pot reaction, generally multicomponent reactions afford good yields.

The indolizines constitute the core structure of many naturally occurring alkaloids (-)*slaframine*, (-)*dendroprimine*, *indalozin* and *coniceine*. The synthesis of biologically active indolizines continues to attract the attention of organic chemists.

The indolizines are most commonly synthesized by sequential *N*-quarternization and intramolecular cyclocondensation reactions or the cycloaddition reaction of *N*-acyl/alkyl bipyridinium salts. These strategies, however, involved multistep synthesis employing two-component reactions and do not represent the goal of an ideal synthesis.

Bis-indolizinic compounds were prepared, by classical reaction, according the retrosynthetic strategy based on cicloaddition reaction (Scheme 2) [14-15].

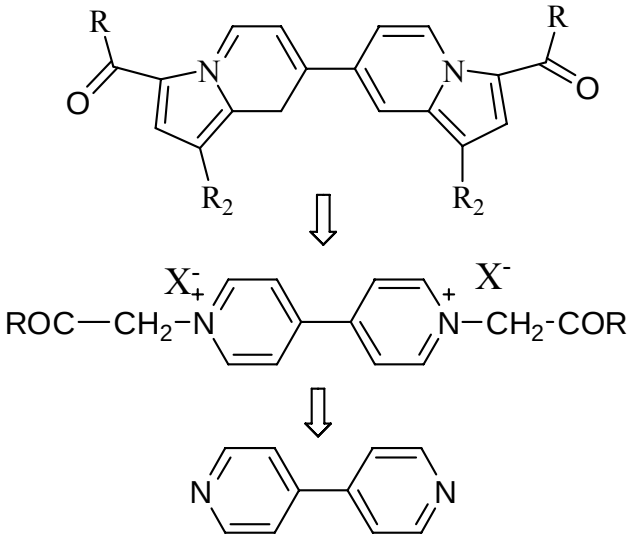

Scheme 2. Retrosynthetic strategy for obtaining of bis-indolizines

It was reasoned that basic alumina can be used as a basic catalyst under microwave energy for *in situ* dipole generation from the *N*,*N*'-biphenacyl bipyridinium salt, which could participate in a [3+2] intramolecular cycloaddition reaction with acetylene dienophiles. Thus, when a three-component mixture of phenacyl bromide, 4,4'- bipyridine, and ethyl propiolate was thoroughly mixed in basic alumina and irradiated in a domestic oven for 10 min, the reaction products was obtained in very good yields In the following table there are the results obtained in synthesis of bis-indolizines by classical reactions, in multistep way and one-pot synthesis.

Table 1

Bis-indolizine's yields by classical reactions, in multistep and one-pot synthesis

Reaction type	Solvent	Activation mode	Time (min)	T (°C)	η (%)
Multistep reaction (second step)	N-methylpirolidone	MW	15	95	70-75
		Δ	300	50	60-65
	No solvent	MW	15	95	67-70
		Δ	300	50	65-70
One-pot reaction	N-methylpirolidone	MW	15	95	72-75
		Δ	300	95	65-70
	No solvent	MW	15	95	70-75
		Δ	300	95	70-75

The usefulness of this methodology lies in the fact that the three-component reactions are carried out rapidly under microwave-promoted environmentally benign, solvent-less conditions to give substituted indolizines in excellent yields. The catalytic effect of basic alumina was found more prominent in solid-phase 3-CRs than liquid-phase 3-CRs (Table 1). The reaction is compatible with substitutents such as aroyl groups and bipyridines. In conclusion, the methodology reported herein denotes a new class of 3-CR, which is expected to be a general route for the facile, one-pot combinatorial synthesis of a wide range of bis-indolizines.

Experimental

General Synthetic Procedure. 4,4'-bipyridine, **1**, (1 mmole), phenacylbromide derivative, **2**, (3 mmole), dipolarophyle,**3**, (3 mmole), and basic alumina (2 g) were added in a 50 mL beaker. The mixture was stirred to obtain a free flowing powder, which was irradiated in a microwave oven at 300 W for an appropriate time (monitored by TLC). After cooling to room temperature, the product was extracted with chloroform (3 x15 mL). The product obtained after removal of solvent under reduced pressure was crystallized from a suitable solvent (EtOAc-petroleum; ether; MeOH). The structure of the bis-indolizinic products, **4**, was confirmed by spectral data and comparison with authentic samples prepared according to literature methods [14-16]. All reactions were carried out in a commercially available BPL BMO 800T multimode microwave reactor having a maximum power output of 800 W operating at 2450 MHz. Mass spectra were recorded using MSQ-Plus spectrometer. Melting points were recorded on a Metler Toledo melting point apparatus and are uncorrected.

Conclusion

A rapid, economic and environmentally friendly method has been developed for bis-indolizine synthesis using KF/basic alumina. The reagent system described here may be a good alternative to well known methods since the cycloaddition proceeds expeditiously with high yields under solvent-free conditions. These procedures are clearly dependent on the reaction medium and mechanisms involved.

Solvent-free organic synthesis offers a lot of advantages connected to safety, enhancement in reactivity and selectivity, cost saving, and energy and pollution prevention. When coupled with microwave irradiation, no thermal effects can be developed, thus allowing considerable improvements over classic procedures.

By this way, it can be improved the selectivity, enhanced the reaction rate and it can be obtained the cleaner products.

Acknowledgment

The authors thank the Romanian National Authority for financial research support (CNMP Nr.71/2007-2010).

References

[1]. Gundersen, L.L., Charnock, C., Negussie, A. H, Rise, F., Teklu, S., Eur. J. Pharmaceut. Sci., 2007, 30,26-35;
[2]. Hao, L., Zhiqiang, X., Shoujun, C., Koya, K., Ono, M., and Sun, L., Org. Process Res. Dev., 2007, 11 (2), 246 -250;
[3]. Landy, D.G. Surpateanu, G., Fourmentin, S., Blach, P., Decockand, P., Surpateanu, Gh., Internet Electronic Journal of Molecular Design, 2005, 545–555;
[4]. Qin, R. T. W., , Dahaen, B. N, Eur J Org Chem, 2006, 20:4658-4663;
[5]. Pessoa-Mahana, H., J. Kosche, et all, Heterocycles, 2008, 75, 8;

[6]. Adam, D., Nature, 2003, 421, 571–572;
[7]. Satya, P., Nanda, P. and Gupta, R., Molecules 2003, 8, 374-380;
[8]. Kappe, C.O., Dallinger, D., Murphree, S.S., Practical Microwave Synthesis for Organic Chemists - Strategies, Instruments, and Protocols, Edition - 2009, Wiley-VCH;
[9]. Caddick, S., Tetrahedron, 1995, 51, 10403–10432;
[10]. Loupy, A., Petit, Hamelin, A. J., Texier-Boullet, F., Jacquault, P., Mathé, D, Synthesis, 1998, 1213–1234;
[11]. Huisgen, R. In 1,3-Dipolar Cycloaddition Chemistry; Padwa, A., Ed.; John Wiley & Sons: New York, 1984; Vol. 1;
[12]. For reviews, see: (a) Lown, J. W. In 1,3-Dipolar Cycloaddition Chemistry; Padwa, A., Ed.; John Wiley & Sons: New York, 1984; Vol. 1, p 653. (b) Vedejs, E.; West, F. G., Chem. Rev. 1986, 86, 941. (c) Tsuge, O.; Kanemasa, S. In Advances in Heterocyclic Chemistry; Katritzky, A. R., Ed.; Academic Press: San Diego, 1989; Vol. 45, p 231;
[13]. For a review, see: Grashey, R. In 1,3-Dipolar Cycloaddition Chemistry; Padwa, A. Ed.; John Wiley & Sons: New York, 1984; Vol. 1, p 733;
[14]. Dinica, R., Pettinari, C., Heterocyclic Comm., 2001,07, 4, 381-386;
[15]. Dinica, R., Druta, I., Pettinari, C., Synlett, 2000, 222, 1013;
[16]. Furdui, B., Dinică, R., Druță, I., Demeunynck, M., Synthesis, 2006, 16, 2640-2642.

THE SOLID-STATE INCLUSION COMPLEX BETWEEN THE MONO-ANION OF CALIX[4]ARENE AND PROTONATED DIAMINO-BICYCLOUNDECANE

Oleksandr Shkurenko[a], Kinga Suwinska[a*], Florent Perret[b], Katia Sigaud[c], Antoine Leydier[c], Said Jebors[c] and Anthony W. Coleman[c*]

[a]*Institute of Physical Chemistry, Polish Academy of Sciences, Kasprzaka, 44/52, PL-01 224 Warsaw, Poland*
[b]*Laboratoire de Chimie Organique 2, ICBMS, CNRS UMR 5246, Université Lyon 1, 43, bd du 11 novembre 1918, 69622 Villeurbanne cedex, France*
[c]*Institut de Biologie et Chimie des Protéines, UMR 5086, CNRS, Université Lyon 1, 7 passage du Vercors, F69367 Lyon, France. Email: aw.coleman@ibcp.fr*

Abstract: Diamino-bicycloundecane mono-deprotonates H-calix[4]arene and the solid-structure of the resulting salt has been determined by X-ray crystallography. Two different complexes are present in the structure with the Diamino-bicycloundecane cation held in the calix[4]arene cavity by CH-p interactions. In the packing there is a hydrogen-bonded polymeric chain. Both the complexes formed layered structures with differing inter-layer distances.

Keywords: Calix[n]arenes, X-ray Crystallography, Structure, Mono-anionic, Diamino-Bicycloundecane, inclusion polymer.

Introduction

The calix[n]arenes are a class of macrocycle organic host compounds widely studied for their complexation properties [1], they have been shown to complex molecules at sizes varying from metallic cations [2], anions [3], small organic molecules [4] through peptides [5] to proteins [6] and DNA [7]. As they possess two different chemistries: at the *para*-aromatic position and at the phenolic hydroxyl position, their selective chemical modify-cation may be achieved [8], and hence groups with divergent chemical and physical properties may be readily introduced at either face.

A wide range of amphiphilic calix[n]arene derivatives have been developed by modification at one or two faces. We have some time been interested in the synthesis of amphiphilic calix[n]arenes having a geometry tuned to the formation of micellar structures, such molecules are based mono-functionalisation at the phenolic face followed by use of quinine-methide substitution at the three remaining phenolic groups [9]. Obviously the key step is the initial mono-substitution.

The synthesis of such molecules has been studied by Casnati *et al.* [10] *via* the 1-3 dialkoxy or tetra-alkoxycalix[4]arenes followed by hydrolysis with respectively 1 or 3 equivalents of trimethylsilyl iodide. We have previously demonstrated mono-substitution of calix[4]arene using potassium carbonate as a base, however yields are very low, ca 10%. Kalchenko has used sodium hydroxide as a base with DMSO as a solvent for mono-substitution [11]. Work by Groenen *et al.* [12] showed that cesium fluoride or potassium fluoride could be used as suitable mono-alkylating agents. An interesting article by Cunningham *et al.* showed that certain organic bases such as diamino-bicycloundecane (DBU) could be used, with total selectivity to mono-deprotonate all the calix[n]arenes [13].

Experimental

Suitable crystals for X-ray diffraction, were grown from an acetonitrile solution of a 1:1 mixture of calix[4]arene and diamino-bicycloundecane by slow evaporation.

The crystal collection and refinement data for 1 are given in Table 1.

H atoms were treated as riding atoms in geometrically idealized positions, with C–H distances of 0.95 (aromatic ring), 0.99 (CH_2), 0.98 (CH_3), 0.88 (NH) and 0.84 Å (OH), and with $U_{iso}(H) = kU_{eq}(C, O)$, where k = 1.5 for the methyl and hydroxyl groups and k = 1.2 otherwise.

Data collection: COLLECT [14]; cell refinement and data reduction: DENZO and SCALEPACK [15]; programs used to solve structure and refine structure: SHELXS97 and SHELXL97 [16]; molecular graphics: Diamond 3.1f [17].

Results and Discussion

While the yields obtained from the use of DBU as a selective mono-deprotonation agent for calix[4]arene are too low to allow its use in the production of mono-O-alkylated calix[4]arene derivatives, during the course of the study suitable crystals for crystallographic study were obtained by slow evaporation from a chloroform-methanol solvent mixture.

Table 1

Crystal data and structure refinement details of 1.DBU

	1.DBU
Empirical formula	$C_{28}H_{23}O_4^-\cdot C_9H_{17}N_2^+\cdot 0.5CH_3OH$
Formula weight	592.73
Temperature (K)	100(2)
Diffractometer	Nonius KappaCCD
Wavelength (Å)	0.71073
Crystal	colourless
Crystal size (mm^3)	0.45 × 0.40 × 0.30
Crystal system	Monoclinic
Space group	$P2_1/c$
Unit cell dimension	
a (Å)	16.9981(2)
b (Å)	19.1230(2)
c (Å)	19.7663(2)
α (°)	90
β (°)	107.8250(4)
γ (°)	90
Volume ($Å^3$)	6116.7(1)
Z	8
Calculated density ($g\cdot cm^{-3}$)	1.287
F(000)	2536
Absorption coefficient (mm^{-1})	0.084
θ Range for data collection (°)	2.97–27.46
hkl Ranges	$-22 \le h \le 22$, $-24 \le k \le 24$, $-25 \le l \le 25$
Reflections collected/unique	90818 / 13966
Completeness (%) to θ	99.9 / 27.46
Absorption correction	None
Refinement method	Full-matrix least-squares on F^2
Data/restraints / parameters	13966 / 0 / 802
Goodness-of-fit on F^2	1.06
Final R indices [$I > 2\sigma(I)$]	$R = 0.041$, $wR = 0.090$
R indices (all data)	$R = 0.049$, $wR = 0.094$

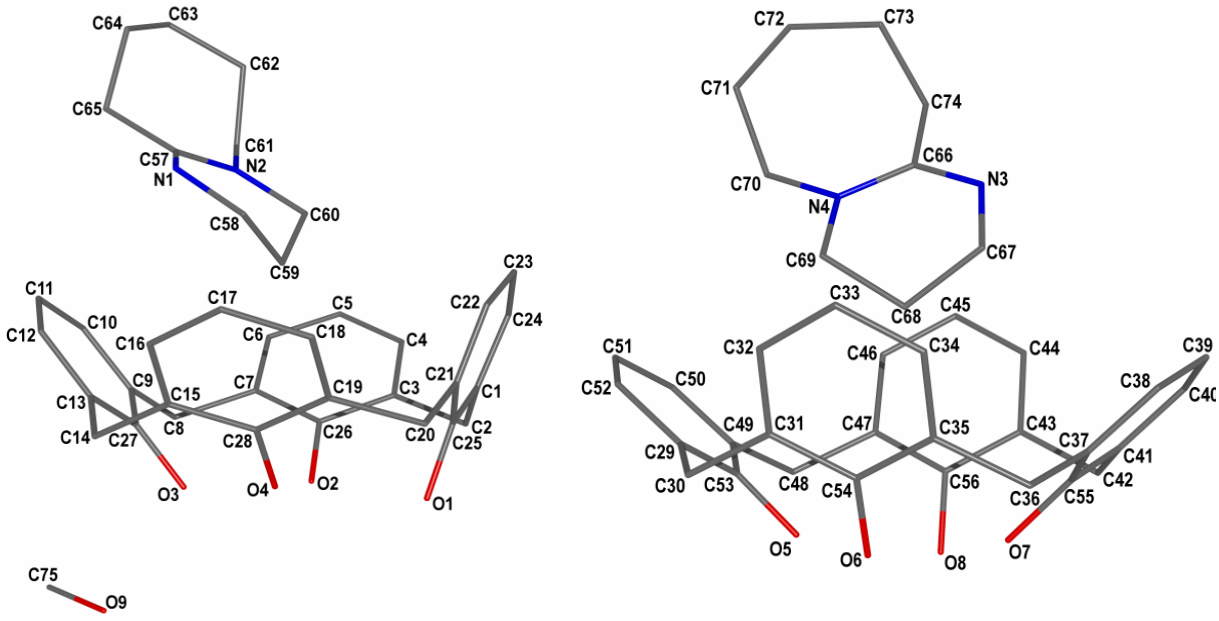

a **b**

Figure 1. The molecular structures of Complexes I and II along with the atom labelling.

The solid-state structure shows a 2:2 complex of two mono-anions of calix[4]arene **1** with two protonated DBU cations and a single molecule of methanol present as a solvate in the structure.

The two different complexes are given, along with atom labelling in Figure **1a** and **b**.

Bond Lengths are given in Table 1 and Bond Angles in Table 2 (for non-hydrogen atoms), atomic coordinates are given in the Supplementary data.

Table 2

Bond length (Å)

Bond	*d*, Å	Bond	*d*, Å
O1—C25	1.373(2)	C35—C54	1.408(2)
O2—C26	1.362(2)	C35—C36	1.517(2)
O3—C27	1.356(2)	C36—C37	1.518(2)
O4—C28	1.372(1)	C37—C38	1.399(2)
C1—C24	1.399(2)	C37—C55	1.401(2)
C1—C25	1.405(2)	C38—C39	1.387(2)
C1—C2	1.522(2)	C39—C40	1.386(2)
C2—C3	1.521(2)	C40—C41	1.395(2)
C3—C4	1.397(2)	C41—C55	1.409(2)
C3—C26	1.402(2)	C41—C42	1.517(2)
C4—C5	1.390(2)	C42—C43	1.518(2)
C5—C6	1.387(2)	C43—C44	1.398(2)
C6—C7	1.394(2)	C43—C56	1.400(2)
C7—C26	1.406(2)	C44—C45	1.389(2)
C7—C8	1.518(2)	C45—C46	1.385(2)

C8—C9	1.521(2)	C46—C47	1.399(2)
C9—C10	1.395(2)	C47—C56	1.401(2)
C9—C27	1.409(2)	C47—C48	1.523(2)
C10—C11	1.390(2)	C48—C49	1.514(2)
C11—C12	1.387(2)	C49—C50	1.398(2)
C12—C13	1.395(2)	C49—C53	1.404(2)
C13—C27	1.410(2)	C50—C51	1.387(2)
C13—C14	1.518(2)	C51—C52	1.387(2)
C14—C15	1.519(2)	N1—C57	1.320(2)
C15—C16	1.397(2)	N1—C58	1.464(2)
C15—C28	1.404(2)	N2—C57	1.325(2)
C16—C17	1.389(2)	N2—C60	1.480(2)
C17—C18	1.387(2)	N2—C61	1.480(2)
C18—C19	1.391(2)	C57—C65	1.498(2)
C19—C28	1.400(2)	C58—C59	1.517(2)
C19—C20	1.519(2)	C59—C60	1.515(2)
C20—C21	1.522(2)	C61—C62	1.525(2)
C21—C22	1.393(2)	C62—C63	1.527(2)
C21—C25	1.405(2)	C63—C64	1.526(2)
C22—C23	1.389(2)	C64—C65	1.539(2)
C23—C24	1.391(2)	N3—C66	1.316(2)
O5—C53	1.355(2)	N3—C67	1.469(2)
O6—C54	1.350(1)	N4—C66	1.324(2)
O7—C55	1.371(2)	N4—C70	1.475(2)
O8—C56	1.381(2)	N4—C69	1.478(2)
C29—C52	1.397(2)	C66—C74	1.498(2)
C29—C53	1.406(2)	C67—C68	1.512(2)
C29—C30	1.515(2)	C68—C69	1.516(2)
C30—C31	1.517(2)	C70—C71	1.526(2)
C31—C32	1.393(2)	C71—C72	1.527(2)
C31—C54	1.410(2)	C72—C73	1.525(2)
C32—C33	1.387(2)	C73—C74	1.540(2)
C33—C34	1.391(2)	C75—O9	1.404(2)
C34—C35	1.392(2)		

An expected the cone conformations of the calix[4]arene mono-anions are stabilized by hydrogen bonds at the phenolic face, distances 2.703(1), 2.524(1), and 2.521(1) Å for anion **I** and 2.559(1), 2.587(1), and 2.788(1) Å for anion **II**. In both cases the two shorter hydrogen bond lengths are associated with the deprotonated phenolic groups.

Table 3

Angles between bonds (Å)

Angle	∠, °	Angle	∠, °
C24—C1—C25	118.1(1)	C38—C37—C36	119.5(1)
C24—C1—C2	120.0(1)	C55—C37—C36	122.0(1)
C25—C1—C2	121.8(1)	C39—C38—C37	121.4(1)
C3—C2—C1	111.1(1)	C40—C39—C38	119.3(1)
C4—C3—C26	118.5(1)	C39—C40—C41	121.4(1)
C4—C3—C2	120.3(1)	C40—C41—C55	118.5(1)
C26—C3—C2	121.2(1)	C40—C41—C42	120.6(1)
C5—C4—C3	121.0(1)	C55—C41—C42	120.8(1)
C6—C5—C4	119.6(1)	C41—C42—C43	111.8(1)
C5—C6—C7	121.3(1)	C44—C43—C56	118.5(1)
C6—C7—C26	118.3(1)	C44—C43—C42	120.0(1)
C6—C7—C8	120.3(1)	C56—C43—C42	121.5(1)
C26—C7—C8	121.3(1)	C45—C44—C43	120.8(1)
C7—C8—C9	115.6(1)	C46—C45—C44	119.5(1)
C10—C9—C27	119.1(1)	C45—C46—C47	121.6(1)
C10—C9—C8	119.9(1)	C46—C47—C56	117.9(1)
C27—C9—C8	121.0(1)	C46—C47—C48	120.0(1)
C11—C10—C9	121.1(1)	C56—C47—C48	122.1(1)
C12—C11—C10	119.5(1)	C49—C48—C47	112.5(1)
C11—C12—C13	121.2(1)	C50—C49—C53	118.5(1)
C12—C13—C27	119.1(1)	C50—C49—C48	122.0(1)
C12—C13—C14	119.9(1)	C53—C49—C48	119.6(1)
C27—C13—C14	121.1(1)	C51—C50—C49	121.0(1)
C13—C14—C15	114.1(1)	C50—C51—C52	119.7(1)
C16—C15—C28	118.6(1)	C51—C52—C29	121.3(1)
C16—C15—C14	120.3(1)	O5—C53—C49	116.5(1)
C28—C15—C14	121.1(1)	O5—C53—C29	122.2(1)
C17—C16—C15	120.9(1)	C49—C53—C29	121.3(1)
C18—C17—C16	119.4(1)	O6—C54—C35	120.2(1)
C17—C18—C19	121.6(1)	O6—C54—C31	120.7(1)
C18—C19—C28	118.4(1)	C35—C54—C31	119.2(1)
C18—C19—C20	120.2(1)	O7—C55—C37	122.0(1)
C28—C19—C20	121.4(1)	O7—C55—C41	117.2(1)
C19—C20—C21	112.6(1)	C37—C55—C41	120.9(1)
C22—C21—C25	118.7(1)	O8—C56—C43	119.7(1)
C22—C21—C20	120.4(1)	O8—C56—C47	118.8(1)
C25—C21—C20	120.9(1)	C43—C56—C47	121.6(1)
C23—C22—C21	121.2(1)	C57—N1—C58	123.4(1)
C22—C23—C24	119.4(1)	C57—N2—C60	120.6(1)
C23—C24—C1	121.4(1)	C57—N2—C61	121.6(1)
O1—C25—C21	120.3(1)	C60—N2—C61	117.7(1)
O1—C25—C1	118.5(1)	N1—C57—N2	122.1(1)
C21—C25—C1	121.2(1)	N1—C57—C65	117.5(1)
O2—C26—C3	117.9(1)	N2—C57—C65	120.3(1)
O2—C26—C7	120.9(1)	N1—C58—C59	108.7(1)
C3—C26—C7	121.1(1)	C60—C59—C58	109.5(1)
O3—C27—C9	120.3(1)	N2—C60—C59	110.2(1)
O3—C27—C13	119.6(1)	N2—C61—C62	114.2(1)
C9—C27—C13	120.1(1)	C61—C62—C63	115.2(1)
O4—C28—C19	117.5(1)	C64—C63—C62	115.3(1)
O4—C28—C15	121.4(1)	C63—C64—C65	113.5(1)

C19—C28—C15	121.1(1)	C57—C65—C64	112.9(1)
C52—C29—C53	118.2(1)	C66—N3—C67	124.3(1)
C52—C29—C30	120.9(1)	C66—N4—C70	121.8(1)
C53—C29—C30	120.9(1)	C66—N4—C69	120.3(1)
C29—C30—C31	114.3(1)	C70—N4—C69	117.9(1)
C32—C31—C54	119.3(1)	N3—C66—N4	122.1(1)
C32—C31—C30	119.7(1)	N3—C66—C74	117.5(1)
C54—C31—C30	121.1(1)	N4—C66—C74	120.4(1)
C33—C32—C31	121.8(1)	N3—C67—C68	109.5(1)
C32—C33—C34	118.8(1)	C67—C68—C69	110.2(1)
C33—C34—C35	121.1(1)	N4—C69—C68	110.3(1)
C34—C35—C54	119.9(1)	N4—C70—C71	113.4(1)
C34—C35—C36	120.0(1)	C70—C71—C72	113.7(1)
C54—C35—C36	120.0(1)	C73—C72—C71	114.6(1)
C35—C36—C37	113.0(1)	C72—C73—C74	114.0(1)
C38—C37—C55	118.5(1)	C66—C74—C73	112.2(1)

The DBU cation **I** is included within the calix[4]arene **I** cavity. There are CH···π interactions between the two hydrogen atoms of the most deeply inserted methylene group, distances of 3.691(2) and 3.572(2) Å and two further interactions between one hydrogen of the other two methylene groups and the other two aromatic rings, distance of 3.604(2) and 3.666(2) Å. The protonated nitrogen of this DBU cation is hydrogen bonded to the deprotonated phenolic hydroxyl group of anion **II**, N–H···O distance 2.791(1) Å.

In the case of the second DBU cation (**II**) CH···π interactions are stronger (3.459(2), 3.345(2), 3.572(2), 3.546(2) Å) which correlates with more flattened conformation for **II** (cone angles of 55.34(3), 86.34(3)° for **I** and 43.27, 86.67° for **II).** The methanol molecule forms hydrogen bond with deprotonated hydroxyl group of **I**, so DBU cation connects with other hydroxyl group *via* hydrogen bond of 2.916(1) Å.

As a result of N–H···O bonding and CH···π interactions (Table 3) each DBU cation binds two neighbouring calixarenes (Fig. 2). DBU cations present in the crystal structure as racemic mixture, so both complexes **I** and **II** are assembled by pairs into syndiotactic H-bond polymer in [201] direction: …-$\mathbf{I}_L$–$\mathbf{II}_L$–$\mathbf{I}_D$–$\mathbf{II}_D$-…

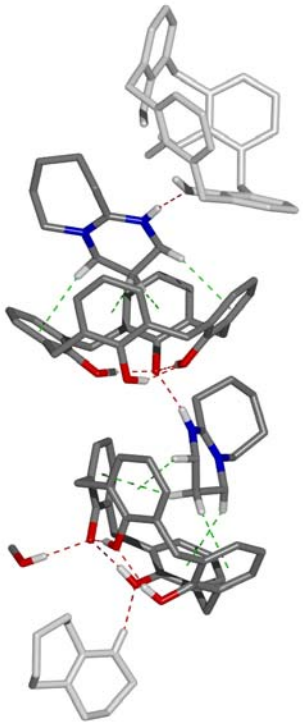

Figure 2. Hydrogen-bonded polymeric chain of 1. Protons not involved in intermolecular interactions or hydrogen bonding have been removed for clarity.

The distance between methanol molecules corresponds to the polymer link length (17.00 Å). All polymeric chains which lie in *xz* plane are parallel, so folded layers consisted of complexes **I** and **II** are anti-parallel (Figure 3a). Hydrogen bonds and contacts, as listed in Table 3, link the units in the chain, and then the inter-chains cohesion is via held electrostatic and van der Waals interactions. The layer formed by calixarenes **I** is thinner than that formed by calixarenes **II** due to the presence of a methanol molecule (Figure 3b).

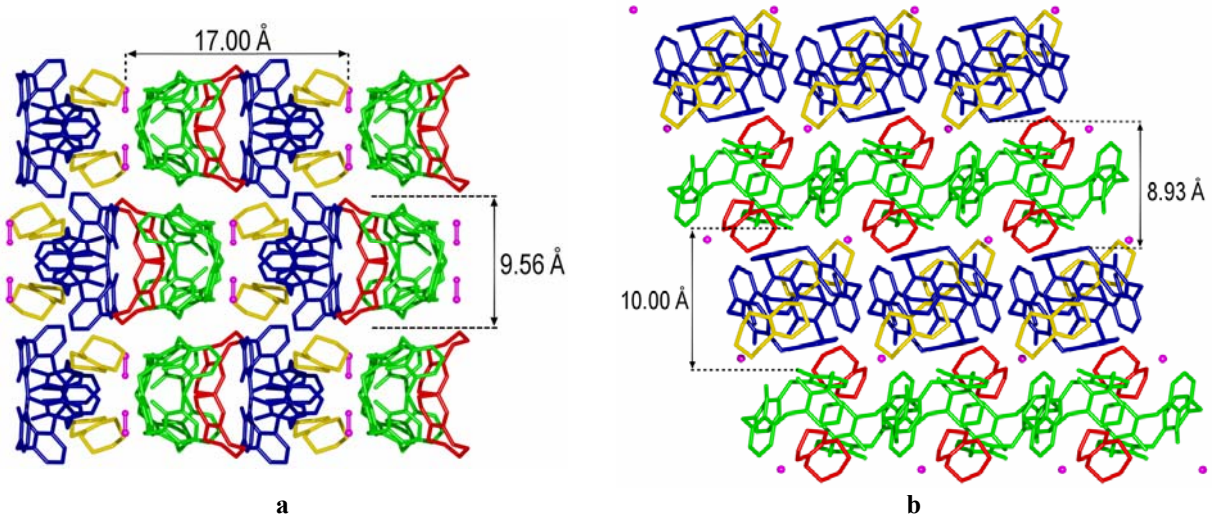

Figure 3. The packing diagrams of the complexes 1. Hydrogen atoms have been removed for clarity.

Table 3

Hydrogen-bond and C−H···π contact geometry

D—H···A	D—H, Å	H···A, Å	D···A, Å	D—H···A, °
O1—H1···O4	0.84	1.89	2.703(1)	163
O2—H2···O3	0.84	1.70	2.524(1)	168
O4—H4···O3	0.84	1.70	2.521(1)	167
O5—H5A···O6	0.84	1.74	2.559(1)	163
O7—H7···O6	0.84	1.76	2.587(1)	167
O8—H8···O7	0.84	1.99	2.787(1)	158
N1—H1···O6^{i}	0.88	1.92	2.791(1)	173
N3—H3···O2^{ii}	0.88	2.07	2.916(1)	162
O9—H9···O3	0.84	1.90	2.741(1)	179
C2—H2A···O9^{iii}	0.99	2.66	3.631(1)	166
C16—H16···O5^{iv}	0.95	2.65	3.542(1)	157
C74—H74B···O3^{ii}	0.99	2.60	3.533(1)	158
C58—H58A···π4	0.99	2.72	3.691(1)	168
C59—H59A···π1	0.99	2.74	3.707(1)	165
C59—H59B···π3	0.99	2.73	3.722(1)	176
C60—H60B···π2	0.99	2.80	3.774(1)	167
C65—H65A···π6^{iv}	0.99	2.66	3.594(1)	157
C67—H67B···π7	0.99	2.78	3.765(1)	173
C68—H68A···π6	0.99	2.40	3.380(1)	172
C68—H68B···π8	0.99	2.49	3.438(1)	160
C69—H69A···π5	0.99	2.74	3.646(1)	152

Symmetry codes: (i) −x+1, −y+1, −z+1; (ii) −x, y+1/2, −z+1/2; (iii) x, 1/2−y, −1/2+z; (iv) 1−x, 1−y, 1−z.

Phenolic ring name in table above is defined by oxygen atom label, for example π1 means phenolic ring with O1 atom.

References

[1]. Gutsche, C.D. Calixarenes Revisited; Royal Society of Chemistry: Cambridge, 1998.

[2]. a) Tu, C.; Surowiec, K.; Bartsch, R.A. Tetrahedron. 2007, 63, 4184-4189; b) Yaftian, M.R.; Razipour, M.R.; Matt, D. JRNC 2006, 270 (2), 357–361; c) Marcos, P. M.; Felix, S.; Ascenso, J.R.; Segurado, M.A.P.; Mellah, B.; Abidi, R.; Hubscher-Bruder, V.; Arnaud-Neu, F. Supramol. Chem. 2006, 18 (2), 147-159.

[3]. a) Klimentova, J.; Vojtisek, P. J. Mol. Struct. 2007, 826(1), 48–63; b) Delaigue, X.; Gutsche, C. D.; Harrowfield, J.M.; Ogden, M.I.; Skelton, B.W.; Stewart, D.F.; White, A.H. Supramol. Chem. 2004, 16(8), 603-609.

[4]. Mutihac, L.; Buschmann, H.-J.; Tudorescu, A.; Mutihac, R. J. Incl. Phenom. Macroc. Chem. 2003, 47 (3-4), 123–128.

[5]. Douteau-Guevel, N.; Perret, F.; Coleman, A.W.; Morel, J.-P.; Morel-Desrosiers, N. J. Chem. Soc., Perkin Trans. 2 2002, 524-532.

[6]. a) Coleman, A.W. ; Perret, F. ; Cecillon, S. ; Moussa, A. ; Martin, A. ; Dupin, M. ; Perron, H. New J. Chem. 2007, 31(5), 711-717; b) Perret, F. ; Lazar, A.N. ; Coleman, A.W. Chem. Commun. 2006, (23), 2425-2438; c) da Silva, E.; Lazar, A.N.; Coleman, A.W. J. Drug Delivery Sci. and Technol. 2004, 14(1), 3–20; d) Memmi, L.; Lazar, A.N.; Brioude, A.; Ball, V.; Coleman, A.W. Chem. Commun. 2001, (23), 2474–2475; e) Oh, S.W.; Moon, J.D.; Lim, H.J.; Park, S.Y.; Kim, T.; Park, J.B.; Han, M.H.; Synyder, M.; Choi, E.Y. FASEB J. 2005, 19(10), 1335–1337.

[7]. a) Zadmard, R.; Schrader, T. Angew. Chem., Int.Ed. 2006, 45(17), 2703–2706; b) Dudic, M.; Colombo, A.; Sansone, F.; Casnati, A.; Donofrio, G.; Ungaro, R. Tetrahedron 2004, 60(50), 11613–11618.

[8]. Thorndorf, I.; Shivanyuk, A.; Böhmer, V. Chapter 2 in Calixarenes 2001, eds Asfari, Z.; Böhmer, V.; Harrowfield, J.; Vicens, J.; Kluwer Academic Publishers: Dordrecht, 2001; pp 26-53.

[9]. a) Suwinska, K.; Shkurenko, O.; Mbemba, C.; Leydier, A.; Jebors, S.; Coleman, A.W.; Matar, R.; Falson, P. New J. Chem. 2008, 32, 1988-1998; b) Mbemba, C.; Sigaud, K.; Perret, F.; Suwinska, K.; Shkurenko, O.; Coleman, A.W. J. Incl. Phenom. Macroc. Chem 2008, 61(1-2), 29-40.

[10]. A.Casnati, A. Pochini, Andrea; R. Ungaro, R. Cacciapaglia, L. Mandolini, J. Chem. Soc., Perkin Trans. 1 1991, (8), 2052–2054.

[11]. Boyko, V.I.; Podoprigorina, A.A.; Yakovenko, A.V.; Pirozhenko, V.V.; Kalchenko, V.I. J. Incl. Phenom. and Macroc. Chem. 2004, 50(3-4), 193-197.

[12]. Groenen, L.C.; Ruel, B.H.M.; Casnati, A.; Verboom, W.; Pochini, A.; Ungaro, R.; Reinhoudt, D.N. Tetrahedron 1991, 47(39), 8379-8384.

[13]. Cunningham, I.D.; Woolfall, M. J. Org. Chem. 2005, 70(23), 9248-9256.

[14]. Nonius. COLLECT. Nonius BV, Delft 1998, The Netherlands.

[15]. Otwinowski, Z.; Minor, W. Methods in Enzymology. Vol. 276, Macromolecular Crystallography, Part A, ed. Carter, C.W. Jr; Sweet, R. M. New York: Academic Press 1997; pp. 307-326.

[16]. Sheldrick, G. M. Acta Cryst. 2008, A64, 112-122.

[17]. Pennington, W.T. J. Appl. Cryst. 1999, 32, 1028-1029.

USE OF ELECTROSPRAY MASS SPECTROMTERY TO STUDY THE INTERACTIONS BETWEEN *PARA*-SULPHONATO-CALIX[4]ARENE AND A SERIES OF SERUM ALBUMIN PROTEINS

Jalil Moubarak, Elodie Moreno, Eric Diesis and Anthony W. Coleman*

Institut de Biologie et Chimie des Protéines, UMR 5086, CNRS, Université Lyon 1, 7 passage du Vercors, F69367 Lyon, France.
Tel +33 472722640; E-mail: aw.coleman@ibcp.fr

Abstract: The binding of *para*-Sulphonato-calix[4]arene to a series of Serum Albumin Proteins has been studied using Electrospray Mass Spectrometry, each protein shows different capacities to interact with *para*-Sulphonato-calix[4]arene, including the number of ligands bound, the Association Constants observed, and the stoichiometries at which the onset of each binding event is observed.

Keywords: Calix[n]arene, *para*-Sulphonato-calix[4]arene, Electrospray Mass Spectrometry, Binding Constants, Complex Stoichiometry, Sequential Binding

Introduction

The calix[n]arenes are amongst the most widely studied organic host molecules, [1] over the last ten years we and others have demonstrated that these synthetic macrocycles have a wide and highly interesting biology. [2] Studies on the interactions of the calix[n]arenes, and in particular the *para*-sulphonato-calix[n]arenes, with bio-molecules have ranged from amino-acids, [3] nucleotides, [4] and steroids [5] through peptides [6] to various proteins, [7] and most recently to cellular biology [8] and in vivo-toxicity [9].

The calix[n]arenes have been shown to have direct biological properties including anti-coagulant, [10] anti-viral, [11] anti-bacterial, [12] and anti-tumoral, [13] activities and also indirect activity where they have been used as colloidal transporters, [14] inclusion compounds for drug solubilisation, [15] protectant molecules against UV degradation, [16] co-crystal formers [17] and to be capable of acting as amplifying systems in neurodegenerative disease diagnostics. [18]

At this time the most studied and also the most versatile of the calix[n]arenes with regard to biological and bio-medical applications is *para*-sulphonato-calix[4]arene. It is usable as a co-crystal former, [17] as an inclusion compound solubilser [15] and for the formation of co-colloids for drug transport. [19] It has been shown to possess no hemolytic properties, [20] does not provoke non-specfic immune responses, [21] has no anticoagulant activity [10] and possesses very low *in-vivo* toxicity, [9] where in mice it is rapidly cleared from the body without accumulation. Thus *para*-sulphonato-calix[4]arene is an excellent candidate for use as a adjuvant for drug transport and delivery.

Of the circulating proteins, the Serum Albumins are the most important class with concentrations in physiological fluids of up to 40g/L. [22] They are well known as anion transporter proteins and may thus act as reservoirs for delivery of negatively charged bioactive molecules. [22] Thus the study of the interaction of *para*-sulphonato-calix[4]arene with various Serum Albumins is of considerable interest, in view of the possible medical applications of this molecule.

We have already reported on the interaction between para-sulphonato-calix[4]arene and Bovine Serum Albumin, (BSA), where three binding sites where observed with Association Constants of 0.77, 0.38 and $0.03 \times 10^{6} M^{-1}$. [23]

Electrospray Mass Spectrometry has been widely developed for the study of the binding of small molecules to proteins, [24] the technique, which is a soft Mass Spectrometric method using low energy for ionisation, can provide information on both the stoichiometry and binding energies, [25] involved in supramolecular complexes and possesses high sensitivity. However, there exists still much discussion on the subject of whether the binding constants derived from ES-MS and the conformations of the proteins in the gas phase reflect conditions in the solution state. [26]

Given that the Serum Albumins are capable of adhering non-selectively to a wide range of surfaces, thus ruling out many analytical techniques such as SPR or HPLC and that they are not suitable for study by NMR due to their high molecular weight, over 65kD, the use of Electrospray Mass Spectromtery (ES-MS) is an excellent tool for the study of binding of ligands to the various Serum Albumins.

In the present work we have studied by ES-MS the interaction of *para*-sulphonato-calix[4]arene with Serum Albumins obtained from Human, (HAS), Goat, (GSA), Pork, (PSA), Rat, (RSA), Rabbit, (RbSA) and Sheep, (SSA). The use of a single substrate molecule with a closely related series of proteins under identical conditions should allow us to have some degree of confidence in the internal consistency of the results and permit quantitative comparisons to be undertaken.

Results and Discussion

The synthesis of *para*-sulphonato-calix[4]arene, 1, below, was carried out using the conditions previously developed for samples to be used in biological studies.[9]

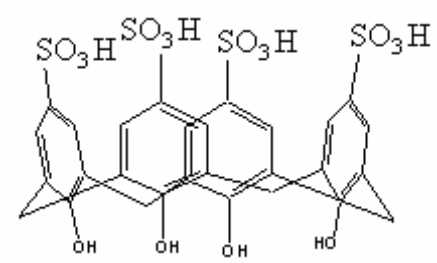

Scheme 1. Molecular Structure of *para*-sulphonato-calix[4]arene, 1.

A typical mass spectrum, at a 1:0.8 ration between *para*-sulphonato-calix[4]arene and Rat Serum Albumin, along with the deconvoluted spectrum are shown in Figure 1a and 1b respectively.

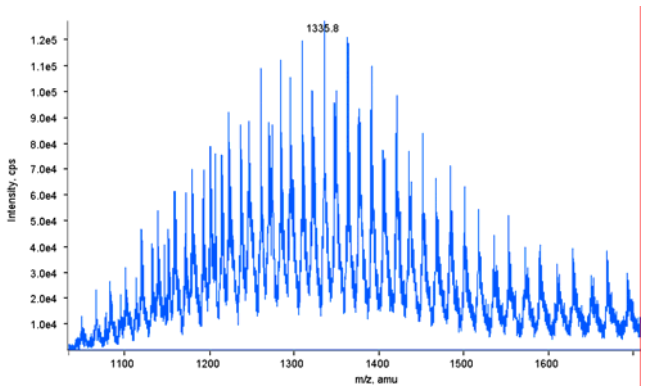

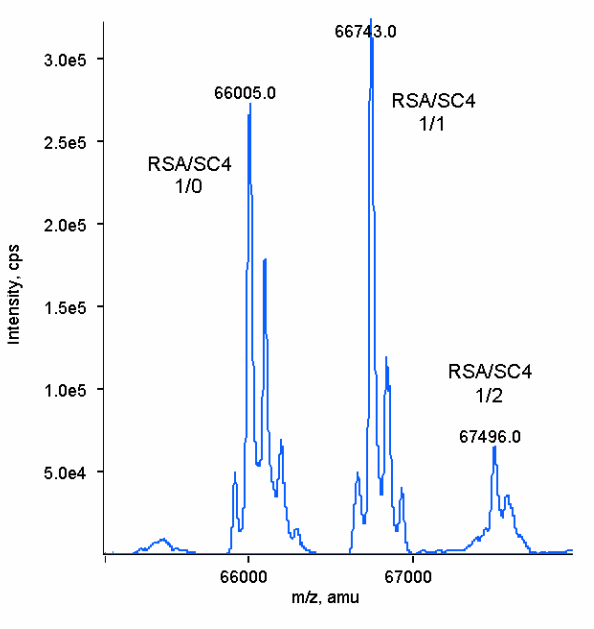

Figure 1a **Figure 1b**

Figure 1, a Native ES-MS spectrum of the complexation of Rat Serum Albumin by *para*-sulphonato-calix[4]arene, 1 at a molar ratio of 1:0.8, and b the deconvoluted spectrum.

The high charge state naturally present on the Serum Albumins leads to median values for observed m/z ratios in the range 1270 to 1390, as given in Table 1. Also in Table 1 are given the number of basic amino-acids, Lysine, Arginine and Histidine present in each protein.

In Table 2 are given the data on the binding of *para*-sulphonato-calix[4]arene to each of the Serum Albumins, along with the Association Constants, $K_{ass,}$ for each of the observed complexes.The Association Constants are expressed in M^{-1} as the mathematical treatment calculates each value as a separate entity.

Evidently a major point concerns the nature of the observed binding, is it specific or non-specific in nature. Given the high, between 90 and 100, number of basic amino acid residues present and that at most a 1:5 stoichiometry is observed, as well as the fact that for BSA up to 60 molecules of *para*-sulphonato-calix[4]arene are non-speficially coordinated to BSA, it would seem that under the experimental conditions used here, the binding can be treated as specific but not necessarily directly applicable to the *in-vivo* situation. In fact given the complexity of physiological media binding data obtained *ex-vivo* must, anyway, be treated with circumspection.

Table 1

Data for the various Serum Albumin Proteins, number of basic amino-acids present, median m/z ratio observed. a Data for BSA from [23] b data unavailable

	BSA[a]	*HSA*	*GSA*[b]	*PSA*	*RSA*	*RbSA*	*SSA*
Lys	59	60	**b**	58	54	58	61
Arg	23	25	**b**	29	27	25	25
His	17	16	**b**	19	15	23	18
Median m/z		1388	1386	1338	1335	1351	1280

Table 2

Association Constants, observed for the complexes between *para*-sulphonato-calix[4]arene and the Serum Albumin proteins. [a] Data for BSA from reference [23]

	BSA[a] 10^6M^{-1}	*HSA* 10^6M^{-1}	*GSA* 10^6M^{-1}	*PSA* 10^6M^{-1}	*RSA* 10^6M^{-1}	*RbSA* 10^6M^{-1}	*SSA* 10^6M^{-1}
1:1	0.77	2.13	0.84	0.52	1.52	1.66	0.16
1:2	0.38	1.06	1.25	0.45	0.91	1.72	1.06
1:3	0.03	0.31	0.27	0.14	0.30	0.49	0.68
1:4	-	0.11	0.08	-	0.10	0.16	0.17
1:5	-	0.03	0.03	-	0.03	-	0.06

Analysis of the Association Constants shows that for all the Serum Albumins, except possibly PSA, there exist two very strong binding sites for *para*-sulphonato-calix[4]arene, with Kass values between $0.8x10^6M^{-1}$ and $2x10^6M^{-1}$ and that the sites are generally capable of accomodating two molecules of *para*-sulphonato-calix[4]arene.

There exists a second apparent type o fbinding site, as described by similarity in the observed Assocaition Constants with values grouped around $0.3\text{-}0.5x10^6M^{-1}$ and that this site only binds one molecule of *para*-sulphonato-calix[4]arene.

Finally two other types of site may exist, one showing Association Constants in the range $0.15x10^6M^{-1}$ to $0.1x10^6M^{-1}$ and the other around $0.03x10^6M^{-1}$. With regard to these last sites their presence is dependent on the animal source of the Serum Albumin.

Of further interest is the fact that there are apparently cooperative binding events in which the first Association Constant is smaller the second, this is particularly the case for Sheep Serum Albumin,(SSA) where for the first binding event a Association Constant of $0.16x10^6M^{-1}$ is observed, after which at higher molar ratios of *para*-sulphonato-calix[4]arene to SSA by two strong binding events with Association Constants of $1.06x10^6M^{-1}$ and $0.68x10^6M^{-1}$ are observed before the second typical binding site at $0.17x10^6M^{-1}$ appears. These results suggest, that in the case of this protein, that complexation at an additional site opens up access for *para*-sulphonato-calix[4]arene to the strong double binding site.

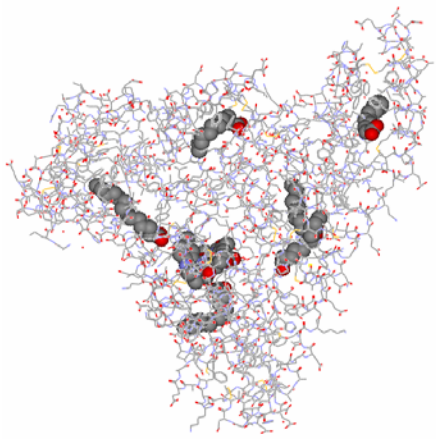

Figure 2, adapted from ref 27, molecular structure of HAS in its complex with myristate, azapropazone and indomethacin, showing the complexed molecules as CPK surfaces to better illustrate the possible binding sites.

The crystal structures of HSA, and more than twenty of its complexes with varying single molecules, and with two and even three different molecules are present in the Protein Data Bank.

Analysis of the binding sites present in the triple complex between HSA, myristate, azapropazone and indomethacin, [27], Figure 2 shows one large site that contains both azopropazone and indomethacin with two myristate anions close by, another quite large site with two myristate anions and two binding sites for one myristate each.

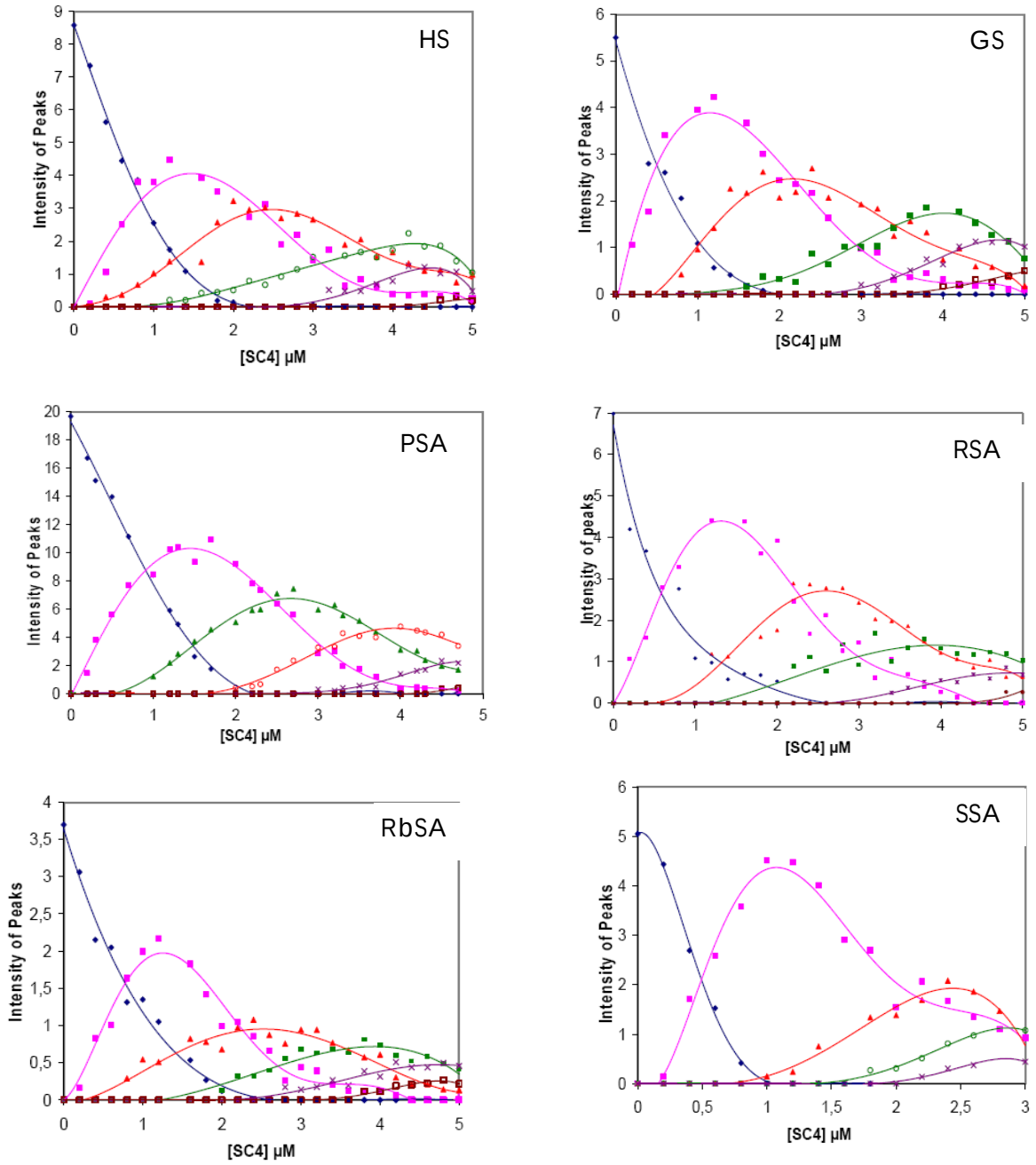

Figure 3. Titration curves for the complexation of *para*-sulphonato-calix[4]arene with the various Serum Albumins as a function of the concentration of *para*-sulphonato-calix[4]arene. Curve fitting has been applied to improve visualization, hence the initial value of the concentration of *para*-sulphonato-calix[4]arene becomes zero.

The observed sites could, thus, correspond to the two strong binding sites of *para*-sulphonato-calix[4]arenefor the large pocket, a second binding site and two weaker binding sites.

In addition to the thermodynamic information on individual binding events, ES-MS provides clear information on the onset of binding events and on the existance of the various binding events as a function of the stoichiometry of the titration, it is one very few analytical techniques that can provide such information. The curves for the variation of each complex are given in Figures 3a-f and the data is summarised in Table 3.

Interestingly for both GSA and, particularly, for RbSA there a lag before observation of the formation of the 1:1 complex, conversely only for HAS are the 1:1 and 2:1 complexes present at the initial extrapolated titration point. For all the other binding events there are sequential and there is never simultaneous formation of more than one stoichiometry. Interestingly for all the proteins other than PSA there is dissymmetry in the 1:1 binding curve with extension out to high *para*-sulphonato-calix[4]arene: protein ratios.

Table 3

Binding Event Onset Stoichiometry Ratios.

	HSA	*GSA*	*PSA*	*RSA*	*RbSA*	*SSA*
1:1	>0	0.03	>0	>0	0.16	>0
1:2	>0	0.46	0.5	0.51	0.72	0.15
1:3	0.69	0.82	1.63	1.22	1.29	1.22
1:4	2.54	2.45	-	2.58	1.8	2.11
1:5	3.88	3.24	-	4.22	-	3.14

Experimental

Sample preparation

Serum albumins were purchased from Sigma and used without further purification. *para*-Sulfonato-calix[4]arenes was synthetised according to the literature method. [9] The mass spectra of solutions containing *para*-sulfonatocalix[4]arene and the relevant Serum Albumins were carried out in a $CH_3OH–H_2O$ mixture (50:50; v/v) with 0.1% of Formic Acid. In the titration experiments, the final concentration of the Serum Albumins was retained constant at 5 pmol/µL. Thus to 10 µL of the Serum Albumin solutions was added increasing volumes of the relevant calixarene solution from 0 to 25 pm/µ, the final volume was adjusted to 1mL. A mass spectrum of each sample was recorded. A minimun of 10 points was required to obtain the best fit for calculating the Association Constant value.

ESI/MS mass spectra

All experiments were performed using a Sciex API 165 quadrupole mass spectrometer, associated with an Electrospray Ionisation (ESI) source operating in the positive ion mode. Compounds were introduced by direct infusion of solutions at 5 µL/min flow rate in a CH_3OH/H_2O (50:50; v/v) mixture containing 0.1% of HCOOH. Mass spectra were acquired at 60V orifice voltage value. The scan range was set at *m/z* 700-2200. Multicharged ion spectra were deconvolved in the 65 to 75kDa mass range with step-size of 0.1Da and 20 iterations were summed to improve the signal to noise ratio. Deconvolution of the raw mass spectra allows observation and subsequent integration of peaks arising from the serum albumin alone and peaks arising from the complexes. It is assumed that the ionisation response factors of the various Serum Albumins and the Serum Albumin-*para*- sulphonato-calix[4]arene complexes are the same.

Calculation of K_{Ass}

For the calculation of the K_D values it is assumed that they are *n* binding sites that are not necessarily equivalent, and where K_D = Dissociation Constant:

$$K_{D1} = \frac{[P][C]}{[PC]} \quad [1]$$

$$K_{D2} = \frac{[PC][C]}{[PC_2]} \quad [2]$$

$$K_{Dn} = \frac{[PC_{n-1}][C]}{[PC_n]} \quad [3]$$

where P is the free serum albumin concentration, C is the free *para*-sulphonato-calix[4]arene concentration, PC is the 1:1 Protein-*para*-sulphonato-calix[4]arene complex concentration, PC_2 is the 1:2 Protein-*para*-sulphonato-calix[4]arene complex concentration and the equilibrium constants can also describe *n* non equivalent binding sites:

$$K_1 = \frac{[P][C]}{[PC]} \quad [4]$$

$$K_2 = \frac{[P][C]^2}{[PC_2]} \quad [5]$$

where $K_1 = K_{D1}$ and $K_2 = K_{D1} \times K_{D2}$. Following the derivation in van Holde's Physical Biochemistry, [28] the relationship below is derived:

$$\frac{[P]+[PC]+[PC_2]+...+[PC_n]}{[P]} = \frac{[C]^n}{K_{D1}K_{D2}...K_{Dn}} + ... + \frac{[C]^2}{K_{D1}K_{D2}} + \frac{[C]}{K_{D1}} + 1 \quad [6]$$

The intercept will be one for a *para*-sulphonato-calix[4]arene concentration of zero. A plot of measured values of $([P]+[PC]+[PC_2]+\ldots+[PC_n])/[P]$ versus added [C] can be fitted to a *n* order polynomial fonction, thus allowing calculation of each Dissociation Constant.

For calculating the association constant, it was assumed that the total signal response for each individual species was proportional to the concentration of that species both in the gas phase and in solution.

K_{ass} is simply $1/K_D$.

Conclusion

The use of Electrospray Mass Spectrometry has allowed the investigation of the binding of *para*-sulfonato-calix[4]arene to a series of Serum Albumin Proteins. There are, depending on the protein, at least three and up to five binding sites observed, with the derived Association Constants varying from 2.14 to $0.03x10^{6}M^{-1}$. Comparison with the crystal structure of a Human Serum Albumin complex suggests that the binding of *para*-sulfonato-calix[4]arene may be correlated with the known anion binding sites. The onset of the formation of each complex is, in general, an independent event particular to the nature of the Serum Albumin.

References

[1]. C. D. Gutsche, An Introduction to the Calix-Arenes, Royal Society of Chemistry, Cambridge, 2008.
[2]. F. Perret, A. N. Lazar and A. W. Coleman, Chem. Commun., 2006, 2425 – 2438. E. Da Silva, A. N. Lazar and A. W. Coleman, Journal of Drug Delivery Science and Technology, 14, 2004, 3-20.
[3]. O. I. Kalchenko, F. Perret, N. Morel-Desrosiers and A. W. Coleman, Journal of the Chemical Society, Perkin Transactions 2, 2001, 258-263. N. Douteau-Guevel, A. W. Coleman, J.-P. Morel and N. Morel-Desrosiers, Physical Organic Chemistry, Perkin Transactions 2, Journal of the Chemical Society, 1999, 629-634. N. Douteau-Guevel, A. W. Coleman, J.-P. Morel and N. Morel-Desrosiers, Journal of Physical Organic Chemistry, 11, 1998, 693-696. O. I. Kalchenko, E. Da Silva and A. W. Coleman, Journal of Inclusion Phenomena and Macrocyclic Chemistry, 43, 2002, 305-310.
[4]. G. M. L. Consoli, G. Granata, E. Galante, I. Di Silvestro, L. Salafia and C. Geraci, Tetrahedron 63, 2007, 10758-10763.
[5]. E. Da Silva, C. Valmalle, M. Becchi, C.-Y. Cuilleron and A. W. Coleman, Journal of Inclusion Phenomena and Macrocyclic Chemistry, 46, 2003, 65-69.
[6]. N. Douteau-Guevel, F. Perret, A. W. Coleman, J.-P. Morel and N. Morel-Desrosiers, Journal of the Chemical Society, Perkin Transactions 2, 2002, 524-532.
[7]. F. Perret, H. Peron, M. Dupin and A. W. Coleman, in Topics in Current Chem, Creative Chemical Sensor Systems, ed T. Schrader, 277, 2007, 31-88, Springer, Berlin. T. Oshima, Y. Baba, K. Shimojo and M. Goto, Current Drug Discovery Technologies, 4, 2007, 220-228.
[8]. R. Lalor, H. Baillie-Johnson, C Redshaw, S. E. Matthews and A. Mueller, J. Am. Chem. Soc., 130, 2008, 2892-2893. R. Lalor, J. L. Di Gesso, A. Mueller and S. E. Matthews, Chem. Commun., 2007, 4907-4909. M. A. Klyachina,V. I. Boyko, A. V. Yakovenko, L. G. Babich, S. G. Shlykov, S. O. Kosterin, V. P. Khilya, V. I. Kalchenko, J. Incl. Phen. Macro. Chem., 60, 2008, 131-137.
[9]. A. W. Coleman, S. Jebors, S. Cecillon, P. Perret, D. Garin, D. Marti-Battle and M. Moulin , New J Chem, 32, 2008, 780-782.
[10]. E. Da Silva, D. Ficheux and A. W. Coleman J.Incl. Phen. Macro. Chem., 52, 2005, 201-6.
[11]. K. M. Hwang, Y. M. Qi, S. L. Liu and W. Choy, J. Chen, Treatment of infection by enveloped virus with calix[n]arene compounds, U.S. Patent , 1995, US 5,312,837.
[12]. P. D'Arcy Hart, J. A. Armstrong and E. Brodaty, Infection and Immunity 1996, 64, 1491-3. J. W. Cornforth, P. D'Arcy Hart, G. A. Nicholls, R. J. W. Rees, J. A. Stock, British Journal of Pharmacology and Chemotherapy, 10, 1955, 73-86.
[13]. A. W. Coleman, A. N. Lazar, L. G. Bagetto, S. Magnard and M. H. Michaud, Dérivés de Calixarènes comme Agents Anticancéreux, 2007 International Patent, PCT/FR2007/051127. C. Geraci, G. M. L. Consoli, E. Galante, E. Bousquet, M. Pappalardo and A. Spadaro, Biocon. Chem., 19, 2008, 751-758.
[14]. P. Shahgaldian, E. Da Silva, A. W. Coleman, B. Rather and M. J. Zaworotko, International Journal of Pharmaceutics, 253, 2003, 23-38.
[15]. W. Yang, M. M. de Villiers, 7, AAPS Journal, 2005, E241-E248.
[16]. M. Pojarova, G. S. Ananchenko, K. A. Udachin, M. Daroszewska, F. Perret, A. W. Coleman and J. A. Ripmeester, Chem Mat, 18, 2006, 5817-5819.
[17]. N. Dupont, A. N. Lazar, F. Perret, O. Danylyuk, K. Suwinska, A. Navaza and A. W. Coleman, CrystEngComm, 2008, *DOI:* 10.1039/b805317k.
[18]. A. W. Coleman, F. Perret, S. Cecillon, A. Moussa, A. Martin, M. Dupin and H. Perron, New J. Chem., 31, 2007, 711-717.
[19]. A. W. Coleman, A. N. Lazar and J.-Y. Renault, Co-colloïdes supramoléculaires obtenus à l'aide de systèmes macrocycliques polyanioniques, French Patent FR 2904782, 2006.
[20]. E. Da Silva, P. Shahgaldian and A. W. Coleman, Int. J. Pharm., 273, 2004, 57-62.
[21]. M.-H. Paclet, C. F. Rousseau, C. Yannick, F. Morel and A. W. Coleman, J.Incl. Phen. Macro. Chem., 55, 2006, 353-8.
[22]. T. Peters Jr, All About Albumin, Academic Press, San Diego, 1995.
[23]. E. Da Silva, C. F. Rousseau, I. Zanella-Cleon, M. Becchi and A. W. Coleman, J.Incl. Phen. Macro. Chem., 55, 2006, 53-9.
[24]. A. J. R. Heck and R.H.H. van den Heuvel, Mass Spectrom. Revs, 23, 2004, 368- 389.
[25]. J. M. Daniel, S. D. Friess, S. Rajagopalan, S. Wendt and R. Zenobi, Int. J. Mass Spectrometry, 216, 2002, 1-27.
[26]. M. C. Jecklin, D. Touboul, C. Bovet, A. Wortmann and R. Zenobi, J. Am. Mass Spectrom, 19, 2008, 323-43.
[27]. J. Ghuman, P. A. Zunszain, I. Petitpas, A. A. Bhattacharya, M. Otagiri, and S. Curry, J. Mol. Biol., 353, 2005, 38-43.
[28]. K. E. Van Holde, Physical Biochemistry, 2end ed., Prentice-Hall, Englewood Cliffs, New Jersey, 1985.

HYBRID ORGANIC-INORGANIC COMPOSITE MATERIALS FOR APPLICATION IN CHEMICAL SENSORS

Anca-Dana Bendrea*, Ana-Maria Catargiu and Mircea Grigoras

"P. Poni" Institute of Macromolecular Chemistry, 41A Gr. Ghica Voda Alley, Iasi-700487, Romania
** Email: anca.bendrea@icmpp.ro, Phone: +40 232 21754, Fax: +40 232 211299*

Abstract: Mesoporous SBA-15/conducting polymers composites, type SBA- polithiophene, SBA-polyaniline, respectively were synthesized and their physical properties were investigated. Polymers molecules were synthesized by chemical oxidative polymerization inside the pores of the mesoporous material by a post-synthesis process. The obtained materials were characterized by X-ray diffraction, scanning electron microscopy, thermal analysis and infrared spectroscopy.

Introduction

Chemical sensors for gases are at the forefront of the information acquisition chain about the environment in which we live. The quality of the air is one of the most important concerns of our society. A large number of gas sensors use the organic components, like porphyrins, phtalocyanines, or doped conducting polymers [1, 2]. Conducting polymers, such as polypyrrole (PPy), polyaniline (PANi), polythiophene (PT) and their derivatives have been used as the active layers of gas sensors since early 1980s [3]. In comparison with most of the commercially available sensors, based on metal oxides and operated at high temperature, the sensors that have conducting polymers like component exhibit many improved characteristics. They have high sensitivities and short response time even at room temperature. This endows conducting polymers sensors with low energy consumption and simple device configuration. The selectivity of sensors can be easily modified by the adjustment of the specific properties of conducting polymers, by introducing different substituents, or copolymerizing with different monomers. However, conducting polymers have several disadvantages like: long-time instability and irreversibility, low selectivity that need to be improved.

To meet the need for analyzing the gas mixture and to overcome the low stability, poor selectivity and high cost problems of popular sensors, organic-inorganic hybrid composite sensors are intensively investigated [4-7]. They can complement the characteristics of pure inorganic and organic materials. It is also observed that hybrid materials have small grain size and high stability in air [8, 9].

In this work we exploit the hybrid organic-inorganic self-assembly approach to prepare mesostructured conducting polymer silica composite particles, type polyaniline/SBA-15 (SBA-PANi), polythiophene/SBA-15 (SBA-PT) respectively. Mesoporous materials are of great interest because of their potential applications in various areas that span from catalysis to drug delivery [10-14].The uniform pore architecture of mesoporous materials make them very attractive as hosts for the encapsulation of polymers. In fact, several reports describe the encapsulation of conducting polymers such as polyppyrole, polythiophene and polyaniline into molecular sieves [15-21]. We focus on conjugated polythiophene and polyaniline, two of the most promising conducting polymers due to a good combination of properties, stability, price and ease of synthesis.

Our mesostructured conducting polymers silica composites particles were prepared via oxidative polymerrization of monomers by iron (III) chloride, in the case of thiophene and ammonium persulfate when aniline is the monomer, in the presence of SBA-15 particles. The obtained composites were characterized by X-ray diffraction, infrared spectroscopy, scanning electron microscopy, thermal analysis and. The preliminary results obtained for composite particles will be used in our further investigation regarding the development of humidity sensors.

Results and discussion

The powder XRD patterns for SBA-15, SBA-15-polythiophene and SBA-polyaniline composites are presented in Fig. 1. The successful formation of well-ordered mesoporous materials with two-dimensional hexagonal (p6mm) structure, with d_{100} spacing of 9.1 nm, follows from the presence of a basal (100) peak, along with (110) and (200) reflections in the low-angle region [22].

The XRD patterns of SBA - composite materials (Fig 1b, 1c) show that the composite materials are not as well ordered as the regular SBA-15, as evidence by the broadening of the (100) reflection peak and the disappearance of the higher order reflection. The XRD data show an increase in the d_{100} spacing from 9.1nm to 15.1nm in the case of SBA –PT composite and to 12.1 nm for SBA- polyaniline samples. This enhancement of d_{100} spacing is attributed to encapsulation of polymers into SBA-15 structures.

The presence of polymers molecules in the mesoporous silica was also confirmed by infrared spectroscopy (Fig. 2). The FT-IR spectrum of silica mesoporous SBA-15 (Fig. 2a) shows typical vibrations of SBA-15 silica framework with the asymmetric Si-O-Si stretch recorded at around 1080 cm^{-1}. The symmetric stretch occurs at 809 cm^{-1}, while the band at 460 cm^{-1} is assigned to the Si-O-Si bending mode [23].

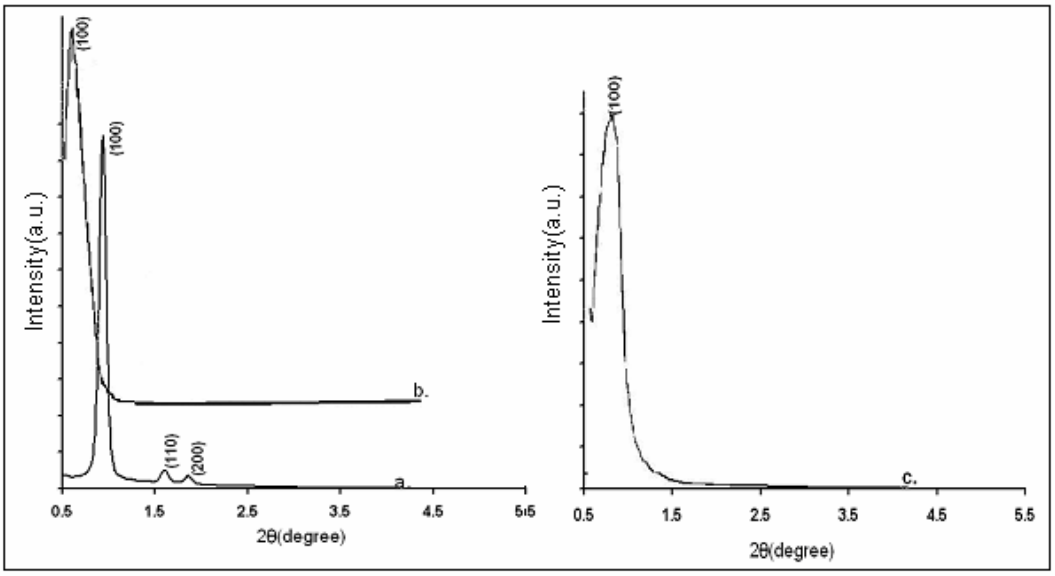

Fig.1. XRD patterns for a. SBA-15, b. SBA-PT and c. SBA-PANi composites

All these vibrations characteristics to silica SBA-15 are presented in the FT-IR spectra of SBA-PT and SBA-PANi, respectively, composites (Fig.2b, 2c), but some of them are shifted due to the presence of polymer. Also, the polythiophene presence in the composite it is confirmed by the absorption peak at 848 cm^{-1} ascribed to the C-H out-of –plane stretching vibration of the 2,5-substituted thiophene ring, which confirmed the polymerization of monomer[24]. The peak at 696cm^{-1} can be assigned to the C-S bending mode, which also, indicates the presence of polymer in the composite structure.

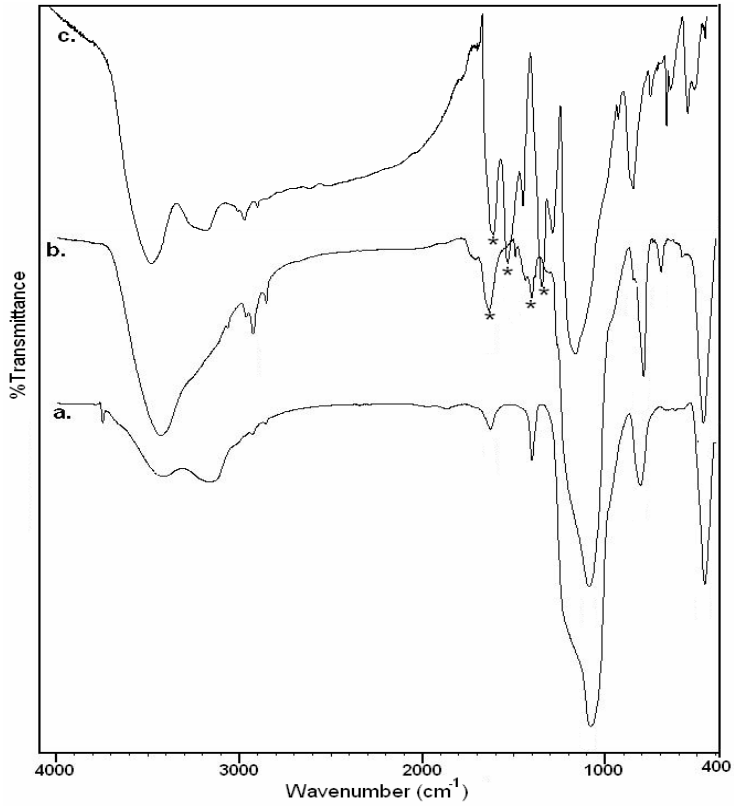

Fig. 2. FT-IR spectra of a.SBA-15, b. SBA-PT and c. SBA-PANi composite samples (* marks some of the polymers characteristics bands)

The FTIR spectra of SBA-PANi composite (Fig.2c) show both, typical vibrations of the SBA-15 silica framework and also display bands associated with PANi at 1564, 1486 and 1299 cm^{-1}. These bands are associated

with the stretching vibrations of the quinoid and benzenoid rings. The band at around 801cm^{-1} is attributed to aromatic C-H bending out of plane of the 1,4-sustituted aromatic rings [25,26].

Further evidence of the presence of polymers was confirmed by TGA analysis as shown Fig.3.

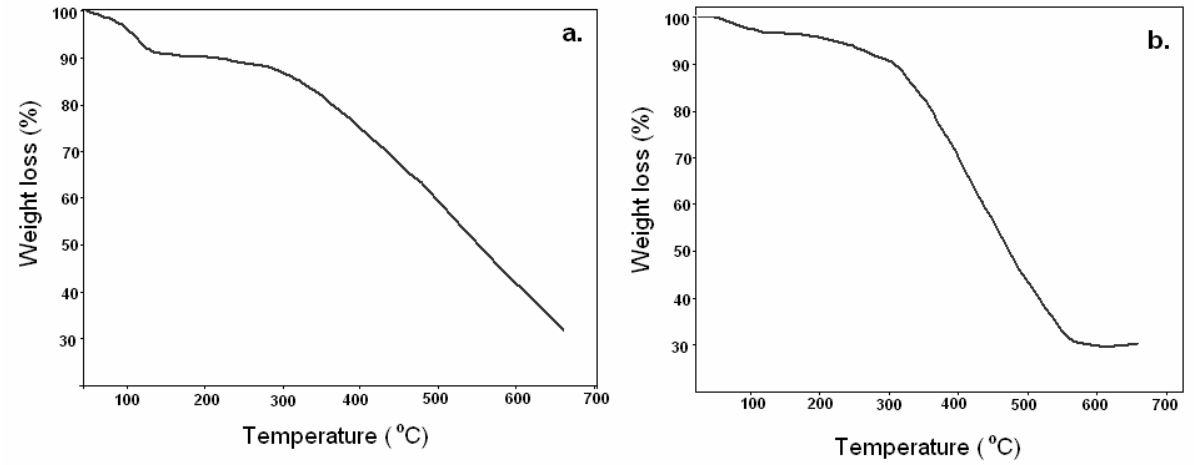

Fig.3. TGA of a. SBA-PANi and b. SBA-PT composite samples

The trend of degradation of the SBA-PANi composites (Fig.3a) is similar to that of pure PANi and show two major step weight loss process. The first step indicates a 9.2 % weight loss at temperatures up to 100°C. This step can be attributed to the expulsion of water molecules and the dopant (HCl) from PANi chain. The second-step weight loss occurs between 315 and 675°C, which is due to the degradation of PANi chain. Note that the decomposition rate when the polymer is encapsulated is very different from the decomposition rate of bulk polymers [17].The decomposition of polymer backbone of pure PANi usually occurs around 300-450°C, but the encapsulated polymer decomposes slowly from about 315 to 675°C.

The thermogravimetric curve of SBA-PT composites (Fig.3b) also reveals two weight-loss steps. The first one, up to 300°C indicates a 5% weight loss is attributed to the evaporation of adsorbed water molecules on the sample surface and to the expulsion of oligomers. The most important weight loss (about 38%) takes place between 300 and 650°C. Above 650°C the organic component is completely decomposed, so the weight loss recorded in this step can be attributed to the inorganic silica.

The minimum temperature in the case of our composites is shifted to a higher temperature suggesting an increase of thermal stability of SBA-polymers composites in comparison with pure polymers, which proved that the encapsulation of polymers into mesoporous silica enhances their thermal stability.

Thermogravimetry was also employed to determine the amount of polymer in the composite samples. It was found that the composites contained 65% of PANi and 45% of PT, respectively. The amount of polymer in the composite was calculated from the mass loss between 300°C, when the solvent was evaporated and 700°C, when the polymer was completely decomposed.

Fig. 4 shows the particle morphology of both SBA-15 and SBA-PT composites observed by scanning electron microscopy (SEM).

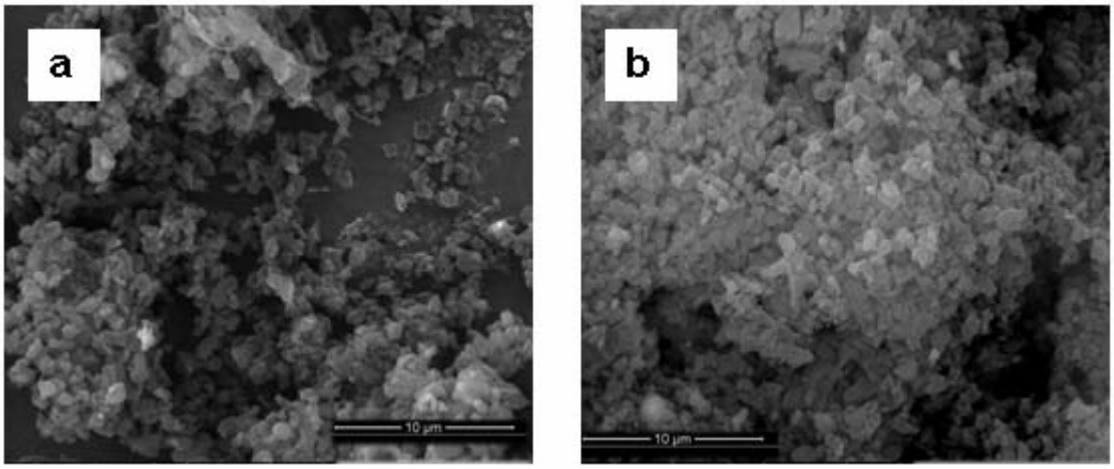

Fig.4. SEM images of a. SBA-15 and b. SBA-PT composites

The SEM images (Fig. 4) reveal that the mesoporous materials are assemblies of many doughnut-like particles being typical of SBA-15 materials [27]. As shown from SEM images, no apparent difference in the particle surface morphology between the SBA-15 and SBA-PT composites (Fig.4b), except the fact that composite structure is more compact than SBA-15. This agglomeration effect is attributed to the presence of polythiophene on composite structure.

Experimental

Tetraethylorthosilicate (TEOS) (98%), hydrochloric acid (37%), fresh distilled thiophene, aniline and ammonium persulfate were purchased from Aldrich. The triblock copolymer Pluronic 123 (P123) was supplied by BASF. Water-free iron (III) chloride, was purchased from Fluka. All chemicals were used as received without any further purification.

Materials Preparation

Silica SBA-15 was synthesized following the literature procedure [22, 26]. 4 g of ploy(ethylene oxide)-poly(propylene oxide) – poly(ethylene oxide) triblock copolymer (PEO_{20}-PPO_{70}-PEO_{20}), Pluronic 123, were added to 150 ml of 1.6 M aqueous solution of hydrochloric acid and stirred for 16 hours. Next, 8.5 g TEOS were added dropwise and the polymer – TEOS synthesis mixture was stirred for 24 hours. The synthesis gel was transferred to Teflon-lined sealed containers and kept at 100^{o}C for 48 hours under static conditions. The final product was filtered, washed with water and dried at 80^{o}C over night. The surfactant, Pluronic P123, was removed by a heat treatment in air, at 550^{o}C, for 6 hours.

Preparation of SBA-PT composites. 0.1g of SBA-15 was dried under vacuum at around 100^{o}C for 24 hours and then placed in 10 ml chloroform (water free) and stirred at room temperature for 2 hours. Next, 0.2 ml thiophene was added to this mixture and stirred at room temperature for another 24 hours. Meanwhile, the dispersion of 0.304 g $FeCl_3$ in 10 ml $CHCl_3$ was prepared and subsequently added to the dispersion of SBA-monomer solution. After 24 hours of vigorous magnetic stirring at room temperature, the composite was extracted with methanol, filtered, washed with deionized water and 2M HCl aqueous solution and dried at 60-80^o C at vacuum. During the extraction step, the color of the composite changed from black (PT in oxidized state) to red (PT in reduced state), indicating successful reduction of the polymer.

Preparation of SBA-PANi composites. 0.1g of SBA-15 was dried under vacuum at around 100^{o}C for 24 hours and then placed in 10 ml of 1M HCl aqueous solution and stirred at room temperature for 2 hours. Next, 0.2 ml aniline was added to this mixture and stirred at room temperature for another 24 hours and than 0.22 g (NH_4) S_2O_8 were added to the reaction system. After 24 hours of vigorous magnetic stirring at room temperature, the composite was extracted with methanol, filtered, washed with deionized water and 2M HCl aqueous solution and dried at 60-80^o C at vacuum. During the extraction step, the color of the composite changed from blue (PANi in oxidized state) to dark green (PANi in reduced state), indicating successful reduction of the polymer.

Materials Characterization

Powder X-ray diffraction patterns were obtained with a Brucker AD8 ADVANCE X-ray diffractometer using CuKα radiation. The FTIR spectra (KBr pellets) of samples were recorded in the range of 4000-400 cm^{-1}, using a Bruker Vertex 70 spectrometer. The SEM studies were performed on samples fixed by means of colloidal silver on copper supports. The samples were covered with a thin layer of gold, by sputtering (Emitech K550X). The coated surface was examined by using an Environmental Scanning Electron Microscope (ESEM) Quanta 200-type, operating at 15 kV with secondary electrons. Thermal gravimetric analysis (TGA) was performed by means of a Mettler Toledo TGA-SDTA 851 device, in air stream, a heating speed of 10 K/min (25-800 ^{0}C range) and the sample weight of 4-6 mg. Constant operating parameters were kept for all the samples in order to obtain comparable data.

Conclusions

This study described the preparation of new organic-inorganic hybrid composites, where organic component is a conducting polymer, type polyaniline, or polythiophene and mesoporous silica SBA-15 represent the inorganic host. In situ chemical oxidative polymerization method of the monomers has been used for the composites synthesis.

The dates obtained from XRD and FTIR analysis show the formation of polymers and the successful encapsulation of them into SBA-15 structure. The morphology of SBA-PT samples was obtained by SEM. By thermogravimetric analysis was reveals the main weight loss and decomposes steps of composites. Thermogravimetry was also employed to determine the amount of polyaniline and polythiophene, respectively, in the composites.

These preliminary results obtained for mesoporous silica-conducting polymers composites will be used in our further investigation regarding the development of humidity sensors.

Acknowledgments

The authors thank the Romanian National Authority for Scientific Research for financial support (Grant PN II-IDEI-963).

References

[1]. McQuade,D. T., Pullen,A. E.& Swager, T. M. Chem. Rev.2000, 100, 2537–2574.
[2]. Gerard, M., Chaubey,A.& Malhotra, B. D. Biosens. Bioelectron. 2002, 17, 345–359.
[3]. Bai, H. and Shi, G., Sensors, 2007, 7, 267-307.
[4]. Guernion, N., B.P.J. de Lacy Costello, Ratcliffe, N.M., Synth. Met.2002, 128,139
[5]. Tandon, R.P., Tripathy, M.R., Arora, A.K., Hotchandani, S., Sens. Actuators B 2006, 114,768-773.
[6]. Ram, M.K., Yavuz, O., Aldissi M., Synth. Met. 2005, 151, 77–84.
[7]. Sadek, A.Z., Wlodarski, W., Shin, K., Kaner, Kalantar-Zadeh, R.B. K., Nanotechnology. 2006, 17, 4488–4492.
[8]. Parch, R., Gangolli, S.G., Matijevic, E., J. Colloid Interf. Sci.1991, 144 (1), 27–35.
[9]. Maeda, S., Armes, S.P., Chem. Mater.1995, 7, 171–178.
[10]. Kresge C.T., Lenowicz M.E., Roth W.J., Vartuli J.C., Beck J.S., Nature,1992, 359, 710.
[11]. Diaz J.F., Balkus Jr. K.J., J. Mol. Catal. B: Enzym.1996, 2,115.
[12]. Jain T.K., Roy I., De T.K., Maitra A., J. Am. Chem. Soc.1998, 120, 11092.
[13]. Ying J.Y., Mehnert C.P., Wong M.S., Angew. Chem. Int. Ed. 1999, 38, 56.
[14]. Vallet-Regi M., Ramila A., del Real R.P., Perez-Pariente J., Chem. Mater.2001, 13, 308.
[15]. Mbaraka I.K., Radu D.R., Lin V.S.-Y., Shanks B.H., J. Catal.2003, 219, 329.
[16]. Wu C.-G., Bein T., Science. 1994, 264, 1757.
[17]. Enzel P., Bein T., J. Phys. Chem.1989, 93, 6270.
[18]. Cho M.S., Choi H.J., Ahn W.-S., Langmuir.2004, 20, 202.
[19]. Cho M.S., Choi H.J., Ahn W.-S., Synth. Met.2003, 711, 135–136.
[20]. Cho M.S., Choi H.J., Kim K.Y., Ahn W.-S., Macromol. Rapid Commun.2007, 23, 713.
[21]. Cardin D.J., Adv. Mater. 2002, 14, 553.
[22]. Zhao D., Feng J., Huo Q., Melosh N., Fredrickson G.H., Chmelka B.F., Stucky G.D., Science, 1998, 279,548.
[23]. Coutinho D., Yang Z., Ferraris J.P., Balkus K.J., J. Micropor.Mesopor.Mater, 2005, 81, 321-332.
[24]. Han M.G., Foulger S.H., Adv. Mater, 2004, 13(4), 301.
[25]. Long, Y., Chena, Z., Duvailb, J.L., Zhang, Z. and Wan, M. Physica B.2005, 370: 121-130.
[26]. Li, P., Yu, B. and Wei, X. J. Appl. Polym. Sci.2004, 93: 894-900.
[27]. Zhao D., Sun J., Li Q., Stucky G. D., Chem. Mater, 2000, 12, 275-279.

IMPLICATIONS OF GLOBAL AND LOCAL MOBILITY IN AMORPHOUS EXCIPIENTS AS DETERMINED BY DSC AND TM DSC

Ion Dranca* and Tudor Lupascu

Institute of Chemistry of the Academy of Sciences of Moldova
3 Academiei Str., Chisinau, MD 2028
Email: drancai@yahoo.com

Abstract: The paper explores the use of differential scanning calorimetry (DSC) and temperature modulated differential scanning calorimetry (TM DSC) to study α- and β- processes in amorphous sucrose and trehalose. Amorphous sucrose was prepared by lyophilization while amorphous trehalose was prepared by dehydration of trehalose dihydrate. The variation in the effective activation energy of α-relaxation through glass transition has been determined by applying an isoconversional method. β-relaxations were studied by annealing glassy samples at different temperatures and subsequently heating at different rates in a differential scanning calorimeter. The effect of heating rate on the β-relaxation peak temperature formed the basis for the calculation of the activation energy. The higher density of glassy trehalose resulted in larger activation energy of α-relaxation compared to sucrose. The effect of temperature on viscous flow was greater in trehalose which can have implications on lyophile collapse. The size of the cooperatively rearranging regions was about the same for sucrose and trehalose suggesting similar dynamic heterogeneity at their respective glass transition temperatures. The activation energy of β-relaxations increased with annealing temperature due to increasing cooperative motions and the increase was larger in sucrose. The temperature at which β-relaxation was detected for a given annealing time was much less in sucrose implying that progression of local motions to cooperative motions occurred at lower temperatures in sucrose.

Keywords: molecular mobility; excipients (sucrose & trehalose); α- and β-relaxations; activation energy; DSC & TM DSC.

Introduction

A number of active pharmaceutical ingredients in the drug development pipelines, are prepared in the amorphous state, in light of their poor aqueous solubility [1]. In addition, many pharmaceutical excipients (an excipient is an inactive substance used as a carrier for the active ingredients of a medication) exist in the amorphous state, or are rendered amorphous in order to obtain the desired functionality [2]. Since amorphous compounds are inherently less stable, both physically and chemically, than their crystalline counterparts, numerous investigations over the last decade expectedly focused on the stabilization of amorphous pharmaceuticals [3-5].

A number of protein pharmaceuticals are prepared by lyophilization, and the stresses encountered during lyophilization can cause destabilization of the protein. Lyoprotectants are excipients (typically disaccharides) which help in the preservation of the native state of proteins either by reducing the conformational flexibility of proteins by being in the highly viscous glassy state or by hydrogen bonding [2]. Crystallization of these lyoprotectants can result in protein destabilization [6-10]. Izutsu et al.[8] reported that devitrification of inositol resulted in the instability of a model protein and addition of water soluble polymers stabilized the protein by preventing inositol crystallization. Sucrose and trehalose are widely used as lyoprotectants. Liao et al.[11] reported sucrose to be more effective than trehalose in stabilizing spray-dried lysozyme. On the other hand, Sun et al.[12] compared the effectiveness of sucrose and trehalose to stabilize protein formulations and attributed the superiority of trehalose to its lower free volume in the glassy state as well as lower free volume expansion coefficient above the glass transition temperature (T_g). Both these properties indicated more restricted molecular motions in amorphous trehalose than in amorphous sucrose, both in the glassy in the rubbery states. The relative effectiveness of maltitol, sucrose and trehalose, three model compounds, depends all the vitrification mechanism and specific interactions in a particular formulation.

Molecular mobility in glassy pharmaceuticals has been studied by differential scanning calorimetry and temperature modulated DSC with the goal of generating information that would aid in the prediction of physical stability. Most of these reports [13-16] deal with the molecular motion associated with glass transition or the cooperative α-relaxation. Information on the mobility below T_g, derived by extrapolation from the data obtained above T_g, is at best an indirect measure of the local mobility or the non-cooperative β-relaxation. These secondary intermolecular relaxations were present in all small molecule organic glasses and are referred to as the Johari-Goldstein relaxations [17,18]. In contrast to α-relaxations, they generally follow Arrhenius kinetics and are characterized by activation energy values that are much smaller than those of α-relaxations.

The β-relaxations, specifically the Johari-Goldstein relaxations, are supposed to be the precursor to the cooperative α-relaxations[19]. Thus their characterization is immensely important both for understanding the nature of molecular motions in the glassy phase and their role in determining physical stability. Hikima et al. concluded that β-relaxation processes control the crystal growth in triphenylethylene [20]. Similar observations were made by Alie

et al. [21] who showed that β-relaxations can control the process of crystal growth of a low molecular weight compound above T_g. Although dielectric spectroscopy has been typically used to study structural relaxations, recently Vyazovkin et al. have shown that it is possible to study both α- and β-relaxations using conventional DSC [22,23]. While relaxations far below T_g are non-cooperative (i.e. β), cooperative α-relaxations evolve as T_g is approached and cause glass transition. By annealing amorphous systems below T_g, followed by rapid cooling and reheating, β-relaxation is manifested by a shallow enthalpic recovery endotherm preceding the T_g. With an increase in annealing time, the enthalpic recovery peak shifts to higher temperatures. This effect was systematically investigated in inorganic glasses [24]. Bershtein and Egorov [25] studied the same effect in polymers and used the relationship between the peak temperature, T_p, and the heating rate, q, to calculate activation energy, E:

$$E = -R\frac{d\ln q}{dT_p^{-1}} \quad (1)$$

Our overall goal is to gain a mechanistic understanding of the differences in the global (glass transition) and local mobility in amorphous sucrose and trehalose In light of the differences in their properties, it will be worthwhile to comprehend the implications of molecular mobility on their role as lyoprotectants. Our first objective is to demonstrate the utility of a macroscopic property, specifically density, as a predictor of the temperature dependence of global mobility. Although the densities of crystalline sucrose and trehalose (anhydrous) are almost the same (~1.58 g cm^{-3}) [4], the density of glassy trehalose (1.54 g cm^{-3}) is higher (lower free volume) than that of glassy sucrose (1.43 g cm^{-3}) [26]. This can be attributed to the nature of hydrogen bonding network present in trehalose (discussed in detail later). Thus we anticipate higher activation energy values through the glass transition for amorphous trehalose compared to amorphous sucrose. Our second objective is based on the hypothesis that the difference in activation energy for global mobility between the glassy and supercooled liquid states would be more for trehalose than for sucrose. In other words, the effect of temperature in reducing the activation energy barrier for the glass to flow would be more in trehalose than in sucrose. Our third objective is to measure the minimum temperature of β-relaxation in amorphous sucrose and trehalose under similar experimental conditions (e.g., annealing time). Assuming that β-relaxations are the precursor to the glass transition or the global mobility, we hypothesize that the minimum temperature of β-relaxation would be more in trehalose compared to sucrose because amorphous trehalose has a higher T_g than sucrose. Lastly, as an indirect proof of the thermally induced progression of local to global mobility, we aim to show that the activation energy of β-relaxation approaches that of the α-relaxation as the annealing temperature approaches T_g

Materials and Methods

Crystalline sucrose and trehalose dihydrate (Sigma, St. Louis, MO, USA) were used as obtained.

Differential scanning calorimetry (DSC)

A differential scanning calorimeter (MDSC 2920, TA instruments, New Castle, DE and Mettler-Toledo DSC 823) equipped with a refrigerated cooling accessory was used. The instrument was calibrated with pure indium and tin. About 15-20 mg of sample was weighed in an aluminum pan which was then crimped non-hermetically.

For sub-T_g measurements (β-relaxation), samples were quench cooled in liquid nitrogen and immediately placed in the DSC cell (Mettler-Toledo DSC 823 and TA Instruments MDSC 2920) maintained at -40°C. The samples were then heated to the annealing temperature and held for 30 minutes. The annealing temperatures were -25, -20, -10 , -5, 0, 5, 10 °C for sucrose and -10, 0, 10, 20, 30, 35, 40, 50, 60, 70°C for trehalose. After completion of the annealing segment, the samples were cooled down to -40°C and immediately heated above the T_g. The heating rates were 10, 15, 20, 25 and 30°C min^{-1}. The resulting endothermic peaks detected upon heating were used to determine the peak temperature by using the standard DSC analysis software (Universal analysis 2000, TA Instruments or Mettler-Toledo, STAR^e 9.01). Prior to these experiments, samples of sucrose and trehalose were heated to 85°C and 155°C respectively and held at the respective temperatures for 5 minutes to erase thermal history.

For the measurements of glass transition or α-relaxation, glassy sucrose and trehalose were heated above their respective glass transition temperatures to erase thermal history. The samples were then cooled to ~40°C below their respective glass transition temperatures at 10, 15, 20, 20, 25 and 30°C min^{-1}. The samples were immediately heated at the same rate as that used for cooling. The cell constant was determined and the temperature calibration of the DSC was performed using an indium standard at a heating rate of 20°C min^{-1}. The validity of the temperature calibration was checked at all the other heating rates used. The heat capacity of sucrose and trehalose was measured using sapphire as the reference. A Mettler-Toledo DSC823e with an HSS7 sensor was employed for performing DSC measurements that were carried out under nitrogen flow (50 ml ·min^{-1}). Heat and temperature calibrations were performed by using gallium and indium standards. Regular DSC runs were conducted by heating the samples from 25 to 90 °C at 0.5–5 K·min^{-1}. The regular DSC was complemented by the recently invented (J. E. K. Schawe, T.

Hutter, C. Heitz, I. Alig, D. Lellinger, Thermochim.Acta 2006, 446, 147) technique of multi-frequency temperature modulated DSC (TOPEM® by Mettler-Toledo). The program temperature for TOPEM® measurements was defined by superimposing the underlying heating rate of 1 K· min^{-1} and a series of stochastic temperature pulses of the 1 K amplitude and the time between the pulses ranging from25 s to 60 s. All measurements were performed at least two times to ensure reproducibility.

An example of a multifrequency DSC measurement for sucrose is given in Figure 1. The real part of the complex heat capacity is evaluated at the frequencies, *f*, from 5 to 25mHz.

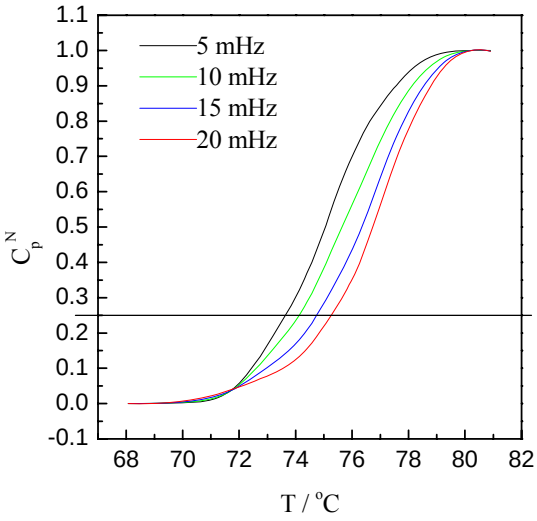

Fig. 1. Frequency dependence of the normalized heat capacity for sucrose evaluated by multifrequency DSC (TM DSC).

Results and Discussions

Variation of activation energy through the glass transition in amorphous sucrose and trehalose

As mentioned earlier, an advanced isoconversional method was used for this purpose. While we provide the highlights here, the details can be found elsewhere [27-29]. Isoconversional methods are used to describe the kinetics of a complex multi-step process by the application of the Arrhenius model to several single-step components or extents of conversion of the process. These methods can be used to evaluate the variation of activation energy, E_α, with the extent of conversion, α, by using different heating rates. Vyazovkin [29] proposed an advanced method which involves carrying out a set of n experiments using different temperature programs, $T_i(t)$, resulting in the determination of a value of E_α that minimizes the following function:

$$\Phi(E_\alpha) = \sum_{i=1}^{n} \sum_{j \neq 1}^{n} \frac{J[E_\alpha, T_i(t_\alpha)]}{J[E_\alpha, T_j(t_\alpha)]} \tag{2}$$

where

$$J[E_\alpha, T_i(t_\alpha) \equiv \int_{t_\alpha - \Delta\alpha}^{t_\alpha} \exp[\frac{-E_\alpha}{RT_i(t)}]dt \tag{3}$$

The advantages of this method over other isoconversional methods [30, 31] are that it uses the actual sample temperature in order to account for the deviation from linear heating or cooling due to self-heating or cooling. Integration over small temperature segments also results in the elimination of error associated with the variation of E_α with α.

The extent of conversion α is determined from the normalized heat capacity, C_p^N , which is evaluated as follows:

$$C_p^N = \frac{(C_p - C_{pg})|}{(C_{pl} - C_{pg})|_T} \equiv \alpha \tag{4}$$

where C_p is any given heat capacity and C_{pg} and C_{pl} are the heat capacities of the glass and the liquid respectively.

In Figure 2, the DSC glass transition events (heating rate: 10°C min^{-1}) in amorphous sucrose and trehalose are shown. The glass transition temperatures (midpoint) of sucrose and trehalose were estimated to be 73 and 119°C respectively. The dependence of the activation energy on the extent of conversion α has been determined by applying the advanced isoconversional method outlined above to the C_p^N (or α) vs temperature data. Figure 2 shows the change in the activation energy as a function of the extent of conversion for sucrose and trehalose. The decrease in activation energy has been plotted against temperature in Figure 3 by replacing α with the corresponding average temperature at different heating rates. The activation energy decreases as the glass transition event progressed. For trehalose the activation energy for α-relaxation decreased from ~348 to ~312 kJ mol^{-1} whereas for sucrose it changed from ~227 to ~198 kJ mol^{-1}. In the glassy phase the low free volume results in large activation energy for molecular motions. As the temperature is increased, the free volume increases, thereby facilitating molecular motion and lowering the activation energy [32].

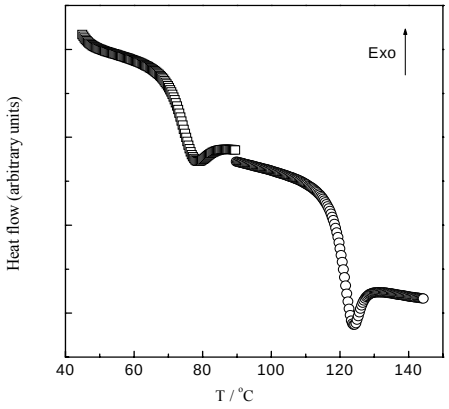

Fig. 2. DSC curves for the glass transition of sucrose (*squares)* and trehalose (*circles)* obtained at 10°C min^{-1}

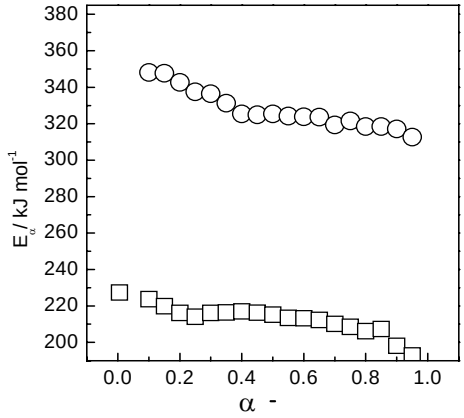

Fig. 3. Variation in the effective activation energy with the extent of conversion from the glassy to the liquid state in sucrose (*squares*) and trehalose (*circles).*

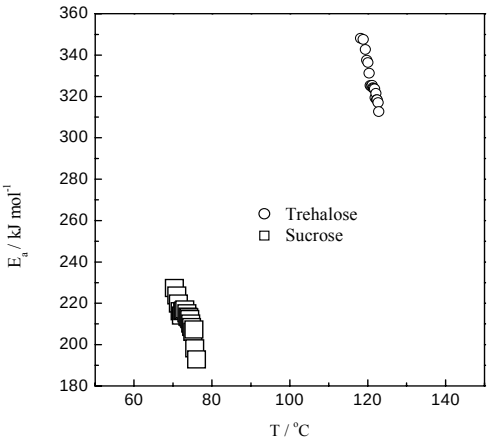

Fig. 4. Variation in the effective activation energy with temperature from the glassy to the liquid state in sucrose (*squares*) and trehalose (*circles).*

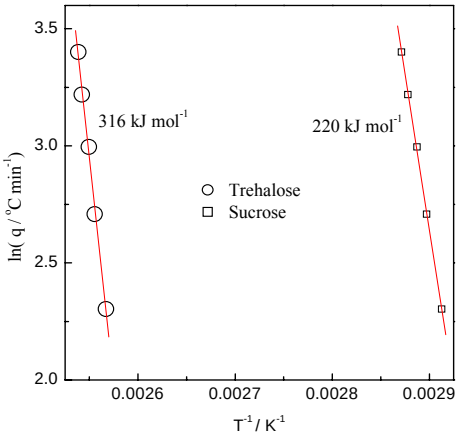

Fig. 5. Evaluation of activation energy (equation 1) of the glass transition in trehalose and sucrose.

The range of activation energy values for trehalose is greater than that for sucrose. Single activation energies for α-relaxation in sucrose (220 kJ mol^{-1}) and trehalose (316 kJ mol^{-1}) were also calculated using Equation 1 and have been shown in Figure 5. Literature reports for activation energy values for trehalose range from 229 to 732 kJ mol^{-1} [33,34] whereas those for sucrose range from 152 to 407 kJ mol^{-1}[33,35]. Despite the range of activation energy values reported, it is clear that amorphous trehalose is characterized by higher activation energy values of α-relaxation compared to sucrose.

Hancock et al. [33] reported similar findings for amorphous sucrose and trehalose based on the activation energy values calculated from the onset, mid-point and offset T_g values. We can therefore conclude that amorphous trehalose has lower free volume and hence more restricted molecular mobility compared to that of sucrose. Sun et al.[12] had earlier reached the same conclusion using the Williams-Landel-Ferry model. The lower free volume of trehalose is probably also reflected in the fact that although both crystalline sucrose and (anhydrous) trehalose have almost the same density (1.58 kg m^{-3}), the density of amorphous trehalose (1.49 kg m^{-3}) is higher than that of amorphous sucrose (1.43 kg m^{-3}) [4]. The higher density of amorphous trehalose could be explained from the hydrogen bonding patterns in the glassy state. Trehalose, composed of two D-glucose rings is bisymmetric compared to sucrose which is characterized by the asymmetry of the constituent glucose and fructose rings. This binary symmetry in the glucose units led Phillips[36] to propose a "tandem sandwich" structure for trehalose. In this structure, strongly bound pairs of glucose rings are alternated with weakly bound pairs resulting in a stable and flexible arrangement. The ethanol side groups of the pyranose rings reside between the rings for weakly bound pairs whereas they lie outside the rings for the strongly bound pairs. Such "sandwich" structures would naturally lead to better packing and hence the higher density of glassy trehalose compared to glassy sucrose where such arrangement is not feasible due to ring asymmetry.

Vyazovkin et al.[32] proposed a variability parameter, ΔE, to describe the rate of decrease of the activation energy with the average temperature:

$$\Delta E = \frac{E_{0.25} - E_{0.75}}{T_{0.25} - T_{0.75}} \tag{5}$$

where $E_{0.25}$ and $E_{0.75}$ are the activation energy values for α=0.25 and 0.75 respectively and $T_{0.25}$ and $T_{0.75}$ are the corresponding temperatures. Δ*E* could be used as a measure of kinetic fragility or deviation from the Arrhenius temperature dependence. These authors showed that the Δ*E* values of various compounds correlated well with the respective values of fragility index. Δ*E* values of sucrose and trehalose were calculated to be -2.3 and -7.2 respectively. Thus although, as mentioned earlier, trehalose is characterized by higher activation energy and hence lower free volume compared to sucrose, the decrease in activation energy per unit of temperature throughout the glass transition is higher for trehalose. This could be explained in light of the fact that sucrose and trehalose liquids have very similar fragility values as detailed below. On the other hand, glassy sucrose and trehalose are characterized by different densities reflecting different free volumes. Since glassy trehalose is more tightly packed compared to glassy sucrose, it is clear that the activation energy barrier for global mobility, required for the glass to start flowing, would be initially much higher in trehalose as was shown above. But since both the liquids are similar in terms of fragility, the effect of increasing the temperature could be expected to have a much greater bearing on the free volume in trehalose. In other words we would expect a greater decrease in activation energy per unit temperature through the glass transition which is exactly what we observed.

The "strength parameter" or the D-value obtained from Vogel-Tammann-Fulcher (VTF) equation could be used as an estimate of kinetic fragility index. Literature VTF D-values for sucrose (7.3) and trehalose (5.1) are similar [13]. Since the kinetic and thermodynamic fragility indices generally correlate well [37], we calculated thermodynamic fragility index using the empirical equation proposed by Wang and Angell [38] :

$$m = 56\frac{T_g * \Delta C_p(T_g)}{\Delta H_m} \tag{6}$$

where we have used experimentally obtained mid-point T_g values of 346 K and 392 K respectively for sucrose and trehalose and $\Delta C_p(T_g)$ value of 0.55 $JK^{-1}g^{-1}$ (188.3 $JK^{-1}mol^{-1}$) for both sucrose and trehalose. The heat of fusion, ΔH_m, for sucrose and anhydrous trehalose were found to be 41.4 kJ mol^{-1} [39] and 53.4 kJ mol^{-1} [40] respectively. Using these values, m was found to be ~88 for sucrose and ~77 for trehalose. Thus although the calculated fragility indices for sucrose and trehalose are in agreement with literature values, the Δ*E* values calculated above indicate a difference in the temperature dependance of activation energy and hence the change in free volume with temperature. The above observation implies that the effect of temperature on the viscous flow of trehalose during glass transition is much more than that of sucrose. This could have implications in bringing about collapse of a lyophilized cake in that a small increase in temperature around the T_g' of a formulation containing trehalose would cause a greater viscous flow than that containing sucrose.

Calculation of the size of cooperatively rearranging regions

The molecular kinetic theory of Adam and Gibbs [41] describes the temperature dependence of structural relaxation in the supercooled liquid phase in terms of the temperature dependence of the size of the "cooperatively

rearranging regions (CRR) ". CRR is the smallest region that can undergo a change in configuration independent of the neighboring molecules in response to an adequate thermal fluctuation. Donth has united the concept of "islands of mobility" proposed by Johari [17] with the defect diffusion model of Glarum [42]. Molecular mobility is facilitated when a "defect" or a locally concentrated high free volume (island of mobility) diffuses due to thermal fluctuations. These defects are heterogeneously distributed in a CRR and the diffusion length of the defect is described by the size of the CRR. The average size of the CRR, ξ, at T_g can be estimated from calorimetric data using the equation for the volume of CRR proposed by Donth [43]:

$$\xi^3 \equiv V_\alpha = \frac{K_B T_g^{\,2} \Delta(C_v^{\,-1})}{\rho(\delta T)^2} \tag{7}$$

where ρ is the density, δT is the mean temperature fluctuation and C_v is the isochoric heat capacity given by

$$\Delta(C_v^{\,-1}) = C_{vg}^{\,-1} - C_{vl}^{\,-1} \tag{8}$$

where C_{vg} and C_{vl} are respectively the isochoric heat capacities of the glass and the supercooled liquid extrapolated to T_g. Hempel et al.[44] derived the following relationship between C_v and C_p:

$$\Delta(C_v^{-1}) = (0.74 \pm 0.22) * \Delta(C_p^{-1}) \tag{9}$$

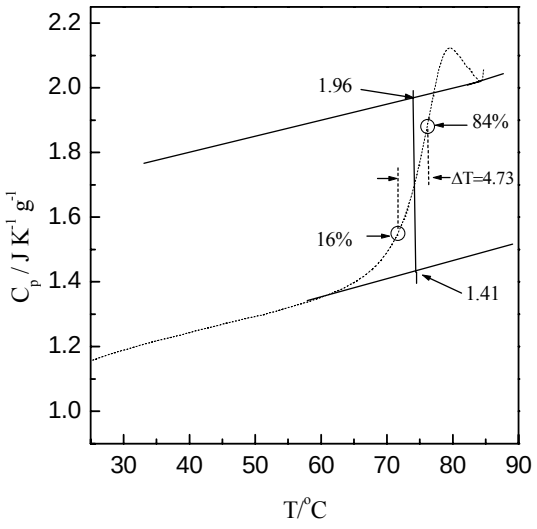

Fig. 6. Temperature dependence of the heat capacity for sucrose. The heat capacity at the glass transition (346 K) changes from 1.41 to 1.96 J K^{-1} g^{-1}. ΔT is determined as the temperature interval in which C_p changes from 16 to 84% of the total Δ C_p.

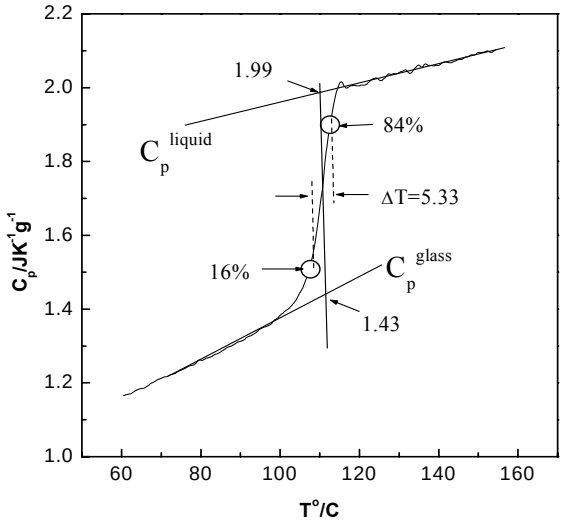

Fig. 7. Temperature dependence of the heat capacity for trehalose. The heat capacity at the glass transition (390 K) changes from 1.43 to 1.99 J K^{-1} g^{-1} . ΔT is determined as the temperature interval in which C_p changes from 16 to 84% of the total Δ C_p. Data are obtained the frequency-dependence of Tg (TOPEM model)

δT is given by (Δ*T*/2.5) [44] where Δ*T* is the temperature interval over which ΔC_p increases from 16 to 84% of the total ΔC_p at T_g. The estimation of Δ*T* for sucrose and trehalose are shown in Figures 6 and 7 respectively. The heat capacity data for both sucrose and trehalose are in excellent agreement with those reported by Shamblin et al.[13] Using equations 7-9, the CRR values were calculated to be 40.4 nm^3 and 35.6 nm^3 respectively for sucrose and trehalose. Assuming a spherical shape, the diameters of the CRR were calculated to be 3.4 and 3.3 nm respectively for sucrose and trehalose. These values are in agreement with the reported range of 2- 5 nm for saccharides and polyalcohols [44].

Since the diameter of the CRR is a measure of the length scale of dynamic heterogeneity, it can be concluded that sucrose and trehalose are characterized by similar dynamic heterogeneity at T_g. The practical implications of these values for CRR could be explained following the argument of Vyazovkin et al.[22].

They found that the critical size of indomethacin nucleus was smaller than that of the CRR and thus it was argued that a critical nucleus could be formed even without involving cooperative motions. In other words,

nucleation (and subsequently crystallization) could occur at temperatures where only local motions exist. We did not find in the literature the data necessary to calculate the critical size of sucrose and trehalose nuclei.

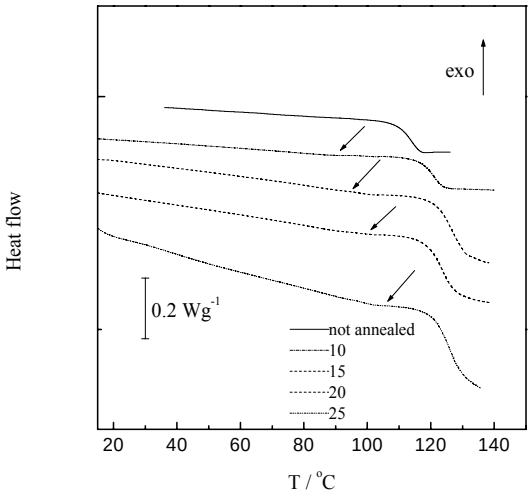

Fig. 8. DSC curves obtained on heating trehalose at different heating rates ranging from 10 to 25°C min^{-1} after annealing for 30 min at 60°C. The heating rates (°C min^{-1}) are shown in the legend. "Not annealed" denotes a curve obtained without annealing at 10°C min^{-1} Arrows show the location of the shallow β-relaxation peaks.

But we could speculate that if the critical size of the sucrose and trehalose nuclei is smaller than that of the corresponding CRR, then nucleation could take place in these systems even in the absence of cooperative motions. Donth[43] also suggested an equation to calculate the number of molecules, N_α, constituting the CRR:

$$N_\alpha = \frac{RT_g\Delta(C_v^{-1})}{M(\delta T)^2} \tag{10}$$

where R is the universal gas constant and M is the molecular weight (342.3 for sucrose and trehalose). N_α was calculated to be 141 for trehalose and 129 for sucrose and again these values are close to those calculated for other structurally similar compounds [44, 45].

Local mobility or secondary relaxations in sucrose and trehalose

In trehalose, β-relaxation peaks were detected after annealing at temperatures ≥ 35°C (Fig. 8) while in sucrose it was ≥ 0°C. The T_p values (Equation 1) were determined from the

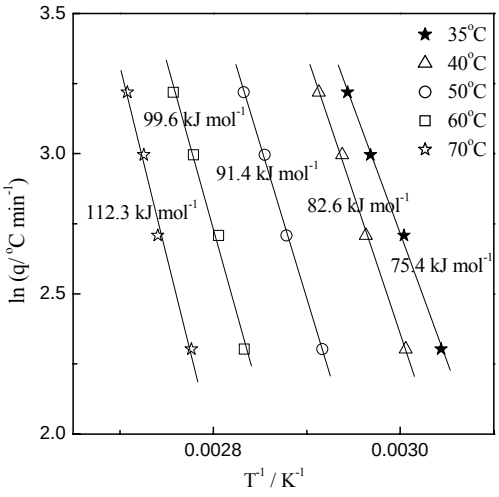

Fig. 9. Evaluation of activation energies from β-relaxation peaks of trehalose annealed at different temperatures (values in °C show the respective annealing temperatures).

DSC curves after appropriate baseline subtraction. The annealing time was 30 minutes. As the annealing temperature increased, the β-relaxation peaks shifted towards the glass transition temperature. We did not use annealing temperatures above the respective upper limits (10°C for sucrose and 70°C for trehalose) to avoid any significant overlap of the β-relaxation peaks with the glass transition.

For each annealing temperature, the β-relaxation peak temperature expectedly increased with increase in the heating rate (Fig. 8). The plots ln q vs T^{-1} are shown in Figs. 9 and 10 for trehalose and sucrose respectively. The activation energy values calculated using Equation 1 are 42, 59, and 74 kJ mol^{-1} for sucrose (Figs. 9 and 11) whereas those for trehalose varied from 75 at an annealing temperature of 35°C to 112.3 kJ mol^{-1} at 70°C (Figs. 8 and 10). These values are much smaller than the activation energies of the α-relaxation of sugars, typically in the 200-400 kJ mol^{-1} range.

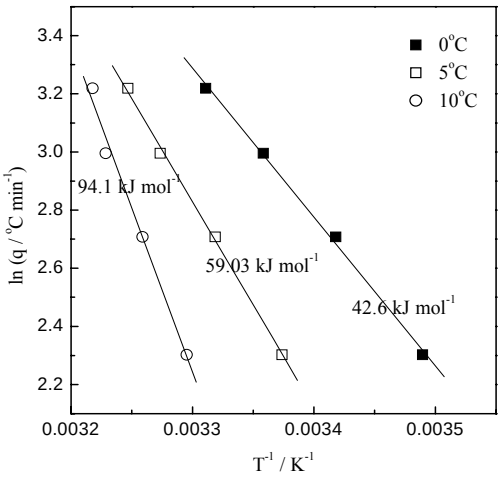

Fig.10. Evaluation of activation energies from β-relaxation peaks of sucrose annealed at different temperatures (values in °C show the respective annealing temperatures).

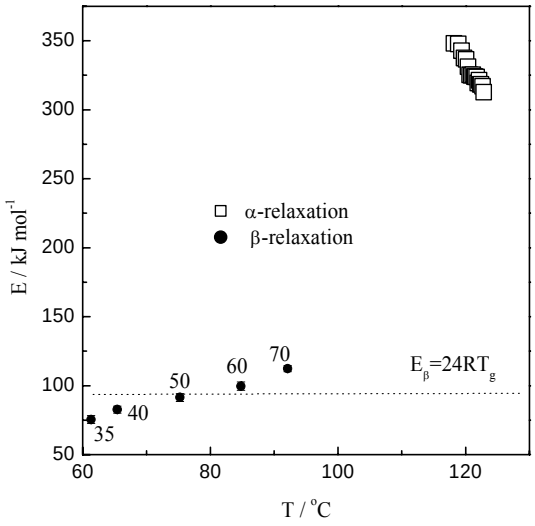

Fig. 11. Variation of the activation energies for the sub-T_g *(solid symbols)* and T_g *(open symbols)* events of trehalose with the average temperature of the process. Numbers by the points represent annealing temperatures. The dotted line corresponds to the value of the activation energy of β-relaxation calculated using Kudlik's empirical equation shown on the plot. Standard deviations of activation energies for β-relaxations are also shown.

The increase in activation energy with annealing temperature is due to the increasing contribution of the cooperative molecular motion that starts to unfreeze as the annealing temperature approaches T_g. Therefore, the activation energy value obtained at the lowest annealing temperature at which β-relaxation was detected is the best approximation of the activation energy of the "true" local molecular motions.

Gusseme et al.[46] reported activation energy values of 47.2 and 85.6 kJ mol^{-1} for the two β-relaxations detected in amorphous trehalose. Of the two β-relaxations, the one with the activation energy of 85.6 kJ mol^{-1} occurs at temperatures close to those in our study. Since calorimetric methods yield activation energy values that are typically within 20% of those obtained from dielectric and/or mechanical spectroscopy[47], our value of 75 kJ mol^{-1} obtained at the lowest annealing temperature probably reflects the contribution from the β-relaxation with the higher activation energy. The contribution from some cooperative motion is also likely. For sucrose, our best estimate of the activation energy of β-relaxation is 42 kJ mol^{-1}, a value in agreement that for other saccharides. The activation energy for β-relaxation was also calculated using the empirical equation, $E_\beta = (24\pm3)RT_g$, derived by Kudlik et al.[48] The calculated and experimental values were in good agreement (Figs. 11 and 12).

It is instructive to evaluate the significance of the annealing temperatures at which β-relaxations were detected. The annealing temperatures ranged from (T_g - 73) to (T_g - 63) for amorphous sucrose (T_g = 73°C) and from (T_g - 84) to (T_g – 49) for amorphous trehalose (T_g = 119°C). As mentioned before, the activation energy increased with annealing temperature indicating an increase in the contribution from cooperative α-relaxations. This observation is clearly in contrast to the generally held belief that mobility in amorphous pharmaceuticals is negligible at or below (T_g – 50).

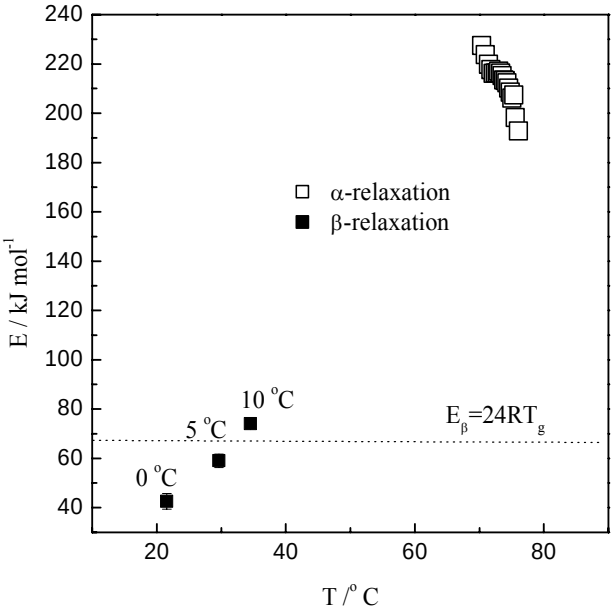

Fig.12. Variation of the activation energies for the sub-T_g *(solid symbols)* and T_g *(open symbols)* events of sucrose with the average temperature of the process. Numbers by the points represent annealing temperatures. The dotted line corresponds to the value of the activation energy of β-relaxation calculated using Kudlik's empirical equation shown on the plot. Standard deviations of activation energies for β-relaxations are also shown.

This becomes especially significant if we consider the fact that the annealing time in all the cases was only 30 minutes. It is clear that increasing the annealing time would result in an increase in the cooperative motions at the annealing temperatures used in our experiments (<T_g-50). Since the average shelf-life of pharmaceuticals is about 2 years, the combination of such long storage (annealing) times and possibly higher storage (annealing) temperatures could result in sufficient mobility in the amorphous matrices of sucrose and trehalose to cause crystallization thereby potentially destabilizing the protein/peptide in the formulation.

The lowest annealing temperature (for the annealing time of 30 minutes) at which β-relaxation was detected for sucrose was much lower than that for trehalose and corresponds to the difference in the T_g of these two compounds. The activation energy of β-relaxation at the lowest annealing temperature for sucrose (~42 kJ mol^{-1}) was also considerably lower than that for trehalose (~75 kJ mol^{-1}) suggesting greater ease in local motions in sucrose that could be very important if molecular mobility is coupled to stability. The increase in the activation energy of β-relaxation with annealing temperature in sucrose (~3.2 kJ mol^{-1} K^{-1}) is *more* than that for trehalose (~1.1 kJ mol^{-1} K^{-1}). This signifies that the effect of temperature on the increase in cooperative α-relaxations is much more in sucrose than in trehalose, attributable to the lower free volume in amorphous trehalose. The implication of this is that even if these amorphous compounds are stored at temperatures < (T_g-50), for the same increase in temperature, the increase in global mobility would be much more for amorphous sucrose. This could ultimately make the amorphous sucrose matrix more prone to instability compared to amorphous trehalose. This is counterintuitive and should not be confused with the fact that sucrose and trehalose, as supercooled liquids, have very similar dynamic fragility values.

Our discussions above focus on the differences in the effects of temperature on the contributions from cooperative motions in the *glassy state*.

Conclusions

The local and global mobility, in two popular amorphous pharmaceutical excipients, sucrose and trehalose, have been compared. Trehalose, having a lower free volume in the glassy state due to a more tightly packed structure, experiences a greater effect of temperature on the reduction in the activation energy barrier for the glass to start flowing. This could be important in causing collapse of a lyophilized cake in that a small increase in temperature around the glass transition temperature of a formulation containing trehalose could cause pronounced viscous flow. In spite of a large difference in T_g, sucrose and trehalose were shown to have similar size of cooperatively rearranging regions (CRR) and also approximately the same number of molecules constituting the CRR, thus implying similar dynamic heterogeneity.

The minimum annealing temperature at which β-relaxation was detected was much lower in sucrose (0°C) than in trehalose (35°C) implying that progression of local motions to cooperative motions occurred at lower temperatures in sucrose. The increase in cooperative motions as a function of annealing temperature was much more for amorphous sucrose when stored below (T_g-50). Thus even a small excursion in temperature could result in significant increase in mobility. This underscores the need to consider the mobility below the T_g of an individual component or the effective T_g of a multicomponent amorphous system.

References

[1]. Pouton, C. W. Formulation of poorly water-soluble drugs for oral administration: Physicochemical and physiological issues and the lipid formulation classification system. Eur. J. Pharm. Sci. 2006, 9:278-287. 2
[2]. Wang, W. Instability, stabilization and formulation of liquid protein pharmaceuticals. Int. J. Pharm. 1999, 185:129-188.
[3]. Yu L. Amorphous pharmaceutical solids: preparation, characterization and stabilization. Advanced Drug Delivery Reviews, 2001, 48:27-42.
[4]. Hancock, B. C.; Zografi G., Characteristics and significance of the amorphous state in pharmaceutical systems. J. Pharm Sci. 1997, 86:1-12.
[5]. Craig, D. Q. M.; Royall, P.G.; Kett, V. L.; Hopton, M. L.The relevance of the amorphous state to pharmaceutical dosage forms: glassy drugs and freeze-dried systems. Int. J. Pharm. 1999, 179:179-207.
[6]. Kreilgaard, L.; Frokjaer, S.; Flink, J. M.; Randolph, T.W.; Carpenter, J. F. Effects of additives on the stability of Humicola lanuginosa lipase during freeze-drying and storage in the dried solid. J Pharm Sci, 1999, 88:281-290.
[7]. Sarciaux, J. M. E.; Hageman, M. Effects of bovine somatotropin (rbSt) concentration at different moisture levels on the physical stability of sucrose in freeze-dried rbSt/sucrose mixtures, J. Pharm Sci , 1997, 86:365-371.
[8]. Izutsu, K.; Yoshioka, S.; Kojima, S. Physical stability and protein stability of freeze-dried cakes during storage at elevated temperatures, Pharm. Res. 1994, 11:995-999.
[9]. Zeng, X. M.; Martin, G. P.; Marriott, C. Effects of molecular weight of polyvinylpyrrolidone on the glass transition and crystallization of co-lyophilized sucrose. Int. J. Pharm., 2001, 218:63-73.
[10]. Passot, S.; Fonseca, F.; Alarcon-lorca, M.; Rolland, D.; Marin. M. Physical characterisation of formulations for the development of two stable freeze-dried proteins during both dried and liquid storage. Eur. J. Pharm. Biopharm. 2005, 60:335-348.
[11]. Liao, Y. H.; Brown, M. B.; Nazir, T.; Quader, A. ; Martin, G. P. Effects of sucrose and trehalose on the preservation of the native structure of spray-dried lysozyme. Pharm Res. 2002, 19:1847-1853.
[12]. Sun, W. Q.; Davidson, P. Protein inactivation in amorphous sucrose and trehalose matrixes: effects of phase separation and crystallization. Biochim Biophys Acta, 1998, 1425:235-244.
[13]. Shamblin, S. L.; Tang, X.; Chang, L.; Hancock, B.C.; Pikal, M. J. Characterization of the time scales of molecular motion in pharmaceutically important glasses. Journal of Physical Chemistry B, 1999, 103:4113-4121.
[14]. Hancock, B, C.; Shamblin, S. L. Molecular mobility of amorphous pharmaceuticals determined using differential scanning calorimetry. 2001, 380:95-107.
[15]. Hancock, B. C.; Shamblin, S. L.; Zografi, G. Molecular mobility of amorphous pharmaceutical solids below their glass transition temperatures. Pharm. Res. 1995, 12:799-806.
[16]. Weuts, I.; Kempen, D.; Six. K.; Peeters, J.; Verrec, G.; Brewster, M.; Van den Mooter, G. Evaluation of different calorimetric methods to determine the glass transition temperature and molecular mobility below T_g for amorphous drugs.2003, Int. J. Pharm. 2003, 259:17-25.
[17]. Johari, G. Intrinsic mobility of molecular glasses. J Chem Phys, 1973, 58:1766 - 1770.
[18]. Johari, G. P.; Goldstein, M. Viscous liquids and the glass transition. II. Secondary relaxations in glasses of rigid molecules. J Chem Phys, 1970, 2372 - 2388.
[19]. Ngai, K. L. 2003. An extended coupling model description of the evolution of dynamics with time in supercooled liquids and ionic conductors. J Phys: Condens Matter. 2003, 15:S1107-S1125.

[20]. Hikima, T.; Hanaya, M.; Oguni, M. Microscopic observation of a peculiar crystallization in the glass transition region and b-process as potentially controlling the growth rate in triphenylethylene. J. Mol. Struct., 1999, 479:245-250.
[21]. Alie, J.; Menegotto, J.; Cardon, P.; Duplaa, H.; Caron, A.; Lacabanne, C.; Bauer, M. 2004. Dielectric study of the molecular mobility and the isothermal crystallization kinetics of an amorphous pharmaceutical drug substance. J. Pharm. Sci., 2004 93:218 - 233.
[22]. Vyazovkin, S.; Dranca, I. Physical stability and relaxation of amorphous indomethacin. J. Phys. Chem. B, 2005, 109:18637-18644.
[23]. Vyazovkin, S.; Dranca, I. Probing beta relaxation in pharmaceutically relevant glasses by using DSC. Pharm. Res., 2006, 23:422-428.
[24]. Chen, H. S. On the mechanisms of structural relaxation in a $Pd_{48}Ni_{32}P_{20}$ glass. J Non-Cryst Solids, 1981, 46:289-305.
[25]. V. A. Bershtein, V. M. Egorov. Differential Scanning Calorimetry of Polymers. ed., New York: Ellis Horwood, 1994.
[26]. Shamblin, S. L.; Taylor, L. S.; Zografi, G. Mixing behavior of colyophilized binary systems. J Pharm. Sci, 1998, 87(6):694-701.
[27]. Vyazovkin, S. Evaluation of the activation energy of thermally stimulated solid-state reactions under an arbitrary variation of the temperature. J. Comput. Chem., 1997, 18:393-402.
[28]. Vyazovkin, S. Modification of the integral isoconversional method to account for variation in the activation energy. J. Comput. Chem., 2001, 22:178-183.
[29]. Vyazovkin S.; Sbirazzouli, N. Isoconversional kinetic analysis of thermally stimulated processes in polymers. Macromolecular Rapid Communications, 2006, 27:1515-1532.
[30]. Ozawa, T. A new method of analyzing thermogravimetric data. Bull. Chem. Soc., Jpn., 1965, 38:1881-1886.
[31]. Flynn, H. J.; Wall, L. A. General treatment of the thermogravimetry of polymers. Journal of Research of the National Bureau of Standards, 1966, 70A:487-523.
[32]. Vyazovkin, S.; Sbirazzouli, N.; Dranca, I. Variation in activation energy of the glass transition for polymers of different dynamic fragility. Macromol. Chem. and Physics, 2006, 207:1126-1130.
[33]. Hancock, B. C.; Dalton, C. R.; Pikal, M. J.; Shamblin, S. L. A pragmatic test of a simple calorimetric method for determining the fragility of some amorphous pharmaceutical materials. Pharm Res., 1998, 15:762-767.
[34]. Green, J. E.; Sitaula, R.; Fowler, A.; Toner, M.; Bhowmick, S. Enthalpic relaxation of convective desiccated trehalose-water glasses. Thermochim Acta, 2007, 453:1-8.
[35]. Bhugra, C.; Rambhatla, S.; Bakri, A.; Duddu, S. P.; Miller, D. P.; Pikal, M. J,; Lechuga-Ballesteros, D. Prediction of the onset of crystallization of amorphous sucrose below the calorimetric glass transition temperature from correlations with mobility. J. Pharm. Sci., 2007, 96:1258-1269.
[36]. Phillips, J. C. Ideally glassy hydrogen-bonded networks. Phys Rev B: Condens Matter., 2006 73:024210-024211.
[37]. Wang, L. M.; Velikov, V.; Angell, C. A. Direct determination of kinetic fragility indices of glassforming liquids by differential scanning calorimetry: Kinetic versus thermodynamic fragilities. J Chem Phys., 2002, 117:10184-10192.
[38]. Wang, L. M.; Angell, C. A. Response to "Comment on 'Direct determination of the fragility indices of glassforming liquids by differential scanning calorimetry: Kinetic versus thermodynamic fragilities' " [J. Chem. Phys. 118, 10351 .2003]. J Chem Phys 118:10353-10355.
[39]. Wang, L. M.; Angell, C, A.; Richert, R. 2006. Fragility and thermodynamics in nonpolymeric glass-forming liquids. J. Chem. Phys., 2006, 125:074505-074501-074508.
[40]. Higashiyama, T. Novel functions and applications of trehalose. Pure Appl Chem., 2002, 74:1263-1269.
[41]. Adam, G.; Gibbs, J. H., On the temperature dependence of cooperative relaxation properties in glass-forming liquids. J. Chem. Phys, 1965, 43:139-146.
[42]. Glarum, S. H. Dielectric relaxation of isoamyl bromide. J. Chem. Phys, 1960, 33:639-643.
[43]. Donth E. The Glass Transition: Relaxation Dynamics in Liquids and Disordered Materials. ed., Berlin: Springer 2001
[44]. Hempel, E.; Hempel, G.; Hensel, A.; Schick, C.; Donth, E. Characteristic length of dynamic glass transition near T_g for a wide assortment of glass-forming substances. J. Phys. Chem. B, 2000, 104:2460-2466.
[45]. Vyazovkin , S.; Dranca, I. Comparative relaxation dynamics of glucose and maltitol. Pharm Res., 2006, 23:2158-2164.
[46]. Gusseme, A. D.; Carpentier, L.; Willart, J. F.; Descamps, M. Molecular Mobility in supercooled trehalose. J. Phys. Chem. B, 2003, 107:10879-10886.
[47]. Vyazovkin, S.; Dranca I. Activation energies derived from the pre-glass transition annealing peaks. Thermochim Acta, 2006, 446:140-146.
[48]. Kudlik, A.; Benkhof, S.; Blochowicz, T.; Tschirwitz, C.; Rossler, E. The dielectric response of simple organic glass formers. J Mol Struct., 1999, 479:201-218.

ON SOME PECULIARITIES OF ETHYL 5-HYDROXY-1,2-DIMETHYL-1*H*-3-INDOLECARBOXYLATE SYNTHESIS

Felix Shepel, Diana Shepel, Fliur Macaev*

Institute of Chemistry of the Academy of Sciences of the Republic of Moldova,
Academy str. 3, MD-2028, Chisinau, Republic of Moldova
Tel +373-22-739-754; Fax +373-22-739-954; E-mail: flmacaev@cc.acad.md

Abstract: The increase of yield up to 63% of ethyl 5-hydroxy-1,2-dimethyl-1*H*-3-indolecarboxylate was obtained via the interaction of *p*-benzoquinone with N-methyl-β-aminocrotone ether in mixture of glacial acetic acid/ethyl acetate.

Keywords: derivatives of 5-oxindole, cardio-vascular remedies.

Introduction

Many physiologically active compounds with a wide spectrum of activities have been found among indole derivatives [1-5]. A representative of this series – preparation "Dimecarbine" - ethyl 5-hydroxy-1,2-dimethyl-1*H*-3-indolecarboxylate has been suggested for treatment of cardio-vascular diseases [6,7].

Results and discussion

It is well known that the chemical reaction forming 5-hydroxyindole derivatives from benzoquinone and β-aminocrotonic esters represents the classical Nenitzescu indole synthesis [8-10].

The synthesis of ethyl 5-hydroxy-1,2-dimethyl-1*H*-3-indolecarboxylate **3** consists of the cycle formation reaction between 1,4-benzoquinone **2** and ester **1** in acetone or 1,2-dichloroethane.

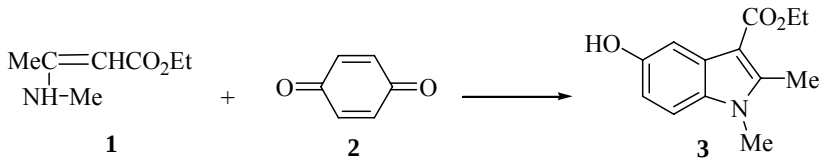

1 **2** **3**

However, both reported methods gave only up to 18% of targeted compound **3.** Such a low yield of the product can, probably, be explained by the instability of benzoquinone due to oxidation, which results in the breaking of the cycle or the polymer formation. Moreover, the spontaneous transformation of quinone into hydroquinone, which, in turn forms with quinone the colored quinhydrone, may influence upon the yield of the final product.

On the other side, it is known the initial interaction of the acetic acid with β-aminocrotonic esters and *p*-benzoquinones leads to the suppression of side reaction [10].

With the optimized conditions in our hands, the scope of the reaction was examined with variety of solvents. Finally, it was find that the replacement 1,2-dichloroethane or acetone by solution of the acetic acid in ethyl acetate leads to the augmentation of the yield of compound **3** up to 63%. It is worth noting that, it is possible to isolate **3** after a single recrystallization of the formed precipitate (look experimental part).

Conclusion

In summary, we have described a reaction of *p*-benzoquinone with N-methyl-β-aminocrotone ether in mixture of glacial acetic acid/ethyl acetate. This method represents a simplicity approach for preparing and isolation of the ethyl 5-hydroxy-1,2-dimethyl-1*H*-3-indolecarboxylate.

Experimental methods

All the used solvents were of reagent quality, and all commercial reagents were used without additional purification. Removal of all solvents was carried out under reduced pressure. Analytical TLC plates were Silufol® UV-254 (Silpearl on aluminium foil, Czecho-Slovakia). IR spectra were recorded on a Spectrum 100 FT-IR spectrophotometer (Perkin –Elmer) using the universal ATR sampling accessory. ^{1}H and ^{13}C NMR spectra have been recorded for $(CD_3)_2SO$ 2-% solution on a "Bruker -Avance III" (400.13 and 100.61 MHz).

Ethyl N-methyl-β-aminocrotonate 1 has been prepared according to the known procedure [7].

Preparation of ethyl 5-hydroxy-1,2-dimethyl-1*H*-3-indolecarboxylate 3. The mixture of **1** (7.9 g, 0.055 mol) and acetic acid (3.2 ml, 0.053 mol) in ethyl acetate (30 ml) were added to a solution of 5g (0.046 mol) of **2** and

glacial acetic acid (2.7 ml, 0.044 mol) in ethyl acetate (35 ml) so that the temperature in the reaction mass does not exceed 30°C (use ice/water bath). The residue was stirred for 1 hour, followed by distillation of the solvent (20 ml) and storing in the refrigerator for 24 hours at 0-10°C. The formed precipitate is separated, washed on filter by means of cold ethyl acetate. In result 7.2 g of solid substance with m.p. 180-190°C is obtained. After recrystallization from ethyl acetate 6.79 g of **3** were obtained. The yield was 63%. M.p. 215-216^{0}C. Lit. [7]. M.p. 210-215^{0}C. IR (ν/cm^{-1}): 3274 (OH), 2991, 2941, 1445, 1375 (Me, CH_2), 2791 (N-Me), 1751 (C=O), 1637, 1622, 1595, 1521, 1479, 1019, 870, 835, 803, 764, 668 (indole), 1333, 1212, 1288, 1093 (C-O). Spectrum NMR ^{1}H (δ, ppm, *J*/Hz): 1.35, t (3H, -CH_2Me, *J*=4), 2.68 s (3H, Me-C=), 3.64 s (3H, N-Me), 4.28, q (2H, -CH_2Me, *J*=4), 6.67, 6.68 d, d (1H, ^{6}CH, $J_{4,6}$=2.4, $J_{6,7}$=8.4), 7.25 d (1H, ^{7}CH, *J*=8.8), 8.47 d (1H, ^{4}CH, $J_{4,6}$=2.4), 8.95 s (1H, OH). Spectrum NMR ^{13}C (δ, ppm): 165.60 (CO_2), 153.10 (^{5}C), 145.67 (^{2}C), 131.14 (^{7a}C), 127.56 (^{3a}C), 111.72 (^{6}C), 110.69 (^{7}C), 105.95 (^{4}C), 102.37 (^{3}C), 59.06 (CH_2), 29.98 (NMe), 14.97 (^{2}CMe), 12.08 (CH_2Me). Mol. For. $C_{13}H_{15}NO_3$. Cal. C 66.94; H 6.48; N 6.0. Find C 67.3; H 6.13; N 6.28.

References

[1]. Macaev, F. Synthesis of spiroindolin-2-ones from 1*H*-indole-2,3-dione. In "*Selected methods for synthesis and modification of heterocycles*". Vol. 3. The chemistry of synthetic indole systems. IBS press, 2004, pp 75-102.

[2]. Landwehr, J.; George, S.; Karg, E. M.; Poeckel, D.; Steinhilber, D.; Troschuetz, R.; Werz O. *J. Med. Chem.* 2006, 49, 4327-4332.

[3]. Srivastava, S. S.K.; Husbands, S.M.; Lewis J.W. *J. Med. Chem.* 2005, *48,* 635-638.

[4]. Bohme, T.M.; Augelli-Szafran, C.E.; Hallak, H.; Pugsley, T.; Serpa, K.; Schwarz, R.D. *J. Med. Chem.* 2002, 45, 3094-3102.

[5]. Swann, E.; Barraja, P.; Oberlander, A.M.; Gardipee, W.T.; Hudnott, A.R.; Beall, H.D.; Moody, C.J. *J. Med. Chem.* 2001, 44, 3311-3319.

[6]. Mashcovskii, M.D.; Medicinal remedies. Chişinău: Cartea Moldovenească, 1990, l, 391.

[7]. Rubtsov, M.V.; Baichikov, A.G. Synthetical pharmaceutical preparates; Medicine, Moscow, 1971, 158-159.

[8]. Nenitzescu, C.D. Chemical Society Bulletin Romania 1929, 11, 37. Chem. Zbl. 1929, 2, S.2331.

[9]. Gil, C.; Brase S. Journal of Combinatorial Chemistry, 2009, 11, 175-197.

[10]. Ronn, M.; McCubbin, Q.; Winter, S.; Veige, M.K.; Grimster, N.; Alorati, T.; Plamondon L. Organic Process Research & Development. 2007, 11, 241-245.